Box 26

A Research Report

The Marysville, Montana Geothermal Project

Final Report

William R. McSpadden
Project Manager

September 1975

Battelle
Pacific Northwest Laboratorie

DISCLAIMER

LEGAL NOTICE

This report was prepared by Battelle as an account of sponsored research activities. Neither Sponsor nor Battelle nor any person acting on behalf of either:

a. Makes any warranty or representation, express or implied, with respect to the accuracy, completeness, or usefulness of the information contained in this report, or that the use of any information, apparatus, method, or process disclosed in this report may not infringe privately owned rights; or

b. Assumes any liabilities with respect to the use of, or for damages resulting from the use of, any information, apparatus, method, or process disclosed in this report.

THE MARYSVILLE, MONTANA GEOTHERMAL PROJECT
FINAL REPORT

23111-01410

to
U.S. Energy Research and Development
Administration

from
Battelle-Northwest
Rogers Engineering Co., Inc.
Southern Methodist University
Systems, Science and Software

September 1975

Battelle
Pacific Northwest Laboratories
Richland, Washington 99352

CONTENTS

SECTION A

INTRODUCTION, SUMMARY, AND RECOMMENDATIONS

W. R. McSpadden, Battelle-Northwest

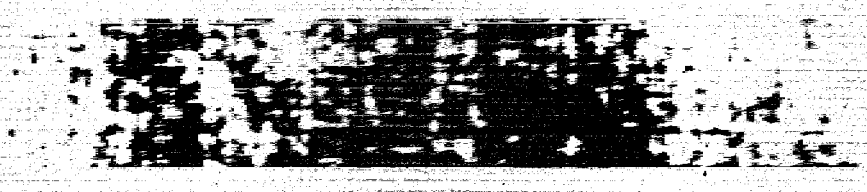

SECTION A INTRODUCTION, SUMMARY AND RECOMMENDATIONS

CONTENTS

INTRODUCTION, SUMMARY AND RECOMMENDATIONS

by
William R. McSpadden
Battelle-Northwest

September 1975

INTRODUCTION, SUMMARY AND RECOMMENDATIONS

William R. McSpadden, Project Manager
Battelle-Northwest

INTRODUCTION

In 1969 a geophysicist, David D. Blackwell, while making regional heat flow measurements in the northwestern United States, discovered a site about 20 miles northwest of Helena, Montana where the geothermal heat flow was about 10 times the regional average. The site aroused scientific interest because there were no surface manifestations such as young volcanics, hot springs, geysers, etc. within 20 miles of the site. Further research showed that this "blind" geothermal anomaly covered a roughly elliptical region about 3 miles long and 1-1/2 miles wide in a mountainous area about 4 miles west of the old gold mining town of Marysville, Montana. The heat source was expected to be a granitic pluton or intrusion of once molten rock with a volume of several cubic miles within about 1.5 miles of the surface and perhaps as hot as 500°C. Resistivity measurements and other data led to the speculation that there was a little water near the heat source. In any event, its exploration was of interest to scientists for several reasons.

Also there was significant economic interest in exploring the source of heat as a potential for the generation of electricity. The process would involve forcing water into the fractured region around the hot rock through one or more wells and extracting steam through other wells to drive electric generators. The energy available from a few cubic miles of hot rock is worth billions of dollars; consequently there was an economic motive for the project. Furthermore the site probably is not unique and many similar sites probably exist in the western part of the United States. If such energy can be made available then less oil is needed to generate electricity.

In the winter of 1972-73 a team of scientists and engineers assembled at Battelle-Northwest in Richland, Washington to prepare a proposal to explore the geothermal anomaly. The principal team members were Donald H. Stewart and William R. McSpadden from Battelle-Northwest (BNW), David D. Blackwell from Southern Methodist University (SMU), and James T. Kuwada from Rogers Engineering Company of San Francisco. Later Systems, Science and Software of La Jolla, California joined the project under the direction of Russell Duff. The proposal was submitted in February 1973 to the National Science Foundation (NSF) with BNW to be the prime contractor. The project was funded in June 1973 with Ritchie B. Coryell of the NSF as the program manager. Between June 1973 and the project completion in June 1975 the project cost approximately $2,240,000. This is the final report of that project.

The final report is organized with independent sections prepared by each contractor. Consequently there is some overlapping information, generally presented from different viewpoints, depending upon the author's part in the project. It was felt that these different viewpoints would be valuable so they have not been edited out. The final report does not repeat the information presented in

earlier project reports, particularly on the environmental analysis, the drill site preparation, and the infrared surveys. However, a limited number of these earlier reports are available from William R. McSpadden.

Briefly the project consisted of geophysical surveys in 1973 and 1974, the drilling of the deep well in the summer of 1974 to a depth of 6790 ft, the coring and logging of the well, the supporting scientific studies, and the data analysis. The well penetrated an extensive hydrothermal zone of about 200°F that was essentially isothermal from 2000 ft to 6790 ft. Scientific studies will continue to better understand the geothermal anomaly but commercial development does not appear feasible at these low temperatures.

DESCRIPTION OF THE MARYSVILLE AREA

The historic gold mining town of Marysville is located approximately 20 miles northwest of Helena, the capital of Montana, as shown in Figure A.1. Many of Marysville's old buildings remain from its gold mining days, a few of which are shown in Figure A.2. The geothermal drill site is located approximately 4 miles west of Marysville in the Empire Valley. Although both Marysville and the drill site are at 5300 ft elevation, they are in different water drainage basins and are separated by Mt. Belmont which rises to 7330 ft. Vegetation of the area is mostly Douglas fir, with open bunch grass regions on the south exposures and narrow stream-bottom meadows. Over 50 years of mining operations have removed all of the large virgin timber so that only second and third generation growth remains. Both the drill site and Marysville can be reached on good dirt roads during the summer months.

Climatic conditions vary considerably over the area with elevation and exposure, and marked contrasts may be found within a few miles. The annual mean temperature at Marysville is 40.7°F, the extreme maximum 91°F and the minimum -22°F. These extremes represent an average of the hottest and coldest days of each year over a 10-year period from 1895 to 1905. Average rainfall for the region is 19.4 inches, while Helena at an elevation of 4157 ft receives only 11.3 inches.

It is impossible to work in this area without becoming aware of the extensive gold mining history of the region over the past 100 years. There have been 15 or more gold mines in the immediate vicinity, the largest of which was the Drum Lummon at Marysville. Gold mining and development of the area was influenced largely by one man, Thomas A. Cruse, founder and developer of the Drum Lummon Mine. Cruse was born in Ireland in 1836 and immigrated to the United States in 1856. In 1868 he appeared in the Helena area and began gold operations near the present site of Marysville. As a result of the discovery of the Drum Lummon he became an extremely wealthy man and dominated the activities of the area until his death in 1914. During this era many other gold mines opened in the area such as the Bald Butte and Empire Mines, and Marysville rapidly grew to a population of more than 5000. By 1880 it had two railroads, six hotels, one bank, four groceries, three churches, 27 saloons, and a wide variety of small businesses.

The geothermal drill site is located near the Empire Mine which was owned by the Empire Mining Company, Ltd. of London which also owned the Drum Lummon

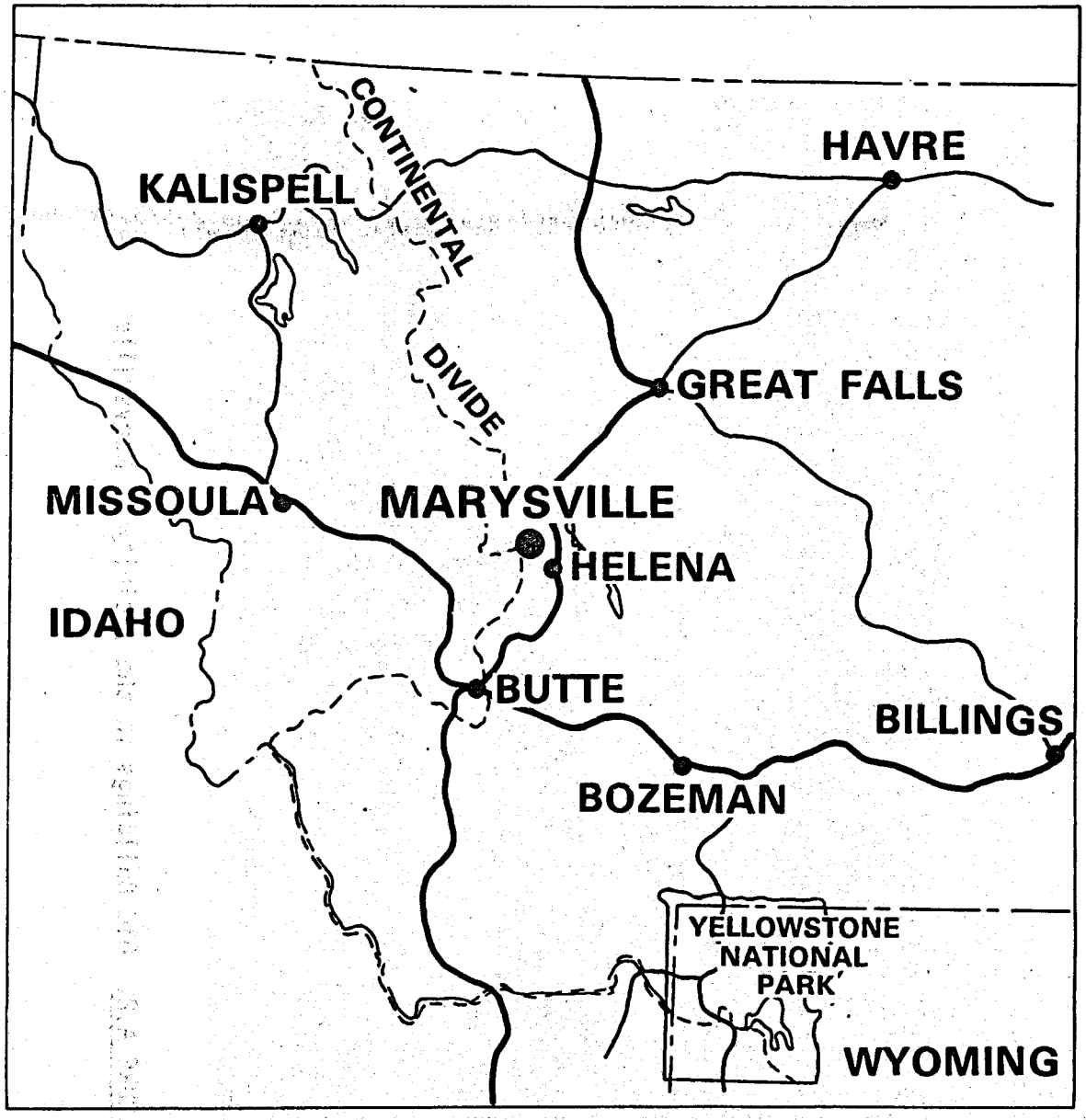

FIGURE A.1. Location of Marysville, Montana

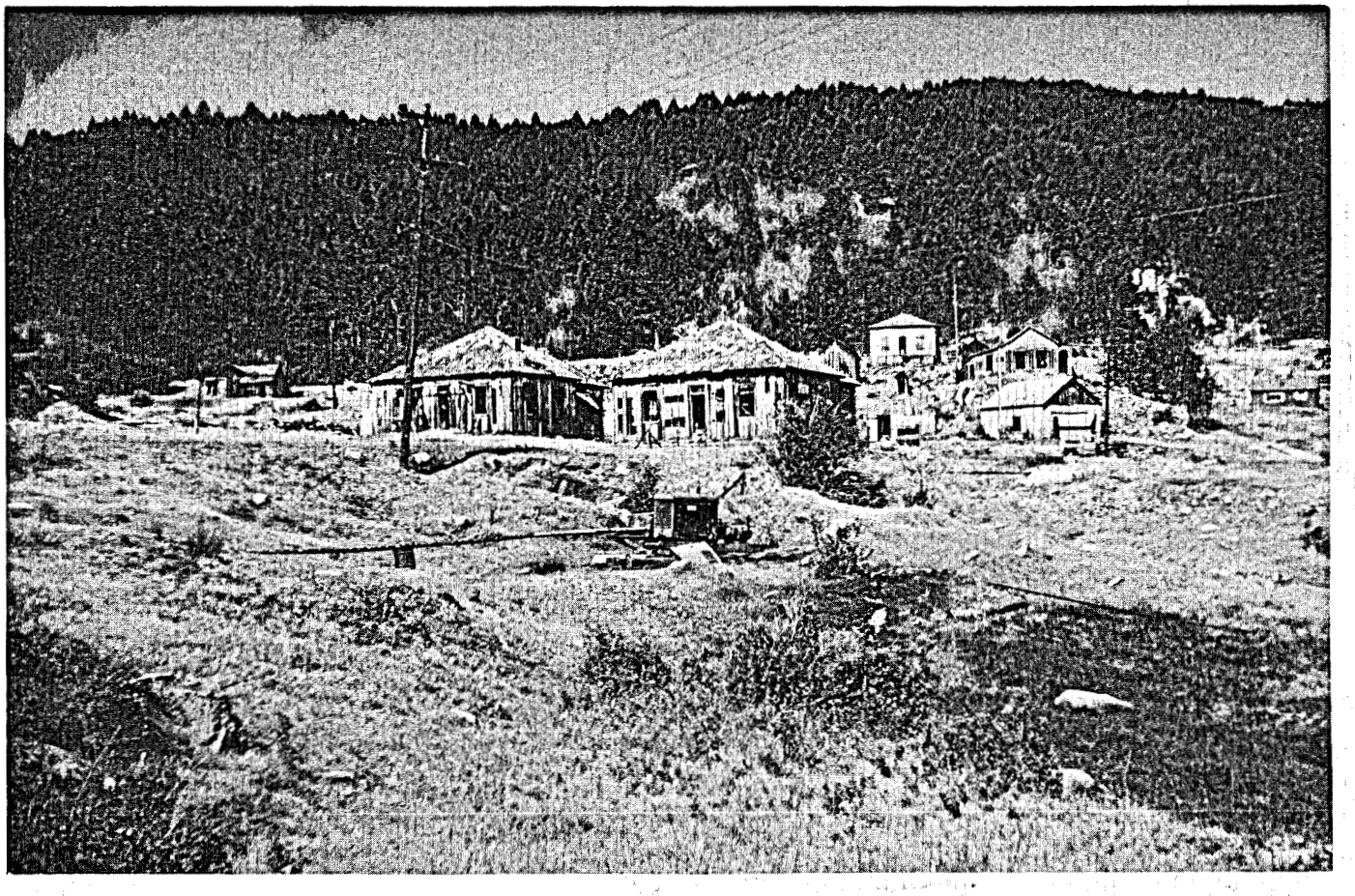

FIGURE A.2. Old Buildings in the Vicinity of Marysville

mine at that time. A large mill was completed at the Empire Mine in 1888 and operation continued until the turn of the century. The mine continued intermittent operation under a variety of owners until the shutdown in 1942 during the war operations. The tailing ponds, a large cyanide mill and a number of buildings still exist in the immediate area of these operations. Although the mine itself is on patented land, all of the operations associated with the geothermal project took place on Federal lands administered either by the Bureau of Reclamation or the U.S. Forest Service.

PROJECT ACTIVITIES IN FY 1974

During the period from 1966 until the beginning of this project in June 1973, David D. Blackwell made extensive heat flow measurements in the vicinity of Marysville under the sponsorship of the National Science Foundation and the U.S. Geological Survey. Heat flow data were obtained from 15 relatively shallow drill holes (less than 1000 ft) which existed in the area as a result of previous mineral explorations. The heat flow from the 15 sites ranged from 3.1 to 19.5 heat flow units (hfu) in $\mu cal/cm^2/sec$. (For comparison, the western Montana average is 1.9 hfu and the worldwide average is about 1.5 hfu.) The maximum heat flow corresponds to a geothermal gradient of 240°C/kilometer. In spite of these extremely high gradients there are no surface manifestations in the form of hot springs or geothermal activities within approximately 20 miles of the site.

After the project began in June 1973, SMU conducted surveys of the geology, heat flow, gravity and magnetic fields, and microseismic noise in the Marysville area. In addition, infrared aerial surveys were conducted by Battelle-Northwest. Heat flow measurements were made in nine additional shallow holes drilled under Blackwell's direction to obtain a better definition of the size of the heat flow anomaly. By October 1973 the results of these various field surveys enabled the team to pick a site for drilling a deep well. The site selected was approximately 1/4 mile downstream from the Empire Mine on land administrered by the Bureau of Land Management (BLM). On October 26, 1973 the NSF conducted a review meeting of the project in Helena which was also attended by members of the State and Federal Government. A preliminary report provided to the reviewers at that meeting was superceded by a first annual report published in June 1974. As a result of the review meeting, NSF authorized the second phase of the work which was to drill the deep well.

Once a decision was made to undertake the second phase, Battelle-Northwest and Rogers Engineering Company prepared a draft environmental analysis for BLM. Additional environmental analyses were conducted by BLM and ultimately they determined that no environmental impact statement would be required for the drilling.

Rogers Engineering Company prepared site engineering surveys and plot plans for the drilling operations. The necessary Use Permits were obtained from the Bureau of Land Management, the U.S. Forest Service, the Montana State Division of Water Use, and the Montana State Lands Department. Following these activities Rogers Engineering Company prepared specifications for the site construction and drilling of the deep well. For the site construction, the low bid was received from and the contract awarded to the William Miller Construction Company, Missoula, Montana in April 1974. Similarly the drilling contract was awarded to the Molen Drilling Company of Billings, Montana in May 1974.

SUMMARY OF DEEP WELL DRILLING OPERATIONS

Under the direction of Winston Bott of Rogers Engineering Company, 90 days of drilling during the summer of 1974 were planned to achieve a target depth of about 6000 ft. The actual drilling began on June 10 and continued until August 30, a period of 81 days ending at a total depth of 6790 ft. Most of the drilling was done with aerated water at rates of 18 to 25 ft/hr. Two major formations were encountered. The upper formation of Empire shale (metamorphosed shale and quartzite) extended to approximately 975 ft, and the remainder of the hole to depth was in the Empire stock (quartz feldspar porphry). There is a gradual change in the Empire stock with depth toward a granite, showing the effects of slow cooling.

The Empire stock is extensively fractured and contains a large volume of water. Water was first encountered at 1525 ft and major water zones were found at 1912 and 3386 ft. However, the many fractures led to speculation that the water zones are interconnected. All of the fracture zones below 1000 ft appear to contain water. We encountered flows in excess of 250 gallons/minute from upper fraction zones into the lower ones. In view of all of the geophysical surveys that had been done at the surface, including electrical resistivity and magnetotellurics, large amounts of water had not been expected.

The hole in the upper 115 ft of the well was drilled to 26 inches in diameter and a 20 inch casing was set and cemented to that depth. Between 115 ft and 1326 ft a 12-3/8 inch casing was set in a 17-1/2 inch hole and cemented in place. Between 1326 ft and 4264 ft a 9-5/8 inch casing was set in a 12-1/4 inch hole, but cementing was not successful and only the lower few feet of the casing were encased in cement. Between 4264 ft and the total depth of 6790 ft a 7-7/8 inch hole was drilled and not cased. Later a cement plug was placed in the bottom of the hole to control water flow, so the hole depth is now 6414 ft. The current status of the well is shown in Figure A.3 along with locations of fracture zones and coring depths. Although a plan for eventual plugging and abandonment exists, the hole will remain open for scientific studies until the summer of 1976. At the present time (September, 1975) the USGS is conducting regional hydrology studies and has sponsored temperature monitoring and water sampling in the well.

LOGGING AND CORING

Schlumberger Well Services contracted to log the well, and their first major logging was conducted to 1326 ft on July 7, 1974 prior to setting the middle-string casing. The second major logging from 1326 ft to 6790 ft was completed on September 10, 1974. These major loggings were to determine: hole dimensions, formation resistivity, formation density and porosity, hydrogen concentration, cement bonding, natural radioactivity, fracture patterns, hole deviation from the vertical, temperature, and water flow. The results clearly show the two major formations, the Empire shale to 975 ft and the Empire stock to depth, as well as the variations within each major zone. The Shale consists of five subzones wherein the physical properties vary significantly. The Stock is basically quartz porphyry which is quite highly fractured and has a bulk permeability that permits large water flow. In addition to the two major loggings, many minor loggings of temperature and water flow were made by Schlumberger and others. Although the technology exists to make adequate flow and temperature measurements at 100°C, the

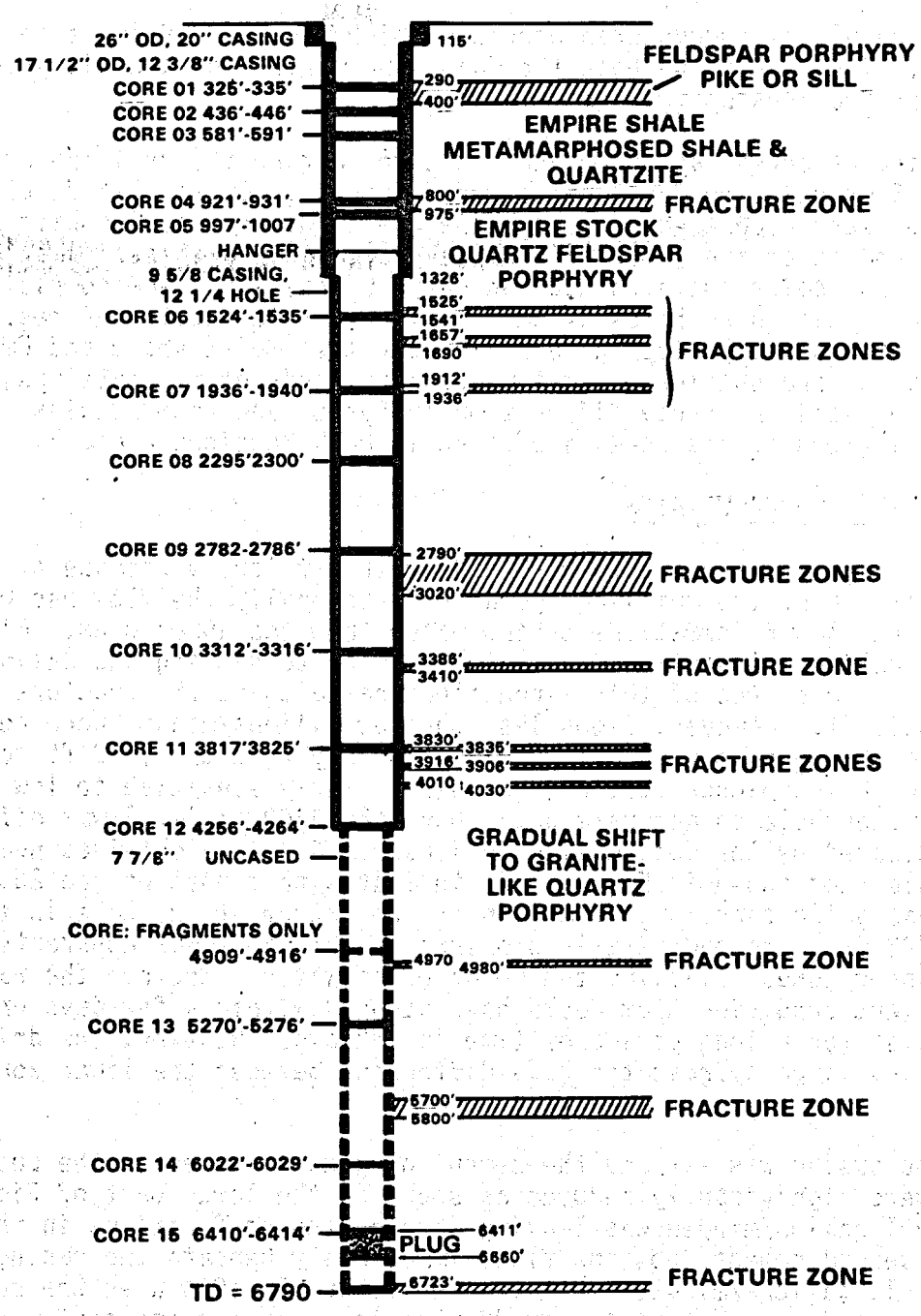

FIGURE A.3. Casing, Coring, and Formation Data, Well No. 1

logging crews regularly encountered problems which made it difficult to obtain reliable data. The results of both the major and minor logs are discussed in detail in other sections of the report.

The cutting of cores was undertaken 18 times during the drilling operations and produced 15 useful cores and one set of fragments. Of the 115 ft cored, 83 ft of useful cores were recovered. Despite the use of diamond coring bits, coring was difficult and expensive (about $1,636/ft recovered) in these formations. The cores were washed, color photographed and cut for analysis. One complete set of core sections is held in archives by SMU for future reference. The results of the core analysis show steeply dipping veins in both the Empire shale and Empire stock. Rock descriptions were obtained from a microscope study of the cuttings, petrographic studies of thin sections, x-ray diffraction analyses, and from studies of the logs. Detailed descriptions of the cores are given in both Sections C and E.

WELL TEMPERATURES AND FLOW RATES

Rock temperature measurements were made with difficulty because of water flow in the hole throughout the drilling operation. Generally the flow has been down the hole with the lower formations taking water from the upper ones. Flows in excess of 250 gallons/minute were encountered prior to setting the casing as shown in Figure A.4. The source of this large flow seemed to be the fracture zone between 3386 ft and 3410 ft. However, flows less than 50 gallons/minute were believed to originate from the upper parts of the hole, probably from the 1912 ft to 1936 ft zone. The open hole spinner test was not particularly sensitive to low flows in the large diameter hole so accurate data above the 3400 ft level was difficult to obtain as indicated by the dotted line in Figure A.4. Data obtained near the bottom of the hole (not shown in Figure A.4) indicates that most of the 250 gallon/minute flow was going back into formation at the bottom of the hole in the fracture zone below 6723 ft. The hydrostatic pressure of this zone was apparently less than that of the upper zones, allowing the downflow of water. Whether the water flow was a local transient condition that would have stopped within a few days or a condition that might exist for a long period of time is unknown. However, the drill stem test did not show any large hydrostatic head difference between the lower zone and the upper zones.

After the casing was set and the cement plug established in the bottom of the hole, flows were significantly reduced as shown in the lower part of Figure A.4. Approximately 1 gallon/minute was leaking through the perforations in the casing made for the second cement job, and flows immediately beneath the casing were approximately 10 gallons/minute. Between September 10, 1974 when the packer flowmeter test was performed and September 22 when the radioisotope test was done, an apparent equilibrium took place in a lower part of the hole since the flow at the 5700 ft level reduced from greater than 30 gallons/minute to approximately 1 gallon/minute. Below the 6000 ft level the flow is zero to the best of our ability to measure it with the isotope test. The flow test made on November 17, 1974 (not shown in Figure A.4.) with the radioisotope instruments showed a maximum flow of about 1 gallon/minute at about 4270 ft, which had reduced to about 0.1 gallon/minute by April 1975.

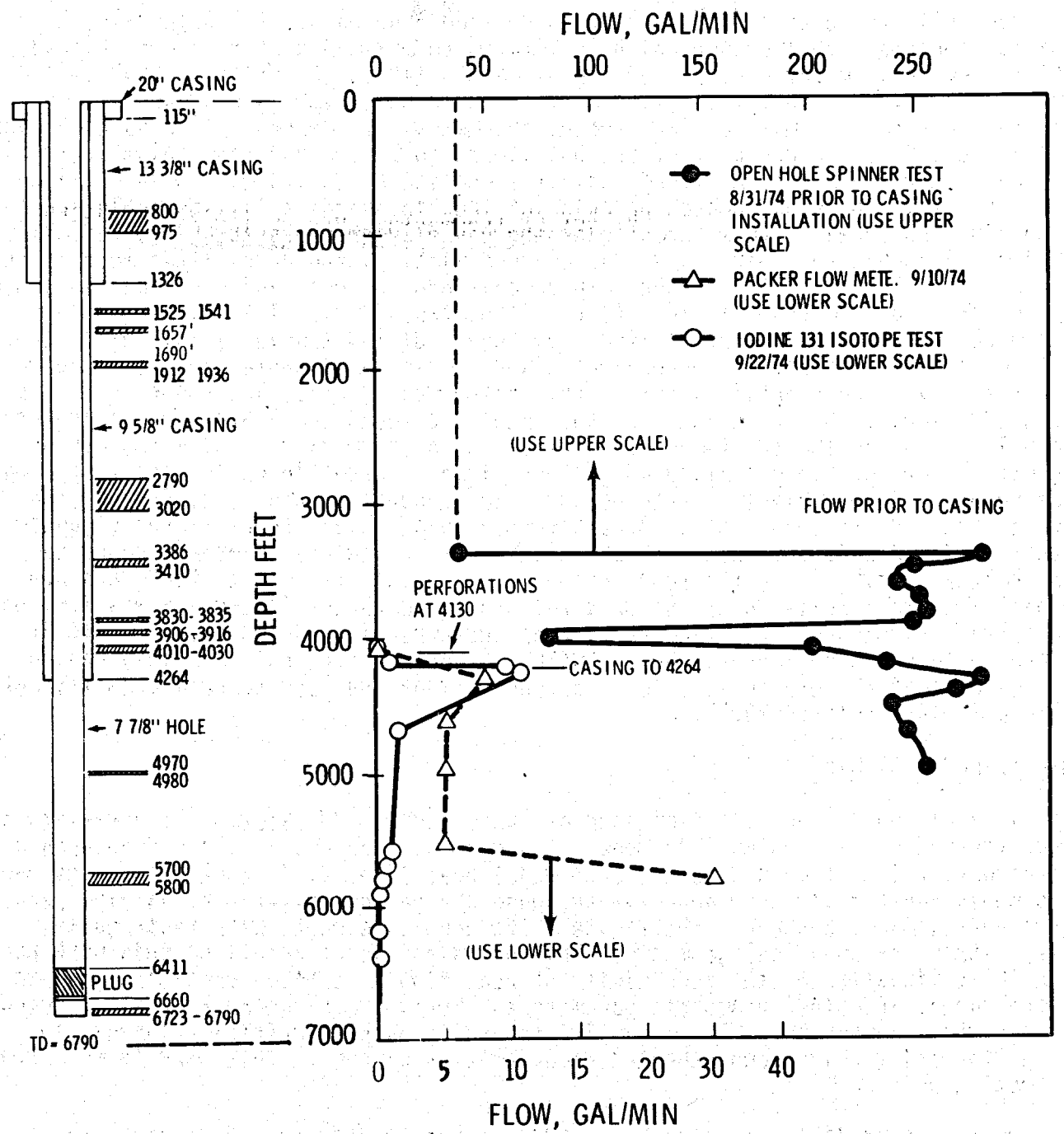

FIGURE A.4. Flow Rates, Well No. 1

Down-hole temperature measurements were made four ways: (a) using Blackwell's resistance element thermometer which is limited to maximum depths of approximately 2500 ft and maximum temperatures of approximately 110°C, (b) using the Schlumberger platinum resistance thermometer, (c) a Kuster down-hole temperature versus time recorder, and (d) maximum reading mercury thermometers. Generally the data obtained by Blackwell in the upper part of the hole tends to complement the Schlumberger measurements shown in Figure A.5, and indicates cooling of the formation as drilling proceeded. The apparent erratic behavior of the fine details is presumably caused by the in-flow of water from formations before and after the setting of the casing. The logging on September 10 (curve 2) occurred within a few hours after most of the cool water in the mud pit had been pumped back into the hole and consequently cooler temperatures were recorded at that time. Also, two additional Schlumberger logs were made approximately 24 hours after the August 31 log (curve 1) and these agree quite closely with those of curve 3 which were obtained on September 21. Temperatures of curve 1 were obtained before the casing was in place and those of curves 2 and 3 afterwards. Water moving down the annulus between the 9-5/8 inch casing and the hole was affecting the temperature readings in the casing. Below the casing the water flows of approximately 10 gallons/minute are sufficiently high to prevent measurement of the ambient rock temperature and generally this condition existed down to the 5700 ft level until about November 1974. Water temperatures slightly less than 200°F were obtained throughout this entire region. Maximum temperature thermometer readings over the same region read consistently 200 to 204°F and are probably the most reliable of the measurements. The Kuster instrument was left on the bottom of the hole for 44 hours between September 19 and September 21 but it showed no temperature increase above 204°F. Since the flow rates in this region are believed to be zero or very low, it appears that the rock temperatures may not be greatly in excess of 200°F.

THERMODYNAMIC STUDIES

In addition to the heat flow studies conducted by SMU (Section E) a variety of other thermodynamic studies were done. Systems, Science and Software developed a two-dimensional heat conduction code to model heat flow. This work by Stanley Hays uses nonlinear functions to approximate phase change and temperature varying parameters near a magma chamber. The finite difference code works with rectangular, axisymmetric, or spherical geometry. The most significant result of this work has been the delineation of the sensitivity of heat flow to surface variations, depth of the magma, and other geometric parameters. For example, changes in the assumed depth of the chamber by as little as 100 meters produced significant changes in the geothermal gradient and other thermodynamic parameters. This work is reported in Section D.

During the drilling operations in 1974 it became evident that a computer simulation of the drilling, based upon a heat flow balance between the drilled formations and the circulating drilling fluids, would be a valuable guide. This was dictated by the difficulty of obtaining estimates of the in-situ rock temperatures while the circulation was in progress, and for perhaps as long as several months after the drilling had stopped. Accordingly, J. R. Sheff of BNW began work on a simulation model. Ultimately this work was shifted to C. A. Oster and Burt Scheffler as Sheff took on other assignments. The results are reported in Section D.

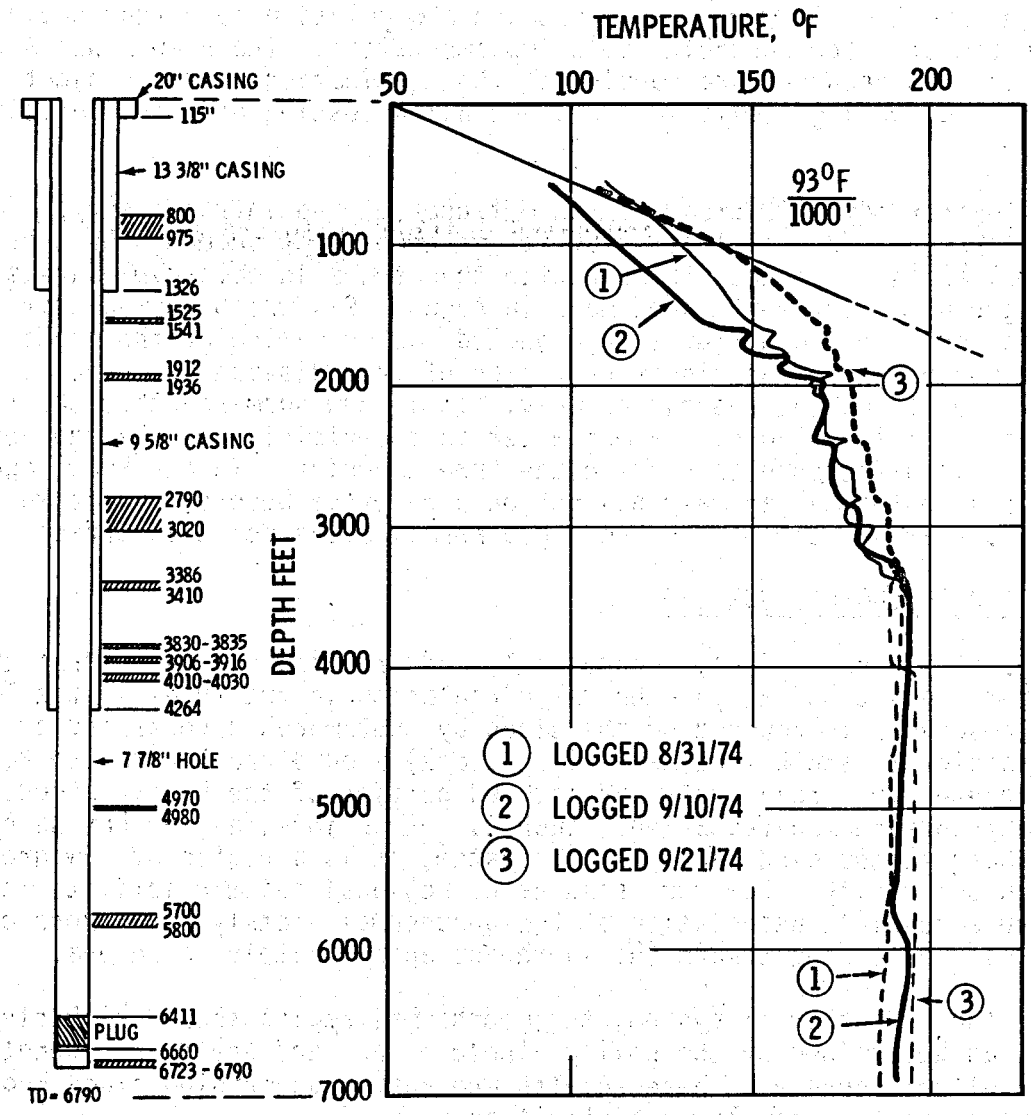

FIGURE A.5. Well Temperatures, Well No. 1

The objective of this work was to produce a simulation code that could be run on a minicomputer for possible field implementation. The result was a code, THERMWEL, which was debugged and running at the termination of the project. Unfortunately time and funding limitations did not allow testing and field applications of the code.

The third thermodynamic study was an offshoot of the infrared survey conducted by BNW in September 1973. In that study it was noted that some of the trees over the geothermal anomaly appeared to be hotter than trees in comparable areas. Accordingly ground measurements were made in August 1974 which showed that the trees were indeed 1 to 2°C warmer than expected. Observation of the trees over a period of 12 months showed no significant sign of tree disease or insect infection which might account for the thermal anomaly. It is now surmised that the roots of the trees are obtaining slightly warmer water in the vicinity of the geothermal anomaly, and this difference is seen in the tree canopies. To our knowledge, this phenomenon of a geothermal anomaly has not been reported before, but it would be of interest to examine some of the known geothermal areas for this effect.

GEOPHYSICAL AND GEOLOGICAL SURVEYS

Analyses of the geological, geophysical, and drilling data show that the geothermal system consists of a hydrothermal circulation in fractures in the Empire stock. The reservoir is bounded on the sides by metamorphic rocks and by a Mesozoic granodiorite stock (the Marysville stock) around the Empire stock, and bounded on the top by a relatively unfractured portion of the Empire stock. The area lacks any surface manifestations, such as hot springs, at the hot water reservoir. Despite the circulating water system, it is a region of low ground noise and low seismicity. However, studies of regional seismic activity in 1973 and 1974 show a possible association of the geothermal anomaly and a zone of seismic activity extending toward the southeast approximately to Helena.

Despite the hydrothermal system, the geothermal region showed high electrical resistivity, as determined by the roving dipole method and the deeper penetrating audiomagnetotelluric survey. These results are rather surprising since known geothermal areas generally show low resistivities.

A negative gravity anomaly is associated with the high heat flow, but these are not associated with any magnetic anomaly. The Marysville stock to the northeast of the geothermal region does have a magnetic anomaly, however, which was useful in determining one boundary of the Empire stock.

An infrared survey conducted in September 1973 failed to show the geothermal anomaly. The aerial survey was conducted in two bands, 3-5μ and 8-14μ wavelengths, from an altitude of approximately 10,000 ft above the terrain. Under ideal conditions a heat flow of 20 hfu would produce a temperature rise of about 0.4°C. However, variations due to water vapor in the air, solar variations, changes in ground slope and the effects of trees and other vegetation produced a poor signal to noise ratio. As noted above, some vegetation was found to have a higher than normal temperature. The infrared survey was presented in detail in the First Annual Report (June 1974) and is not repeated here.

Heat flow, correlated with other geophysical surveys, proved one of the most useful techniques for this project. As noted in the paragraph on FY 1974 activities, heat flow was measured at 15 sites prior to 1973, at nine sites drilled in 1973 and at four new sites drilled in 1974. Heat flow and geothermal gradient data were corrected for terrain variations and found to vary from 19.5 hfu (240°C/kilometer) to 3.2 hfu (43°C/kilometer) with rather sharply defined boundaries on the north and east sides (abutting the Marysville stock). Values on the south and west sides diminished more gradually, as did the gravity anomaly. Additional areas of high heat flow may exist to the south, but time and money limitations prevented further exploration here.

Geologic mapping in 1973 and 1974 proved very significant in providing a framework for understanding the geothermal anomaly. These studies consisted of structural geology, metamorphic petrology, neutron activation analysis of the igneous rocks and identification of lithologic units of the Precambrian Belt Series and the plutonic and volcanic igneous rocks. There are at least four major normal faults which may have played a part in the emplacement of the geothermal source. These are generally east-west faults dipping to the south. The mapping identified a dome-like structure that correlates approximately with the high heat flow. The petrology studies indicate that the Empire stock was much larger than suspected and perhaps underlies most of the dome southwest of the Marysville stock.

COST SUMMARY

The total expenditures for the Marysville Geothermal Project to date (September 1975) are $2,240,000, which are detailed in Table A.1. This includes an obligation of approximately $50,000 for plugging and abandonment of the hole at some future date. Site restoration costs are included in this latter figure.

The total footage drilled, including 1556 ft of reaming the upper levels for large size casing, was 8346 ft. Since the direct drilling costs were $633,993, the average linear drilling cost is $76/ft. However, coring costs were high because of very slow cutting rates (0.5 to 4.0 ft/hr) of the diamond coring bits. The 82.5 ft of recovered core cost an average of $1,636/ft.

RECOMMENDATIONS

It is highly probable that other geothermal systems like Marysville exist in the western part of the United States and elsewhere, some of which can be expected to have temperatures high enough for commercial exploitation. Because so much data are available on the Marysville system, it can serve as a testing and research area to help locate and understand similar systems. Accordingly, it is recommended that (a) pump tests be made to determine reservoir production characteristics, (b) additional heat flow wells be drilled to the south of the anomaly to close the heat flow contours and complete the study, and (c) the existing well be held open for research and equipment testing.

With respect to geothermal exploration and national resource assessment programs, many additional wildcat wells will be drilled in the next 10 years. If we use the oil industry's success ratio of about one successful well in 10 tries for

TABLE A.1. Cost Summary of the Marysville Geothermal Project

Geosciences Surveys, Core Analysis and Data Reduction	$ 332,786
Site Preparation and Field Office Operations	107,751
Direct Drilling Costs	633,993
Coring Costs	134,970
Casing, Cement and Wellhead Equipment	196,759
Well Logging and Testing	52,664
Engineering and Drilling Supervision	178,051
Thermodynamic Studies and Infrared Survey	81,924
Environmental Analysis, Fracture Analysis, Logging Analysis	158,866
Project Management	211,700
Drilling Arbitration Costs	33,648
Miscellaneous Other Costs	66,888
Plugging and Abandonment (Estimate)	50,000
Project Total	$2,240,000

geothermal estimation, we can expect a very high ratio at nonproductive wells. Accordingly, research should be pursued to reduce the cost of locating and assessing new geothermal areas. A national program could produce refined geophysical exploration techniques, new drilling and coring techniques, and use of existing slim hole drilling technology as an exploration technique. Better logging service at high temperatures is needed, and the integration of modern computer technology for rapid data reduction in the field should be undertaken. The need for all of these techniques and services was experienced on the Marysville Geothermal Project.

ACKNOWLEDGEMENTS

Although many people contributed to this project, the support of Ritchie Coryell and David Lombard of our sponsoring organizations was essential. Throughout the period of transfer from NSF to ERDA they provided help and continuity. Most of the major contributions from the contractor organizations are identified herein by the authorship of sections of the final report. The exceptions are Donald Stewart of BNW, James Kuwada of Rogers Engineering Company, and Russell Duff of Systems, Science and Software, who contributed throughout the project with management advice and support. The work of Laura Koester and Sally Rogers in administering contracts at Battelle-Northwest is greatfully acknowledged, as is the technical editing of Lonnie Foley. The efficient work of Joanne Perry, Darlene Couch, and Peggy Snyder, our secretarial staff, helped keep the project on schedule, and generally helped make order out of potential office chaos.

This work was sponsored by the National Science Foundation from June 1973 to January 1975 and by the Energy Research and Development Administration from January 1974 to completion in July 1975.

PROJECT REPORTS

The following reports were published in connection with this project:

1. The Marysville, Montana, Geothermal Project Preliminary Report to Research Applied to the Nation's Needs (RANN) National Science Foundation, November 12, 1973.

2. Statement of W. R. McSpadden to U.S. House of Representatives' Committee on Science and Astronautics, The Subcommittee on Energy, Hearings on H.R. 8628, "Geothermal Energy Development Corporation Act," in Richland, WA, September 11, 13 and 18, 1973.

3. Statements of W. R. McSpadden and D. D. Blackwell to U.S. House of Representatives' Committee on Science and Astronautics, The Subcommittee on Energy, Hearings on H.R. 11212, "The Geothermal Energy Research, Development, and Commercial Demonstration Act of 1973," in Richland, WA, February 11, 1974.

4. Specifications for Construction of the Drill Site for the Deep Geothermal Research Well, by Rogers Engineering Co., Inc., April 1, 1974.

5. Specifications for Drilling The Deep Geothermal Research Well, by Rogers Engineering Co., Inc., April 1, 1974.

6. Environmental Analysis of Cooperative Research Contract for The Marysville, Geothermal Project (Deep Research Well Phase), Bureau of Land Management, District Office, P.O. Box 4427, Missoula, MT 59801, April 1974.

7. The Marysville, Montana Geothermal Project, First Annual Report, Part I, by Battelle-Northwest to National Science Foundation, June 1974.

8. First Annual Report, Part II, Geological and Geophysical Exploration at Marysville Geothermal Area: 1973 Results, by Southern Methodist University; with a section on "Contemporary Seismicity in the Helena, Montana, Region," University of Utah, to National Science Foundation, June 1974.

9. Marysville Geothermal Anomaly Thermodynamic Studies, Agreement No. B-809, Systems, Science and Software, SSS-IR-74-2389, August 15, 1974.

10. Marysville Geothermal Project Plan and Estimate for Plugging and Abandonment of the Deep Well, by Rogers Engineering Co., Inc., July 1975.

11. The Marysville, Montana Geothermal Project, Final Report, by Battelle-Northwest, Rogers Engineering Co., Southern Methodist University, and Systems, Science and Software, September 1975.

IDENTIFICATION OF KEY PERSONNEL

SPONSORS

- National Science Foundation, Washington D.C.
  Ritchie B. Coryell, Program Manager

- Energy Research and Development Administration, Washington D.C.
  David B. Lombard, Program Manager

CONTRACTORS

- Battelle-Northwest (BNW), Richland, Washington, Prime Contractor
  Donald H. Stewart, Manager, Geothermal Programs
  Wm. R. McSpadden, Project Manager

- Rogers Engineering Company (REC), San Francisco, California
  James T. Kuwada, Vice President
  Winston Bott, Project Engineer

- Southern Methodist University (SMU), Dallas, Texas
  David D. Blackwell, Associate Professor
  Department of Geological Sciences

- Systems, Science and Software (SSS), LaJolla, California
  Russell E. Duff, Manager, Radiation and Fluid Physics Division

FEDERAL GOVERNMENT LIAISON

- Bureau of Land Management, John Fields, Robert Newman, David Pickett, Missoula, MT

- Environmental Protection Agency, James Shaw, Denver, CO

- U.S. Geological Survey, James Hinds, Billings, MT

- U.S. Forest Service, Wm. Taliaferro, Helena, MT

STATE GOVERNMENT LIAISON

- Office of Lieutenant Governor, William Christiansen, Helena, MT

- Department of Intergovernmental Relations, Raymond Dominick, State Liaison, Helena, MT

- Environmental Quality Council, Walter Enderlin, Helena, MT

- Department of Fish and Game, James Posewitz, Helena, MT

STATE GOVERNMENT LIAISON (Continued)

- Department of Natural Resources and Conservation, Lynn Brant, Ron Guse, Helena, MT
- Department of State Lands, Sharon Solomon, Helena., MT
- Montana State Historical Society, Harriet Meloy, Helena, MT

NSF REVIEW COMMITTEE (Helena, October 26, 1973)

- Jesse C. Denton, University of Pennsylvania
- Charles R. Draper, Montana Division, Planning and Economical Development
- Gerald W. Johnson, Director, Division of Applied Technology, USAEC
- L. J. Patrick Muffler, US Geological Survey, Menlo Park
- Robert Newman, Bureau of Land Management, Missoula, MT
- Dan H. Pyfer, Montana Power Company, Butte, MT
- Henry J. Ramey, Department of Petroleum Engineering, Stanford University
- Robert C. Scott, Environmental Protection Agency, San Francisco, CA
- Morton C. Smith, Los Alamos Scientific Laboratory
- Lillian K. Stone, Office of Environmental Projects Review, Washington, DC

SECTION B

DRILLING REPORT

Winston Bott, Rogers Engineering Company

SECTION B DRILLING REPORT

CONTENTS

LIST OF FIGURES

DRILLING REPORT

by
W. F. Bott
Rogers Engineering Company

September 1975

DRILLING REPORT

W. F. Bott

Rogers Engineering Company

Introduction

This Drilling Report describes the engineering and drilling management activities of Rogers Engineering Co., Inc., in carrying out its CY 1974 and 1975 responsibilities on the Marysville Geothermal Project.

These responsibilities include: (1) contacts with governmental agencies for coordination and approval of plans, and acquisition of necessary permits (except those acquired by Battelle Northwest Laboratories); (2) completion of plans and specifications for site preparation, and award of contracts for this work; (3) preparation of plans and specifications for drilling the deep well, issue bid invitations to selected list of drilling contractors, and award of drilling contract; (4) preparation of procurement specifications and award of contracts for auxiliary drilling services and permanent equipment; (5) supervision of site preparation; (6) supervision, direction and management of the total drilling operation, performing the functions of both Drilling Engineer and Operator; (7) compile a report of drilling operations; (8) if drilling results favorable, commence design of test facilities and preparation of feasibility report.

This report will not touch on details of the temperature surveys, the lithology, or the geophysical logging program, as these matters were the responsibility of Battelle Northwest Laboratories and Southern Methodist University, and are covered separately in this volume.

The office engineering work carried out during the winter 1973 and early spring 1974 culminated in the award of contracts for the various phases of the work during the month of May. The William G. Miller Construction Company, of Missoula, Montana commenced work on site preparation on 3 May, 1974. The construction schedule called for completion by 1 June, 1974; however, a twelve-inch snowfall on 19 May caused a one week delay in completion of the earth work, so the drilling rig mobilization could not start until 4 June.

Molen Drilling Co., Inc., of Billings, Montana, was awarded the drilling contract, and their Rig No. 4 spudded in the deep well on 10 June, 1974. At a 2:00 p.m. public ceremony, Lt. Governor Bill Christensen of Montana operated the lever to start the rotary drill turning.

The planned first phase of the drilling operation was to set 20-inch conductor casing at 250 feet. The rock formations proved

much harder to drill than anticipated, so the 20-inch pipe was set at 115 feet. Similarly, the 13-3/8 inch surface casing of the second phase was set at 1,326 feet instead of the planned 2,500 feet, again due to hard drilling of the 17-1/2 inch hole in the quartz feldspar porphyry of the Empire stock. (Major changes from the original plans, such as this, were made after consultation with BNW, SMU, USGS, and all other appropriate agencies).

Large unexpected volumes of water entered the bore hole from numerous intermittent fractured zones below 1,500 feet, and this caused additional changes in the drilling plans. The 12-1/4 inch hole was carried to 4,256 feet instead of the planned 4,000 feet, as fractured conditions at the planned depth would not provide a competent anchor point for the 9-5/8 inch casing.

Installation of the 9-5/8 inch casing was delayed until after the barefoot 7-7/8 inch bottom segment of the hole was drilled to postpone the anticipated cementing problems caused by the heavy formation water flows between 1,800 and 3,800 feet. This decision was possible because the formation was competent and free from sloughing, such that setting the 9-5/8 inch casing could be deferred until after it could be determined from the 7-7/8 inch bore hole results whether it would be of value to case the hole. Costs of the cementing job were considered unpredictable and potentially excessive, and might well have depleted the budgeted funds before reaching total depth, had not the above drilling plan been adopted.

The hole was bottomed at 6,790 feet after penetrating a severely fractured zone at 6723 feet. Final drilling conditions indicated heavy flow of water down the hole and into the fracture zone at the bottom. When the 9-5/8 inch pipe was finally set at 4,256 feet, after the hole was logged, the cementing did, indeed, prove difficult. It was only anchored by a cement plug at the bottom to stop water flow. The formation water prevented getting the desired good bond; however, the bond obtained proved adequate to seal off the water flow in the hole.

Core cutting with diamond bits in the Empire stock proved more difficult and costly than anticipated. As a result the amount of core taken was only 82.4 feet instead of the planned 300 feet.

The original proposal budget dated February 2, 1973, set out a cost estimate for the Rogers Engineering CY 1974 project activities of $1,009,200. The program contemplated drilling the deep well to 6,000 feet. The summary of actual costs (Figure B.1) shows that the activities as carried out cost $1,304,188. However, the deep well was drilled to 6,790 feet instead of 6,000.

The increase which was authorized by NSF, reflects the general inflation of drilling costs that has occurred since February, 1973, as well as higher than anticipated costs of the core drilling and well logging. Unit drilling costs are discussed in the Cost Analysis section.

PLANNING AND CONTRACT DEVELOPMENT

Planning, General

During January, February and March of CY 1974, Rogers Engineering completed the planning for the site preparations and drilling operations which was begun in August 1973 with site selection and survey. Input was furnished to Battelle Northwest Laboratories as required for the environmental analysis and for permit applications to the various governmental agencies. The U.S. Bureau of Land Management was consulted on a continuing basis as the site layout was developed, and that agency's requirements were incorporated into the site preparation and drill site construction plans and specifications.

Planning, Site Preparation

Plans and specifications for construction of the drill site were publicly advertised and filed with the Montana Contractor's Association, and bids were publicly opened on 17 April in Helena. Of the three qualified bids received, William G. Miller Construction Company, of Missoula, Montana, was the low and successful bidder, for a lump sum bid of $38,047. Lindsay Drilling of Clancy, Montana was the low and selected bidder for the water well drilling.

Planning, Drilling

As the planning for drilling the deep well evolved, three fundamental controlling factors became clear:

(1) The national and worldwide energy crisis was creating a rampant inflation of costs in the drilling industry, and the probability of drilling this wild-cat research well within the authorized budget using the normally accepted conventional techniques was diminishing rapidly from month to month. It was this realization that caused Rogers Engineering to investigate the possibility of using the latest improved drilling techniques (untried in geothermal drilling) that held promise of increasing drilling rates and reducing rig time on the project. This study led to the decision to use air drilling or an air-water-foam hybrid system, since penetration rates by this method had been known to exceed conventional mud drilling by factors of from 2 to 5.

(2) The demand for drilling rigs was rapidly escalating and doubt was developing if this project, far removed from active drilling areas, would attract the kind of experienced drilling contractor desired, and remain within the budget constraints that applied.

(3) Given the expectation of ultra-high temperature bore-hole conditions, extremely hard drilling in igneous rock, plus the need

to use advanced techniques to stay within budget, it became clear that the required expertise to direct the operation would not be found embodied in any one individual, or in any one drilling contractor organization. Rogers Engineering concluded that it would be necessary to orchestrate the most advanced, specialized expertise of all segments of the drilling and drilling service industries in order to accomplish the objectives.

Inputs on the unique problems of the project were received from the leading companies in drilling mud service, cementing service, air drilling service, diamond core drilling, mud logging, and drill bits and tools. The information obtained was used by the Rogers Engineering staff drilling consultants in preparation of the drilling plans, drill rig specifications, and the specifications for auxiliary drilling services and equipment.

For the drilling contract a list of qualified bidders was compiled which included those with geothermal well drilling experience, as well as the leading responsible oil and gas well drilling contractors in the Rocky Mountain region. Eleven contractors from this list requested plans and specifications and the opportunity to bid. Bid opening was set for 29 April 1974, at which time only three bids were received. The bids were as follows:

(1) Molen Drilling Co., Inc., Billings, Montana:

Day Rate:	$150 per hour
Mobilization in and out:	$ 35,000

(2) Geo-Drilling, Inc., Phoenix, Arizona:

Day Rate:	$200 per hour
Mobilization in and out:	Cost plus nominal fee: $100,000 estimated

(3) Big Chief Drilling Co., Oklahoma City, Oklahoma

Day Rate:	$180 per hour
Mobilization in and out:	$230,680

The bidding confirmed the virtual explosion of drilling costs to a new level much higher than existed when the project budget was proposed. The Molen bid was substantially less than the other two, but even so was in excess of the budget, assuming the use of conventional mud drilling and that the full estimate of 90 days would be required. The Molen day rate, for instance, was $150 per

hour, while the budgeted figure used was only $110 per hour, predicated on the day rates quoted at the time the original estimate was made.

The aforementioned study of advanced drilling techniques had shown that conditions in this hole would probably be favorable for use of an air drilling system. Accordingly it was recognized that the increased penetration rates to be expected from such a system could reduce the rig time on the well sufficiently to compensate for the higher level of unit costs revealed by the bidding, and offer some expectancy that the drilling program might be accomplished within the budget. J. T. Kuwada communicated the bid data and the above analysis thereof to Battelle Northwest and National Science Foundation, and the decision was returned, through channels, to proceed. It was understood that Rogers Engineering would utilize the drilling techniques most likely to accomplish the work within budget and exert maximum effort toward that objective; however it was also understood that if unexpected problems developed (as is always possible in such a wildcat well) the budget could be increased by a reasonable amount if required.

From the standpoint of experience in drilling large bore geothermal wells, Big Chief Drilling Co. was the preferred contractor. However, their bid of $230,680 for mobilization and demobilization of their rig (from Stockton, California to Marysville, Montana and return) was considered too great a premium to pay for this benefit.

The Molen and Geo-Drilling rigs were inspected and an in-depth comparison was made between the two bids. Geo-Drilling's advantage of crew experience on large bore geothermal wells was persuasive, but was not sufficient to overcome the large excess of their bid over Molen's. The contract was awarded to Molen Drilling Co., Inc. on the basis of their low bid; however, it was recognized that certain "trade-offs" had to be acknowledged. Molen's crew was not experienced in drilling large bore geothermal wells, so it was estimated that this could be translated into four days additional rig time over the length of the project. After allowing for this, there still remained a large cost advantage in accepting Molen's low bid; and only by using Molen was there a chance of doing the project within the budget.

In Molen's favor were: (1) a good record of employee loyalty, demonstrated by a low turnover rate of their rig crew personnel; (2) a good reputation within the drilling industry of the region as a responsible and capable drilling contractor, and (3) the fact that Molen was a Montana firm and this was a Federally funded program.

SITE PREPARATION

General Summary

Mountain construction work above 5,000 feet in western Montana generally doesn't start before June 15th, so starting the site preparation work on May 3rd was crowding the season somewhat. However, the weather smiled on the Miller Construction Co. for the first 16 days and 80 percent of the work was completed on May 19 when a 12-inch snowfall caused a one week delay. The Contractor William G. (Bill) Miller, deserves much credit for the extra effort and dedication with which he overcame this set-back and completed the work in time for the drilling rig to start moving in on June 4, 1974.

Some adjustments to the drill site layout were required after the drilling contract was let, in order to accommodate the equipment of the rig that was selected. However, this possibility had been anticipated in the site work contract and the extra work was accomplished at contract unit prices. The total cost of site preparation was within the budgeted amount.

Protection of Empire Creek

The location of the deep well in the narrow Empire Creek valley required extreme precautions to prevent drilling fluids and petroleum products from contaminating the creek water. All pits were lined with plastic. The site was laid out without changing the course of the creek, and the edges of the creek were faced with native rock riprap to protect against erosion and siltation.

Water Supply

The State of Montana Water Resources Department required that the project get its potable water and water for the drilling operations from wells, rather than from Empire Creek, if possible. Accordingly bids were invited and Lindsay Drilling (low bidder) was awarded the job of drilling a well adjacent to the drill site. It was hoped that one well, or at most two wells, would produce the minimum requirement of 30 gallons per minute at a reasonably shallow depth.

However, the first well revealed no significant aquifer, only meager amounts of water production from intermittent thin fractured lenses. At 150 feet production was only 12 gpm. The well was carried to 305 feet and developed a maximum flow of 26 to 28 gpm. The cost was over $6,000, compared to the authorized budget of $4,000.

In view of the high cost of this small quantity of ground water, the Montana Water Resources Department issued a temporary

permit for the use of creek water for peak demand. It was decided to provide the balance of the minimum estimated requirement by building a pond on Empire Creek immediately upstream from the office area on the site. The cost of the pond was less than the cost of a second well. A pipe large enough to carry the full flow of the creek was placed at the bottom of the dam in the creek bed, with a sluice gate to control the pond level and the creek flow. With this arrangement, the creek flow was maintained at normal level throughout the drilling operations and an adequate reserve of water was assured for the drilling operation.

The water well supplied most of the requirements throughout the project. Water was pumped from the pond only during the high demand of cementing operations and during several electric service interruptions, and this was done without jeopardizing normal stream flow in Empire Creek.

DRILLING

First Phase - Set 20-inch Conductor Casing

The first phase of the drilling operation was to drill a 26-inch diameter bore hole to 250 feet for the 20-inch conductor casing. This interval was first drilled 12-1/4 inches in diameter, then opened to 17-1/2 inches and finally to 26 inches in two stages. The Empire shale formation proved much harder to drill than anticipated, starting immediately under the shallow layer of overburden, so with the approval of the U.S. Geological Survey it was decided to run the 20-inch casing at 115 feet instead of the programmed 250 feet. This decision was based on the fact that the presence of the hard rock down to that depth provided a competent formation for cementing the conductor pipe.

Due to the hardness of the formation, the recommended mill tooth bit for medium hard formation had to be replaced after only 29 feet with a carbide insert bit made for hard formations. The initial drilling of the 12-1/4 inch pilot hole was done with foam drilling fluid instead of the air as planned, due to a cracked head on the large air compressor. Penetration was slow, around 1 to 2 feet per hour, down to 150 feet. At that point, on June 11, 1974, heavy drill collars arrived and bit weight was increased. Penetration improved to 10 to 12 feet per hour. The slope of the time-depth history of the well (Figure B.2) indicates the average drilling or penetration rate for the well.

Mud was used to open the hole to 17-1/2 inches and 26 inches because the air rotating head furnished by Air Drilling Services was not operating satisfactorily. Opening the hole to 26 inches progressed easily for 75 feet but slowed drastically and wore out the first cutters by 90 feet. The second set of cutters were worn out by 115 feet. The next 26 inch hole opener, with carbide insert cutters, made only six inches in six hours. The high drilling torque used made exceedingly rough drilling and made drill collar break-out difficult; therefore the 26 inch hole was bottomed at 115 feet.

Second Phase - Set 13-3/8 inch Surface Casing

The plan for the next phase was to drill a 17-1/2 inch hole to 2500 feet and set 13-3/8 casing to that depth. However, the reduction of the 20-inch conductor pipe to only 115 feet dictated a corresponding reduction of the water string to a maximum depth of 1,500 feet. The 12-1/4 inch pilot hole was drilled to 1,526 feet, after which an array of Schlumberger geophysical logs were run under the direction of Battelle Northwest Labora-

tories. Schlumberger's temperature logging tool failed to perform at this stage, so Dr. Dave Blackwell and his associates from Southern Methodist University used their thermistor equipment to acquire the temperature data.

The pilot hole was then reamed to 17-1/2 inches diameter down to 1,326 feet, and the 13-3/8 inch casing was cemented from there back to the surface.

Drilling mud was used as the fluid in this interval, because of some indication of sloughing gravel when the pilot hole was washed out below the shoe of the 20-inch casing with the foam system.

The drilling rate was less than acceptable so higher bit weights and rotation speeds were used to increase penetration rates. This was a calculated trade-off against reduced bit life. The formation below 1,000 feet was a very hard competent quartz prophyry, and therefore the surface casing string was set at 1,326 feet instead of 1,500 to save drilling time and costs. Hole deviation built up to 5-3/4 degrees during this interval, but was successfully reduced to desired limits by using the pendulum effect with reduced bit weight, followed by a return to normal bit weight with increased stabilization.

The Molen crew's lack of experience in handling large pipe had been apparent in running the 20 inch casing, so for running the 13-3/8 inch pipe a special casing setting crew was brought in (WISCO, of Williston, S. Dakota).

Third Phase - Set Intermediate Casing

It had been planned to use straight air drilling below the surface string, but due to difficulties experienced in drying the hole, a mist drilling fluid was used in drilling out from the 13-3/8 inch casing. The combination of the mist and the air hammer drill produced penetration rates as high as 28 feet per hour with the 12-3/4 inch bit. At about 1,800 feet, water started entering the hole at about 100 gpm and increased to about 1,000 gpm at 1,932 feet. This influx of water filled the reserve pit and operations had to be shut down to pump out the reserve pit. This excess fluid had to be trucked several miles to a specially designated dumping area.

It became clear quickly that the cost of hauling away this unexpected volume of water would be unacceptable. Since the static level of the water was several hundred feet down the hole, a test was run to see if the excess water would return to the formation when pumped back into the well bore. The test was suc-

cessful, so while it was desirable for well logging and geophysical determinations to minimize disturbances, the excess water was pumped back down to the producing zones, and the excess water hauling operation was terminated.

Drilling was resumed and after a period of experimentation a successful aerated water system was devised. With air and foam chemicals the amount of aeration of the fluid column was varied to achieve a balance between the hydrostatic head in the well and the formation water pressure. With this balance the formation water was held back while the circulating system in the well bore operated in normal fashion providing a good return of cuttings.

As drilling proceeded the bit penetrated numerous heavily fractured zones which would either produce large volumes of water, or would accept fluids, depending on the hydrostatic head of the column in the bore hole. The principal fracture zones are shown in Figure B.4. At times it was advantageous to increase aeration and produce water, filling up the reserve pit, and at other times it was advantageous to reduce or eliminate aeration, thus drilling with straight water from the reserve pit. The latter method was used principally to dispose of excess water, and during coring operations.

While drilling with straight water (no aeration) return flows did not reach the surface; in other words, the lost circulation zones or fractures accepted the drilling fluids and the cuttings from the bit. This variable system was used all the way to total depth (6,790 feet). After hole depth reached 3,500 feet a jet air sub was installed at 1,300 feet to assist in lifting the fluids from the hole.

The hole size was reduced to 7-7/8 inches at 4,256 feet, although the original plan was to reduce at 4,000 feet. This change was made because of the indication of fractures from 4,000 to 4,200 feet, and a more competent zone was sought in which to bottom the 9-5/8 inch casing.

The aerated water drilling regime proved most advantageous in this lower portion of the hole with penetration rates up to 28 feet per hour. Gross footage per day of over 400 feet was achieved. Total depth was declared at 6,790 feet after penetration into a heavily fragmented zone threatened to stick and trap the drill string.

A series of Schlumberger geophysical logs were run before setting the intermediate 9-5/8 inch casing. Turbine flow meter tests showed substantial water flows from upper zones to the bottom of the hole. The 9-5/8 inch casing was set on the shoulder

at 4,256 feet, but it was cemented at the bottom only, to permit maximum salvage later if it is not needed. The WISCO casing crew was called again to run the 9-5/8 inch casing.

A cement bond log was run after the first attempt to cement the bottom 700 feet of pipe, but it showed a maximum of only 10 feet of good bond, at 4,190 to 4,200 feet. A squeeze job was attempted with perforations at 4,130 feet. Another bond log was run and showed no change in the amount of bond as a result of the additional cement. Budget limitations precluded further effort to improve the cement bond, so it was decided to drill out the shoe of the 9-5/8 inch casing and check for bond right at the bottom. The final bond log showed at least 3 feet of good bond at the shoe, and a flow meter check indicated that the casing as cemented had virtually stopped the flow of water in the hole immediately below the casing.

A cement plug was then spotted near the bottom of the hole over an open-hole packer, and final temperature and water flow tests were run. These tests indicated substantial success in eliminating down-hole water flows.

The Schlumberger crew finished the logging on September 10, 1974. After the rig crew installed the Christmas tree, the drill rig was released at 8:00 p.m. on that same date.

CORING OPERATIONS

Coring, General

Cores were cut with diamond core bits, using unaerated water for the drilling fluid. The greater hydrostatic head of this denser drilling fluid caused lost circulation, which resulted in no drilling returns. Each core drilling sequence was thus limited by the amount of water in the reserve pit. The aeration in the drilling column was increased for a time before each core was to be taken, to allow the well to produce sufficient water to fill the reserve pit. This fluid was then used, with no returns, during the coring operation. Straight water was used for core cutting for maximum cooling of the diamond bit while penetrating the highly abrasive granite formations.

Christensen diamond core bits were used throughout the coring program. A total of 114.5 feet of formation was core drilled and a total of 82.5 feet of core was recovered, a recovery rate of 72%. Coring in the Empire metamorphosed shale down to 975 feet was quite difficult, but yielded generally good results. Below 975 feet, however, the quartz feldspar porphyry (granite) was extremely difficult to core with diamond bits and presented a severe challenge to core drilling experts. Very little to no recovery was obtained on four core intervals. Inadequate stabilization of the 7-7/8 inch core bit in the 12-1/4 inch hole allowed the bit to walk around the bottom face of the hole and damaged the core head. Only 7 inches of the 5 foot interval cored was recovered on one core interval, and no recovery was obtained in the subsequent two core intervals.

At this point Rogers Engineering requested a conference with Christensen Diamond Products management to resolve the problems. As a result of the meeting, pinned stabilizers were utilized to prevent lateral bit travel at the start of a core and allow the stabilizers to slide up the outer core barrel tube as coring progressed. This, together with a change of core engineer personnel, produced better results thereafter.

Coring Rates and Costs

Coring Summary (Figure B.5) presents the coring results. The core penetration rate varied from 0.5 to 4.0 feet per hour. The coring operation occupied 99 hours of rig time in coring and 114 hours of roundtrip time. The average penetration rate was 0.83 feet per hour and the average cost of the cores was $1,177 per foot cored, or $1,636 per foot recovered. (These cost figures for coring include rig time and hourly pro-rata share of all accessory costs).

COST ANALYSIS

General Costs

The gross amount expended on the Marysville Goethermal Well No. 1 project during CY 1974 and 1975 by Rogers Engineering Co., Inc. was $1,363,702. This figure includes certain expenditures not directly chargeable to the drilling and related operations, as follows:

(1)	Cost of arbitration of contractor's claims	$ 33,648
(2)	Estimated re-sale value of wellhead and casing hardware purchased but not used due to unexpected results of the drilling	20,650
(3)	Cost of study for plugging and abandonment of the deep well	5,216
	Total Non-Drilling Expenditures	$ 59,514

Deduction of the non-drilling expenditures from the gross expenditure yields a total of drilling and related costs of $1,304,188. A detailed summary of the costs included in this total is shown in Figure B.1.

The major categories of costs, expressed as a percentage of the total, were as follows:

	Cost	Percentage of Total Cost
Site preparation and Field Office Operation	$ 107,751	8.2%
Direct Drilling Costs, including Coring	768,963	59.0%
Casing, Cement, Wellhead Equipment	196,759	15.1%
Well Logging and Testing (Direct Cost, not including Rig Time	52,664	4.0%
Engineering, Drilling Supervision, Procurement, Expediting & Misc.	178,051	13.7%
	$1,304,188	100 %

Comparative Costs

To get a realistic comparison with commercial drilling costs in the industry, it is necessary to deduct the portion of the

total cost that was chargeable to strictly research objectives: principally the costs of the extensive coring program and the logging and testing activities.

An additional adjustment of comparative per foot drilling cost should be made due to the drilling sequence dictated by the geophysical logging program. In order to log the hole, it was necessary to drill the upper 17-1/2 inch and 26 inch hole in multiple runs because the logging tools were limited to a 12-1/2 inch maximum hole size.

Allowing a conservative saving of four days for eliminating one drilling pass in the upper 1,326 feet, and deducting the direct costs and the rig time and associated extra costs of the coring, logging, and testing programs, leaves a direct drilling cost of $522,830, or $77 per foot. (Casing, well head and cement not included).

DISCUSSION OF RESULTS

Drilling Procedures

The pre-spud decision to provide air drilling service as a supplement to conventional mud drilling equipment proved a fortuitous one, although the advantages of the air system were not fully realized in the large bore upper segments of the hole.

Where mud was used (in reaming the 17-1/2 inch and 26 inch holes, and in drilling the 12-1/4 inch pilot hole from 290 feet to 1,524 feet) penetration rates varied from two to ten feet per hour. Below 1,524 feet, while drilling with air mist and a percussion hammer drill, penetration ranged consistently from 12 to 28 feet per hour. After water influx damped out the effectiveness of the hammer drill below 1,912 feet, drilling with an aerated water system achieved consistent penetration rates of from five to 24 feet per hour.

An added advantage of the air drilling experienced was increased drill bit life, as shown in Figure B.6.

Hole Deviation

Control of drift was more difficult in the Empire shale, from 300 feet down to 975 feet, than in the quartz porphyry below. After drift built up to over 5 degrees in the shale, drilling had to slowed to bring it under control. A "full hole" stabilizer arrangement was then used to maintain control.

Tendency to drift was slight to moderate while drilling with 12-1/4 inch bit in the Empire stock. When bit size was reduced to 7-7/8 inches, hole deviation increased markedly. The decision was made and approved to accept up to 15 degrees deviation so that maximum drilling rpm and weight-on-bit could be utilized to maximize penetration for the final run to bottom. The final deviation survey showed a drift of slightly over 12 degrees at bottom.

Drill Bits

The metamorphosed shale and quartzite of the Empire Shale, and the quartz feldspar porphyry of the Empire Stock both proved to require bits for harder formation than drill bit vendor engineers had anticipated. The cutting structure of the Security-Dresser H-100 bits, for extra hard formations, held up better than other cutters. However, the best bearing performance was by the Hughes journal bearing bit (only one available to the project due to limited supply).

The short bit life of the large hole openers as shown in Figure B.6, resulted from a deliberate trade-off in which higher

than normal drilling rpm and bit weight were used to achieve more rapid penetration and consequently less rig time. The higher rpm actually resulted in less shock of the drill rig and tools, because the fractures of the formation caused greater "torquing" at slow to moderate rpm than at the higher rate.

Coring Bit Problems

As noted in the coring section, the diamond core bits performed satisfactorily in the metamorphosed shale, even though the formations were heavily fractured. In the quartz porphyry however, the more abrasive nature of the formations consumed the diamonds of the cutting structure at a rapid rate, resulting in unacceptably high bit cost and slow penetration. This is in contrast to the carbide insert tricone drill bits, which performed better making hole in the quartzite than in the Empire shale.

The superior performance of button bits versus diamond bits in granitic rocks should add further impetus to the drilling bit industry's efforts to develop button-type core bits in anticipation of greater use in such formations in the future search for geothermal resources.

Analysis of Rig Time

Figure B.3 displays a distribution of rig time on location according to the major operations. Of significance is the fact that basic new-hole drilling used only 42.08 percent of rig time. Reaming with hole-openers to larger hole size used an additional 8.65 percent. The scientific information gathering operations (coring and bore hole logging) used a total of 24.23 percent of rig time. Equipment repairs required 13.07 percent of rig time of which 79 percent were paid for by the drilling contractor.

Drilling Contract Administration Problems

In awarding the contract to the low bidder, some trade-offs, such as possible lower efficiency and performance by the Contractor's personnel, were recognized in electing to use a small local contractor organization.

Such a trade-off proved to be a reality in the area of contract administration. The Contractor was delinquent in submitting cost data, billing and documentation for reimbursable third-party and freight charges. Also, when such bills were finally received they contained charges for basic rig equipment that were not reimbursable under the Contract, and for rig repairs that were not reimbursable. These deficiences resulted in the disallowance by the Engineer of approximately $167,000 of Contractor claims.

The Contractor then demanded arbitration of his rejected claims. Accordingly a three-man arbitration panel of the American Arbitration Association was convened in Billings, Montana, for a total of seven days beginning June 9, 1975. The results of the arbitration proceeding are as follows:

Total Contractor Claims Disallowed by Engineer	$167,000
Less Claims Approved by Engineer after Proper Documentation	(23,138)
Less Claims Awarded by Arbitration Panel	(25,234)
Total Claims Denied by Arbitration Panel	$118,628

Although the Contractor was not successful in collecting on the majority of what Rogers considered unsupportable claims, the costs of defending the claims in the arbitration proceedings became an added cost factor to the project. These costs included the services of Roger's project management personnel, legal counsel, expert witnesses, plus their travel and per diem expenses, and American Arbitration Association's administrative fees and expenses, for a total of $33,648. The conclusions of the arbitration panel fully supported and justified this effort and expense by Rogers Engineering to reject ungrounded claims by the drilling contractor.

Item	Budget Totals	
Site Preparation & Equipment		
Site Preparation, including Telephone and Electric Power Construction	$ 81,714	
Trailer, Truck & Office Equipment	5,687	
Field Office Operations & Maintenance	14,470	
*Potable Well Drilling & Pump	5,880	$ 107,751
Drilling Costs		
Well Drilling	509,226	
Drilling Bits	77,045	
Coring Tools, Bits & Services	66,424	
Air Drilling Services and Equipment	76,178	
Drilling Mud and Service	19,547	
Mud Logging	20,543	$ 768,963
**Well Casing	134,287	
*Well Head Equipment	13,647	
Cementing	48,825	$ 196,759
***Bore Hole Logging	42,689	
Drill Stem Testing	9,975	$ 52,664
Consulting Engineering, Procurement, Expediting, Drilling Supervision	166,194	
Travel & Per Diem	11,716	
Report Reproduction	141	$ 178,051
Total		$1,304,188

*Net cost after estimated resale credit.

**Net cost after estimated resale credit of unused casing hanger. Does not reflect credit for resale of 9-5/8 inch casing if recovered in future. That credit is reflected only in the separate study of Plugging and Abandonment by Rogers Engineering Co., Inc.

***Transferred to Rogers Engineering Co., Inc. budget from BNW in original proposal.

FIGURE B.1. Summary of Drilling Costs
Marysville Geothermal Project

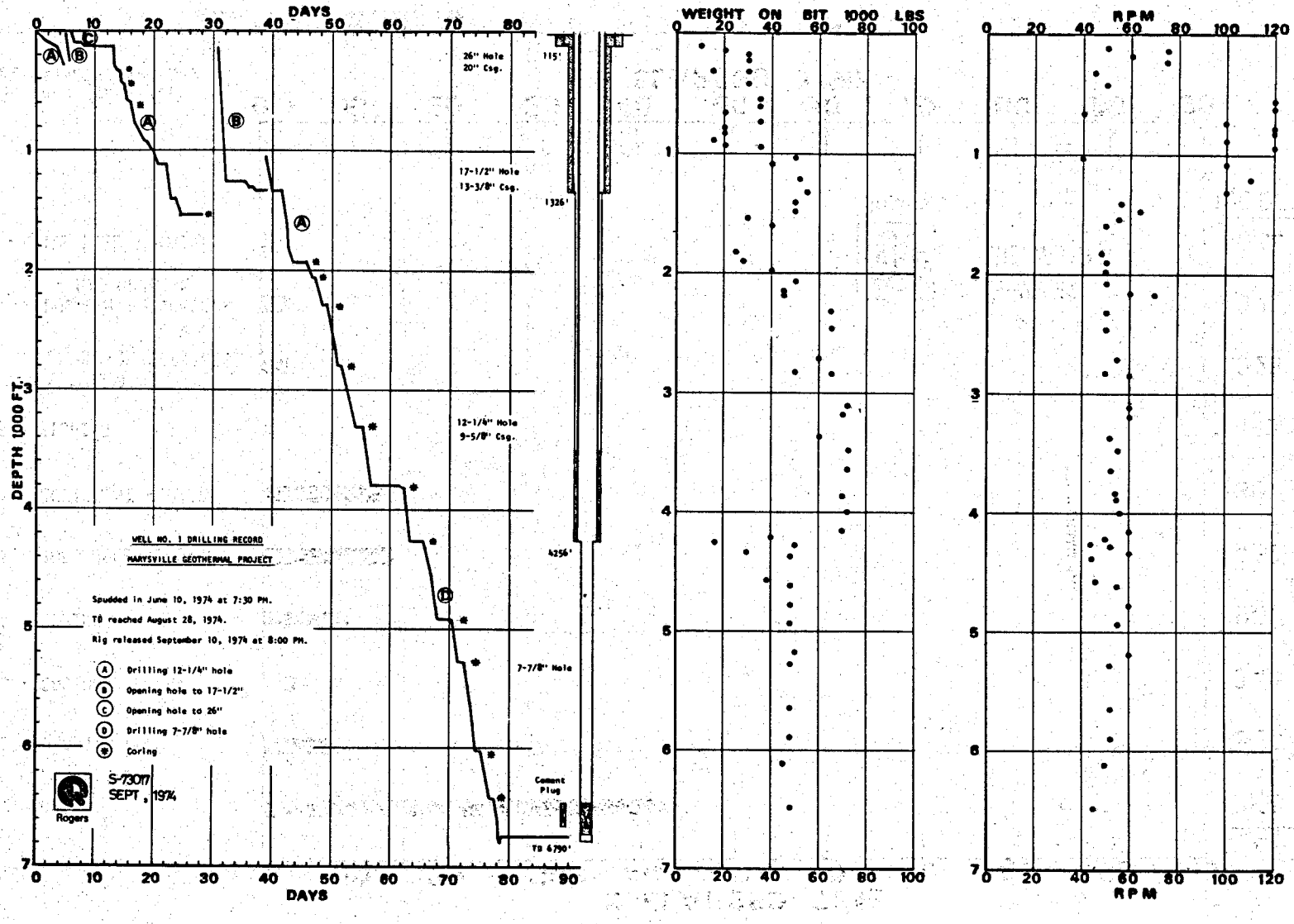

FIGURE B.2. Well No. 1 Drilling Record
Marysville Geothermal Project

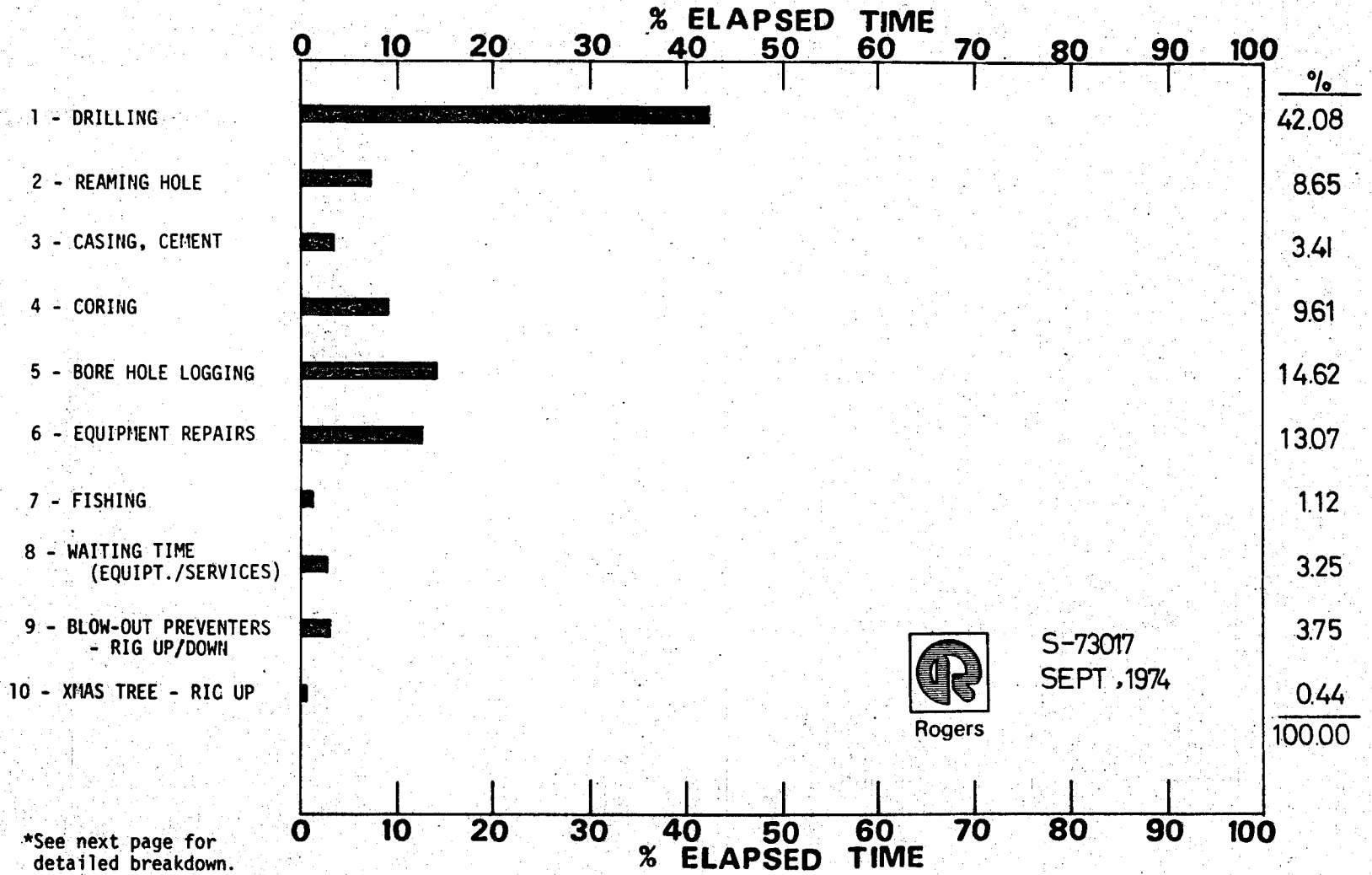

FIGURE B.3. Marysville Well No. 1 Rig Time Distribution

	ACTIVITY		PERCENT OF TOTAL RIG TIME
1.	Drilling		42.08
	a. Drilling Hole	25.17	
	b. Round Tripping - Drilling	12.05	
	c. Conditioning Hole, Mixing Mud	3.60	
	d. Magnaflux Drill Collars	1.26	
2.	Reaming Hole		8.65
	a. Reaming and Opening Hole	6.67	
	b. Cleaning Out Pilot Hole	1.98	
3.	Casing, Cement		3.41
	a. Running Casing	0.94	
	b. Cementing Casing	1.05	
	c. Waiting on Cement	0.74	
	d. Cement Plugs	0.16	
	e. Drilling Cement Out of Casing	0.52	
4.	Coring		9.61
	a. Cutting Core	4.42	
	b. Round Trip-Coring	5.19	
5.	Bore Hole Logging		14.62
	a. Geophysical Surveys	1.30	
	b. Temperature Surveys, SMU	4.82	
	c. Temperature Surveys, Schlumberger	3.86	
	d. Drill Stem Testing	0.67	
	e. Round Tripping, Drill Stem Tests	2.05	
	f. Fluid Flow Surveys	0.76	
	g. Cement Bond Surveys	0.41	
	h. Water Sampling	0.19	
6.	Equipment Repairs		13.07
	a. Equipment Repairs, Rig	10.32	
	b. Equipment Repair, Operator Charge	2.75	
7.	Fishing		1.12
8.	Waiting Time (Equipment/Services)		3.25
9.	Blow-out Preventers - Rig Up/Down		3.75
10.	Xmas Tree - Rig Up		0.44
			100%

FIGURE B.3-A. Marysville Geothermal Well No. 1
Breakdown of Drilling Rig Time

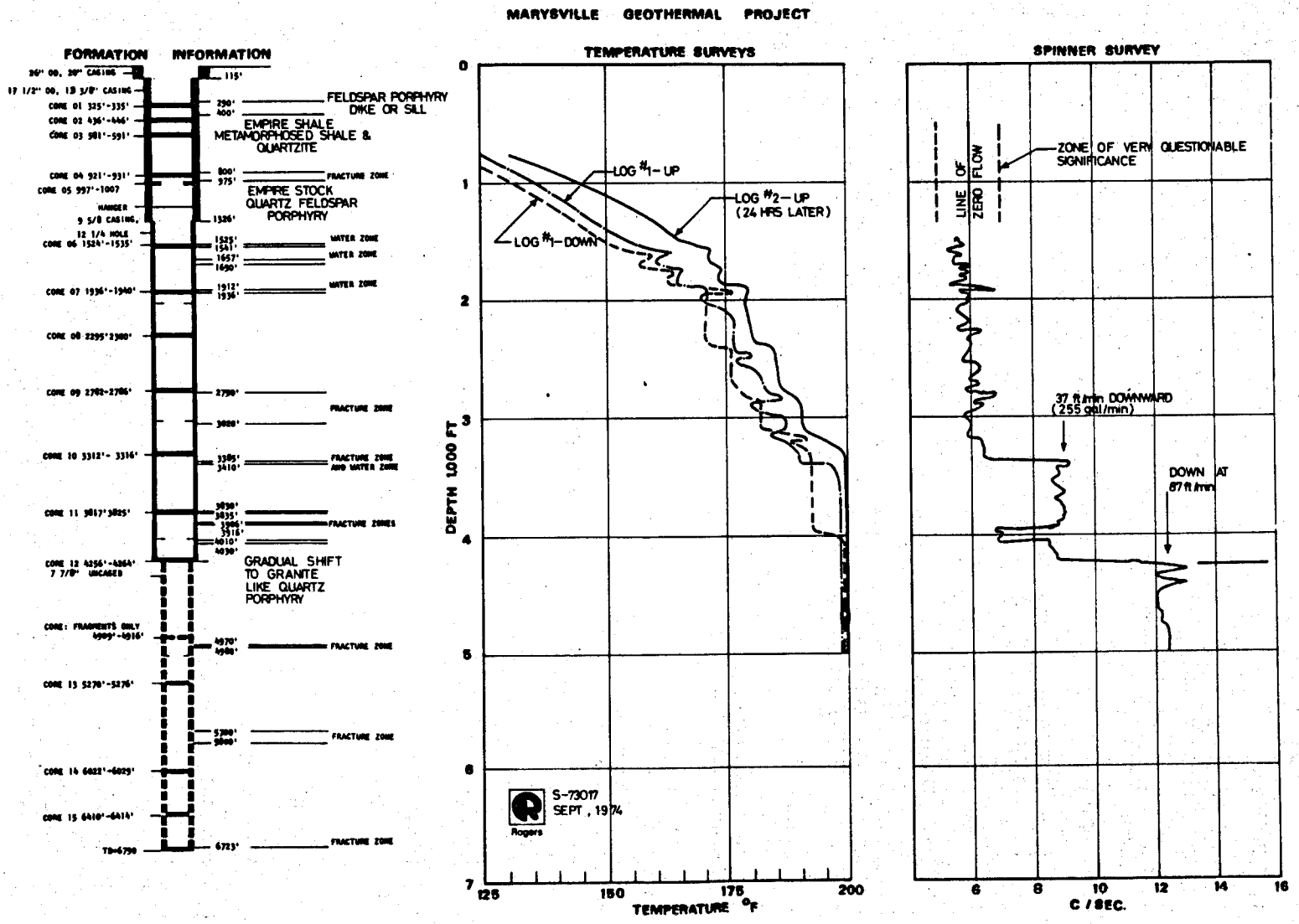

FIGURE B.4. Fracture Zones, Temperature Surveys and Spinner Surveys

Coring Interval No.	Depths	Cored	Coring Rate Ft/Hr	Core Recovered	Core Diameter	Remarks
1	325 - 335	10'	2.1	10'	4"	
2	436 - 446	10'	5.0	6'-10"	4"	
3	581 - 591	10'	2.2	9'-8"	4"	
4	921 - 931	10'	3.3	10'	4"	
5	997 - 1007	10'	1.7	10'	4"	
6	1524 - 1530	6'	0.9	5'-10"	4"	
7	1936 - 1940	4'	1.4	7"	4"	Core head broke.
8	1942 - 1943	1'	0.3	0	4"	Metal in hole.
9	2042 - 2042.5	0.5'	0.3	0	4"	Damaged core head.
10	2295 - 2300	5'	0.7	4'-7"	4"	
11	2782 - 2786	4'	0.5	2'-8"	5-1/4"	
12	3312 - 3316	4'	0.7	3'	5-1/4"	
13	3817 - 3825	8'	0.8	5'-2"	4"	Undersized core.
14	4256 - 4264	8'	1.5	5'	5-1/4"	
15	4909 - 4916	7'	1.0	0	4"	Fragments recovered in junk snatcher.
16	5270 - 5276	6'	1.0	3'	4"	
17	6022 - 6029	7'	1.3	4'-1"	4"	
18	6410 - 6414	4'	1.1	2'	4"	
		114.5'	1.2 Avg	82'-5"		

Total Rig Time Spent on Coring: 99 Hours

Total Rig Time Spent on Core Round Tripping: 114 Hours

Cost of Rig Time for Cores Recovered: $ 71,781

Cost of Coring Tools, Bits & Services: $ 64,219

Average Cost of Cores Per Foot Recovered:

$1.636

Rogers

S-73017
SEPT., 1974

FIGURE B.5. Coring Summary
Marysville Geothermal Project

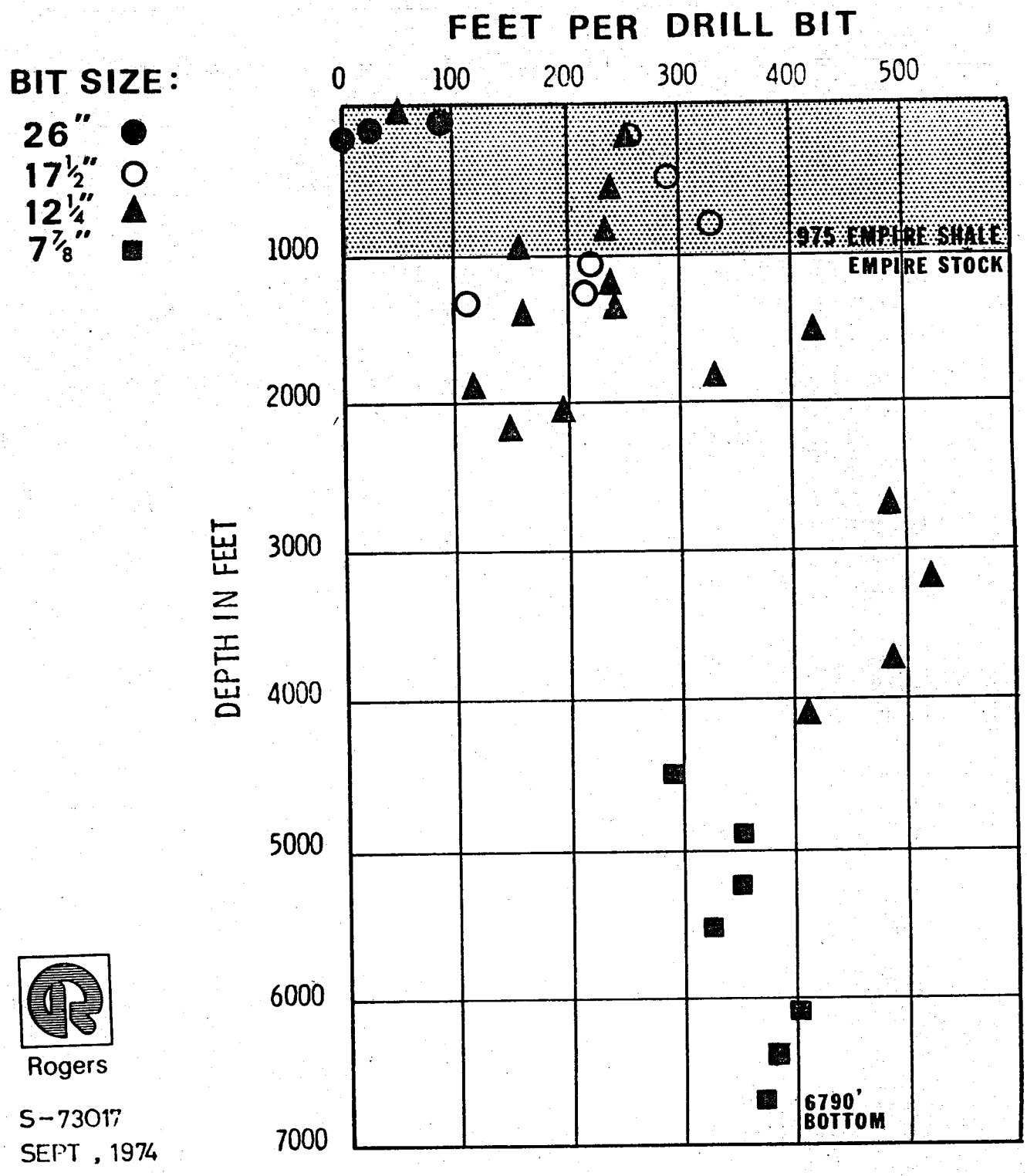

FIGURE B.6. Drill Bit Life for Marysville Geothermal Project

APPENDIX B.1

LIST OF SUBCONTRACTORS - MARYSVILLE PROJECT

SITE WORK SUBCONTRACTORS

	Subcontractor	Type of Work	Amount of Contract
(1)	Foundation and Materials Consultants, Inc. Attn: Robert L. Holm 839 Front Street Helena, Montana 59601	Soil Tests and Analysis	$ 335
(2)	V. T. N., Inc. (Helena) Attn: Dave Twiddy Helena, Montana 59601	Site Survey	1,686
(3)	Lindsay Well Drilling Attn: Wesley Lindsay Clancy, Montana 59634	Potable Water Well	6,200
(4)	William G. Miller Construction Co. Attn: William G. Miller P. O. Box 1033 Missoula, Montana 59801	Site Grading and Construction	50,994

DRILLING SUBCONTRACTORS

(1)	Molen Drilling Co., Inc. Attn: Vern Molen, Pres. Billings, Montana 59103	Drill the Deep Well	487,165
(2)	Air Drilling Services, Inc. Attn: J. Brodie Pugh 4 Sedgewick Drive Englewood, Colorado 80110	Air Drilling Service	73,631
(3)	Baroid Division of NL Industries, Inc. Attn: Leroy D. Greener Roundup, Montana 59072	Drilling Mud Service	19,547
(4)	Dowell Division of Dow Chemical Co. Attn: G. J. "Bud" Durborow 216 Security Life Building Denver, Colorado 80202	Well Cementing Service	48,611

LIST OF SUBCONTRACTORS - MARYSVILLE PROJECT

	Subcontractor	Type of Work	Amount of Contract
(5)	Continental Laboratories, Inc. Attn: Billy R. Roush, V. P. 1744 Mullowney Lane Billings, Montana 59102	Mud Logging Service	20,543
(6)	Schlumberger Well Services Attn: Harold Darling Havre, Montana 59501	Well Logging (Geophysical)	40,157

APPENDIX B.2

LIST OF SUPPLIERS OF DRILLING EQUIPMENT AND SERVICES

MARYSVILLE PROJECT

	Name of Supplier	Equipment/Service Supplied	Amount
(1)	The Bovaird Supply Co. P. O. Box 2590 Tulsa, Oklahoma 74102	20" Casing	$ 5,845
(2)	Republic Supply P. O. Box 1995 Oklahoma City, Oklahome 73101	9-5/8" Casing	73,584
(3)	Vinson Supply Co. P. O. Box 1860 Tulsa, Oklahoma 74101	13-3/8" Casing	33,837
(4)	Continental Emsco Co. P. O. Box 22558 Dallas, Texas 75284	Drill Bits: Security - $58,645 Hughes - 10,992 Smith - 6,723	76,360
(5)	Christensen Diamond Products P. O. Box 387 Salt Lake City, Utah 84110	Diamond Core Bits, Tools and Engineering Service	64,219
(6)	Hycalog, Inc. P. O. Box 15372 Houston, Texas 77020	Diamond Core Bit & Tool	1,883
(7)	Core Laboratories, Inc. Box 10185 Dallas, Texas 75207	Core Boxes	302
(8)	Cavins Corp. P. O. Box 8013 Houston, Texas 77004	Junk Snatcher, Rental and Engineering Service	8,543
(9)	Gray Tool Co. P. O. Box 2291 Houston, Texas 77001	Well Head Valves, Casing Hangers	32,806
(10)	Valve Services, Inc. 13060 E. Firestone Blvd. Santa Fe Springs, Ca. 90670	Well Head Valve	4,014

APPENDIX B.2 (Cont'd)

LIST OF SUPPLIERS OF DRILLING EQUIPMENT AND SERVICES

MARYSVILLE PROJECT

	Name of Supplier	Equipment/Service Supplied	Amount
(11)	Williston Industrial Supply Corp. P. O. Box 1323 Williston, N. Dakota 58801	Casing Handling Tools and Crew	3,507
(12)	Casper Machine Shop P. O. Box 2995 Casper, Wyoming 82601	Cut Threads on Casing	$ 13,986
(13)	Colona Division of AMPCO-Pittsburgh P. O. Box 360897 M Pittsburgh, Pennsylvania 15251	Casing Thread Protectors	423
(14)	AMF Tuboscope, Inc. P. O. Box 808 Houston, Texas 77001	Casing and Drill Pipe Inspection	4,661
(15)	Kuster Company P. O. Box 7038 Long Beach, Ca. 90807	Down-hole Temperature Recorders	1,575
(16)	C. A. White P. O. Box 156 Casper, Wyoming 82601	Portable Wire Line	903
(17)	Shafco Industries, Inc. P. O. Box 575 Buena Park, California 90620	Well Head Fittings	713
(18)	Lynes United Service, Inc. 1562 Cleveland Place Denver, Colorado 80202	Drill Stem Testing	2,501
(19)	Johnston-Schlumberger P. O. Box 36369 Houston, Texas 77036	Drill Stem Testing	7,474
(20)	TRW Mission Manufacturing Co. P. O. Box 40402 Houston, Texas 77040	Air Hammerdril Rental	1,035

APPENDIX B.2 (Cont'd)

LIST OF SUPPLIERS OF DRILLING EQUIPMENT AND SERVICES

MARYSVILLE PROJECT

	Name of Supplier	Equipment/Service Supplied	Amount
(21)	Acme Tool Co. Casper, Wyoming 82601	Fishing Tool Rental	$ 6,679
(22)	Drilco, Division of Smith International Casper, Wyomiing 82601	Stabilizers, Reamers, and Subs	$ 43,604

SECTION C

LOGGING AND CORING

Well Logging

P. N. LaMori, Battelle-Northwest

Log Data Evaluation

G. Coates, Schlumberger-Doll

Temperature and Flow Measurements

P. N. LaMori and J. R. Sheff, Battelle-Northwest

Core Documentation, Reconstruction and Photography

P. N. LaMori, Battelle-Northwest

SECTION C LOGGING AND CORING

CONTENTS

LIST OF FIGURES

LIST OF TABLES

WELL LOGGING

by
P. N. LaMori
Battelle-Northwest

September 1975

WELL LOGGING

P. N. LaMori
Battelle-Northwest

Well logs are commonly made both during and after drilling to determine characteristics such as lithology, fracture patterns and physical properties of the drilled formations and to determine certain conditions in the well such as its deviation from the vertical, its mechanical dimensions, and conditions on temperature and water flow. Good well logging requires the use of sophisticated scientific techniques developed over many years of research by the oil industry. Logging services for field operations are available from a number of companies who truck their equipment to your site and perform logging services under contract. For this project an agreement was made with an industry leader, Schlumberger, whereby the logging would be done by the Schlumberger Well Services Corporation for the normal charge rates, and interpretation of the logs would be provided by Schlumberger-Doll Research Laboratories. The project is particularly indebted to Dr. James Moran, Director, Schlumberger-Doll Research Laboratory, for providing the services. In addition to the logging done by Schlumberger, temperature logs and directional surveys were undertaken by project personnel using the instruments and equipment available at the site.

Major loggings were done by Schlumberger on two occasions just prior to the setting of the casing, the first on July 7, 1974 to a depth of 1326 ft, and the second on September 10 to 6790 ft. At these times a complete suite of logs were taken as described below. Minor loggings involving only temperature and flow were undertaken in 1974 on August 29, September 21, October 21, November 16 and in 1975 on April 23. The composite set of both major and minor loggings include:

1. The bore hole caliper log and sonic log with gamma ray (measures hole diameter, acoustic velocity, and natural radioactivity in the rock).

2. The dual induction laterolog (determines the formation resistivity by eddy current induction and flow of a focused direct current).

3. The formation density gamma ray log (determines the formation density, hole diameter, and natural radioactivity).

4. Compensated neutron log (measures the formation porosity and hydrogen concentrations by means of a neutron source).

5. Electrical survey (measures resistivity of the formation).

6. 4-Arm Digital Dipmeter (measures the dip angle and dip direction of fractures and bedding planes by correlating changes of formation electrical resistivity).

7. The directional survey (measures deviation of the hole from the vertical and the compass bearing of the deviation).

8. Temperature logs (measured with platinum resistance thermisters, maximum rating thermometers, and the Kuster time-temperature downhole recorder).

9. The water flow logs (measured with an open hole spinner, the Packer Flowmeter, and with the radioisotope flowmeter).

The results of these loggings are discussed in detail in the following sections, as well as elsewhere in the report.

The directional survey is presented in this section. Figure C.1 shows the directional computations of the hole from the dipmeter results. The hole deviation begins with an easterly drift caused by the bit riding up on the dip of the Empire shale. This direction continues in the Empire quartz porphyry until about 2100 ft where the direction changes abruptly because of attempts to control deviation several times in the next 2500 ft. Below 5000 ft the drift is always to the northwest (at nearly 293°) and at an angle of 10° to 11° from the vertical. The cores from these depths all showed fractures normal to their axis, indicating that these fractures dipped at 10° with 113° bearing. Table C.1 summarizes the directional survey data at 100 ft intervals.

The details of the individual logs are rather voluminous and therefore will not be reproduced in this report. The information is stored at Battelle-Northwest and can be examined on request.

Schlumberger

DIRECTIONAL LOG

COMPUTED

COUNTY LEWIS & CLARK
FIELD or LOCATION WILDCAT
WELL MARYSVILLE GEOTHERMAL NO. 1
COMPANY BATTELLE N.W.

COMPANY BATTELLE NORTHWEST

WELL MARYSVILLE GEOTHERMAL NO. 1

FIELD WILDCAT

COUNTY LEWIS & CLARK STATE MONTANA

LOCATION SW/NE

Sec. 32 Twp. 12N Rge. 6W

Other Services:
LL-7 BHC-GR
FDC-GR TEMP.
CNL-GR

Permanent Datum: GL ; Elev.: 5340
Log Measured From KB , 20 Ft. Above Perm. Datum
Drilling Measured From KB

Elev.: K.B. 5360
D.F. ----
G.L. 5340

Date	8-31-74			
Run No.	TWO			
Depth—Driller	6790			
Depth—Logger	6726			
Btm. Log Interval	6725			
Top Log Interval	1390			
Depth intervals between shots -	100'			
Casing—Driller	13-5/8 @1326	@	@	@
Casing—Logger	1326			
Bit Size	12-1/4, 7-7/8			
Type Fluid in Hole	WATER-FRESH			
Dens. / Visc.	--- --	/	/	/
pH / Fluid Loss	--- -- ml	/ ml	/ ml	/ ml
Source of Sample	PIT			
Rmf @ Meas. Temp.	---- @ -- °F	@ °F	@ °F	@ °F
Rm @ BHT	2.61 @205 °F	@ °F	@ °F	@ °F
Time Since Circ.	34 HRS.			
Max. Rec. Temp.	205 °F	°F	°F	°F
Equip. / Location	5640 / CUB	/	/	/
Recorded By	PODOLL-BRUHN-HURTT			
Witnessed By	LAMORI			

FIGURE C.1 Directional Computations from Dipmeter Results

TABLE C.1. Directional Survey Summary

Depth[a]	Degrees Drift	Azimuth	Feet X Deviation	Feet Y Deviation	Inches Diameter 1-3	Inches Diameter 2-4
116	2.1	43	0.00	0.00		
200	2.1	58	2.27	1.92	18.0	18.0
300	1.5	107	5.04	3.28	13.1	13.0
400	1.6	109	7.74	2.64	13.5	13.2
500	2.5	111	10.94	1.36	14.3	14.3
600	3.3	111	15.71	- 0.39	13.4	13.4
700	3.7	109	21.31	- 2.64	13.3	13.3
800	4.6	92	28.58	- 3.91	13.2	13.7
900	5.0	88	37.03	- 3.95	13.2	14.5
1000	5.7	84	46.40	- 3.23	13.8	14.0
1100	5.7	85	56.36	- 2.31	13.5	13.5
1200	5.8	85	66.34	- 1.45	13.5	13.4
1300	5.7	82	76.22	- 0.24	12.8	12.7
1400	5.7	83	86.09	1.03	12.7	12.7
1500	5.9	83	96.09	2.22	12.8	12.5
1602	4.1	93	104.84	2.32	12.8	12.2
1702	2.8	74	110.66	2.77	13.0	12.5
1802	2.7	63	114.90	5.00	13.0	12.5
1902	1.6	62	117.99	6.53	13.1	13.5
2002	1.5	61	120.54	7.69	13.5	13.2
2102	1.1	61	122.46	8.67	13.3	12.9
2202	0.8	48	123.73	9.58	13.1	12.8
2302	0.4	349	124.15	10.38	12.8	12.6
2402	0.9	290	123.28	11.04	12.9	12.6
2502	0.9	288	121.70	11.57	12.9	12.6
2602	0.9	285	120.34	12.03	13.1	12.7
2702	1.2	276	118.61	12.36	13.2	12.7
2802	1.2	264	116.36	12.42	16.2	12.6
2902	0.8	254	114.74	11.93	14.6	12.5
3002	0.5	272	113.62	11.80	17.8	12.5
3102	0.7	50	114.07	12.45	13.0	12.6
3202	0.5	41	114.82	13.21	13.2	12.6
3302	0.7	23	115.28	14.03	13.0	12.5
3402	1.3	16	115.99	15.59	13.3	12.6
3502	1.9	16	116.80	18.34	13.1	12.5
3602	2.3	27	118.02	21.68	13.0	12.7
3702	3.1	18	119.90	26.19	12.9	12.5
3802	3.6	16	121.60	31.90	13.0	12.5
3902	3.3	8	122.86	37.68	12.9	12.5
4002	3.2	3	123.22	43.36	12.7	12.5
4100	3.3	350	122.60	48.84	12.9	13.0

a. In feet from Kelly Bushing

TABLE C.1. (Continued)

Depth[a]	Degrees Drift	Azimuth	Feet X Deviation	Feet Y Deviation	Inches Diameter 1-3	Inches Diameter 2-4
4200	3.7	332	120.43	54.38	12.8	12.2
4308	5.3	319	115.46	60.87	8.6	8.2
4400	6.5	302	108.10	66.71	8.8	8.1
4500	6.9	297	97.76	72.34	8.7	8.4
4600	7.3	298	86.59	77.97	9.1	8.3
4700	7.7	295	75.03	83.94	9.0	8.1
4800	8.5	294	62.12	90.04	8.5	8.0
4900	9.0	296	48.08	96.07	8.3	8.0
5000	9.4	288	33.34	102.15	8.4	8.1
5100	8.9	289	18.56	108.22	9.1	8.0
5200	9.0	289	4.05	113.72	8.4	8.0
5300	8.6	293	- 10.11	119.39	9.1	8.1
5400	8.7	293	- 23.77	125.41	9.0	8.0
5500	8.4	290	- 37.76	130.82	8.4	8.2
5600	8.8	293	- 51.67	136.26	8.5	8.0
5700	9.7	292	- 66.73	141.60	9.7	7.9
5800	10.3	296	- 83.64	148.86	8.4	8.1
5900	9.6	299	- 98.45	157.08	8.6	8.1
6000	10.2	296	-114.10	164.50	8.2	8.0
6100	10.5	296	-130.42	172.47	8.3	8.1
6200	11.5	295	-147.41	180.27	8.3	8.0
6300	12.0	292	-166.63	188.13	8.2	8.0
6400	12.3	289	-186.47	195.44	8.5	8.0
6500	12.6	293	-206.78	203.01	8.0	7.9
6600	13.2	299	-226.72	212.54	8.3	8.0
6700	14.5	296	-248.35	223.50	8.4	8.3

a. In feet from Kelly Bushing

LOG DATA EVALUATION

by
George Coates
Schlumberger-Doll

September 1975

LOG DATA EVALUATION

George Coates

Schlumberger-Doll

Battelle-Northwest et al, in conjunction with the National Science Foundation, elected to drill a borehole in the Marysville, Montana area to evaluate the geothermal anomaly located there.

Surface and shallow-hole geophysical data strongly implied the source of heat was a recent magma chamber, near the surface, which was barren of aquifers. The borehole was deemed necessary to prove or disprove this postulation.

If borne out, the well would become a part of an experimental power system designed to utilize the dry-rock for heating injected water, which would then be withdrawn through a second, nearby well. For the development of such a system it is necessary for fluid movement to occur between the two wells either through existing permeable conditions, or, if inadequate, through induced permeability.

The intended use of logs was to provide a measure or indication of existing porosity/permeability conditions.

LOGGING PROGRAM

The logging program was designed to take advantage of the "fracture" response of each device or combination of devices. This, of course, is necessary since no single technique can be relied upon to find fractures.

The other constraint on selecting a logging program was the environmental factors, the primary one being the high temperatures expected, (500°F at 5,000 ft depth). This possibility prompted the decision of making three separate logging runs, (at 2,500 ft, at 4,000 ft, and at TD).

The basic logging program was to consist of the Laterolog (LL-7), Sonic (BHC), Neutron (CNL), Dipmeter (HDT) and of prime interest, multi-recording of Temperature (HRT), to be modified as dictated by encountered formations. The Density (FDC) and electric-survey (ES) were added later to aid Battelle in their correlation to surface conditions.

FRACTURE DETECTION

Since no single method can reliably locate fractures, the approach was taken that, of the methods tried, the more that indicate fractures the better the chance that a fracture really exists.

One reason a single method is unreliable is due to the sensitivity of most logs to particular geometrical orientations of the fractures. To better illustrate this a discussion of each method follows:

Resistivity

The Resistivity device, since the basic matrix can be considered non-conductive, responds to the presence of conductive fluids. Thus resistivity is a porosity measurement providing the open pore/fracture spaces are water-filled, which, of course, is the case here. With electrode devices such as the LL-7, or ES, fracture response, especially high angle fracturing, is indicated by an apparent "porosity" which is too high compared to other porosity measurements which gives an unaffected value of porosity, such as the Neutron log.

In a vertical electrode configuration this is caused by a "shorting" of current paths which reduces the amount of voltage needed to maintain the current flow. This reduction in voltage is analogous to an increase in porosity. However, in the case of low angle fractures the "shorting" of the electrode is minimal and the amount of porosity shown will not be anomalous, thus requiring the use of another fracture detector method for these (Figure C.2).

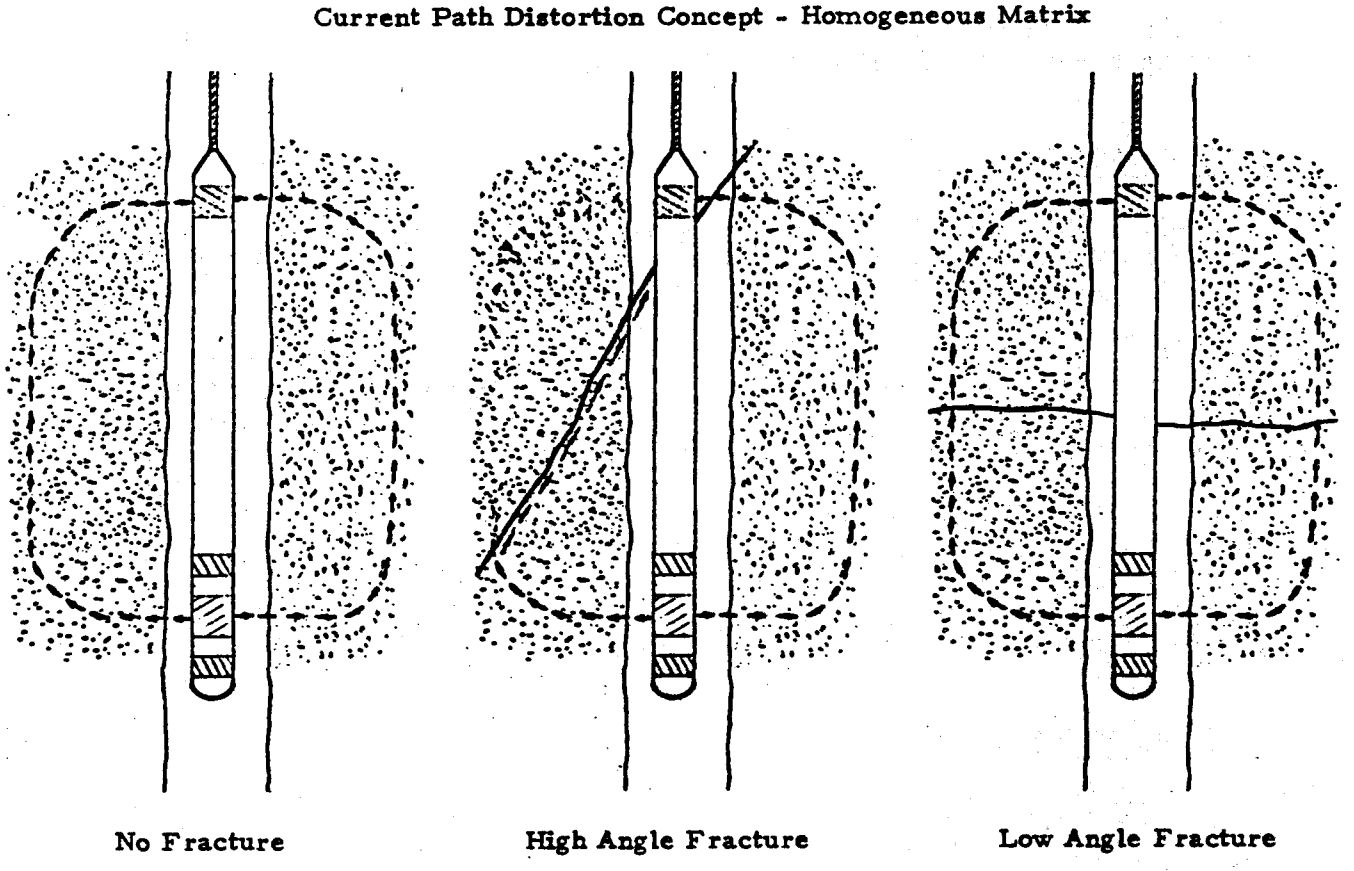

FIGURE C.2. Resistivity Fracture Detection

Sonic

The presence of low-angle fractures is detectable from anomalous values on a travel time recording (Δt) by events which were attributed to cycle-skipping or missed measurements during the time-cycle requirement of the tool. Such events occur when the signal level drops below a bias level which controls the time-cycle measurement. The skipping with the BHC is not always obvious or always due to fracturing, thus reducing the reliability of this method.

Observing the amplitude of the compressional arrival is a common method closely related to cycle-skipping but it has been susceptible to misinterpretation due to poor acoustic coupling between borehole fluids and some types of matrices.

A more successful method of fracture detection with the BHC system has been the Variable Density-Amplitude recordings.

In this type of recording, fractures are normally associated with distortions of the sound pulse wave train caused by reflections of the sound wave due to the interruption of the wave's uniform front by the presence of materials having widely different acoustic properties such as water (fracture) and the basic rock matrix (granite).

In the variable-density recording the wave train is recorded as a function of travel time, the positive half-cycle black, negative white, the intensity of the respective half-cycles being directly modulated by their amplitudes. A fair-to-good fracture finding ability has been demonstrated. This is usually done by noting distortion of the recorded wave train both in frequency and amplitude. Quite often these recordings are so complex, as they are here, that they can only be used to locate zones of fracturing instead of discrete fractures (Figure C.3).

Density

The response to fractures exhibited by FDC is to only show an apparent porosity increase. This, in normal practice, is often disguised by lithologic variations. In this well the lithology is relatively constant so the system is less ambiguous than normal.

A second method found to work in some localized situations is the correlation of the correction curve ($\Delta\rho$) to fractures. This technique is generally only partially successful since hole rugosity can cause a similar response. If significant activity exists though on the $\Delta\rho$ curve in apparently smooth hole, there is a good chance fractures exist, such as at 5450-54 ft on Figure C.4.

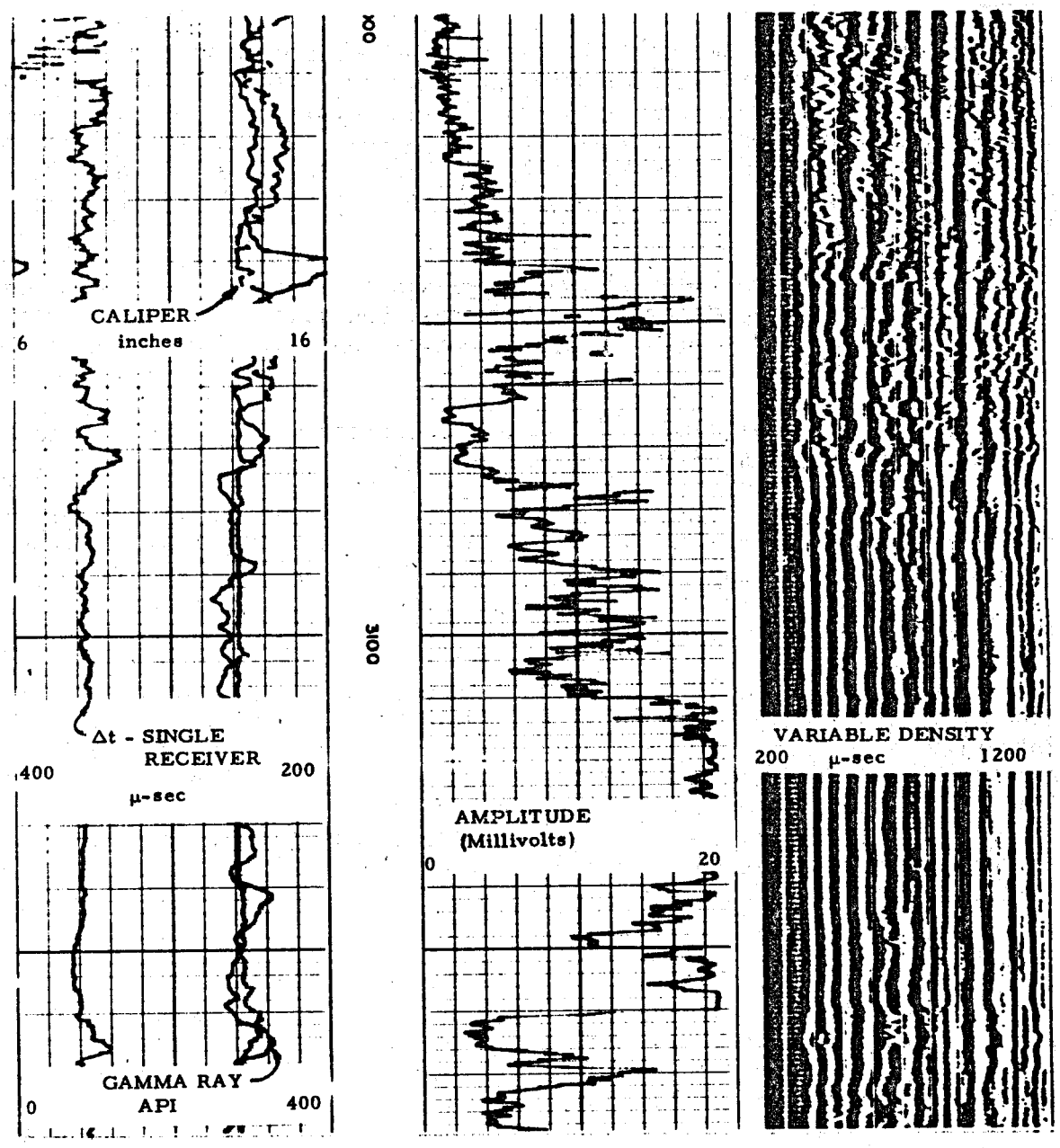

FIGURE C.3. Example Log of Variable-Density Recording of Sonic Wave Train and Companion Data

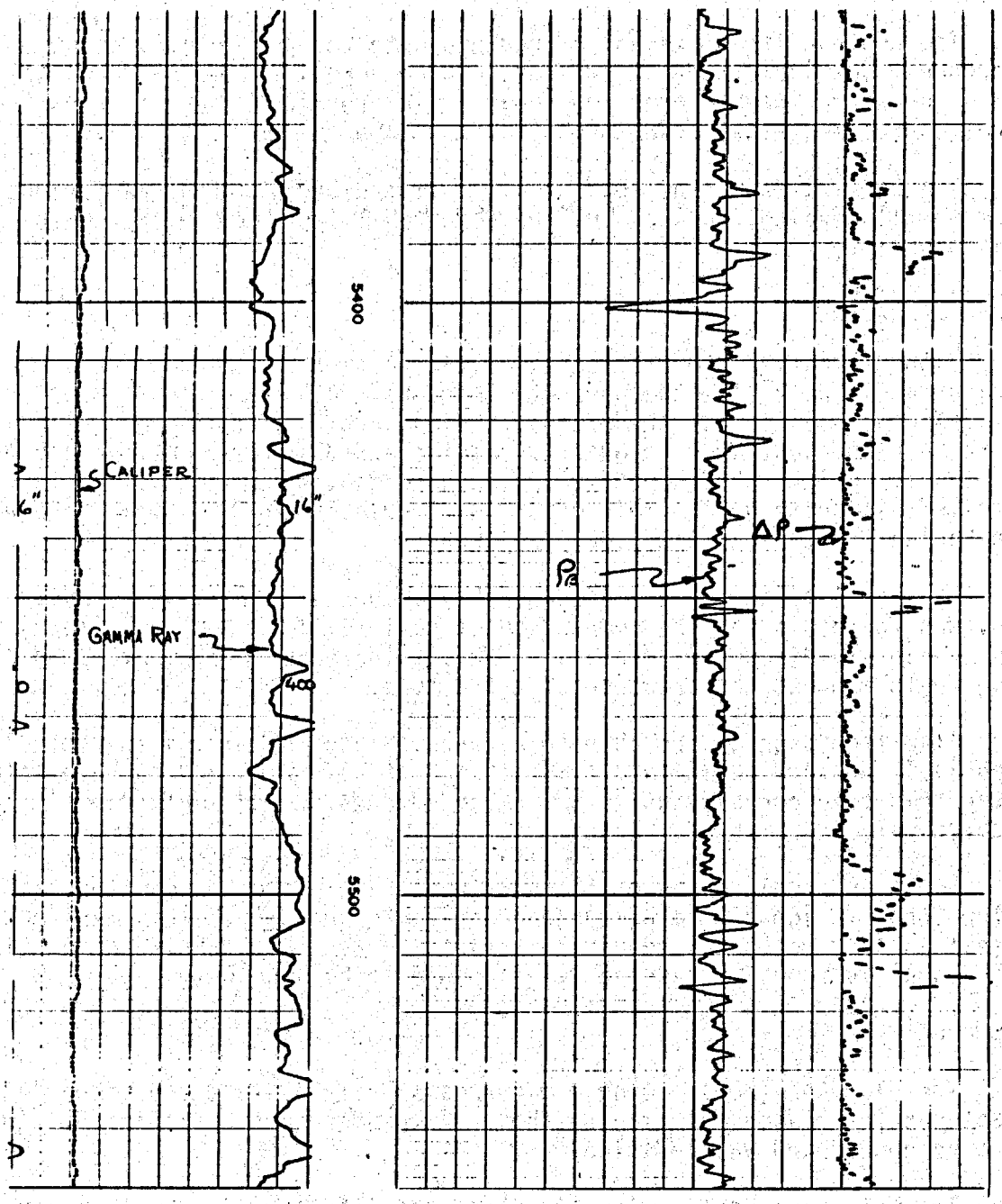

FIGURE C.4. Example FDC Log Showing Bulk Density Recording (ρ_B) and the Compensation Curve ($\Delta\rho$)

Neutron

The neutron itself is not a fracture detector per se but, being a hydrogen index indicator, it provides a good porosity index when water is the major source of hydrogen. Of course, intergranular porosity and fractures containing water show themselves the same to the neutron system.

The CNL is, as is the FDC, usually limited by lithology variations in normal well logging, but, again, the essentially constant matrix helps allay this problem.

ϕ_{SND} Versus ϕ_{RES}

Without knowledge of the exact matrix parameters, though, we are unable to accurately determine the porosity from the individual logs. However, a simultaneous solution of the BHC(S), CNL(N), FDC(D) logs (ϕ_{SND}) calibrated to known responses, such as quartz, calcite and dolomite, provide a value of porosity which, though not 100 percent correct when other minerals are involved, is quite good. This occurs particularly in this case where we are basically dealing with a quartz porphyry.

This ability to achieve a reasonably accurate profile of porosity also provides the basis for the comparison of resistivity "porosity" (ϕ_{RES}) which was previously discussed. Thus an apparent increase in ϕ_{RES} over and above ϕ_{SND} would suggest the presence of a fracture.

Also from ϕ_{SND} we are able to back-calculate the matrix characteristics, especially density (ROGA) and travel time (Δt_{ma}), necessary to have calculated this same porosity using the recorded density and sonic data respectively.

Since the sonic measures the shortest travel time through the rock, it often tends to ignore the presence of fracture porosity. This manifests itself in this method by requiring a fictitiously fast matrix travel time (<50 μsec) in the time average relationship to balance ϕ_{SND}.

Dipmeter

The dipmeter (HDT), being a microresistivity system, can often detect fractures for reasons similar to those discussed under resistivity. They must be opened and water-filled.

The method is most applicable where the lithology is constant and is not troubled by bed boundaries.

Detection of fractures by the dipmeter gives the added benefit of providing an accurate orientation, dip and azimuth, of the fracture plane. This could prove significant in selecting the site of the next well if needed, as well as aiding in understanding the direction fluids could be expected to move most readily.

GENERAL EVALUATION AND FRACTURE LOCATION

A general description of the well from log data and drilling reports indicates two main matrices: Empire shale from surface to 975 ft, and Empire stock from 975 ft to 6790 ft (TD).

The "shale" actually consists of five sub-intervals which display notable changes in logging characteristics as distinguished on the presentation of the attached log.

Interval I (Surface to 310)

This interval appears to be highly interbedded. Hole conditions prevent quantitative evaluation. The variation in apparent grain density (ROGA - Track 2 of Film No. 1) with porosity indicates lithology changes though some of this is undoubtedly due to hole rugosity.

Interval II (310 to 400)

This interval is more stable though some variations exist. The matrix characteristics, apparent grain density (ROGA) = 2.8 g/cc, apparent matrix travel time (DTMA) = 40 μsec, and $\phi_{SND} \approx 8$ p.u. average, suggest a different lithology. Some indications of fracturing exist though very slight. Gamma ray shows slight reduction. This is probably the dike (or sill) mentioned in the drilling report.

Interval III (400 to 590)

This interval again appears to be highly interbedded though hole rugosity again interferes with analysis. Some indication of mineral veining or major fractures exist (408, 438, 445, 527). High apparent grain density and low apparent matrix travel time are possibly due to hole rugosity, but ϕ_{SND} and ϕ_{Rt} agreement suggest total porosity approximately correct which in turn implies ROGA and Δt_{ma} approximately correct. Normal log analysis would have called section more "shaly" due to these responses.

Interval IV (590 to 800)

This interval is similar to the first though hole conditions are improved and data more quantitative. ROGA $\approx$ 2.8 and $\Delta t_{ma} \approx 45$ varying with porosity again suggests interbedding.

ϕ_{SND} versus ϕ_{Rt} response suggests heavy fracturing and possibly some veining ($\sim$680 ft). This zone has a slightly higher gamma ray level than the first zone, possibly indicating less "weathering".

Interval V (800 to 970)

Again hole conditions interfere with analysis; $\phi_{SND} - \phi_{Rt}$ comparison indicates heavy fracturing; otherwise log responses are similar to Interval III except veining indications are absent.

This is probably a highly metamorphosed section and could represent a transition from Empire shale to the Empire stock. Could be a rubble.

WATER FLOW ENCOUNTERED

The well, drilling with air, encountered a significant inflow of water around 1900 ft depth. This provided the first indication that major quantities of water were present in the area.

An additional 1500 ft of drilling showed a very distinct reduction in the geothermal gradient and it in fact appeared to go to zero (no further increase in temperature with depth).

This altered the concept of a dry magma chamber. It also eliminated the need for the intermediate logging run; so the drilling operation continued to 6790 encountering numerous indications of fracturing.

The inflow of water continued and seemed quite capable of maintaining a constant head in the well at 600 ft surface. Much of the deeper drilling, with aereated water, was without returns. Attempts to establish circulation with water failed and in fact indicated adequate porosity and permeability to handle all the water provided. Fluid movement between levels was thought to exist leading to the decision to add flowmeter logs, and later tracer logs, to determine if such flows truly existed and, if so, which intervals were giving and which were taking. The decision to stop at 6790 ft was incurred by the extreme evidence of heavy fracturing and the tendency of the drill-pipe to stick at this depth.

EMPIRE STOCK EVALUATION

The Empire stock, a quartz porphyry basically, but altering to granite characteristics occasionally, was first encountered on the initial logging run at 970 ft depth (see attached log). The first 500 ft (970 ft to 1500 ft) or so appears to be a transitional matrix on the logs and probably represent a variation in the cooling rate causing metamorphic variation. From there to TD the logs indicate a relatively constant lithology with localized variations.

FRACTURE INDICATION

The fracture indication methods worked much as expected and in fact so well that to point out all the indications from each method would fill many pages and really contribute very little to the overall picture.

Only minor indications of fracturing in the stock occur down to 1350 ft depth. From there to 1900 ft depth the frequency of occurrence of indications increases slightly with no major anomalies evident.

From 1900 ft to 2600 ft depth the frequency of indications picks up with a very strong indication in several places, but particularly at 2410 (dips are in the 50° to 60° range with azimuth varying from northeast to southwest) (51° at 210°). From 2600 ft to 3150 ft depth the frequency of occurrence lessens though two strong indications are found, one at 2920 ft (dip 65° south), the other at 3040 ft depth (dip 70° southwest).

It is important to remember that borehole conditions can be a strong influence and may actually be masking fracture indications by causing distortions of a single log measurement, especially the ϕ_{Rt} to ϕ_{SND} comparison.

Considering the matrix, though, any hole irregularity must be studied closely since enlargement may itself be a fracture index.

From 3190 ft to 3650 ft depth the frequency of indications again increases. Many strong indications are found, the most significant are at 3280 ft, 3340 ft, 3370 ft to 3420 ft, 3528 ft and from 3615 ft to 3635 ft depth.

The 3370 ft to 3420 ft interval is especially interesting. It appears exceedingly anomalous on all porosity logs and the resistivity logs. Dip is 60° northeast. It appears to be a vein of unknown material from the log standpoint.

Slight hole irregularities occur at the boundary of this interval but other than that hole rugosity does not appear to be a problem. Though fracture indications exist through the interval, the strong anomalous log responses suggest that other factors may be involved.

The 3650 ft to 3950 ft interval is remarkably void of fracture indications which is quite evident on several logs, particularly resistivity and $\Delta\rho$. The major anomaly within this interval is the high apparent porosity found from 3828 ft to 3850 ft and from 3905 ft to 3935 ft. Dip is around 40° northward. The fact that ϕ_{Rt} is less than ϕ_{SND} might suggest a slight change in mineralization (that these are separate lithologic beds is suggested by the caliper). Of course, the possibility that low angle fractures may also exist must be considered though not felt too likely.

From 3950 ft to 4100 ft depth we find another interval where the frequency of fracture indications increases with major anomalies at 4020 ft and 4038 ft depth.

Though the frequency of indications tends to decrease in the 4100 ft to 4950 ft interval, there are major indications of fractures at 4218 ft, 4422 ft, and at 4600 ft (dip is about 40° to 60° northwesterly to southwesterly). This interval also contains zones with apparent porosities which do not appear to be fractured. This may be due to a lithology variation again since "bedding" is again suggested by the caliper response.

The interval from 4950 ft to 5000 ft depth contains one of the strongest indications of fractures yet encountered (dip is 37° to south-southeast). It is followed by a zone (5000 ft to 5150 ft depth) which is nearly without fracture indications.

This latter interval is significant though in the amount of rugosity indicated by the caliper. This might suggest a highly stressed zone which breaks easily as the stress loading is locally varied.

The remainder of the well shows a high frequency of fracture indications with major indications in the intervals 5610 ft to 5630 ft, 5730 ft to 5740 ft (dip 46° to north-northeast), 5900 ft to 6300 ft (dip 55° southeast), 6450 ft to 6455 ft (dip 50° to west-northwest), and 6645 ft to TD (dip 60° to southwest).

The above analysis is primarily to show the general pattern of fracture indications observed using the methods discussed earlier. It seems quite evident that considerable fracturing exists and in fact, some indication of fracturing is evident throughout the well. The lateral extent is, of course, unknown.

DIPMETER INDICATIONS

Fracture indications are similarly evident on the HDT. The important feature shown by the dipmeter though is the high dip angle of most of the fractures and the zones which are apparently rubblelized or broken so badly that correlatable dipmeter responses cannot be discerned, (Figure C.5).

It is interesting to note also that the hole enlargements are "elliptical" and have a similar long axis azimuth orientation (east-northeast). These conditions are particularly evident just above what appear to be bed boundaries.

The hole enlargement may be only on one side, a possibility we cannot prove since all calipers are averaged readings of the sides involved though some evidence of this is suggested on FDC (Figure C.6) such as at 4340 where the FDC caliper shows smooth hole but ρB-$\Delta\rho$ are very active. Comparison to HDT calipers shows rugosity does exist, possibly the cause of the $\Delta\rho$,ρB activity.

FLUID MOVEMENT

As noted earlier, the presence of in-hole fluid migration established a need for additional logs which could define where fluids were entering and exiting and the amounts involved.

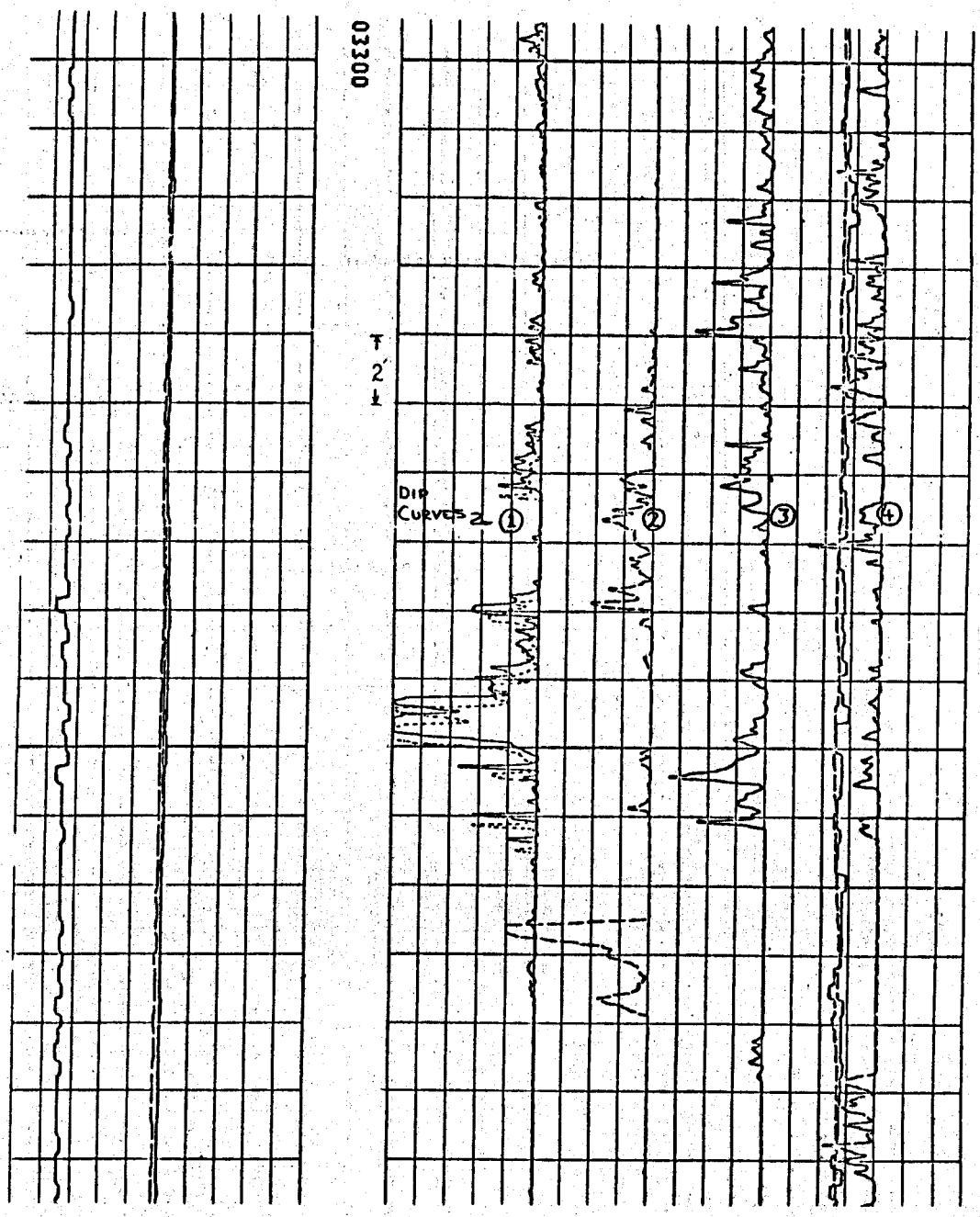

FIGURE C.5. Example Dipmeter Recording Illustrating Contrasting Response Between Four Independent Recordings

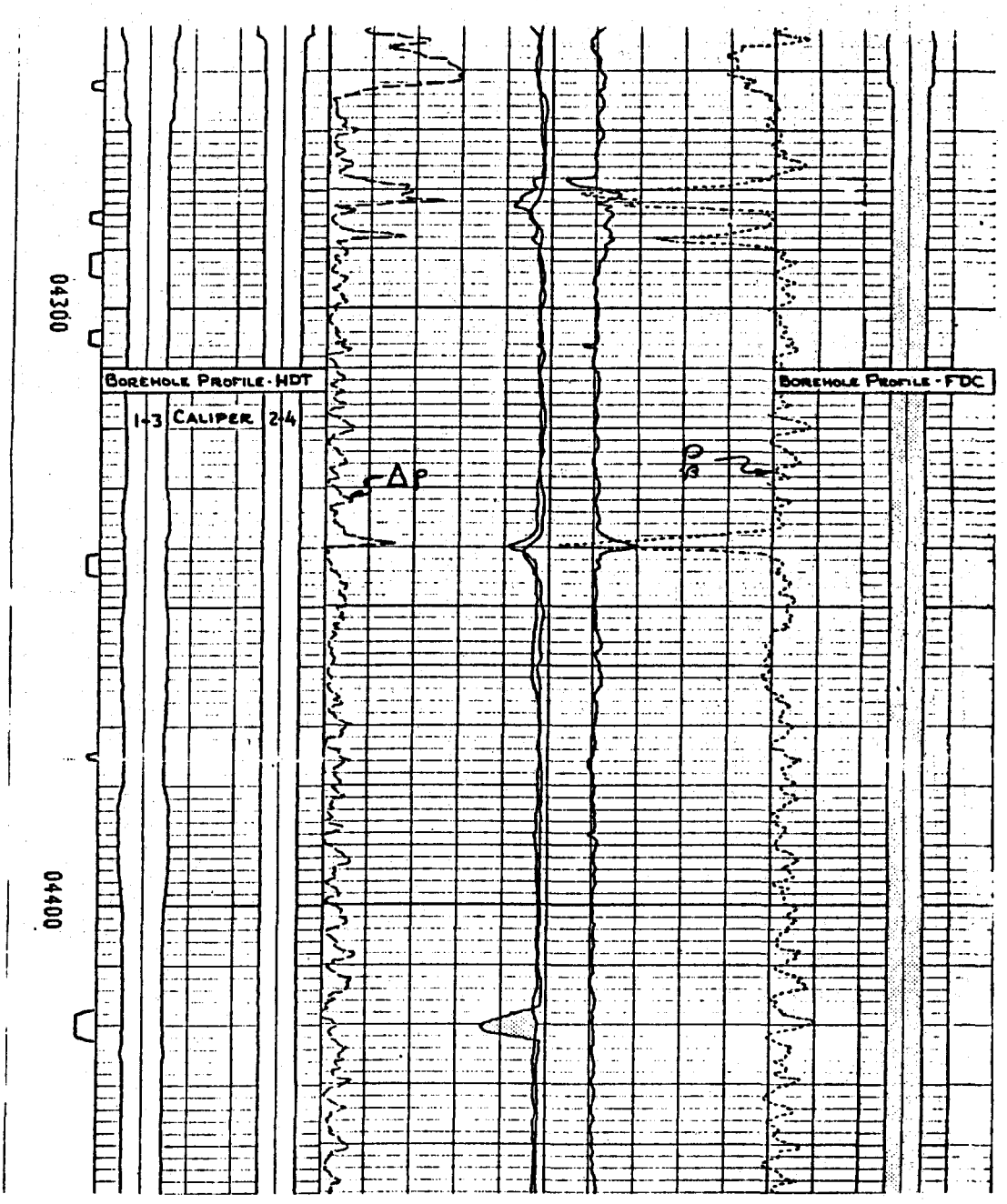

FIGURE C.6. Example of Computed Log Illustrating Ellipticity of the Borehole as Shown by the FDC and Dipmeter (HDT) Calipers. Also illustrates FDC's caliper's apparent lack of hole rugosity in contrast to the activity observed on the $\Delta\rho$ curve.

The flow-rate determination has been difficult to quantitatively define because of seemingly conflicting answers. For example, the very high flow rates defined by a packer-flowmeter run (dated September 10, 1974) failed to exist on subsequent flow measurements. Since this recording was made shortly after setting a cement plug (from 6400 ⟶ TD), the high flow might be due to a short-lived convection cell induced by the heat generated in the setting cement. It is also difficult to visualize any possible uni-direction flow of this magnitude (>1,000 bbls/day) that would have allowed the cement plug to remain in place.

Generally, the in-flowing water is located in the 1500 ft to 3500 ft interval and the present out-flow restricted to the 4500 ft to 5800 ft interval.

More precise location of the in-flow points has been prevented by the presence of casing (set at 4256 ft). The existing flow seems to be occurring behind pipe since the maximum flow rates are directly below it, with no evidence of increase in flow elsewhere.

The geothermal profile (Figure C.7, P. N, LaMori's figure) seems consistent with a hot-water convection system.(1) The reversed gradient below 3500 ft is not in itself unusual but coupled with a downflow of fluid is presently unexplained.

Speculative reasoning tends to favor the two as being hydraulically separated, the lower zone at a lower hydrostatic pressure and independent of the upper system.

FLOW RATES

The flowmeter flow rates, especially the full-bore, were badly hampered by debris in the hole (cuttings) which kept jamming the spinner. Best estimates indicated 280 bbls/day below casing on September 10, 1974; subsequent tests, primarily using radioactive isotope tracer techniques, showed a decline in flow rates such that the latest recording (November 16, 1974) found only 60 bbls/day.

CONCLUSION

The presence of abundant fracturing in the Marysville, Montana, Geothermal Well is well evidenced from the logging data, particularly in the intervals which appear to support the fluid dynamics (1900 ft to 3400 ft and 4500 ft to 5900 ft).

---

(1) Kruger and Otte, Geothermal Energy, p. 76.

TEMPERATURE AND FLOW MEASUREMENTS

by
P. N. LaMori and J. R. Sheff
Battelle-Northwest

September 1975

TEMPERATURE AND FLOW MEASUREMENTS

P. N. LaMori and J. R. Sheff

Battelle-Northwest

TEMPERATURE MEASUREMENTS

The temperature measurements were some of the most important that would be made during and after the drilling of the well. The expected temperature gradient was 175°C/km (96°F/1000 ft);(1) we also expected that the drilling operation would temporarily alter this by decreasing the temperature in the deeper portions of the hole and increasing it in the upper portions.* Consequently, the possibility of a temperature rise to 350°C at 2 km was included in our plans and was expected to cause difficulties with all the logs, including the temperature log.

In anticipation of this temperature rise we made arrangements with Schlumberger representatives to have the high temperature "geysers type" tool at the site for logging. These tools have successfully operated to 315°C (600°F). The tool was to be specially calibrated and air freighted into the drill site. Additionally, the cable on the logging truck was changed from the standard polyethelyne to teflon, which would provide greater than 300°C capability.

As indicated in the logging section, the temperatures were not expected to cause problems (i.e., >350°F) in the upper part of the hole. However, the temperature instrument did not function adequately during the initial logging to 1500 ft and the results obtained were completely unsatisfactory. We believe these difficulties were caused by the instrument being air freighted to the site. Apparently, logging tools handle axial stresses quite well but are susceptible to damage from radial and bending stresses. Such stresses seem to be unavoidable when shipping 12-ft long by 2 in. diameter instruments over long distances. We reappraised the Schlumberger temperature logging program, and decided that to avoid future failures in obtaining results two logging tools would be brought to the site. This proved to be better but was not completely satisfactory.

Fortunately, Blackwell had his temperature logging equipment available and we were able to obtain good measurements of temperature on July 7, 1974, at which time logging to 1500 ft was completed, as discussed in Blackwell's Section on Temperature Measurements. The data are as expected and show values at the hole bottom only slightly less than 87°C. At this point we concluded that we were still in a conductive system.

---

* For the case of a conductive anomaly, the decrease near the bottom of the hole is proportional to the circulation time of the coolant.

(1) D. D. Blackwell, et al., The Marysville, Montana Geothermal Project, NSF-RANN Grant No. GI 38972, Technical Report, Part 2, April 1974.

At 1800 ft water started entering the hole at an estimated 100 gallon/minute. At 1900 ft this inflow increased significantly (estimated at 1000 gallons/minute). Shortly after this temperature measurements by Blackwell showed a large decrease in the gradient below 1500 ft (see Blackwell's section for details). The important point here is that we had obviously entered a region of water with convective heat flow. The water continued to flow into the well for the remainder of the drilling (T.D. 6790 ft). It was obvious that the flow from 1900 ft would dominate temperature measurements and make it difficult to measure the true gradient.

As discussed in the drilling section, the large influx of water caused severe difficulties with water disposal, which resulted in a different drilling strategy. The water in the reserve pit was used for drilling and then pumped into the formation until the pit was empty. Then the water in the hole was air lifted out until the pit filled with water. This process was continually repeated during the drilling of the last 4500 ft of hole. The net result was a continual cooling of the whole well bore and an additional cooling of regions near fractures which accepted the cold water.

During the drilling and after the first logs, various methods were used to measure the temperature. These methods, discussed elsewhere in the report, demonstrated that the temperature in the well never exceeded 200°F. The placement of maximum reading thermometers on a Haliburton line gave readings of up to 250°F. However, these thermometers were not enclosed in pressure tight cases, and it has since been demonstrated that the apparent increase in temperature was caused by the hydrostatic pressure of the water on the thermometer bulb.

The next complete temperature survey of the well occurred August 29 after completion of drilling. In addition to the calibration of the temperature instrument by Schlumberger, it was also calibrated on the floor of the rig by measuring the boiling temperature of water. Temperature measurements were made with the two instruments, and in each case data were taken as the probe dropped down the hole and again as it was pulled up. Generally the two runs do not produce identical results.

The first run had unusual deflections in the curve, which looked like instrumental errors. The upward measurement produced a deflection at 4000 ft which has not been seen again and which cannot be related to any other observation. Otherwise the data appear reasonable.

The second measurement may have a calibration error in that it gave readings that looked good but were at a higher temperature than the first measurement. The data for the second curve are plotted in Figure C.7. We identify three regions on the curves: the low temperature conductive region from the top down to about 1500 ft, the high temperature convective region below 3400 ft, and a transition region between. This latter region has a series of temperature fluctuations (depression and peaks) that suggest zones of water influx and exit, and regions where no water flows.

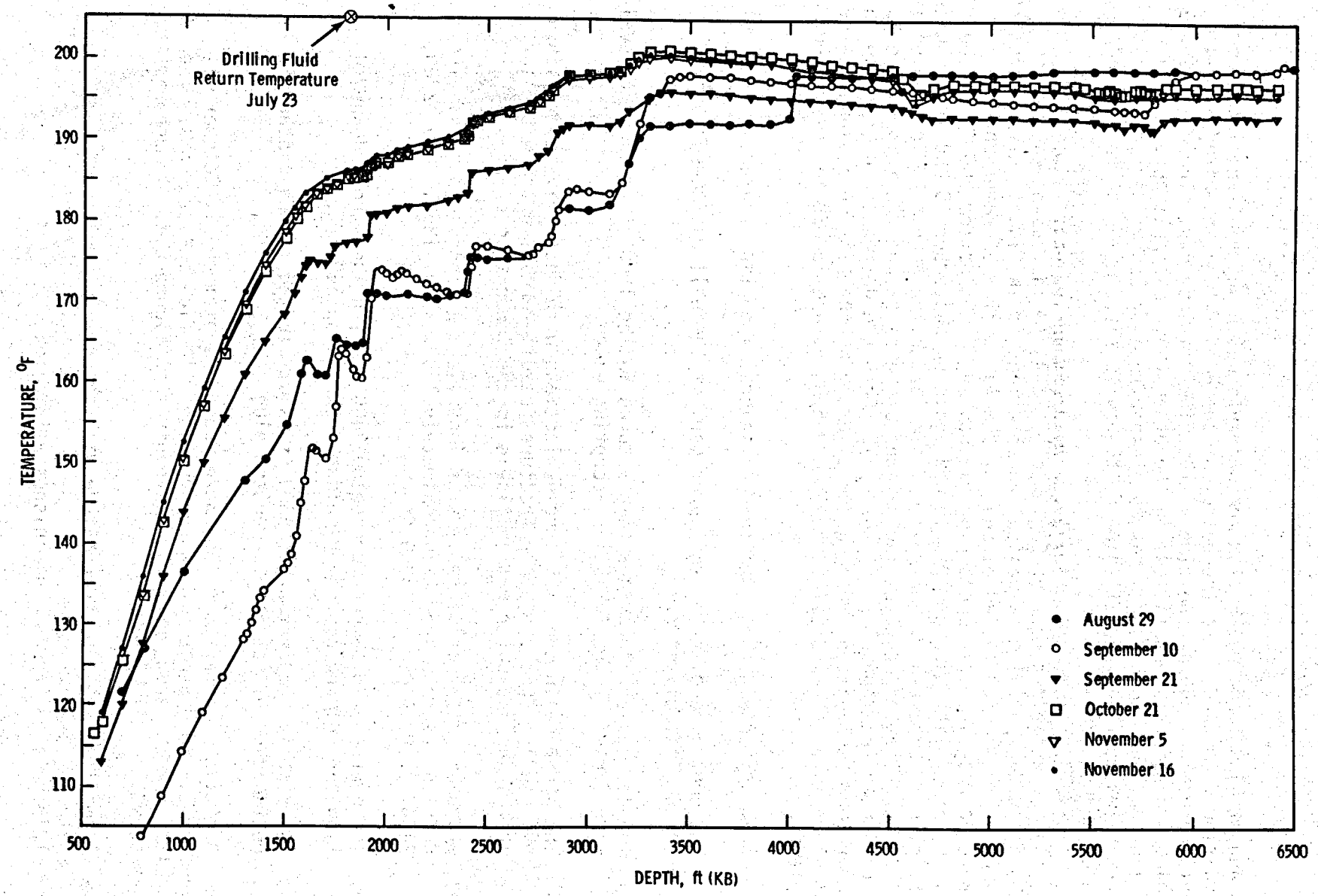

FIGURE C.7. Temperatures in the Marysville Geothermal Well

On August 31 we made water flow measurements which showed significant downward flow from 3400 ft to the bottom of the hole. Two temperature measurements were also made at the time of the flow measurements. In one case the Schlumberger instrument failed, in the other their calibration faltered during the run, indicating a maximum temperature of 220°F instead of the correct 200°F. The general shape of the curve was similar to the second run of August 29.

During the first week of September, the 9-5/8 in. casing was set to 4256 ft and a special crew was called to cement it in place. After attempts to cement the casing failed because of the large flow of water and the many open fractures, a cement plug was poured in the bottom 200 ft of the hole. The well temperature was logged again on September 10 and the results are shown in Figure C.7. This log is similar to the August 29 log Number 1 except that the temperature fluctuations are greater and the temperature is depressed in the upper part of the well. Both the decrease and increase in temperature fluctuations were caused by emptying the 250,000 gallon reserve pit water into the annulus between the 9-5/8 in. and 15-5/8 in. casing on September 9.

Examination of these data reveals several important features:

1) The general cooling of the upper part of the well was caused by the inflow of cool water.

2) The deflections to colder temperatures in the 1500 ft to 3400 ft levels were caused by the formation accepting water.

3) The decrease in the ΔT of the deflections with depth may be explained by assuming that the upper fractures readily accepted the water so that less cold water was available to the lower fractures.

4) There are alternating regions of impervious and pervious rock. The pervious regions are at approximately 1500, 1700, 1850, 2000, 2300, 2400, 2700, 3100, and 3300 ft.

5) The decrease in temperature below 3400 ft with the strong downward flow can only be caused by colder rocks below 3400 ft.

6) The rise in temperature at 5800 ft is attributed to the exothermic heat caused by setting the bottom plug.

Additional temperature logs were made on September 21, October 21, November 5, and November 16 in conjunction with flow measurements. The results of these temperature logs are given in Figure C.7. In general the logs show the following:

1) A small increase of temperature with time;

2) This rate of increase diminishes with time;

3) Three regions - Conductive to 1500 ft
Convective below 4600 ft, and essentially isothermal at ≈195°F
Transition between

4) Continued smoothing out of the deflections above 3400 ft;

5) Development of deflections below 4500 ft;

6) Isolation of the negative temperature slope to the 500 - 4500 ft region.

An additional temperature log was made on April 23, 1975. The results of this are shown as run 1 in Figure C.8. We again had difficulty with the Schlumberger instrument. An additional instrument was flown in, but, while the results appeared significant, the calibration was obviously wrong (run 3, Figure C.8). It gave a maximum temperature of 215°F, while the maximum reading thermometer on the new instrument showed 203°F. The qualitative sense of the data indicates a further refining of what occurred in the previous three logs. The breaks in the curve at 2400 ft, 2700 ft, and 3300 ft suggest that water flowing down the well behind the casing is existing at these depths.

The sharp decrease in temperature at 4600 ft may be caused by a source of colder water crossing the well at that point. The decrease in temperature at 5600 ft and 5700 ft may be explained by a similar cause.

This data cannot be used for quantitative determination of temperature. A fair estimate of the temperature may be made by shifting the depressed portions of run 1 up to make a continuous curve with the parts of the data that were taken before the instrument failed. This produces a maximum temperature of 203°F, which is in agreement with the maximum temperature thermometers. Using this estimate, there appears to be little temperature change in the well since the fall of 1974.

As noted in the above paragraphs, many problems were encountered in making temperature measurements in the deep well. Similar comments apply to the flow measurements, described in the following section. The problems fall into three types: instrument failure, calibration errors, and operator errors. All three types occurred during the logging program, and the subcontractor (Schlumberger) had difficulty providing the quality of service needed for the measurements of temperature and flow. However, those logs that are used more routinely in the oil fields were obtained with little difficulty, and the quality of interpretation provided by the Schlumberger-Doll Research Laboratory was excellent.

In conclusion, the temperature measurements in the Marysville geothermal well show that an isothermal zone of about 195°F was encountered from approximately 3000 ft to a depth of 6700 ft. How much deeper this

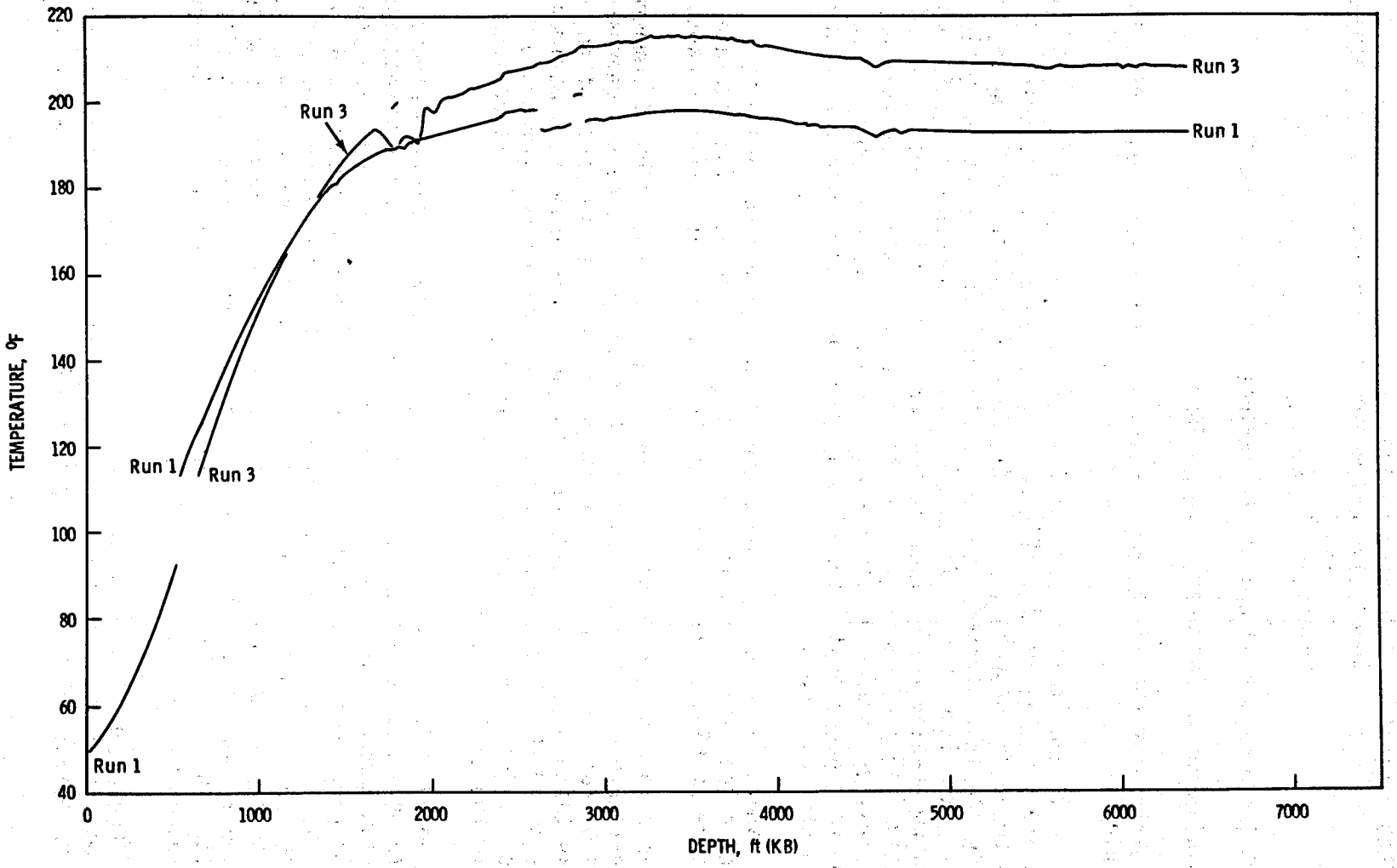

FIGURE C.8. Results of Temperature Log for April 23, 1975

zone extends is not known, but the zone may be a portion of a large convective cell with the water moving through the fractures in the quartz porphyry and limited by its bulk permeability. The heat source driving the convection cell was not located but may be at considerable depth. Heat transport in the region from 1500 ft to about 3000 ft is governed by a combination of conduction plus limited convection in isolated aquifers. Above 1500 ft, heat transport is essentially conductive as shown by the linear gradient.

FLOW MEASUREMENTS

Because of the discovery of water influx to the well, flow measurements were added to the logging program. Table C.2 lists the dates and kinds of flow measurements made by Schlumberger in the Marysville well.

TABLE C.2. Flow Parameters in Marysville Well

Date	Depth Range (ft)	Flow Instrument	Flow Range	Notes
Aug 30, 1974	1000-5500	Full Bore Spinner	0-9000 B/D Down	Much plugging
Sept 10, 1974	4130-5600	Packer Flow	200-560 B/D Down	1 questionable measurement at 5600 ft,1000-10,000 B/D
		Full Bore Spinner		Unsuccessful
Sept 21, 1974	4130-6400	Isotope Injection	1-505 B/D Down	
		Full Bore Spinner	?	Unsubstantial Results
Nov 19, 1974	4130-6400	Isotope Injection	1-505 B/D Down	
		Full Bore Spinner		
April 24, 1975	4130-4600	Isotope Injection	0-48 B/D Down	Reverse in flow
	4600-6400	Full Bore Spinner	0-10 B/D Up	Below 4600 ft

August 30

The full bore spinner was chosen because it is the best flowmeter for large flows. The flowmeter was dropped into the hole and pulled out of the hole at a nearly constant rate. From the difference in the rate of rotation and other parameters it is possible to develop a relationship between spinner revolution rate and flow. Figure C.9 shows the combined up and down spinner data with the calculated flow.

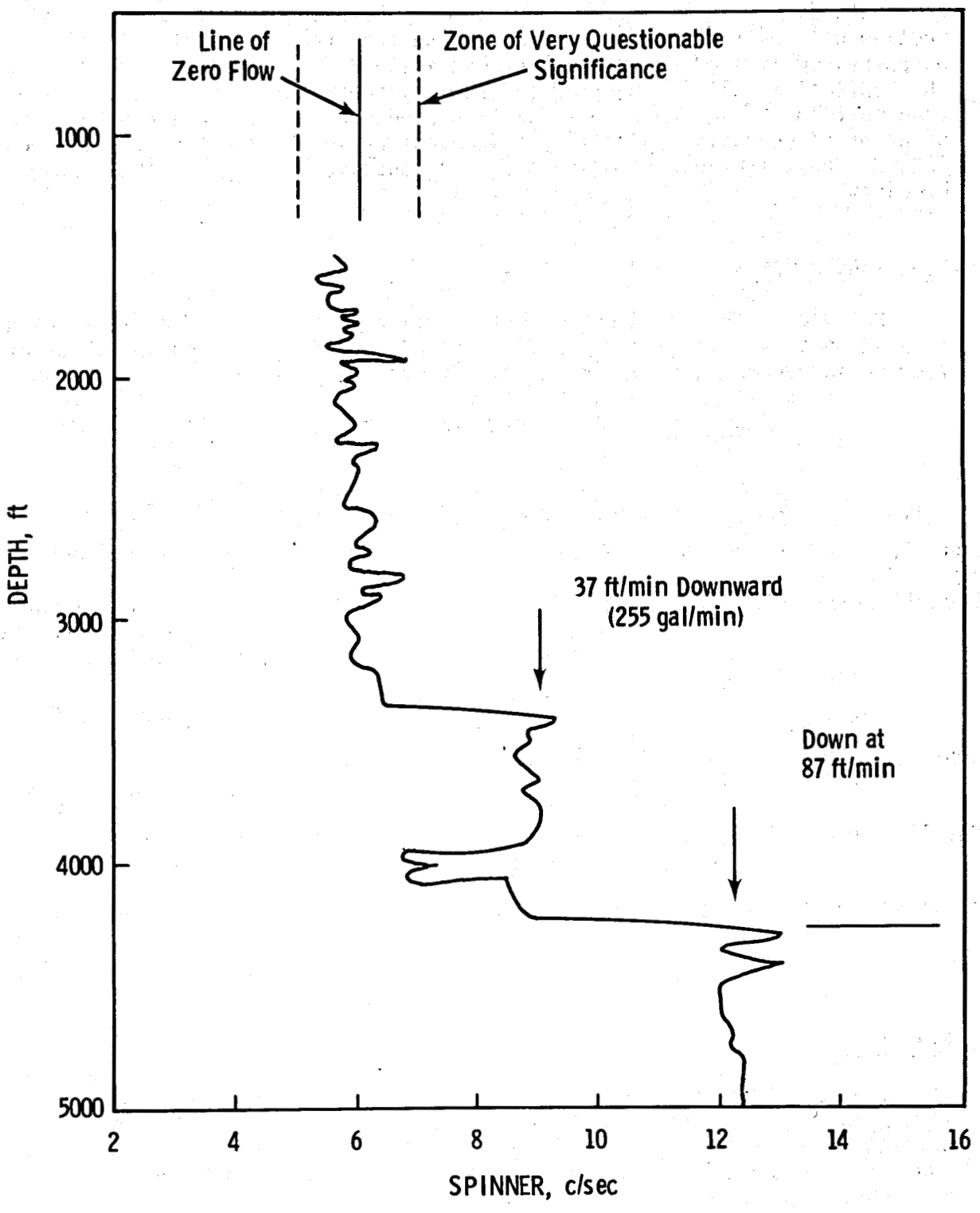

FIGURE C.9. Summary of the Spinner Flowmeter Data

The significance of the smaller variations in the curve cannot be evaluated. There may be some relation to possible variations in flow, but lack of control of other variables (e.g., probe velocity, hole diameter, etc.) is significant enough to produce the effects. Another problem was the plugging of the spinner by small flakes of quartz porphyry, 1/2 in. to 2-1/2 in. diameter x 1/10 in. thick. Apparently the amount of this material increased with depth so that, except in one case, we were unable to keep the instrument unplugged below 5100 ft. Unfortunately this was on the initial run, and the data was not recorded. The indications were that the high flow continued unabated to the hole bottom.

The spinner flow test shows essentially zero flow (i.e., low to zero) at depths less than 3400 ft where the flow abruptly goes to 9000 B/D downward, although during the drilling we had observed that from 1900 ft to 2100 ft we could produce 1000 g/m or 34,000 B/D by air lift pumping. Apparently the upper zones are in hydrostatic equilibrium, or have only low flow. The spinner is insensitive to small flows, which may explain the discrepancy. Another possible explanation is that the 3400 ft fracture zone is the bottom plug of a tank and is emptying from there. This explanation has problems on two counts: 1) the increase in flow with depth should be gradual because the other fractures would still have some flow; and 2) the temperature data suggest that the fracture zones are separated and not easily connected.

The sharp changes in flow near 4000 ft are probably not real; they are only observed on the probe up-run. It has been suggested that a partial plugging of the spinner caused the decrease. The increase in RPS at 4250 ft was caused by a change in hole size.

September 10

This full bore spinner was used in the hole but showed only small signs of flow and was not sensitive enough; thus, a packer flowmeter was used to better define the flow in the hole. A packer flowmeter consists of a spinner with an inflatable rubber bag. The bag expands against the wall of the hole and forces all the fluid through the spinner, thus making it quite sensitive to small flows. The results of the packer flowmeter tests are given in Table C.3.

TABLE C.3. September 10, 1974 Packer Flowmeter Tests

Depth, ft	Flow Down
4290	280 B/D
4640	200 B/D
5000	200 B/D
5540	206 B/D
6000	
6190	1000-10,000 B/D
6385	

Except for the last three points the data seem quite reasonable. The flows are considerably less than on August 31, but in the intervening time the hole was cased, cemented and a plug placed at the bottom. While the cement job around the casing was not good, the flow should have been severely restricted. The spinner galvonometer reading was pegged at 40 rps, with the bag uninflated in order to estimate the high flow at the bottom.

The explanation for this apparent high flow is not known. It could be an instrument error, or it could possibly be due to some special condition in the hole at the time of observation. The temperature curve of September 10 showed an abrupt increase at 5750 ft which has been attributed to the exothermic heat caused by the setting of the cement plug at the hole bottom. It is suggested that this exothermic reaction sets up a convection cell between 5750 ft and 6400 ft. The convective cell is terminated by the sink/source region between 5600 and 5750 ft. If this explanation is valid, then the rapid convective flow in the hole could be observed with the flowmeter.*

The packer flowmeter gives excellent results when working properly, but we experienced significant equipment problems before the equipment was used. The tearing of the inflation bag terminated our use of the packer, for no replacement bags were readily available for our hole size. Use of the packer cost about $2000 extra because of hot-shot air freight and technician travel charges; thus, we decided to use the isotope injection flowmeter for future flow tests. This instrument also had the advantage of greater sensitivity at low flows.

September 21

On September 21 we examined the flow in the well with the isotope injection flowmeter. A small quantity of radioactive material** is injected into the hole at a known depth; two counters are placed known distances away from the injection point and the time for the radioactive material to pass is noted. From this and the hole diameter the flow can be calculated.

In principle this is very simple but certain problems arise. For instance, different velocities may be observed for the two detection points. This can be caused by real changes in flow in that region or by turbulence,

* C. Clavier of Schlumberger offered this explanation. It is based on the fact that the hole deviates 15° from the vertical in this region, and therefore the tool would have a tendency to lie on the bottom (down) side of the hole. The heated convecting water would rise on the top (up) side of the hole and descend on the bottom side of the hole, thus showing a downward flow as was observed. If the bag is inflated, it should block the convection and normal flow should be observed. We attempted this, with no effect. However, the bag was observed to be torn on removal from the hole. Thus, without knowing when the bag tore, we are not certain of the validity of this explanation.

** We used ^{131}I so as not to cause harmful environmental effects; this material has an 8 day half life, thus decaying quickly.

small convection cells, or Brownian mixing. We have not attempted to distinguish among these causes in our analysis and have averaged the results of the two counters. This is justified because, at the present, there seems to be no real significance to these variations. Certainly in the case of low flows Brownian mixing is an acceptable explanation.

This apparent mixing and low flow spread the detection peaks out and decreased the count rate to the point that precise definition of the peak maximum became impossible. As a result, it became standard practice to drop the counters a distance below the injection point and pull the counters through the injected material. The flow rate was calculated the same way as before, except this procedure sharpened up the peaks and permitted detection of the flow when it was so slow as not to pass the counters in a reasonable waiting period (30 to 60 min).

Using this technique it is possible to detect flows as small as a few barrels a day. A gamma log of the hole was made both before and after the isotope injections. This permitted a further examination of the flow in the slow flow regions. When the flow was too slow to be observed by the two normal techniques, the last gamma log often showed the direction of the flow. The results of the September 21 isotope injection flow tests are given in Table C.4.

TABLE C.4. September 21, 1974 Flow in Marysville Well

Depth	Down Flow B/D	Notes
4038.5	∿2	Not significant, only 8 in. displacement
4188.5	61	Below perforations
4258.5	510	Just below casing
4268.5	499	Difference between 510 not significant
4688.5	54	
5588.5	52	
5688.5	27	
5788.5	5.6	
6188.5	5.2	Just at limit of detection
6388.5	7.0	

The full bore spinner test run on this same date proved insensitive to these low flows and the data were not analyzed.

The results of the isotope injection test show significant flow coming from behind the casing. This flow certainly has components above 4130 ft, the depth of perforations. The 510 B/D flow from the casing shoe compared to the 200 B/D observed on September 10 may not be significant. The measurements were made by two different techniques and comparison may be difficult; for example, the packer may not have entirely closed off the outside flow. A second explanation centers on down hole pressure changes. A third explanation involves the cement. The casing was cemented for the

second time on September 9. While the cement bond log showed no bonding to the casing, it is quite likely that the cement filled in some of the space between the casing and the hole wall. The flowing water would wash this out with time, thus causing an increase in flow.

The flow measurements show significant decreases between 4300 ft and 4700 ft and between 5600 ft and 5800 ft. This is consistent with previous and later flow data. These regions also showed significant changes in the temperature-depth data, which will be discussed in a later section.

November 19

The flow was measured in the hole on November 19, using the isotope injection technique. The results are given in Table C.5.

TABLE C.5. November 19, 1974 Flow in Marysville Well

Depth	Down Flow B/D
4188.5	small to 0
4388.5	32
4488.5	27
4568.5	19
4788.5	18
5598.5	12
6028.5	~0
6366.5	~0

The observed flow has continued to decrease. The significant changes (decreases) in flow observed previously near 4600 ft and 5600 ft continue.

April 24

The next injection tests were made on April 24, 1975 with the isotope injection tool. The results of this test are given in Table C.6.

The most significant result found here is the change in direction of flow to upwards at depths below 4600 ft. The result is startling, and while the magnitude of the flow is subject to uncertainty, the direction is not. The data continues to show the significant change in the amount of flow near the 5600 ft level.

The explanation for these results is not readily apparent. The initial potential (P) in the well appeared to be $P_{3400\ ft} > P_{4600\ ft} > P_{5600\ ft} > P_{6400\ ft}$. The present potential (P) in the well appears to be $P_{3400\ ft} > P_{4600\ ft} < P_{5600\ ft} \leq P_{6400\ ft}$. The possibility of error in the data has been examined. While uncertainties exist in the value of the measurements, there appears to be no possibility for errors in direction.

TABLE C.6. April 24, 1975 Flow in Marysville Well

Depth	Flow B/D (Direction) From Injection Log	Flow B/D (Direction) From Gamma Log
4150	17.3↓	7.0↓
4270	47.8↓	could not find
4490	26.8↓	could not find
4600	0	? 4.8↑ could be 4490 ft test flowing down
4750	8.2↑	10.0↑
4750	9.6↑(taken on 4850 ft test)	--
4850	3.8↑	11.0↑
5400	8.9↑	12.9↑
5900	2.2↑	5.0↑
6200	∿1 ↑	6.0↑

WATER LEVEL

Table C.7 presents estimates of the water levels in the Marysville well obtained during the Schlumberger loggings and the methods of detection. In general, the approach was to note a sudden change in the logging tool reading as it was lowered into the well and attribute the depth of this change to the observation of the fluid level. The ability to detect this level is a function of the sensitivity of the instrument as well as the rate of descent. The rate of descent is about 1 ft/sec. The instruments appear to be fairly sensitive. Both temperature tools showed thermal inertias of less than a few seconds (actual time is unknown). The High Resolution tool uses a bare resistance wire as the measuring element and is sensitive to about 0.1°F. The Production Temperature Tool appears to have a thin metal covering and is sensitive to 0.04°F. The temperature gradient is computed over a 2 ft interval. The spinner should also react quickly upon entry into the fluid.

All the indicated depths are measured from the Kelly Bushing of the drilling rig, that is, 20 ft above ground level. Errors associated with locating this point should be about 1 ft or less. Thus it seems likely that all of these measurements should have precisions of better than 5 ft. Furthermore, with the exception of the 0 point, all the measurements should err in the same direction (i.e., long) because of cable velocity, so they may in fact be closer than the 5 ft.

Another possible source of error exists in that the loggings were done on two different Schlumberger trucks using two different wire types and sizes. The errors thus introduced were never rigorously evaluated. An evaluation from Schlumberger indicates that these errors are very small, i.e., less than 6 in.

TABLE C.7. Tabulation of Water Level in the Marysville Well

Date	Depth (Ft)	Truck	Method
Uncased			
8-29-74	600*	Havre	Noted on logs. Method of detection unknown. May be estimate.
8-31-74	561	Havre	Production Temperature Tool
8-31-74	565	Havre	Spinner Tool
Cased			
9-10-74	576	Havre	High Resolution Temperature Tool and Gradient
9-21-74	553	Casper	Production Temperature Tool
10-21-74	552	Casper	Production Temperature Tool and Gradient
11-16-74	547-548	Casper	Production Temperature Tool and Gradient
4-23-75	547-548	Havre	Production Temperature Tool and Gradient

* This is probably not accurate

A review of water level determination by use of Schlumberger Logs indicates that we probably obtain precisions of about 2 ft. Thus there seems to be a slight rise of the water level with time but no significant changes since November 1974. The change observed on September 10 may be related to the rapid addition of 250,000 gallons from the reserve pit on September 9, but why this should lower the level has not been studied.

CORE DOCUMENTATION, RECONSTRUCTION AND PHOTOGRAPHY

by
P. N. LaMori
Battelle-Northwest

September 1975

CORE DOCUMENTATION, RECONSTRUCTION AND PHOTOGRAPHY

P. N. LaMori
Battelle-Northwest

CORING AND RECOVERY

The general description of the coring operations and associated problems is described in the Drilling Report. Because of the difficulties in the coring operation, removal and recovery of the core pieces from the core barrel and subsequent handling were often difficult. As noted in the Drilling Report, the length cored and recovered was usually significantly less than the 10 ft planned before drilling began.

The core was removed from the core barrel on the floor of the drill rig. In almost every case, because of wedging, the bottom part of the core had to be driven out of the slips with a sledge hammer, thus causing breakage of that part of the core. All portions of the cores were highly fractured when removed from the core barrel; this no doubt reflected the fractured and veined nature of the rock. Thus the cores had a marked tendency to come out of the core barrel in pieces from 1 in. to 12 in. long.

Great care was taken in removing these pieces and placing them into the core boxes in proper order. The core barrel was unloaded from the bottom up. The pieces were removed and passed to those loading the core boxes so that the top/bottom relationship was maintained. During this process the pieces were washed with water. The full core boxes were then stored in a secure place. However, despite this care, more than a few errors in placement were found during subsequent reconstruction.

DOCUMENTATION AND RECONSTRUCTION

SMU personnel performed the immediate documentation by marking and identifying each piece in the order and direction found in the core boxes. The immediate documentation provided a valuable first record of the cores. P. N. LaMori performed the more detailed documentation and reconstruction of the cores. During the reconstruction and documentation the fractures and veins were catalogued and analyzed. After reconstruction and documentation, the cores were photographed.

The cores were reconstructed so that the pieces would represent a single piece with breaks. In almost every case it was possible to do this unequivocally, albeit sometimes with considerable difficulty. Core 13 was so highly fractured, and broken up into approximately 1 in. to 2 in. thick discs, that it was never totally reconstructed.

Because the cores were not oriented with respect to true north during drilling, the bearing could not be determined. An arbitrary north was assigned for convenience in reconstruction, marking, description, and analysis. The assigned north was normally the major knife scribe cut along the length of the core by the core barrel. However, slippage along natural fractures often allowed the core to rotate somewhat during cutting.

During reconstruction the core was laid horizontally within the 90° angle of a section of angle-iron supported on wooden blocks. After the core was reconstructed, each piece was numbered, measured in length along the north line and described. The numbering system used for core pieces was sequential: 1, 2, 3, . . , starting from the top. The numbering system used for cores was a four digit code in which the first two digits were the core number and the last two digits the piece number, e.g., the eighth piece in Core 11 would be numbered 1108. Each core was assembled for photography with the top of the core on the right side of the photograph; the numbers read "right side up" when the core is viewed in this position. Each core was measured and marked with yellow dots every inch and yellow lines every 10 in. along the assigned north line. The marks and numbers were kept as small as possible to minimize contamination. For the photographic record, the cores were rotated approximately 120° and 240° clockwise when viewed from the top. Small dots were placed every 10 in. along the length of the core at the 120° and 240° lines. These markings were used for scale in the photography.

PHOTOGRAPHY

We decided to use photography as the primary method of recording the original physical state of the cores in addition to the visual petrographic descriptions and the analysis of the fractures. This decision was responsible for choosing the method of markings described above. Using that particular marking method and a short descriptive caption, it is always possible to uniquely identify each section and measure the scale from the photographs.

Because of the decision to use photography as a major recording device, a series of test pictures were taken to determine the method that gave the best information. The following parameters were studied:

1. color photography
2. black and white photography
3. exposure variables
4. over and under exposure effects
5. direct or indirect light
6. wet or dry samples
7. film properties
8. processing problems
9. use of a polarizing filter
10. length of core to be on a frame
11. use of lens of different focal lengths.

Not all of these variables were studied as intensively as others and we are not positive that the best method was found. We do believe that a very good and easily workable method was obtained, one that was sufficient for the needs of the project.

Once it was decided that a 35 mm film could give sufficient resolution and lack of grain for 8 in. by 10 in. picutres, the choice of a camera was not a variable. After considering the needs of the project, it was decided that the normal focal length lens would serve satisfactorily, providing that three pictures at different distances were made of each core. Thus the camera and lens used were YASHICA J-5 (circa 1965), f 1.8, 55 mm YASHINON lens with a built point light meter.

The chosen method of photography was to shoot in direct sunlight using normal exposure times. The camera was mounted on a tripod with a remote shutter release to minimize movement. A polarizing filter was used to reduce the glare caused by the sun on the samples which were wet. The polarizing filter required using two additional f stops.

Kodak CPS color negative film was used. This film has an ASA speed of 100 but is still sufficiently fine-grained to give the detail needed. The film provided excellent detail and gave excellent color reproduction with the wet samples. An additional cost advantage was that the ektacolor process could be processed at Battelle Laboratories. This also gave us excellent control on the final pictures. Black and white pictures were not made because it was decided that they could be made later, if needed, from the color negatives. Complete sets of color photos are held at BNW and SMU and the films are held at BNW. Information about roll number, picture number, f-stops, speed, etc. can be obtained from BNW.

The reconstructed cores were photographed from three distances except in cases where the core length recovered was so small as to make the longer distances unnecessary. The core was photographed in the horizontal position with the 0° (north bearing) mark on top. The camera was at a height of 5 ft and at a distance just sufficient to frame the core length (about 18 ft away for a 10 ft long core). This was not done for the 120° and 240° rotations. The core was then photographed from a distance just sufficient to frame 30 in. sections (approximately 4-1/2 ft away) at a camera height of 3 ft. This was done with 0°, 120°, 240°, in the vertical direction. In the case of Core 12 the photography was at 180°. The fractures present made other rotations impractical in this case. This core was also photographed with the camera pointing at the normal to the N-S line (i.e., 90°) without rotation of the core. The small yellow dots or lines at 10 in. provide scale for the pictures. It is possible to reconstruct a total picture of the core from these photographs at three rotations. Thus all features of the core can be seen in the photographs.

An additional set of pictures were taken to provide more detail. These are pictures of 10 in. sections taken from a distance of 2 ft. These pictures were taken at 0°, 120°, 240° rotation with the camera directly above the rotation angle. Again, complete reconstruction of the cores is possible at three rotations. On an 8 in. by 10 in. format this provides about a 75 percent scale picture of the core.

Selected pictures of the cores are presented in Figures C.10 to C.19. These photographs demonstrate the core photograph as well as the rock and fractures, discussed in the following section, found in the Marysville well.

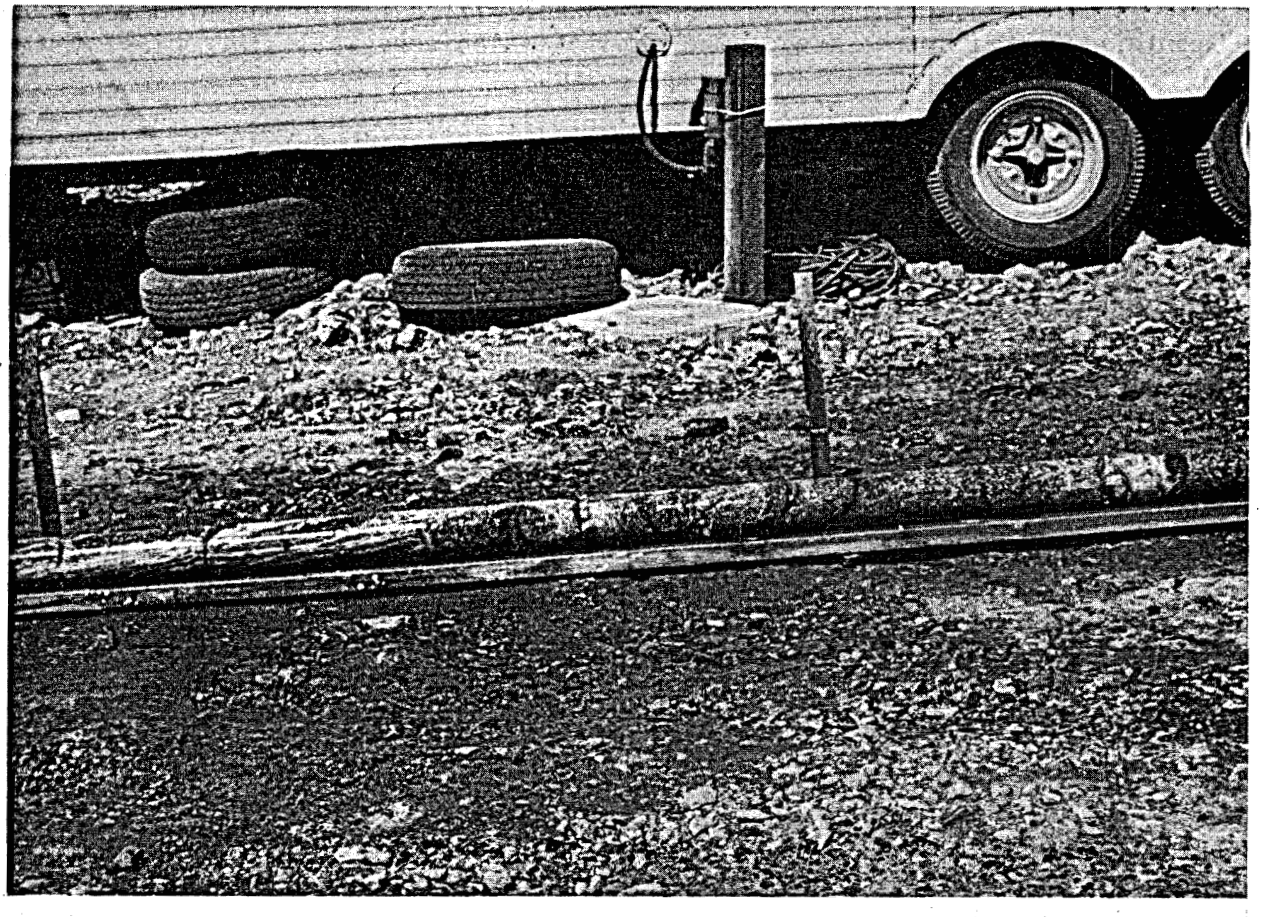

Figure C.10. Core 1 0 in.-120 in. 0° Rotation. Picture Demonstrating Full Core Length of Feldspar Porphyry Dike or Sill.

FIGURE C.11 Core 1 90 in.-120 in. 0° Rotation. Picture Demonstrating 30 in. Section. Note steeply dipping veins.

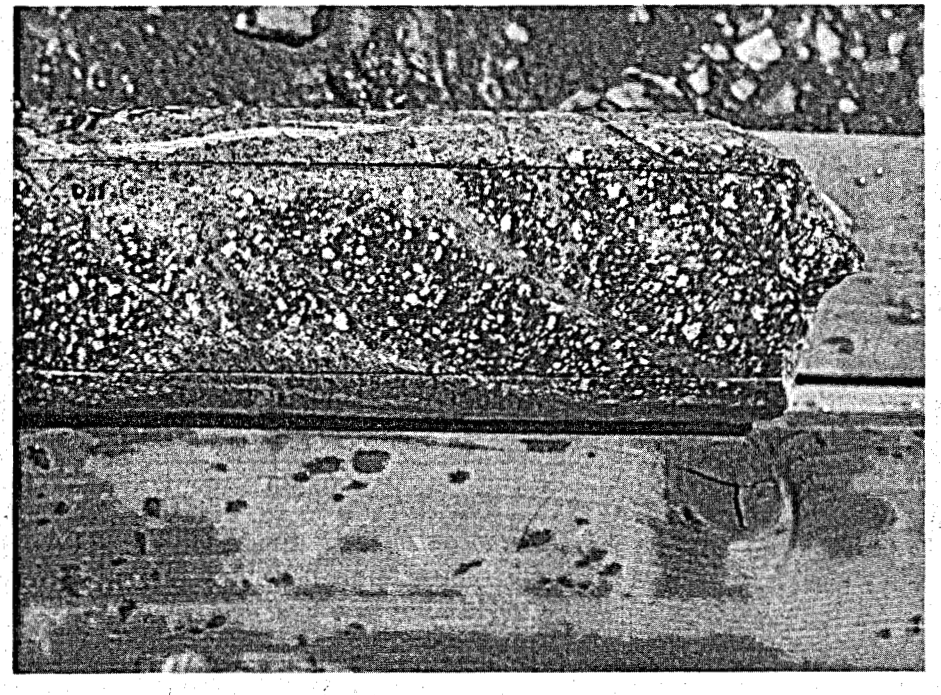

FIGURE C.12 Core 1 110 in.-120 in. 0° Rotation. Picture Demonstrating 10 in. Section.

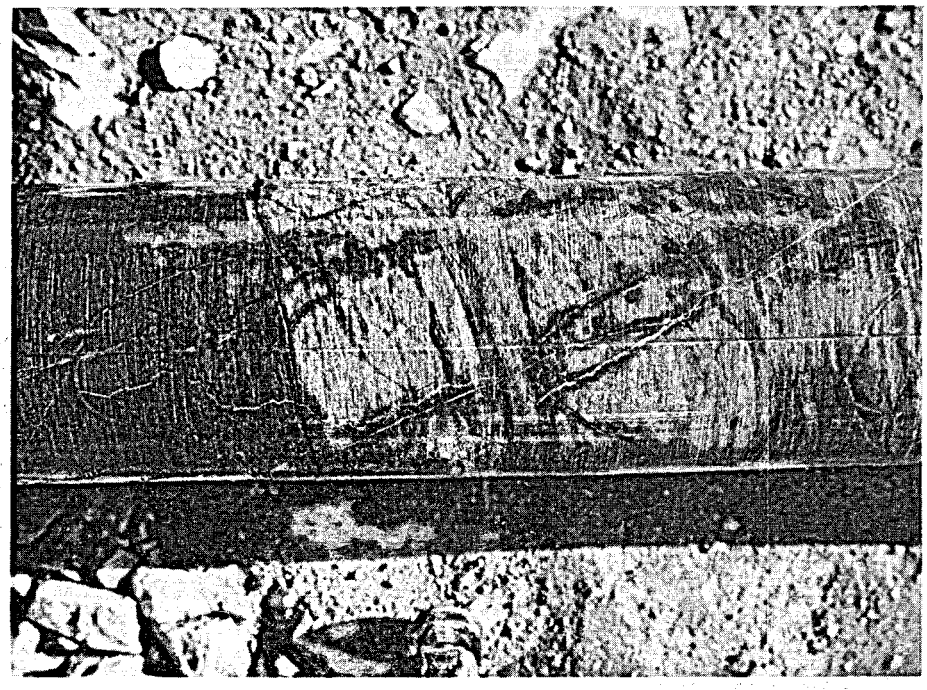

FIGURE C.13 Core 3 20 in.-30 in. 240° Rotation. 10 in. Section of Empire Shale Showing Some Steeply Dipping Veins and General 45° Dip of Shale.

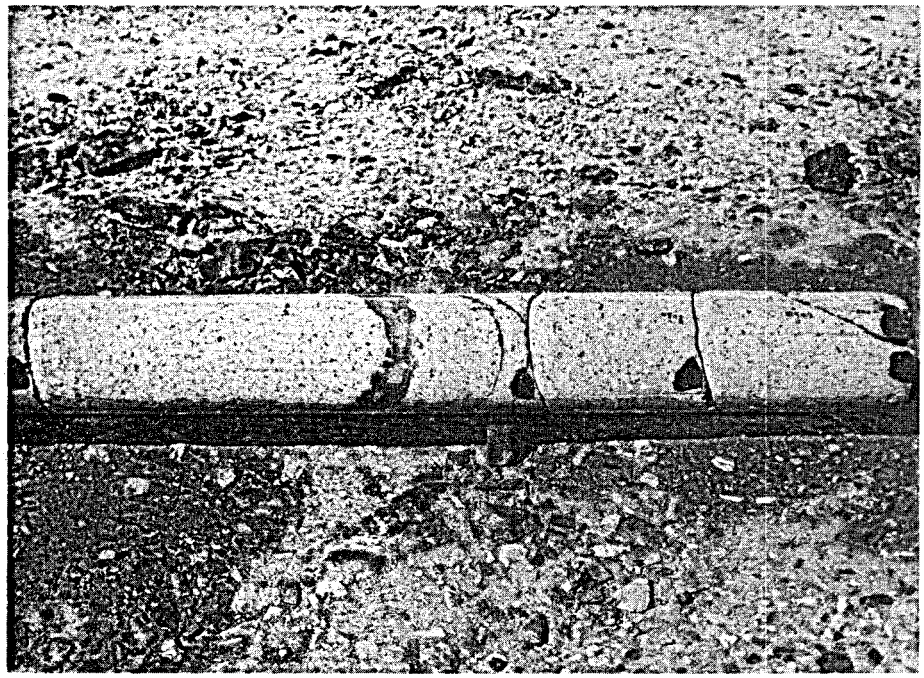

FIGURE C.14 Core 5 0 in.-30 in. 0° Rotation. Upper Section of Empire Stock. This piece shows molybdenum mineralization. Note rotation of knife edges at breaks between pieces.

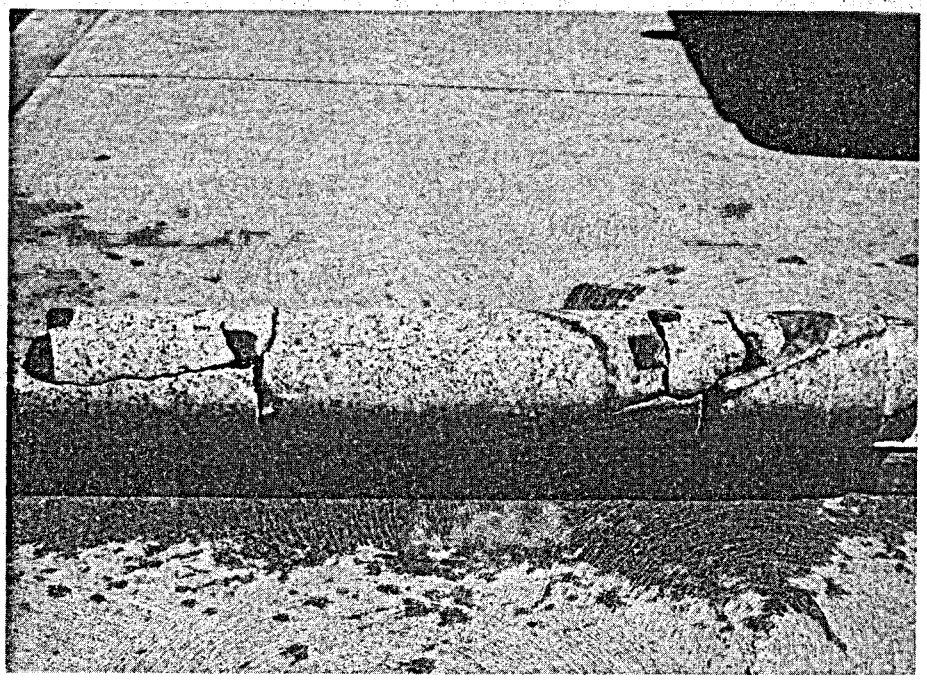

FIGURE C.15 Core 9 0 in.-34 in. 0° Rotation. Note steeply dipping parallel veins. One is filled with massive $Si0_2$ material, probably opal.

FIGURE C.16 Core 12 30 in.-62 in. 0° Rotation. Note two major fracture sets, one normal to the core axis, one steeply dipping.

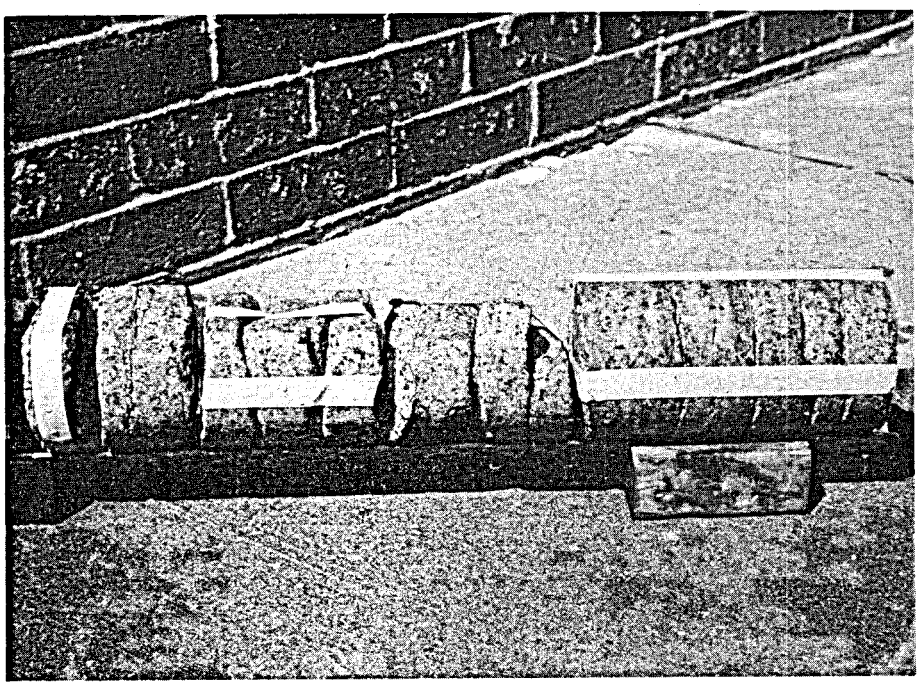

FIGURE C.17 Core 13 Selected Pieces. Note two major fracture sets; one normal to the core axis is easily discernable. Obviously open at depth. Some surfaces show slickensides. Another steeply dipping set is visible. Rock is unweathered quartz porphyry granite.

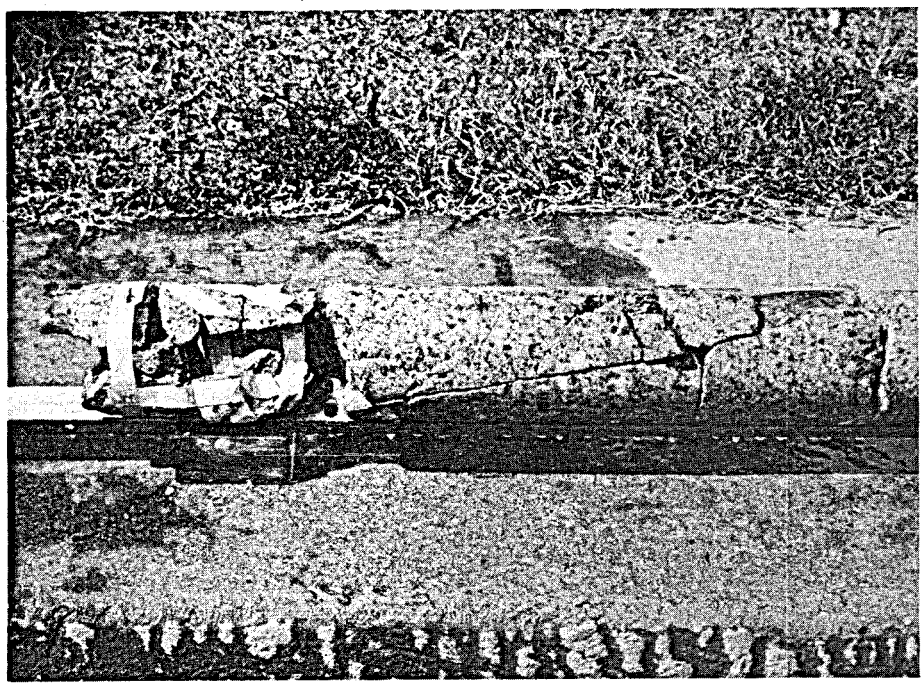

FIGURE C.18 Core 14, 30 in.-60 in. 90° Rotation. Two Distinct Fracture Sets Observed in Cores 12 and 13. Also a less well-defined steeply dipping set whose plane normal is the same as the more defined set. Highly broken up section is from end of the core and was removed from the slips with a sledge hammer.

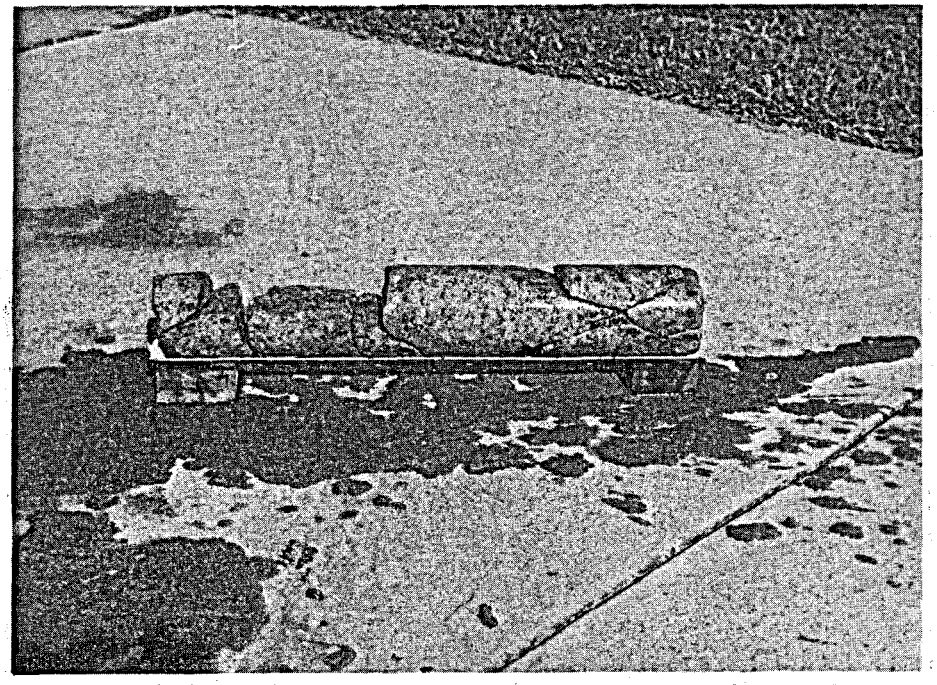

FIGURE C.19 Core 15 0 in.-23 in. 0° Rotation. Shows the Two Steeply Dipping Fracture Sets

CORE FRACTURE ANALYSIS

During the documentation and reconstruction of the cores, the fractures and veins were analyzed and described. The detailed results of this analysis are contained in Appendix C.1.

A general description of each core was made from the hand specimen. This description is given as an introduction to the section on the fractures and veins in the Appendix. The fracture and vein types were catalogued for each core in order to systemize the analysis. Each piece was labeled (as described in the documentation section) and marked at 1 in. intervals along the arbitrary "north" line.

The core pieces were then put singularly or in a small number into a Christensen goniometer. This enabled one to measure the strike, dip and dip direction of all the prominent fractures and veins. The distance at which the top or bottom of the vein intersects the core was also noted (+ sign for top, - sign for bottom). This permitted a complete description of the fractures and veins and, when correlated with the photographs, provided a complete record.

In general all the cores were highly fractured and had a large number of veins. This was especially true in the Empire shale. Here, the cataloguing and analysis was quite tedious and time consuming. This problem was aggravated by the fact that the core recovery was 10 ft for the upper cores

while it was much less for the deeper cores. Because of time limitations, the fractures and veins in Core 4 were not analyzed; however, Core 4 is quite similar to Core 3, and both are from the Empire shale.

RESULTS

The initial plan was to go through an exhaustive series of analyses of the fractures and veins. This would have been of value for the hot dry rock development plan. When the geothermal system was found to be water dominated, this analysis would have still been valuable in understanding the fluid flow. However, because of time and funding limitations, the analysis was done only in a qualitative way. These qualitative results are important and, when combined with the dipmeter log information, suggest a quantitative interpretation that helps to understand the hydrothermal system present at the Marysville geothermal anomaly.

All the cores show very steeply (45° to 70°) dipping veins. These veins often appear as two distinct sets with their poles contained on a plane normal to both sets. In the Empire shale the sets are not tight, i.e., the strike varies considerably about the mean, while in the porphyry the strikes appear to be less variable. Cores 2, 3 and 4 show the Empire shale dipping about 20° to 40°. Below 4000 ft all the cores show a pronounced set of fractures that are normal to the core axis.

Since the cores were unoriented, it was hoped that the use of surface measurements, dipmeter results and the goniometer analysis would result in a suggested orientation of some of the cores. Time and budget constraints have prevented such analysis.

Core 2 shows a large number of indications that the Empire shale has a 305° strike and 35° dip to the west. Since the strike is arbitrary in the cores, we might correlate it with the surface geology observations of a generally westerly dip and north strike.(1) This amounts to a rotation of about 55° of the core axis to bring it into alignment with the surface data.

The hand calculated dipmeter results show steep major dips to the southwest and less frequently to the northwest in the bottom half of the Empire stock (see section on logs). George Coates (Log Data Evaluation Section) has also reported that the hand calculations produced some results with 10° to 15° dip to the southeast for the lower Empire stock. The cores showed many fractures normal to their axis in this part of the hole. The cores, however, were 7° from vertical at 4500 ft, and this gradually increased to 15° at TD (6790 ft). All during this time the hole azimuth was bearing at 295° ± 5°. If one correlates this with the known tendency of the hole to drill normal to the bedding (i.e., fractures), we can then start to orient the bottom cores as to N-S. If one correlates the set of steeply dipping fractures

(1) Marysville, Montana Geothermal Project, "Geological, Geophysical Exploration at Marysville Geothermal Area, 1973 Results."

observed in the cores* with the hand calculated dipmeter results, it is possible to infer an orientation. While these results are by no means conclusive, there is a certain consistency that suggests our consideration. Our inference is that the fractures normal to the core axis dip 7° to 15° at 110° true bearing and the major steep set dips at about 225°.

* The two sets were evident; however, one set was present much more strongly than the other set.

APPENDIX C.1

FRACTURE NOTES

CORE 1

325 to 335 ft, Feldspar porphyry dike or sill

Large numbers of 1 to 5 mm anhedral to rounded feldspar crystals in a dark groundmass, highly banded with dark material. At bottom of core, dark minerals alter to greenish material (chlorite). Many veins consist of thin and wide microcrystalline quartz, often with dark alteration bands; calcite or calcite plus fluorite; or thin streaks of dark material. Most have high dips. There is no obvious preferred orientation, but some of the filled fractures become vertical, especially near the bottom of the core. Several dark zenoliths (1 to 2 cm) are found near the top.

The major scribe line has been rotated slightly between some sections of the core, indicating fracture and break up during the coring. Some veinings are completely closed with a smooth coring surface; others show grooves in the coring surface, indicating a tendency to weakness. Truly open fractures are not apparent, but open spots are evident along some solution-filled cracks. Several episodes of induration are indicated with offset along pre-existing filled veins.

FRACTURE TYPES

1. Thin, dark veins, little or no parting, branching and irregular
2. Wide quartz-microcrystalline and gray
3. Thin quartz-microcrystalline and gray
4. Partings (contain calcite)
5. Calcite and fluorite filled, 5 to 10 mm wide, near vertical

FRACTURE NOTES

Core 1, Piece #1
Length 22 1/2 in., Diameter 4 in.

Location Inches	Strike	Dip	Dip Direction	Type	Notes
-29*	52°	60°	142°	2	6 mm wide.

* means bottom point of vein or fracture.
No sign means top point

A series of partings emanating from the top of the core 1 in. with a strike of 130°, very steep dips. Some are well cemented with quartz (called foliation parting).

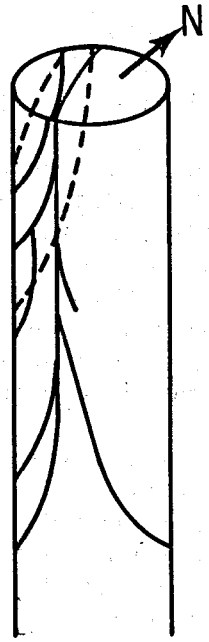

SKETCH 1

Location Inches	Strike	Dip	Dip Direction	Type	Notes
--	125-135	75-90	215°	3-4	About 6 partings
--	125-135	75-90	20°	3	Only 1 to 2 partings
1.2	160°	28°	250°	1	
0.9	175°	23°	265°	1	
2.0	165°	50°	255°	1	
4.1	245°	10°	335°	1	
7.7	193°	30°	283°	1	
10.9	48°	52°	138°	1,4	Combination, some quartz.
13.1	271°	40°	1°	1-4	
12.1	45°	60°	135°	3	Offset by above fracture.
11.9	275°	54°	5°	1-4	
18.3	42°	38°	135°	4	
17.8	208°	42°	298°	1	

A distinct parting with strike at 32°, dip angle 230° and dips 90° to 45° ending in rock and other fractures at about 12 in.

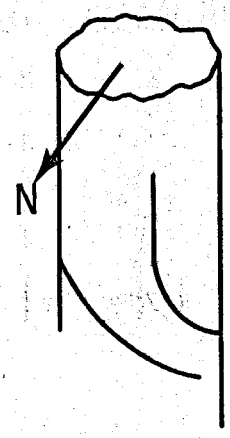

SKETCH 2

Many other less defined indurated veins exist.

Location Inches	Strike	Dip	Dip Direction	Type	Notes
22.3	56°	18°	146°		Broken fracture between #1 and #2.

Core 1, Pieces #2, 3, 4
Length 22.8 to 28.3 in. along true "N" line. N scribe mark rotated to 5°.
This was determined by fitting #2 into #1. #3 chloritized.

Location	Strike	Dip	Dip Direction	Type	Notes
24.4	10°	40°	100°		Fracture between #2 and #3.
27.9	354°	8°	86°		Fracture between #3 and #5.
23.5	120°	80°	210°	4	Fracture between #3 and #4, some pieces missing.
Core 1, Pieces #5, 6					
-29.0	195°	20°	285°		Breakoff between #5 and #6 seems to end at break between #4 and #6.
-32.5	182°	65°	272°	4	

The above is part of a series of the foliation partings (as above). Another parting is:

-35	150°	85°	260°		
31.4	35°	62°	125°	2	5 mm thick.
34.6	47°	45°	137°	3	1.5 mm thick.
37.3	273°	10°	3°	3	0.5 mm thick.
30-42	308°	80-90°	220°	4	Side parting at 220°.
41.2	15°	53°	107°	3	Offset by next vein.

Location	Strike	Dip	Dip Direction	Type	Notes
39.3	165°	50°	225°	3,4	Top 1" dips at 80°.
42.7	175°	58°	265°	4	
45.2	203°	46°	293°	4	
45.0	121°	65°	211°	4	
47.6	71°	55°	161°	1	
52.7	59°	53°	149°	1	Extends into #7.
54.8	48°	55°	138°	3	Goes into #7.
52	180°	60°	270°	4	Break between #6 and #7. Another subparallel but unbroken fracture exists about 1/2" higher and 190° strike.

Core 1, Piece #7
Length 55.8 to 68.9 in. along true "N" line

58.6	208°	35°	298°	1	
60.4	242°	38°	332°	1	2-3 mm wide.
66.0	15°	70°	105°	2	Extends into #8.
63.3	115°	70-80°	205°	4	Extends into #8.
60.5	115°	80-90°	205°	4	Extends into #8.
64.3	225°	35°	345°	1	
65.2	255°	35°	345°	1	Close to above.

Several other (partial) near vertical partings exist, strike approximate N-S.

Core 1, Pieces #8, 9
Length 69.2 to 97.0 in. along true "N" line

N scribe rotated -40° from original scribe. This was determined by 66.0 in. quartz vein plus several other minor fracture lines. Apparently 0.3 in. of core lost.

Location Inches	Strike	Dip	Dip Direction	Type	Notes
80.8	350°		42°	80°	Smeared out.

This particular piece starts the greenish apparently chloritized section which has a new type (5) veining, wide (several mm) with calcite plus fluorite. This veining is essentially vertical and has about 90 to 120° strike. The fluorite appears to be later than the calcite, as it is in the center, sometimes enclosing small calcite particles, sometimes in contact with enhedral calcite grains and sometimes cutting the calcite. Much pyrite throughout. Some pyrite in the center of calcite (as fluorite is).

A series of type 5 (2-4 veins)

Location Inches	Strike	Dip	Dip Direction	Type	Notes
78-81	115°	60-90°	205°	5	Exiting bottom of #7.

The top 10 in. of #7 contains a series of discontinuous fractures randomly oriented.

90.5 and 93.5	110°	80°	190°	5	Two veins extend out bottom.

The calcite-fluorite vein appears to be part of a larger system which has chloritized steeply dipping several inch-wide band in the dike rock. They are definitely later than the 80.8 quartz vein, as it is offset in several places by the calcite-fluorite veins.

Core 1, Piece #10
Length 97.0 to 109 in.

N scribe rotated approximate 35° to the original N scribe. The series of type 5 veins (3-4) extending from #9 continue through #10 and are the major veinings. The strike is still between 100-115°. The dips are about 80 to 90° with the dip direction 190°. This is accompanied by a 2 in. band of greenish alteration (chloritization?). Other veins are evident but they are much less distinct than the above. The high angle dip parting (type 4) seems to have been replaced by type 5 in the lower core section.

Location Inches	Strike	Dip	Dip Direction	Type	Notes
99.7	50°	70°	140°	1	
103.3	237°	38°	327°	1	

A partial vein (1) at 105.7 in.

Core 1, Piece #11
Length 109.1 to 119.0 in.

N scribe rotated -33° from original N scribe. The type 5 veins have now changed strike to 95° and 3 major veins are extending from above into this piece. Their thickness has reduced to 2 to 3 mm.

Location Inches	Strike	Dip	Dip Direction	Type	Notes
113.4	43°	63°	133°	3	
--	177°	57°	267°	4	Extends from top center, no real definite bottom.
115.8	2°	50°	92°	1	

Bottom of core shows no definite planar breaking surface.

CORE 2

437 to 447 ft, Empire shale

Black to dark green color near top, with more buff color near bottom. The very top piece shows that the core barrel not centered when it was first run.

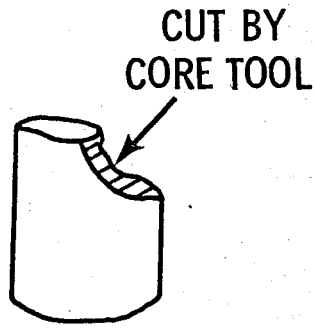

SKETCH 3

The core "appears" to have a "bedding" of about 45°, but it is difficult to be certain because of coring marks. Need to cut and polish the core to be certain. There is a distinct set of filled fractures sub-parallel to this and normal to this. Most of these fractures are filled with 1 to 2 mm wide calcite. One of the apparent bedding fractures (calcite-filled) has slickensides. If dip is to the west, keying of the "fault" suggests a strike or lateral movement to the north. There is another set of veins that are almost vertical and are calcite- and fluorite-filled. These are similar to type 5 in the first core. Most of the veins branch in many directions.

FRACTURE TYPES

1. Parting
2. Small calcite-filled veins
3. Large calcite-filled veins

4. Not used

5. As in Core 1

FRACTURE NOTES

Core 2, Pieces #0201, 0202
Length 0201 - 0 to 4.5 in.
0202 - 4.5 to 10.6 in.

Location Inches	Strike	Dip	Dip Direction	Type	Notes
0.1 - 1.5	211°	60 - 90°	301°	5	Several 1 mm veins coalescing into large vein at 90° dip, 5".
--	259°	90°	--	5	Vertical fracture ~1" in from 349° coalescing with above.
4.9	5°	59°	95°	1	
All down the core	320°	45°	50°	--	Bedding (a series of essentially parallel slightly darker lines.
4-6	155°	55°	245°	2	A series of fine fractures (1/2 mm) may be related to 0.1" to 1.5". Fracture extends into #0203.
7.9	63°	75°	153°	2	

Core 2, Pieces #0203, 0204
Length 0203 - 10.8 to 14.3 in.
0204 - 14.3 to 15.4 in.

13.5	9°	40°	99°	2?	Break between #0203 and #0204 has slickensides.
1-1/2" in on top	38°	70-80°	128°		Extends into next section.
11.5	358°	58°	88°	2	A couple of others 2" to 3" higher.
-15.5	334°	57°	64°	2	Extends down to #0210; probably connects with big vertical fracture.
12.8	103°	80-90°	193°	5	

Core 2, Pieces #0205, 0206, 0206a, 0207, 0208
Length 16.5 in. to 22.5 in.

This section contains a series of broken small pieces; #0208 is the largest. The section begins with the fracture between #0204 and #0205 which shows some slickensides with approximate strike slip striations on #0204. The corresponding parts appear to be missing on #0205.

Location Inches	Strike	Dip	Dip Direction	Type	Notes
13.7	5°	57°	95°	2?	Break between #0204, #0205.
16.9	275°	36°	5°	?	Break between #0206, #0207.
18.0	356°	48°	86°	2	
17.9	126°	80°	216°	5	Start of big vein extending into #0214.
	85°	75-90°	175°	2	From #0204.

Core 2, Pieces #0210, 0211
Length 22.5 to 30.0 in.

The surface between #0210 and #0211 shows good slickensides with distinct strike-slip striations with the last movement, apparently right lateral. This was deduced from keying of the pieces plus calcite filling a void left by the movement. The movement is difficult to verify by offset of any fractures.

Location Inches	Strike	Dip	Dip Direction	Type	Notes
	100-110°	85-90°	195°	5	Big one from above.
	75°	85-90°		2,5	From #0204.
22.5	295°	53°	215°	2?	Fault between #0210, #0211.
25.0	158°	62°	248°		
23.7	111°	60°	201°	1	
25.5	120°	60°	210°	1	
--	105°	50°	295°	2	Coalesces with big vein at 25.0" at 315° and 23.5".

The pieces contain many other small fractures of widely varying orientation. There is one fairly significant piece missing at 90° (1/4 in. thick) from #0211. There appears a series of sub-parallel dark veinings to the break between #0210 and #0211.

Core 2, Piece #0212
Length 30.0 to 37.9 in.

This piece has the veins coming in from above at steep dip (e.g., big one) 25.0 in. (62° dip and 75° strike). These have branchings and offshoots. There appears a general trend of color banding and minor fractures with strike 295°, dip direction 25° and dip 45° ± 15°.

Location Inches	Strike	Dip	Dip Direction	Type	Notes
-32.4	297°	27°		1,2	Coalesces into big vein.
-34.3	297°	27°		1,2	Dip variable, coalesces into big vein.
--	Rear vertical #2 veining at 35.4" and 45°, surface a continuous saw tooth type 2 extension of -32.4" from about 31.5".				

Core 2, Pieces #0213, 0214
Length 0213 - 37.9 to 41.1 in.
0214 - 41.1 to 46.6 in.

Rock continues to show general 300° to 313° strike, 30° to 45° dip, of color bands and some thin dark and/or calcite-filled veins.

Location Inches	Strike	Dip	Dip Direction	Type	Notes
38.0	121°	63°	211°	2	
38.5	121°	60°	211°	2	
38.9	0°	40°	90°	2	
39.7	15°	70°	105°	1	
	Dip becomes 85° at 41.0"				
	Strike has 20° component also, which is break between #0213 and #0214.				
38.4	10°	20°	100°	2	5 mm wide, offset by a thin vertical fracture.

Big calcite fluorite veining from above ends at 44.5 in.

Core 2, Pieces #0215, 0216
Length 0215 to 49.7 in.
0216 to 55.7 in.

49.2	135°	43°	225°	2	Break between #0215, #0216.
48.2	135°	67°	225°	1	Partial 2 ends at above.
50.6	136°	53°	226°	3	5 mm wide, has parting in center.
48.4	298°	48°	28°	2	
49.7	295°	41°	25°	2	
52.3	303°	51°	33°	2	
53.1	303°	51°	33°	2	Goes into #0217, #0218.

Several other partings exist with similar strikes and dips to above two fracture sets. The general rock dip direction seems to be 40°.

Core 2, Pieces #0217, 0218, 0219
Length 0219 - 57.0 to 60.5 in.
0217, 0218 - Smaller with #0217 about 1-1/2 in.
Broken--pieces missing
End of #0219 are ground off, not vein fractures.

-60.0	293°	60°	23°	3	Goes into #0217, #0216.

There are several type 1 fractures parallel to this in a 203° direction beginning 1 in. away. The piece shows a couple of type 2 vertical fractures.

Core 2, Pieces #0220, 0221
Length 0220 - 60.7 to 67.2 in.
0221 - 67.2 to 68.5 in.

Has 60° dip fracture that extends it to 71 in. There is a piece missing from dip to #0222 at 71 in. These two pieces fit together, but the break between #0219 and #0220 does not permit orientation with the rest of the core. I have oriented them by the slight indication of a general bedding trend and type 1 fractures of the whole core.

Vertical fractures (2) approximately 320° strike in middle of #0220 extending to 62 in.

Location Inches	Strike	Dip	Dip Direction	Type	Notes
61.9	37°	69°	127°	2	Becomes diffuse, ends at #0221.
65.0	313°	45°	43°	3	Extends beyond #0221.
63.3	296°	52°	26°	2	Several small fractures coalese with 65.0".
65.0	206°	72°	296°	2	
68.0	130°	56°	220°		Break at end of #0221.
62.3	237°	68°	327°	2,3	

Core 2, Pieces #0222, 0223
Length 71.0 to 82.3 in.

These two pieces contain a large number (approximately 50) of type 1 fractures, all with 305° strike, 35° dip directions and approximately 40° dip. The alignment between these rocks and #0221 is tenuous at best and based mostly on these fractures.

-82.2	224°	78°	314°	2	1 to 2 mm wide vein.
74.3	243°	50°	333°	2	
76.8	205°	48°	295°	2	Break between #0222, #0223.
78.5	278°	45°	368°	2	Coalesces with -82.2".
72.5	123°	79°	213°	2	

Core 2, Piece #0224
Length 82.7 to 92.7 in.

Has about a dozen of type 1, strike 307°, 37° dip direction, 40° dip.

83.6	100°	60°	190°	2	
87.5	3°	70°	93°	2	
88.0	263°	80°	353°	2	Extends only 2".
88.3	257°	56°	347"	2-3	Extends into #0224. Has been offset.

At 120°, #0224 has type 3 vein from top to 85 in., with an 85 to 90° dip. This does not show in #0223.

Core 2, Piece #0225
Length 92.8 to 100.5 in.

This piece is oriented by a major calcite-filled vein, 2 cm thick, containing fluorite.

Location Inches	Strike	Dip	Dip Direction	Type	Notes
93.0 (top)	192°	69°	282°	--	Major vein.
97.5	295°	58°	20°	2	Goes through major fracture.
95.3	285°	73°	15°	2	Very thin. Extends through major fracture.

This piece also has several other minor veinings.

Core 2, Piece #0226
Length 100.8 to 107.0 in.

The end of the above major fracture goes out of this piece; also the 97.5 fracture forms the top, and a section between # 0225 and #0226 is missing there. This piece has two major calcite-fluorite veinings not parallel to above, one about 1 cm wide, the others just visible at the very bottom of the piece and probably 2 to 3 cm wide.

Location Inches	Strike	Dip	Dip Direction	Type	Notes
101	315°	65°	45°	--	1 cm wide, major fracture.
-108	23°	63°	113°	--	

CORE 3

18 pieces, 120.9 in.

The core is in excellent shape, with almost no missing or badly broken up sections. There appears to be vein material missing between #0308 and #0309. This has made reconstruction of the core difficult at that point since the vein may have been 1/2 in. thick (similar to #0312). However, reconstruction of the core shows no rotation of the knife edge grooves, suggesting that no rotation occurred here either. The matching of structural evidence on both sides of the boundary is consistent with this reconstruction.

FRACTURE TYPES

The core has the following easily identifiable fracture types--using the major knife edge as north:

1. Steeply northeast dipping, with very thin (1/2 mm) vein of calcite (?) or quartz (?) showing pyrite. There is a distinct dark alteration zone around the vein.

2. Not quite as steeply northeast dipping quartz veins. These are wider than above (up to several mm) and generally show little or no alteration zone. May have thin calcite layer between it and shale.

3. Wide (1 cm) veins of calcite quartz, fluorite, pyrite, chlorite, and a white fibrous material. The white fibrous mineral makes up the contact with the shale and is layered with some of the chlorite. Northwest dipping and about 120° angle with type 2.

4. These are not really identifiable fractures but are the general trend of the breaks between core pieces. These form a shallow ($\sim$ 20°) dip to the southwest. The surfaces appear to be shale. This dip follows the general trend found in the color banding of the core and suggests a general formation dip. This is definitely shallower than the inferred dip from Core 2.

5. A few only, green color banding, 1 mm thick, no alteration outside.

FRACTURE NOTES

Core 3, Pieces #0301, 0302
Length 0 to 10.3 in.

Location Inches	Strike	Dip	Dip Direction	Type	Notes
1.8	43°	74°	133°	2	
7.3	320°	75°	50°	2	End in #0304, thickness varies.
--	75°	80°	165°	2	Enters at center top #0301.
0.5	333°	67°	63°	1	Four closely spaced.
1.0					
1.2					
1.3					
5.7	350°	68°	80°	1	
6.0	347°	65°	65°	1	Three closely spaced.
6.5					
7.3					
-7.5	355°	67°	85°	1	
-3.3	347°	75°	77°	1	
--	160°	50°	250°	1	There are 3 to 4 similar partial parallel fractures in 1" above.
-3.1	227°	50°	317°	2	
6.0	165°	20°	255°	4	Between #0301, #0302.
9.3	189°	22°	269°	4	Between #0302, #0303.

Core 3, Piece #0303
Length 10.3 to 22.6 in.

Location Inches	Strike	Dip	Dip Direction	Type	Notes
10.8	351°	71°	81°	1	Top in #0302, branches to at least two more fractures.
12.0	345°	70°	75°	1	Top saw toothed.
13.8	334°	70°	65°	1	
13.8	325°	70°	55°	1	
16.0	323°	65°	53°	1	
#0303 shows a series of faint cracks with	180°	25°	270°	--	
The rock shows several nonplanar irregular 2 veins.					
20.4	334°	70°	64°	1	
The piece has many other small veins (type 1).					

Core 3, Piece #0304
Length 22.6 to 38.9 in.

24.9	172°	start=55° most=70°	262°	5	
25.8	330°	81°	60°	1	

This piece also has several irregular type 2 veins nearly vertical (dips 75° to 85°) with the general 330° strike, e.g., one starts in #0303.

17.5	3°	80°	93°	2	
29.5	330°	80°	60°	2	
22,22.5	338°	74°	68°	1	Starts in above piece.
30.4	0°	55°	90°	1	
27.8	163°	15°	253°	4	Dark lineations.
25.4	163°	32°	253°	4	Dark lineations.
-37.2	333°	~75°	63°	1	
22.3	190°	20°	280°	4	Break between #0303 and #0304.

This section has a great number of other partial fractures of various orientations (mostly type 1) that are too varied to itemize.

Core 3, Pieces #0305, 0306
Length 38.9 to 48.3 in.

Location Inches	Strike	Dip	Dip Direction	Type	Notes
39.5	340°	83°	70°	1	
41.0	325°	75°	55°	1	
38.5	180°	15°	276°	4	Break between #0304, #0305.
38.5	235°	70°	325°	5	Starts in #0304.
42.5	161°	15°	251°	4	Break between #0305, #0306.
45.9	19°	75°	109°	1	

The type 2 vein from #0304 extends through these two pieces.

Core 3, Piece #0307
Length 48.3 to 60.6 in.

47.7	177°	14°	267°	4	Break between #0306, #0307.
50.2	26°	75°	116°	2	2 mm wide.

The long type 2 vein from several pieces up ends in #0307 at 54 in. at 260°.

51.5	332°	75°	62°	1	2 type 1.
and 52 52.5	66°	82°	156°	2	Disappears at about 57".

A fracture starting at 31.2 in. in #0304 exits #0307 at 61 in. It bows into the middle of the core and is type 1 with areas of distinct white veining, strike 290°, enters and leaves rock at 180°. Many other type 1 trends.

Core 3, Piece #0308
Length 60.6 to 67.7 in.

61.1	83°	80°	173°	1	
--	330°	85 to 80°	60°	1	Starts at 58" in the middle of #0307.
-66.5	358°	78°	86°	1	Branches off at 57" in the middle of #0307.
-62	0°	75°	90°	1	Has connecting loop with 66.5".
60.1	170°	28°	260°	4	Break between #0307, #0308.
66.8	152°	35°	242°	-	Break on bottom of #0308.

The space between #0308 and #0309 is probably a type 3 fracture with the piece missing.

Core 3, Pieces #0309, 0310, 0311, 0311a
Length 0309 - 68.0 to 72.7 in.
0310 - 72.7 to 76.3 in.
0311, 0311a - 76.3 to 77.0 in. fits between parts of 2 fractures.

Location Inches	Strike	Dip	Dip Direction	Type	Notes
67.3	128°	28°	218°	--	Top of #0309.
-73.4	328°	50°	58°	2	3 mm wide, ends at top of #0309.
--	337°	60°	67°	2	Second branch 2" below.
72.3	166°	6°	256°	4	Break between #0309, #0310.
70.3	349°	63°	79°	1	
70.3	349°	74°	79°	1	Second radiating fracture.
74.2	172°	58°	262°	3	Contact between #0310, #0311, #0311a, and #0312.
-77.5	186°	24°	266°	4	Break between #0310, #0311, and #0311a ends at 74.2" fracture.

There are a whole series of type 1 fractures extending through #0309 and #0310 with 70° dips and 100° strike. These have no definite beginning or end. There are numerous other fractures (types 1 and 2) in the section.

Core 3, Piece #0312
Length 1 cm

This is the type 3 vein between #0313, #0311 and #0310.

Core 3, Piece #0313
Length 77.7 to 80.3 in.

Location Inches	Strike	Dip	Dip Direction	Type	Notes
-77.9	355°	60°	85°	2	Ends at #0313.
79.4	180°	30°	270°	4	Break between #0313, #0314.

Core 3, Piece #0314
Length 80.3 to 95.7 in.

81.7	116°	54°	206°	2	
83.7	165°	20°	255°	4	No break.
86.3	354°	59°	84°	2	Ends at fracture below.
88.2	7°	48°	97°	2	

There are a series of type 1 fractures with 60° dip, strike ~0° and 90° dip direction starting in middle of top of the piece.

Location Inches	Strike	Dip	Dip Direction	Type	Notes
89.0	2°	60°	92°	1	Two ~1/2" apart.
87.8	238°	81°	378°	2	Extends through #0315-end of core.
90.5	225°	80°	315°	1-2	
93.0	357°	55°	87°	2-3	

Both #0314 and #0315 have apparent bedding dips of 30° and strike 164°

Core 3, Piece #0315
Length 95.7 to 109.8 in.

95.4	343°	50°	73°	2	
--	165°	31°	255°	4	Many bedding lines on piece.
108.1	170°	20°	260°	4	Break between #0315 and #0316.

Core 3, Pieces #0316, 0317, 0318
Length 110.0 to 120.4 in.

107.5	193°	50°	273°	1
103.5	105°	49°	195°	2
103.5	150°	58°	240°	2

CORE 4

921 to 931 ft, Empire shale

The core is quite similar to Core 3 in most respects. The color is black-green at the top, grading into dark browns and back to blackish green near the bottom. The general dip shows as very thin dark lines or color banding. The dip angle appears to be 20° to 30°. Side by side comparison with Core 3 shows the dip of Core 4 to be greater. The type 1 fractures of Core 3 are only occasionally evident. There appears to be three additional sets of veining, one nearly vertical, and the two ≃ 60° dip with a 180° different dip directions. The large veins appear to be fluorite free in contrast to Core 3. The fractures between pieces generally do not have the same dip and strike of the bedding. Fracture types will be the same as Core 3 except for the absence of fluorite in type 3 (quartz-calcite-pyrite + unidentified white mineral assemblage). Because of the similarity between cores and the time limitations, this core was not analyzed.

CORE 5

997 to 1007 ft, quartz porphyry

This core shows several stages of fractures and veins. The earliest appears to be the dark bluish green ones which vary in thickness from very few mm to 50 mm. There are later quartz veins and then fractures which have alterations. Some are nearly vertical and others about 30° from the vertical. There are many veins of vertical and 30° from vertical which do not show up well unless the rock is wet. These have a pinkish alteration zone around them. There appears to be a large number of veins and fractures.

FRACTURE TYPES

1. Narrow fracture surface alterations.
2. Quartz-filled.
3. Greenish-bluish alteration zones from porphyry-quartz appear to have not altered various widths.

Core 5, Pieces #0501, 0502
Length 0.0 to 7.0 in.

Location Inches	Strike	Dip	Dip Direction	Type	Notes
-4.5	315°	60°	45°	1	Break between #0501, #0502.

Core 5, Piece #0503
Length 7.0 to 12.3 in.

There are two 90° dip fractures (entering from above and below) near mid-rock, one at 70° strike, the other at 90°. The 70° appears to be quartz-filled. The 90° appears to be solution altered, type 1.

Core 5, Piece #0504
Length 12.3 to 28.5 in.

The 70° strike vein gradually turns away from 90° dip. The 90° strike vein (270° also) changes to 315° and decreases dip exiting at 23.5 in.

Location Inches	Strike	Dip	Dip Direction	Type	Notes
12.3	50°	45°	140°	3	2 mm wide, displaced by 70° strike vein.
13.1	42°	50°	132°	3	2-3 mm wide, goes only part way through rock.

Location Inches	Strike	Dip	Dip Direction	Type	Notes
15.8	44°	45°	134°	3	25 mm wide cut by both 70° and 90° veins, offset by 70° 12 mm.
23.0	218°	53°	308°		Greenish alteration, offset by 70°.
-23.5	311°	70°	41°		90° one from above.

Core 5, Pieces #0505, 0506, 0507, 0508
Length 0505 - 28.5 to 33.5 in.
0506 - 33.5 to 38.2 in.
0507 - 38.2 to 43.4 in.
0508 - 43.4 to 50.6 in.

-49.3	268°	67°	358°	1	

Near vertical crack at 190° strike.

#0509 - Number not used.

Remainder of core not analyzed.

CORE 6

10 pieces, 68 in., 1524 to 1529.8 ft, grey quartz feldspar porphyry.

Quartz phenocrysts 3 to 10 mm with rounded and sharp orthoclase phenocrysts ≈ 3 to 10 mm are dark pinkish except in the top 5 in. where they are very light pink. The surface of the core is sparsely pockmarked with what appears to be kaolinized feldspar (plagioclase ?). Much of the plagioclase is altered as is some of the orthoclase. The breaks between pieces are essentially horizontal. This corresponds to the major mineralization (pyrite plus quartz and molybdinite). Some steeply dipping fractures and veins are present. There does not appear to be any offset of veins. It seems likely that the fractures were made after vein (filled fractures). This core does not have the well healed pink veins in Core 5 that appear on wetting.

FRACTURES TYPES

1. Near horizontal vein of pyrite plus quartz and molybdinite.
2. Near horizontal vein of fractures, very slight rust alteration.
3. Steeply dipping vein of pyrite plus quartz and molybdinite.
4. Steeply dipping fractures, very slight rust alteration.

Core 6, Pieces #0601, 0602, 0603
Length 0601 - 0.0 to 6.7 in.
0602 - is side of #0603.
0603 - 6.7 to 11.0 in.

Location Inches	Strike	Dip	Dip Direction	Type	Notes
-2.7	132°	85°	222°	-	3 mm wide, chlorite and pyrite and others, vein only one in this core.
(-14.0)	305°	81°	35°	4	Starts in middle of top of #0301. It is the break between #0302, #0303.
-	-	-	-	4	Rear vertical 3/8" in at 240°. Only evident on break between #0601, #0603.
6.3	82°	11°	172°	2	
-14.0	Rotates from 305°-290°	85°	35°	4	
14.7	105°	85°	195°	4	
10.3	130°	10°	220°	2	Break between #0603, #0604.

Core 6, Piece #0604
Length 11.0 to 20.9 in.

18.0	200°	55°	290°	-	Very thin fracture.
20.2	325°	5°	55°	1	Single vein branches into 4 in one spot.

Core 6, Piece #0605
Length 20.9 to 34.7 in.

Location Inches	Strike	Dip	Dip Direction	Type	Notes
20.4	68°	20°	158°	2	Break between #0604, #0605.
32.2	125°	70°	215°	4	Goes into pieces below.
-	193°	85°	-	4	Makes a scallop at 103° - 1/4" into core.
27.5	220°	5°	310°	1	
	-	≈0°	-	1	Break between #0605, #0606.

Core 6, Piece #0606
Length 34.7 to 45.0 in.

38.7	180°	10°	270°	1	Extends from 330° to 150°, ends at steep fracture.
37.2	-	≈0°	-	1	Ends at 32.2" fracture extension, on 220° side.
-	≈300°	85°	30°	3	Ends at 32.2" fracture. Goes into pieces below.

Core 6, Pieces #0607 and #0610 (out of order)
Length 0607 - 45.0 to 48.9 in.
0610 - 48.9 to 53.9 in.

The ≈300° strike vein from above (≈310° in these pieces) dominates #0607 and #0610. The side veins are generally stopped at the fracture into east and west side.

Location Inches	Strike	Dip	Dip Direction	Type	Notes
47.8	-	0°	-	1	East side, very thin.
47.4	64°	18°	154°	1	West side, very thin.
48.3	276°	8°	6°	1	2 mm wide, west side.
48.9	93°	≈10°	183°	2	Break between #0607, #0610.
≈49	-	≈0	-	1	Both sides 2 mm thick, some branches.
52	-	≈0	-	1	Both sides 2 mm thick, some branches.
52.7	19°	160°	109°	1	Both sides 2 mm thick, some branches.

These last three contain numerous branches with vertical and high angle connections.

(-58.8)	130°	61°	220°	3	Ends in #0608, west side only.
53.9	25°	10°	115°	-	Break between #0610 and #0608.
48.1	116°	63°	206"	3	Ends at ≈49" vein.

Core 6, Piece #0608
Length 53.9 to 62.5 in.

-60.8	129°	52°	219°	3	West side has flat branch at 58.5".
57.0	-	-	-	1	North appears and ends at -60.8" vein.

Near vertical fracture from above ends at ≈57".

61.7	0	20°	90°	1	Flattens out and becomes 5 mm wide in #0609.
61.2	163°	42°	253°	3	Goes into #0609.

A bent vein that strikes at 340° and dips ≈25° in each direction. East at -64.0 in., west at 64.8 in.

CORE 7

1936 to 1936.7 ft.

Core 7, Piece #0701
Length 7.2 in.

Rock altered from two cores above. Color very light pink orthoclase which is probably some altered grey quartz phenocrysts, some white plagioclase, and green altered plagioclase. Almost all dark minerals have been altered to greenish color (chlorite ?). Rock shows one vein, 5 mm quartz-filled at -2.3 in., 60° dip. It has greyish metallic mineralization in one part of vein. Rock also shows a broken out piece which is the result of a fracture, has 75° dip and is 90° clockwise from the vein. Top is at 3.7 in.

CORE 8

2295 to 2299.6 ft, white-grey quartz - orthoclase porphyry
Length 55.3 in.

Rock seems to be more granitic than those from above. More dark minerals than Core 7 with biotite present. Hornblende altered to chlorite, although the greenish material may be altered plagioclase and in some cases altered orthoclase. Orthoclase white with very light pink cast. Phenocryst size ≈ 3 to 10 mm. Although altered, the core is less altered than Core 7 and more than Cores 5 and 6. The core is only slightly veined and shows few fractures. The bottom of the core shows an open fracture which has a coating of calcite or quartz. There are also open voids in a few spots on the cores. The only mineralization may be with the bottom fractures as they have dark vein filling in places.

Pieces #0801 to #0808 contain ≈ 1 in. diameter regions of alteration that are different, suggesting xenoliths.

FRACTURE TYPES

1. Thin, dark, healed fracture.
2. Open and healed with larger openings filled with calcite or quartz.

Core 8, Piece #0801
Length 0.0 to 10.0 in.

Location Inches	Strike	Dip	Dip Direction	Type	Notes
2.1	325°	27°	55°	1	Has two other partial branches.

The piece contains a very thin (type 1) fracture at about 0° that does not appear to go through it.

9.8	120°	10°	210°	-	Break between #0801, #0802.

Core 8, Piece #0802
Length 10.0 to 20.2 in.

A type 1 fracture (vein) that is in #0801 becomes evident in #0802, strike = 55°, dip = 78°. It enters #0802 about middle of top.

Location Inches	Strike	Dip	Dip Direction	Type	Notes
19.2	135°	15°	225°	1	Break between #0802, #0803.

Core 8, Pieces #0803, 0804, 0805, 0806
Length 0803 - 20.2 to 21.8 in.
0804 - 21.9 to 23.7 in.
0805 - 23.8 to 27.0 in.
0806 - 27.3 to 30.0 in. although only 220° to 360° part present*

Breaks between #0803, #0804 and #0804, #0805 ≈ parallel to that between #0802, #0803, but there is no evident reason for this.

-27.0	40°	35°	130°	1

Core 8, Piece #0807
Length 30.1 to 36.1 in.

The missing piece from 240° to 360° seems to be caused by a V-shaped fracture.

Core 8, Piece #0808, Length 36.1 to 40.9 in.

Core 8, Pieces #0809, 0810, 0811
Length 0809 - 40.9 to 45 in.
0810 - 45 to 50 in.
0811 - 50 to 55.3 in.

41.0	300°	85°	45°	2

This starts out as a single fracture in #0809 but becomes several parallel fractures in #0810 and #0811 and two at the exit from #0809. These are open in #0810 and #0811. Also showing about 1 in. toward the center is a faint fracture which becomes more evident in #0810 and #0811. It does not seem evident in #0808. In #0810 these two fracture sets are subparallel, with the second one at 315° strike. Both lose dip in #0811 with the first exiting at 52.8 in. and 60° dip and the second continuing at ≈ 70° dip.

* Further reconstruction changed this.

CORE 9

2782 to 2784.9 ft, altered quartz, feldspar porphyry
Length 34.2 in.

Similar to Core 7. Has definite greenish cast with few dark minerals remaining. Feldspars are altered. It has a steeply dipping quartz-filled (4 mm) fracture that dominates. A parallel fracture is unfilled. It has a few other beaded quartz-filled fractures that are thin with larger alteration zones. Shows some horizontal fractures. No voids for fracture voids. There is pyrite in the rock and in the veins.

FRACTURE TYPES

1. Thin quartz-filled altered rock.
2. Thick quartz-filled, not as much alteration.
3. Unaltered fractures.

Core 9, Piece #0901
Length 0.0 to 8 in.

Location Inches	Strike	Dip	Dip Direction	Type	Notes
0.0	44°	58°	134°	1	Main branch.
-	61°	50°	151°		Secondary branch which circuits piece and comes out near top center. There are several parallel cracks between two branches on west side.
2.0	90°	70°		1	The big quartz-filled vein becomes part of this at 8" and this one disappears. This one joins 0.0 for a few inches in east.
3.6	80°	65°	170°	2	The big quartz-filled vein.

Pieces #0902, 0902a, 0903 extend to 10.5 in. but are broken off from big vein.

Core 9, Pieces #0904, 0904a, 0905
Length 0904 - 9.0 in. - #0904 is back part of #0905
0904a - is small 2 in. extension of #0904
0905 - 10.5 to 24.7 in.

At 9.5 in. #0904 has horizontal fracture (3). Until about 14 in., #0904 has parallel fracture (3) to big vein. There is a thin unaltered vein that crosses #0903, #0905 at 310° strike and 50° dip.

Location Inches	Strike	Dip	Dip Direction	Type	Notes
12.2	32°	50°	122°	1	This quickly separates into two fractures of unequal intensity of alteration. The second is 1" above the first and is more intense on bottom 1/2 of loop than the above.
17.0	93°	80-85°	183°	3	Becomes break between #0909, #0908.

Core 9, Pieces #0908, 0909
Length 0908 - 25.0 to 34.2 in.
0909 - fractured off at #0908

CORE 10

3312 to 3314.7 ft, length 32.0 in., grey quartz - feldspar porphyry

Not as many dark or altered dark minerals as before. Orthoclase is a very slight pink. The most obvious feature in the featureless rock is the 10 mm wide quartz veins in the upper 20 in. of the core, which are near vertical. The veining is not very planar and is quite different from that previously seen. It appears to be well bonded to the rock; the contacts are sharp and unaltered and the veins have small angular pieces of the main rock in it. In hand specimen these small inclusions do not appear altered. The core shows three major fractures all with similar strikes and steep dips (two at 60° and one at 45°); these fractures appear to be partially open. The 45° fracture is broken and shows secondary quartz, most of which appears to have grown into a void as crystal faces are evident. It appears possible to blow through the unfractured 60° crack. #1001 has an open fracture (by blowing) of at least 5 in. Other greenish alteration veins (1 to 2 mm) are evident.

Core 10, Piece #1001
Length 0.0 to 17.0 in. (V's out at end)

Location Inches	Strike	Dip	Dip Direction	Type	Notes
-4.3	152°	43°	242°	1	
4.3	285°	20°	15°	1	Has opening.
2.7	142°	52°	232°	1	
6.0	180°	26°	270°	1	All about parallel and very fine.
6.5	180°	26°	270°	1	
7.3	180°	26°	270°	1	

Two major quartz at ≈90° dip 100° strike. They stop at the +4.3 vein.

Location Inches	Strike	Dip	Dip Direction	Type	Notes
11.1	83°	58°	173°	2	Break between #1001 and #1004.

There are many other partial #1 veins throughout.

Pieces #1002, #1003 are parts of #1001.

Core 10, Pieces #1004, 1005
Length 1004 - 15.7 to 22 in.
1005 - part of #1004

19.4	83°	43°	173°	2	Break between #1004 and #1007.

There seems to be a series of open holes at 50° dip.

Core 10, Pieces #1006, 1007
Length 1007 - 21.3 to 32.0 in.
1006 - part of #1007

19.4	83°	65°	173°	2	Not broken apart, starts as above.
28.3	83°	45°	173°	?	May be type 2, only not well defined.
21.5	133°	68°	223°	1	
27.5	270°	80°	360°	2	Terminates at 19.4" - 65° dip.

CORE 11

3817 to 3822.4 ft, length 65 in., grey quartz porphyry

Plagioclase feldspars are highly altered to pale greenish chalky substance. Orthoclase whitish, looks somewhat altered, dark minerals look like biotite and hornblende, no gangue. The core appears to have a common strike and dip (≈60°) for the veins and cracks. Most veins are similar. All the breaks between the pieces are nearly horizontal, have been polished and appear to have 1/8 to 3/4 in. of material missing. This is the first time that this effect has been so pronounced in any core. It suggests that there are horizontal planes of weakness that we obliterated in the coring process.

Core 11, Pieces #1101, 1102
Length 1101 - 0.0 to 7.2 in.
1102 - 7.4 to 15.4 in.

Location Inches	Strike	Dip	Dip Direction	Type	Notes
-10.5	171°	75°	261°	1	Black line.
-10.5	171°	82°	261°	1	Black line.
-2.9	171°	72°	261°	1	Green line.
5.5	191°	63°	281°	1	Greenish black line.
7.4	200°	74°	290°	1	Black line becomes type 2 at bottom.
6.5	200°	72°	290°	1	Green.
12.5	183°	69°	273°	1	Very thin green line

There is another crack at 13 in. but only can be seen on ends.

Core 11, Pieces #1103, 1104
Length 1103 - 16.3 to 20.3 in.
1104 - 20.4 to 26.0 in.

17.8	170°	78°	260°	2	Goes to 23.0" and then exits at 20° dip.
18.8	170°	60°	260°	2	Branch loop of above.
-	188°	70°	278°	2	Comes from 17.8 at 20.0".

Core 11, Piece #1105
Length 26.3 to 34.6 in.

29.8	203°	56°	293°	1-2	Stops at about 33".
31.4	183°	56°	273°	2	Top of vein at 168° - strike from bottom.
31.8	185°	55°	275°	2	Dip flattens out to 45° in #1106.

There is a heavy mass of quartz vein similar to that found in Core 10 from 32.5 to 36 in., strike 150°, dip 83°.

Core 11, Piece #1106
Length 34.7 to 39.0 in.

34.2	189°	71°	279°	2	Starts in #1105.

Core 11, Piece #1107
Length 39.5 to 45.6 in.

Core 11, Piece #1108
Length 46.0 to 53.3 in.

Location Inches	Strike	Dip	Dip Direction	Type	Note
46.0	182°	57°	272°	1	Green line

Core 11, Piece #1109
Length 53.5 to 59.3 in.

Slight vein at 340°.

Core 11, Pieces #1110, 1111, 1112
Length 1110 - 59.4 to 61.2 in.
1111 - 61.5 to 65.0 in.
1112 - part of #1111

59.8	177°	63°	267°	-	Break between #1111, #1112, only nonhorizontal break.

CORE 12

Length 61.5 in., quartz feldspar porphyry granite

Plagioclase altered to greenish clay-like material, orthoclase pinkish, altered some. 10% biotite plus hornblende grain 8 to 10 mm. Upper 30 in. a single piece, bottom 30 in. contains two well-defined fracture sets, one horizontal, the other near vertical ≈75°. Core contains a few greenish vitreous veins, a few mm thick. These all have similar strikes (about the same as the steep fractures and dips (45°). These fractures are listed below.

Horizontal fractures at 44.0 in., 47.2 in., 48.6 in., 49.9 in., 50.8 in., 52.8 in., 54.1 *in., 55.6 *in., 57.1 *in., 58.3 *in., 60.1 in., and 61.6 in.
*These have one or two parallel fractures, close by, that extend a few inches around the circumference.

Steeply dipping fractures--two main fractures both with strike 278°, dip 75°, dip direction 80°. The dip and strike will vary over parts of the fractures. One fracture starts at 24.8 in. and ends 56.0 in. The other ends at 61.5 in. and seems to stop at #1208 near 45 in. Both fractures have regions with more than one fracture running parallel.

In the region of the horizontal fractures each piece is defined by the horizontal fractures and split by the steep fractures. Each horizontal slice is defined by a number (attached to the largest piece); the other pieces are called a, b, c, etc.

Core 12, Piece #1201
Length 30.8 in.

Location Inches	Strike	Dip	Dip Direction	Type	Notes
-3.6	330°	45°	60°		Contains brecciated rock, sharp boundaries 2 cm wide in spots, 2 mm in others.
-4.9	335°	60°	65°		Part of above.
6.0	10°	43°	100°		
24.9	310°	30°	40°		
26.4	310°	60°	40°		

Core 12, Piece #1202, 1203
Length 1202 - 30.8 to 35.5 in.
1203 - ?

Core 12, Pieces #1204, 1205
Length 35.5 to 43.9 in.

Break between #1202 and #1205, which may be a horizontal fracture.

-40.7	305°	51°	35°
-39.0	267°	32°	357°

See photographs for other pieces.

CORE 13

5270 to 5273 ft, length 36 in., quartz porphyry granite

Granite with pink orthoclase rock is only slightly altered. The core is highly fractured. Partial reconstruction shows the dominate fracture as horizontal with a frequency of about 1 in. These fractures are open when not broken. They show strictions which are along the strike of a second fracture system which has dip ~70° to 90°. Vertical fracture appears to be in the core.

CORE 14

6022 to 6026.5 ft, length 53 in., quartz-feldspar porphyry granite

Coarser grained than Core 13, especially the orthoclase. Plagioclase altered to green mineral, biotite present. The core shows an open horizontal fracture pattern and a steeply dipping fracture pattern which has the same strike and dip. The latter is probably not open. The fractures provide the break between pieces except for those pieces fractured when removing from the core barrel. This consists of the last 10 in. of the core, and

this part has only partially been reconstructed. There is a void region between #1401 and #1402 which is filled by some of the pieces - 14A, 14B, 14C, 14D, 14E. #1401 can be oriented by the near vertical fracture and should stand off several in. In view of the simplicity of the fractures and the large number of broken pieces, this rock will be photographed without turning as #12 was. Lower case letters, e.g., 1401, 1401a, have been used to denote small pieces obviously broken off a large piece. The core shows cavities which appear to be caused by gas bubbles during solidification. Quartz and orthoclase single crystals are growing into them.

Horizontal fractures - 1.6, 2.6, 3.0, 4.0, 5.5, 7.0, 8.7, 12.1, 13.2, 14.7, 15.8, 17.3, 19.8, 20.8, 22.5, 25.6, 28.3, 23.0, 32.0, 33.5, 39.5.

Near vertical fractures - same strike, dip = 75°. The ones that are not broken show rusty alteration along the core.

CORE 15

6410 to 6411.9 ft, length 23 in., quartz-feldspar porphyry granite

Coarse grained orthoclase, slightly larger than Core 14. Altered plagioclase. Miralitic cavities but not as large or as numerous as Core 14. It appears that the horizontal fractures are not present here. However, two sets of ≈60° dipping fractures exist. They make ≈60° angle with each other.

Location Inches	Strike	Dip	Dip Direction	Type	Notes
-9.1	82°	66°	172°		
-9.1	265°	72°	355°		
11.6	256°	59°	346°		

Another fracture ≈ parallel to the 82° strike is at the end of the core.

THERMODYNAMIC STUDIES

Marysville Geothermal Anomaly Thermodynamic Studies

S. D. Hays, Systems, Science and Software

Computer Simulation of Drilling Thermodynamics

C. A. Oster, Battelle-Northwest and
W. A. Scheffler, Joint Center for Graduate Studies

Direct Tree Temperature Survey, August 1974

J. R. Eliason, Battelle-Northwest

SECTION D THERMODYNAMIC STUDIES

CONTENTS

LIST OF FIGURES

LIST OF TABLES

MARYSVILLE GEOTHERMAL ANOMALY THERMODYNAMIC STUDIES

by
Stanley D. Hayes
Systems, Science and Software

September 1975

MARYSVILLE GEOTHERMAL ANOMALY THERMODYNAMIC STUDIES

Stanley D. Hays
Systems, Science and Software

INTRODUCTION

Systems, Science and Software (S^3) has been under contract to provide thermodynamic studies of the Marysville geothermal anomaly. Background information on the geology and the project in general can be found in Reference 1. Briefly, with respect to these studies, Blackwell, during his heat-flow studies found surface heat flow of unusual magnitude near the town of Marysville, Montana. There is no other evidence on the surface of a heat source in the region. Subsequent studies were interpreted to indicate a hot, dry magmatic intrusion of perhaps 100-km^3 volume within 2 miles of the surface. Blackwell has developed a model which matches the heat flow and gravimetric measurements reasonably well. However, the results of drilling which became available after the bulk of this study was completed indicate that the heat source was warm water close to the surface.

S^3 used a two-dimensional heat conduction code to model heat flow with highly nonlinear functions that define the phase changes and temperature-varying thermodynamic parameters. Rectangular, axisymmetric or spherical geometry can be investigated in two- or pseudo-three-dimensional modeling. The basic computational scheme is implicit, finite difference and runs in energy space. The first studies were planned in conjunction with Blackwell to match his model as closely as possible within the geometric constraints of the code. A quote from Reference 2 gives a brief description of the Marysville model; and Figure D.1 is a map of the model from the same reference:

> "The heat flow data were interpreted assuming a particular type of model for the heat source. The type of model assumed was an instantaneous heat source in which the body was assumed to be emplaced at a constant temperature, in a medium of uniform thermal properties, and to cool by conduction alone subsequent to the emplacement (see Blackwell and Baag, 1973). No addition of material was allowed after the emplacement of the body and no convection occurred within the body. The emplacement temperature was assumed high enough to include both the latent heat and the emplacement temperature. The model used was based on prismatic units with a square surface 1/2 km in dimension and with arbitrary length, buried at some depth below an isothermal boundary (the surface). A model was built up of these single prisms by superposition. The algorithm was based on an equation in Carslaw and Jaeger (1959, p. 62). This equation was used with the method of images (to match the constant boundary temperature) and was differentiated so that the quantity calculated was the surface

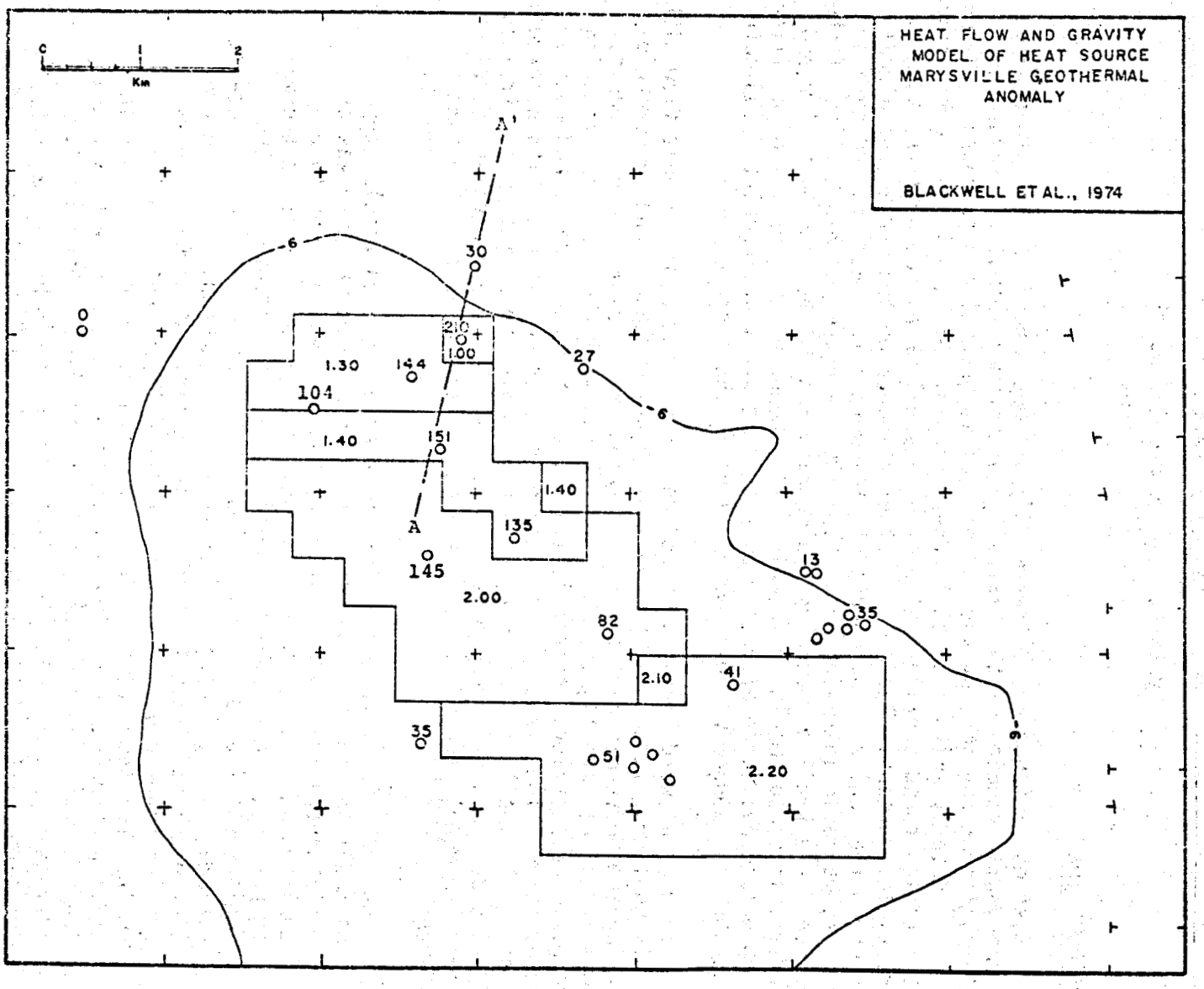

FIGURE D.1. Model of Heat Source for the Marysville Geothermal Anomaly from Reference 2

geothermal gradient. The heat flow data were then fitted using this particular interpretation model."

The results from the S^3 comparison calculations were reported in Reference 3, relevant portions of which are included below where needed for comparisons. Case 1 most nearly matches Blackwell's model near the center of the hot body. It provides the reference data against which many of the subsequent nonlinear cases are compared.

RESULTS

Perhaps the most outstanding result has been the delineation of the sensitivity of heat flow to geometry. This was indicated in the two cases reported in Reference 3 where only the depth of the hot body was varied between 1 and 2 km. The peak surface temperature gradients that were calculated were approximately 450° and 150°C/km. This type of sensitivity is also indicated for the shape of the topography. Variations as small as 100 m in depth produce significant changes in the calculated parameters such as the temperature gradients. Uncertainties in the location of the hot body and limitations inherent in two-dimensional modeling combine with this geometric sensitivity and make it difficult to assess accurately such parameters as age and measured gradients. However, even with these limitations it has been possible to bracket the depth, age, and energy content, and to deduce what part of the core may still be molten.

The effects of including the heat of fusion were found to be significant. It was during this part of the study that the possibility of a still molten core was discovered. Blackwell agreed that a molten core is possible; however, he was not optimistic about the detection possibilities because of the small size of the molten core, if it exists, and the low probability of having detectors in the correct locations with respect to both the source and the core in the rugged terrain.

If the core is still molten, it means that there is a lot of energy still available from the latent heat of fusion. Whether this energy is practically accessible or not depends on the thermal conductivity of the hot rock and the technology of energy removal. If the molten core is only 3 km^3 ($\sim$3 percent of the total estimated volume) there is 7.5×10^{17} cal in the transition phase between 700° and 820°C. That is enough energy to keep a 1000-MW power station running for 25 years, assuming a 25 percent overall efficiency.

Another related conclusion from these studies is that the initial heat content of the body may have been 40 to 50 percent higher than the estimate based on the linearized model. The initial estimate assumed a heat capacity of 0.2 cal/gm-°C to 1000°C which represents a total specific internal energy of 200 cal/gm. The Smithsonian Tables give four values for the specific heat of granite of composition similar to that in the Marysville region. When fitted with a curve and integrated to 700°C the specific energy curve

that results is nearly a straight line with a slope of approximately 0.26 cal/gm-°C. There is 95 cal/gm in the phase transition between 700°C and 820°C, so the total specific internal energy is 284 cal/gm if the initial temperature is taken to be 850°C, which is just molten. This is 42 percent more energy than the initial estimate.

When the energy function described above was included in the simulation, a part of the core remained above 820°C for a time of about 8000 years and above 700°C (partially molten) to beyond 20 ky. When temperature dependent conductivity data were included the core temperatures remained high for much longer. Uncertainties in these results are due to geometry, lack of convection in the S^3 model, and unknown initial temperature.

Near surface temperature gradients were not found to be very sensitive to changes in the nonlinear thermodynamic characteristics. However, temperatures within the hot body were found to be quite sensitive to these characteristics, even when the initial temperature of the linear model was raised to compensate for neglecting the phase change of the granite. For example, at 10 ky and 2.4 km depth on the center line (well within the hot body) the difference in temperature between the linear case, started at 1000°C and the fully nonlinear simulation, started at 850°C is 240°C or about 35 percent.

DISCUSSION

Case 1 will be referred to many times below as it most closely matches Blackwell's analytic model near the center of the hot body. It is fully described in Reference 3, but will be outlined here for convenience. Case 1 assumes a flat earth, two-dimensional model of the Marysville geothermal anomaly which was computed in rectangular geometry (the body is assumed infinitely long) with constant thermodynamic parameters which were the same as those used by Blackwell. The hot body was 2 km below the flat surface, 2.6 km wide and 3 km deep. A diagram of the configuration is included in Figure D.2. The initial temperature was 1000°C for the hot body and 0° for the surroundings. All the material was granite. Case 2 was identical, except the depth was 1 km. The near-surface geothermal gradient (hereinafter simply referred to as the gradient) over the center of the hot body is shown in Figure D.2 as a function of time for Cases 1 and 2 and for two other intermediate depths.

Geometric Sensitivity

The sensitivity of gradients and temperature profiles to the geometry of the simulation was investigated by four types of calculations:

1) Examples similar to Cases 1 and 2 were studied at intermediate depths of the hot body.

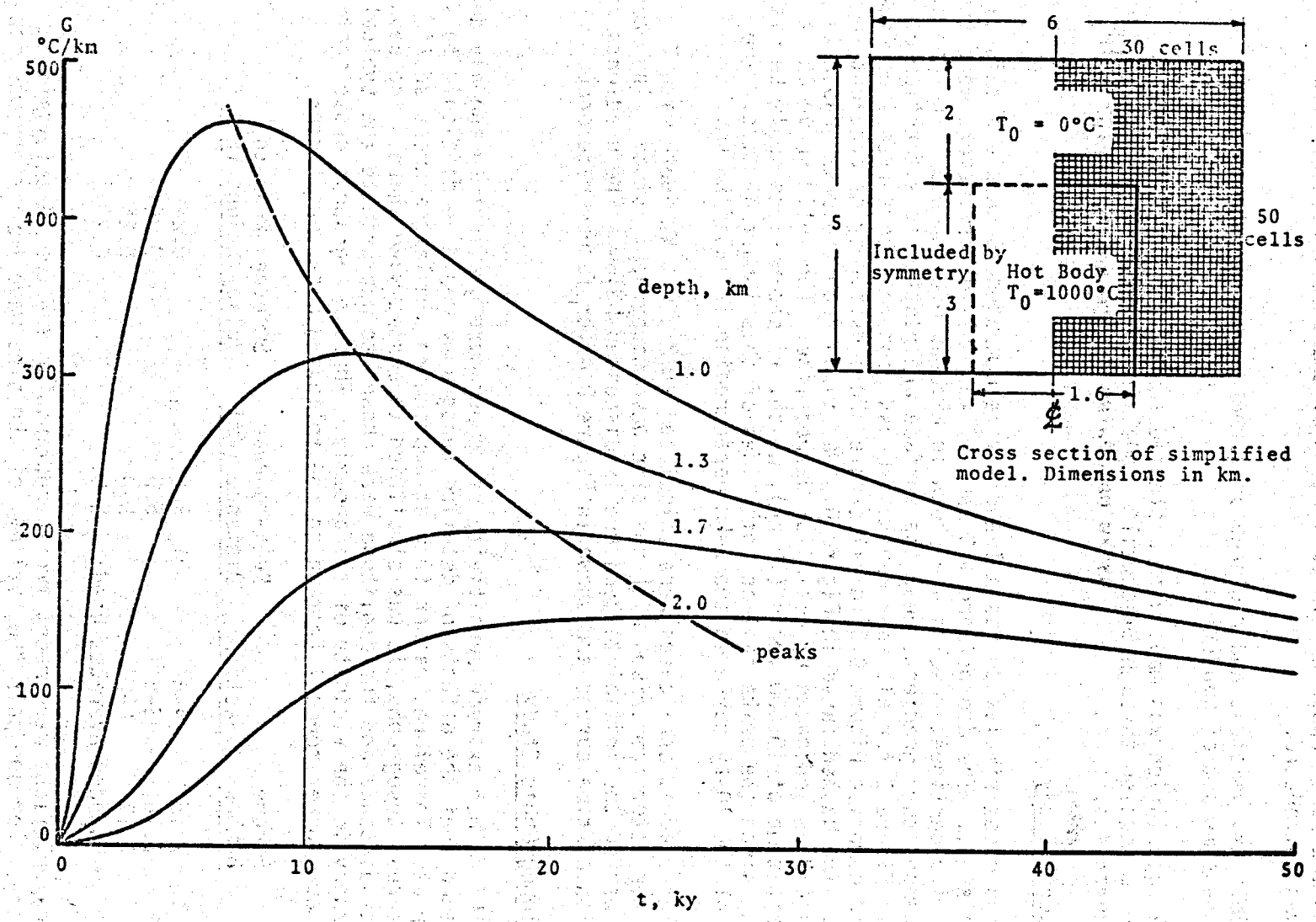

FIGURE D.2. Gradient Versus Time on Centerline for Different Depths of Hot Body

2) A simple sine wave topography that had characteristics similar to the real topography in the region of the anomalous heat flow was introduced.

3) Both axisymmetric and rectangular geometry was investigated under the same set of conditions.

4) A calculation was made with a stepped top on the hot body similar to a section through Blackwell's model in a N-S direction at the North end.

Depth Study

Two cases similar to Cases 1 and 2 were computed to complete this part of the study. The depths were 1.3 and 1.7 km. All other factors were the same. The pertinent results are shown in Figures D.2 and D.3. The centerline temperature gradients near the surface are plotted as a function of time in Figure 2 for all four depths. Cross plots of the curves from Figure D.2 comprise Figure D.3 to illustrate the sensitivity of gradient to depth. The dashed curve in Figure D.3 was taken from the peak gradients in Figure D.2 as indicated by a similar dashed line. The solid curve is at a constant time of 10,000 years (10 ky), which, if shown alone could be misleading since the peaks fall on both sides of this important time. The slope of the 10-ky curve in the 2-km depth region is 165°C/km/km.

Three additional cases were calculated at 2 ± 0.1 km depth with T_0 = 850°C for later comparison with the sine wave topographic study. The reason for lowering the initial temperature is discussed below. The gradients as a function of time curves are shown in Figure D.4 for future reference.

Topographic Study

The rather extreme sensitivity of temperature gradient to anomaly depth indicated that the effects of detailed topography would be difficult to interpret. Therefore, rather than attempting to simulate a cross section of the real topography, it was simplified to a sine wave shape. The peak-to-peak distance and the amplitude were chosen to approximate the typical topography in the vicinity of the anomaly. Three topographic cross sections are shown in Reference 1 from which the following data were taken:

Figure Number	Section	Peak-to-Peak Distance (km)	Smoothed Peak-to-Valley Height (km)
2.15	A-A'	3.5	0.2
2.16	B-B'	5.5	0.25
2.17	C-C'	5.0	0.25
Rounded Averages Used:		5.0	0.2

Four calculations were made, two in rectangular and two in axisymmetric geometry. For one pair the "valley" of the sine wave topography was centered over the hot body and in the other the peak was so centered. The

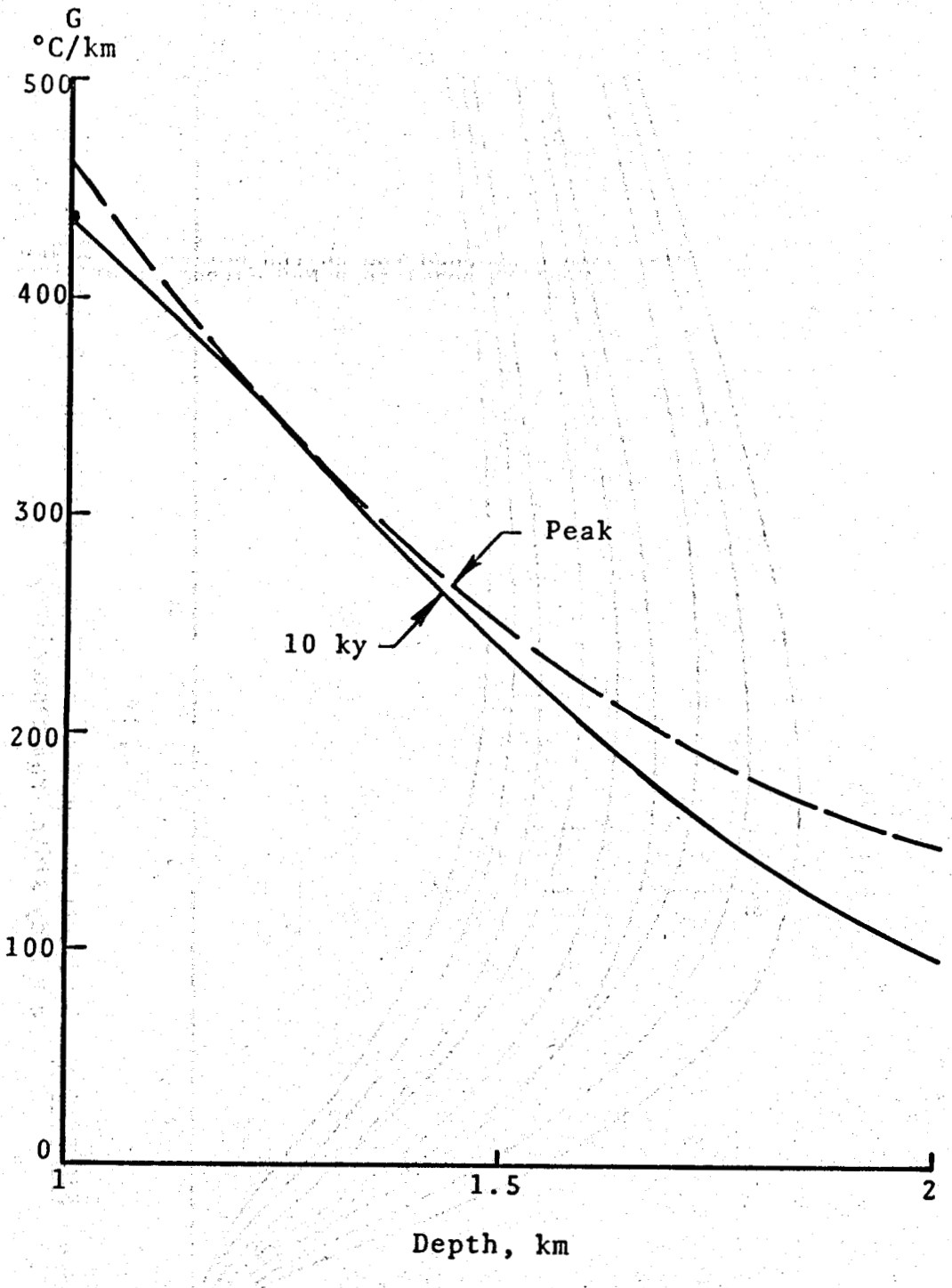

FIGURE D.3. Gradient Versus Depth for Conditions Noted on Figure D.2

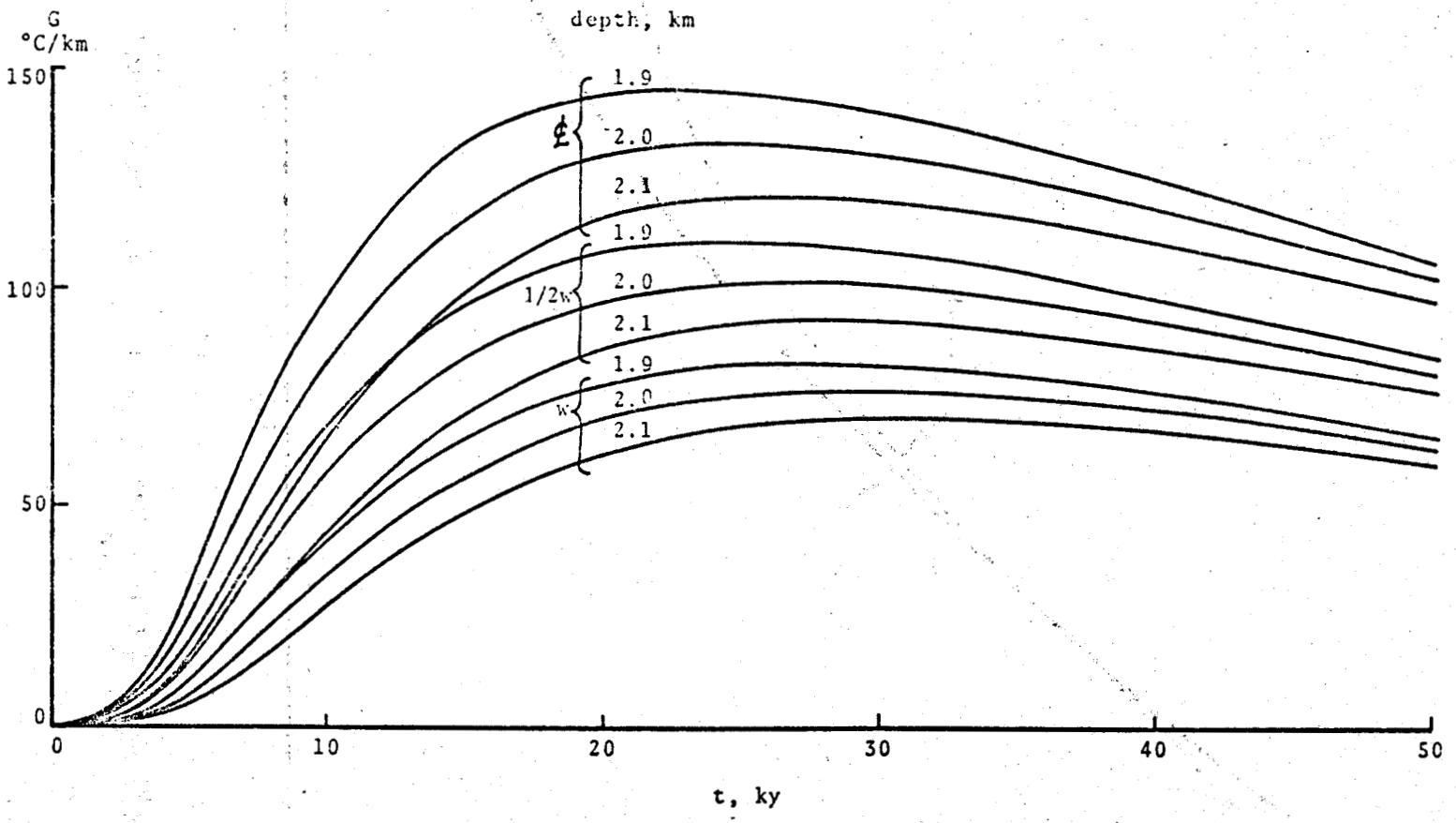

FIGURE D.4. Gradients Versus Time for Case 1 with Depth = 2 ± 0.1 km. w = body width from centerline.

sine wave had to be approximated by rectangular grid lines. Therefore, the upper rows of cells in the grid were gradually reduced in height from the usual 100 m to 20 m in the top 12 rows. This is illustrated in Figure D.5 which shows the valley-centered case; the hill-centered case is similar.

The solid lines in Figure D.6 give the gradients as a function of time for the valley-centered case calculated in plane geometry. The lower dashed curve is the gradient on the centerline for the sine wave topography, but this was calculated in axisymmetric geometry. Because the heat can escape from all sides of the hot body in axisymmetric geometry and the body is effectively smaller than the infinitely long body of the plane cases, the axisymmetric gradients are much lower. Since the real body is probably about three times as long as it is wide, the correct curve must be between the rectangular and axisymmetric curves, probably closer to the former.

Figure D.7 is similar to Figure D.6 except it shows the hill-centered case. Figures D.8 and D.9 show the axisymmetric gradient curves.

The sensitivity of heat flow to minor changes in geometry is as great in this topographic study as in the flat earth study discussed earlier. The need for full three-dimensional modeling of real topography is apparent.

These cases with simplified topography offer an excellent opportunity to test Birch's analytical method (Reference 4) for topographic correction of thermal gradients. If it is assumed, as done in the numerical calculations, that the topography has persisted indefinitely in its present state, then Birch's formula simplifies to:

$$T(z) - \alpha' \bar{h}(\infty) = T_s + \alpha[z - \bar{h}(\infty)]$$

$$\bar{h}(\infty) = \sum_{\text{rings}} \bar{h}_r \frac{\Delta\Omega r}{2\pi}$$

T_s = present surface temperature

α = the true undisturbed geothermal gradient in flat topography

α' = the change of surface soil temperature with elevation

$$\Delta\Omega_r = 2\pi \left[\left(\frac{r_1^2}{z^2} + 1 \right)^{-1/2} - \left(\frac{r_2^2}{z^2} + 1 \right)^{-1/2} \right]$$

$T(z)$ and z are the present uncorrected temperatures at depth, and the depth, respectively

$\bar{h}_r$ is the difference in elevation between the collar of the drill hole and the average elevation of the rth ring

r = radius of the ring.

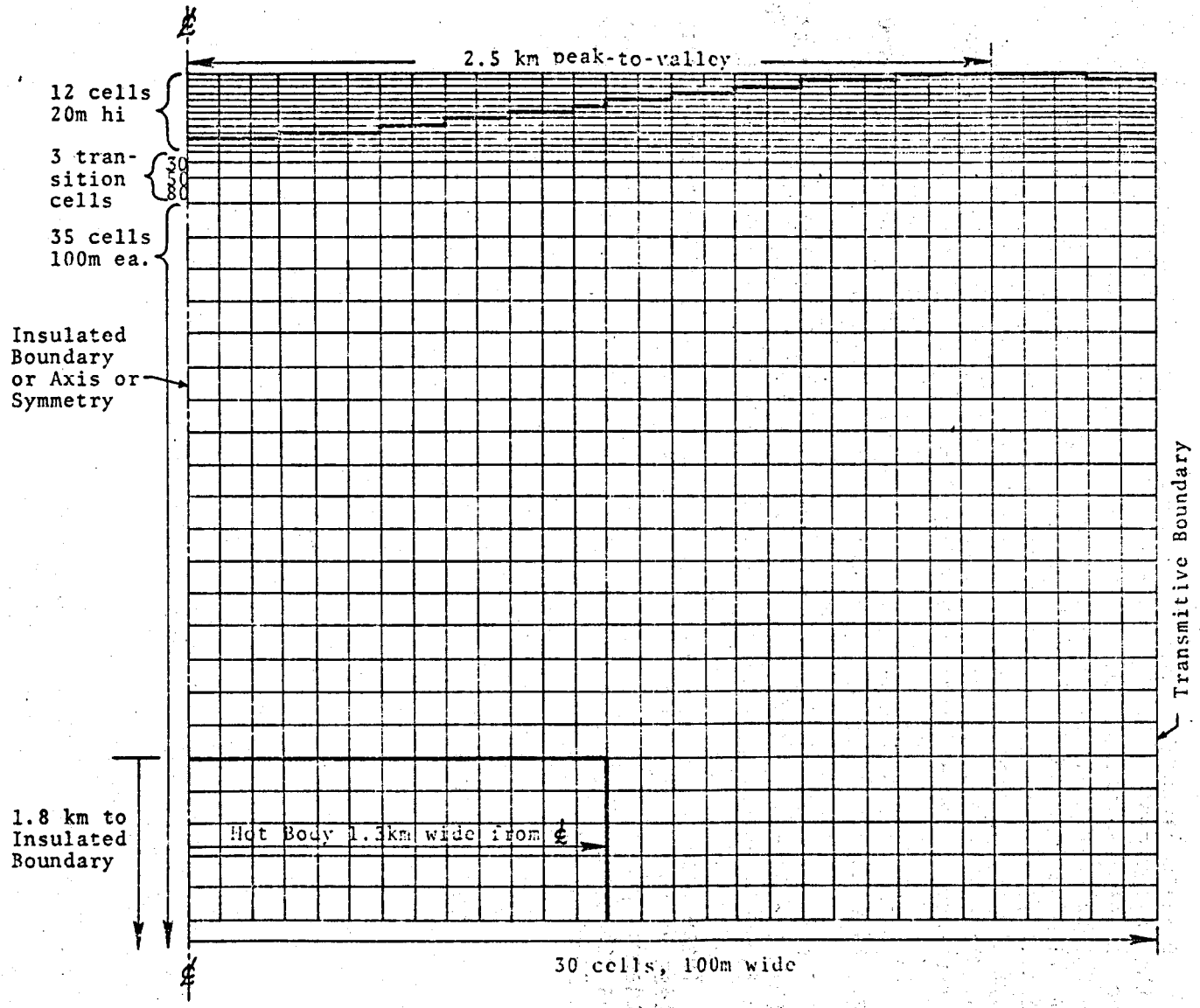

FIGURE D.5. First Topographic Model

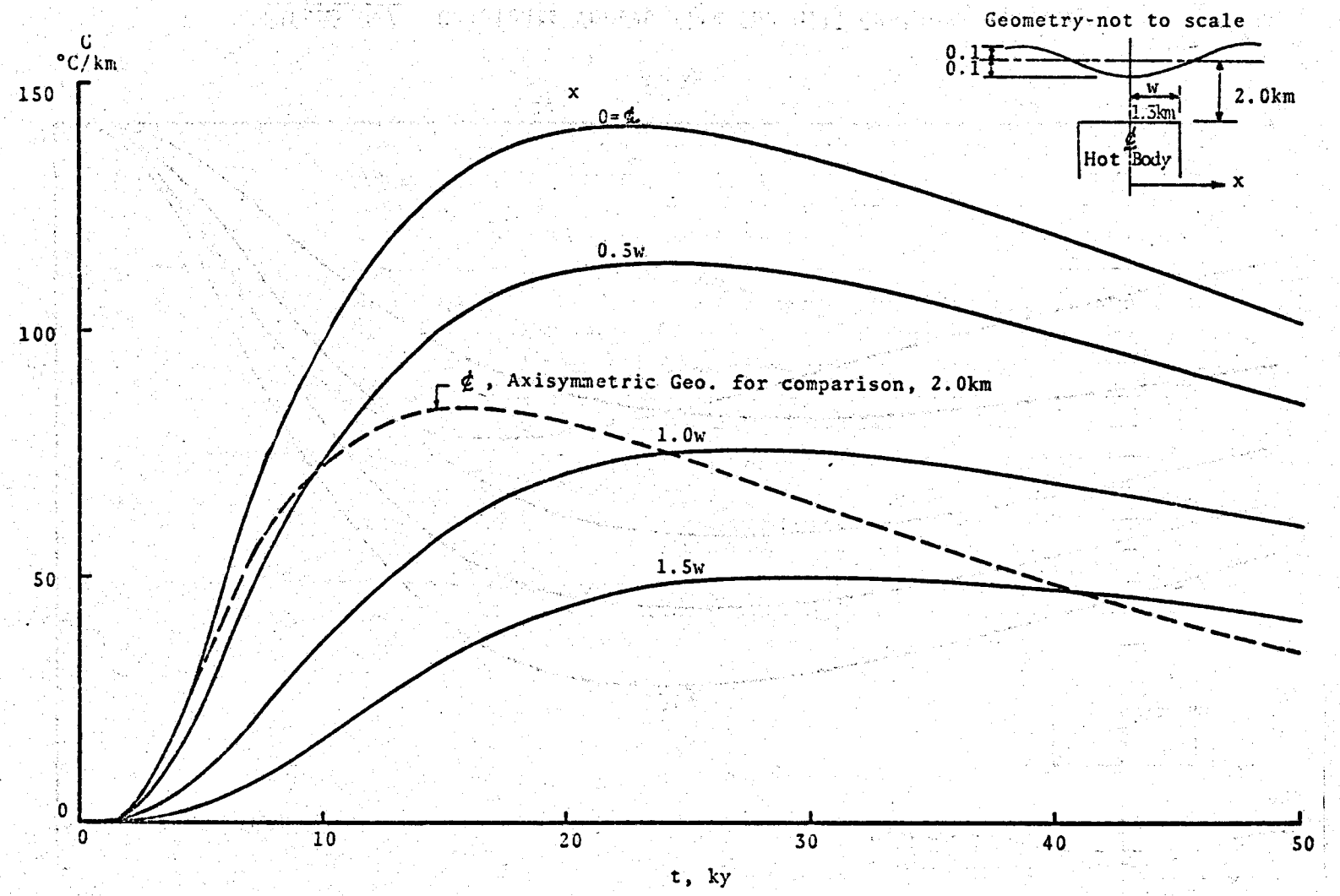

FIGURE D.6. Gradients Versus Time for Valley-Centered Topography-Rectangular Geometry

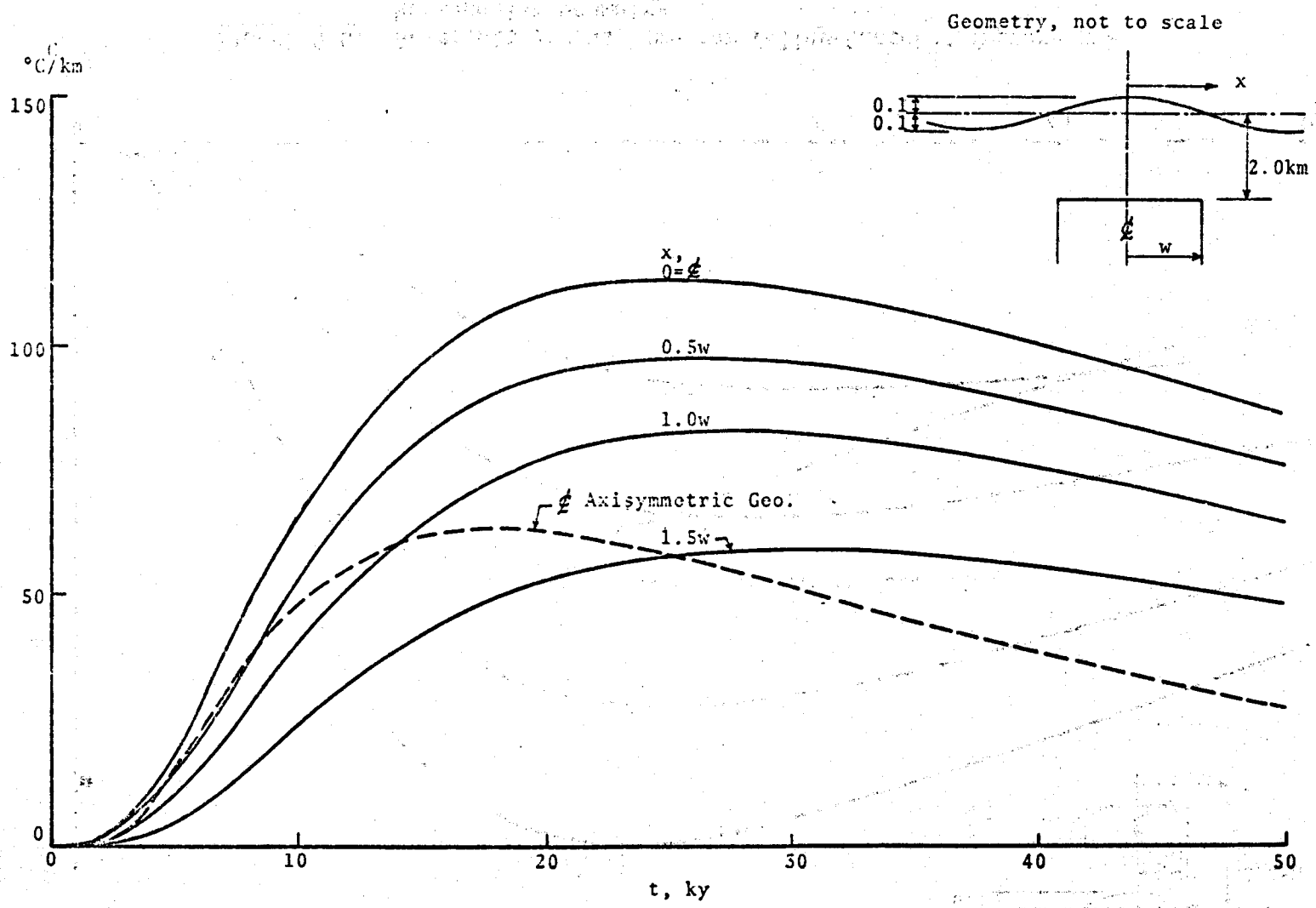

FIGURE D.7. Gradients Versus Time for Hill-Centered Geometry

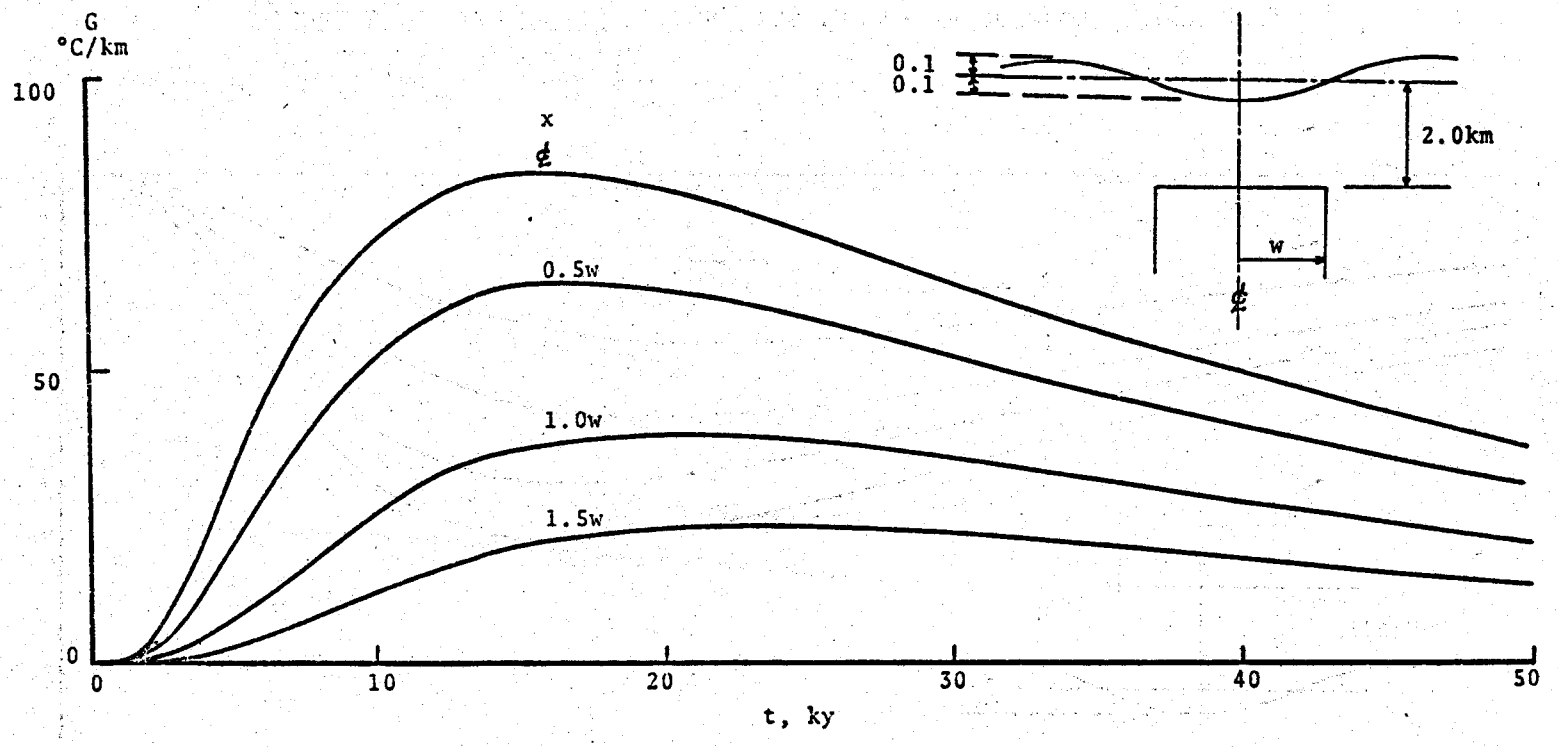

FIGURE D.8. Gradients Versus Time for Valley-Centered Topography, Axisymmetric Geometry

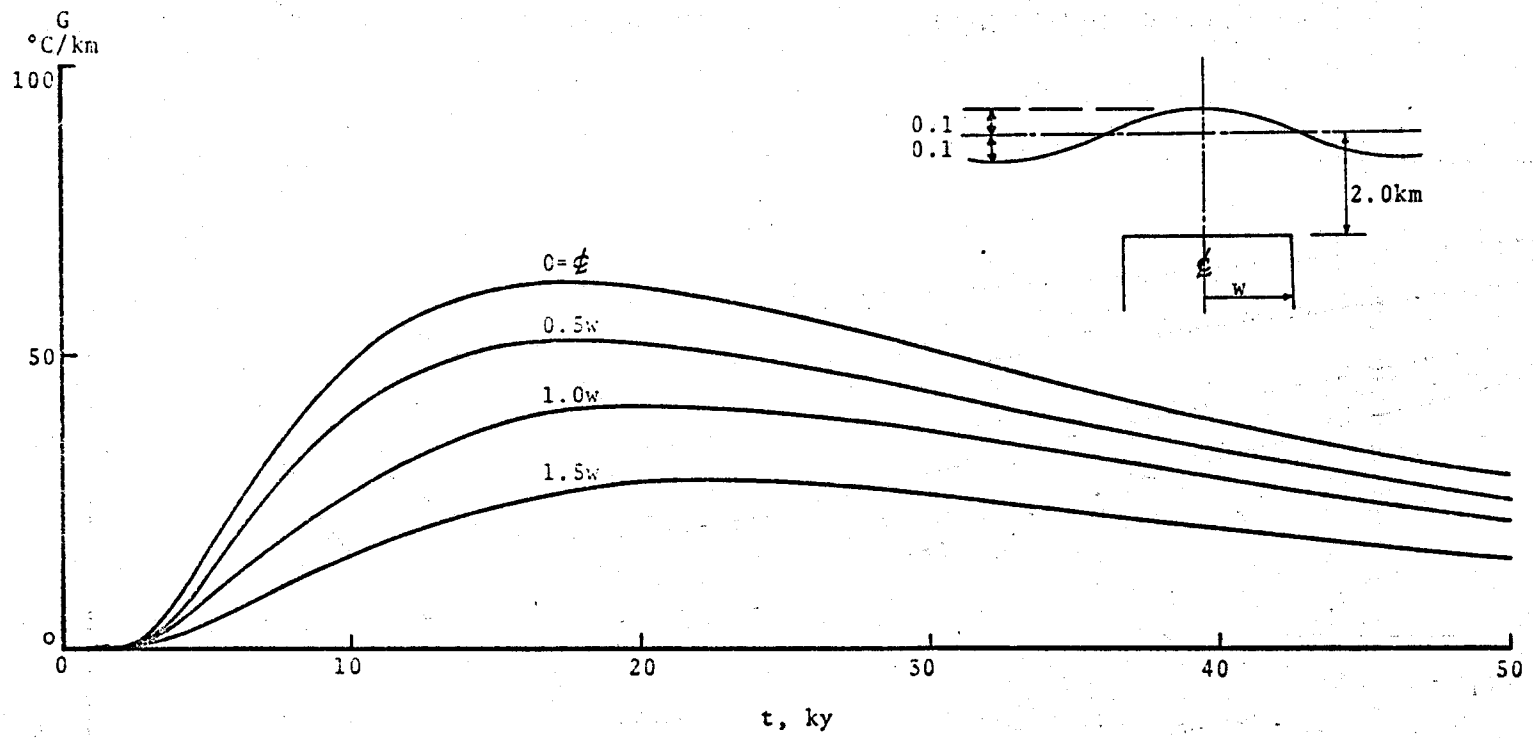

FIGURE D.9. Gradients Versus Time for Hill-Centered Topography, Axisymmetric Geometry

The temperature gradients which are measured in relatively shallow holes near the surface must be corrected for the irregularity of the surface. The general tendency is for gradients to be too low at locations which are above the average surroundings (on a hill) and too high in regions which are low. Both cases approach the true gradient with increasing depth.

Birch's method makes use of the average elevations of annular rings around the collar which must lead to some inaccuracy in the case of real terrain. However, for the sine-wave terrain assumed in these calculations, his method, if precise, should produce the same results as a flat terrain with the same elevation as the $\bar{h}(\infty)$ in the sine-wave case.

The formula given above was programmed and data on the sine-wave cases were input as if these were real terrain. Since the computations were made in the axisymmetric mode, the steps used to approximate the sine-wave terrain (Figure D.5) formed annular rings of constant elevation. Hence, there were no approximations in the input to Birch's formula. Because the earth-air interface had a constant 0°C boundary condition, α' was zero. An example of results of the comparisons at 10 ky are tabulated below where G* is the Birch corrected gradient.

Gradient, °C/km at 10 ky

	G	G*	G_{flat}
Hill	37.5	40.9	42.1
Valley	60.0	54.6	53.0

These comparisons between methods are considered to be good. The difference between the Birch method and the computer simulation is only 3 or 4 percent. Fundamental differences in the comparison are that the hot body was 2.6 km in diameter in the simulation and 10 ky old whereas Birch's method assumes that it is semiinfinite and that gradients have come to equilibrium.

An attempt was made to recalculate the corrected gradient for hole DDH-23 (where the anomaly was drilled) reported by Blackwell. The method described above gives the corrected gradient, G*, as a function of depth. The topographic data around hole 23 was divided into 20 concentric rings of 0.1 km width and the elevations were read at 20° intervals from a topographic map and then were averaged for each ring. The results of the calculation are:

Depth, m	G*, °C/km
100	144.6
200	175.3
300	192.5
400	203.8
500	211.7

When these were compared with Blackwell's computed G* of 173.6°C/km the difference caused some concern which led to a careful comparison of methods. There were some relatively minor differences in data reading, but the important difference is that Blackwell's calculation was confined to the depth region of the temperature measurements which were between 15 and 49 m. In this region of relatively extreme topography at the shallow depths the correction is not very good, so the corrected gradient varies with depth. At the shallow depths the results compare favorably and are well within the commonly accepted errors for this type of situation.

Hot Body Shape

Sensitivity to depth and topography indicated that there could also be a sensitivity to body shape. At early times this is the case as is shown by one example. However, after about 8 ky the effects of body shape smoothed out. The shape used in this example was taken from a cut A-A' through the northerly end of Blackwell's model (see Figure D.1) in a N-S direction. The small step in the model from 1.3 to 1.4 km depth was omitted. Figure D.10 contains a scaled diagram of the hot body shape which was calculated in rectangular geometry and the gradient as a function of time curves. These gradient curves have the usual appearance after about 8 ky, but the smoothing effect can be seen more easily in Figure D.11. Temperature profiles at a depth of approximately 1/2 km are shown in Figure D.11. At early times the raised edge of the hot body is apparent in the profiles, but after 8 ky the heat source appears to have lost the memory of its original shape. By 15 ky the profiles are almost identical to those from a simple flat-topped body. The dashed line in Figure D.11 is such a profile. On the basis of this one example it can be concluded that it is not necessary to attempt to model the shape of the hot body with precision for data at times of current interest (>8 ky).

Thermodynamic Parameters

Initial Values

As discussed in Reference 3 it was agreed that these simulations should start with the same linear thermodynamic approximations that were used in Blackwell's analytical model, namely:

$$\rho = 2.5 \text{ gm/cc}$$

$$C_v = 0.2 \text{ cal/gm-°C}$$

$$K = 0.007 \text{ cal/cm-gm-°C.}$$

The initial temperature, T_0, was assumed to be 1000°C which approximated the amount of specific internal energy in granite up through the phase change (which really is complete at about 820°C). All of the cases in Reference 3 and those discussed above have employed these linear approximations. The only exception has been to lower T_0 to 850°C for some cases that are to be compared with some later nonlinear cases that were started with T_0 just above the phase transition.

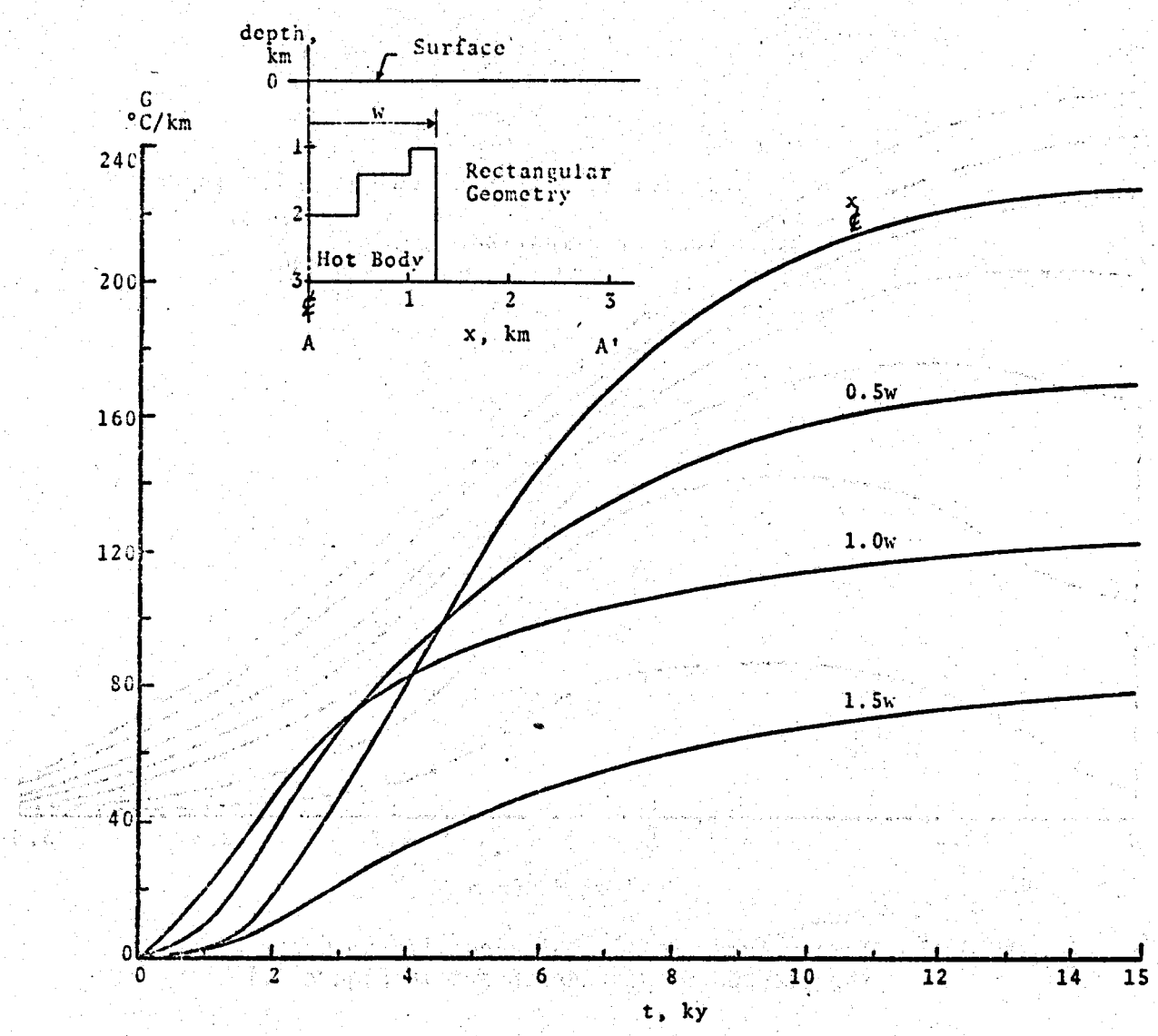

FIGURE D.10. Gradients Versus Time for Stepped Hot Body

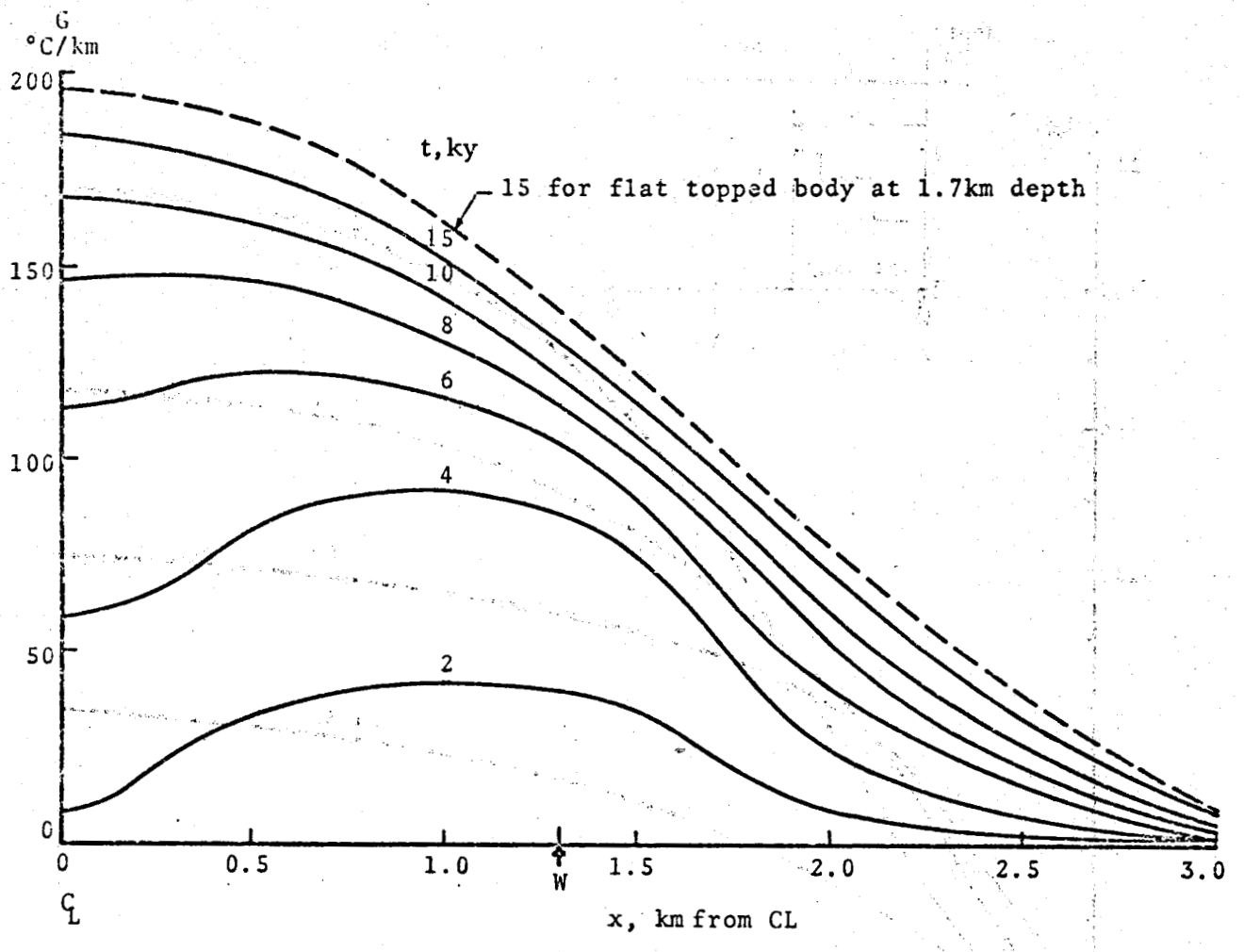

FIGURE D.11. Temperature Profiles at About 1/2 km Depth Above the Stepped Body. See insert in Figure D.10.

Current Values

A literature search was made and several experts in the field of material properties of hot and molten granite were consulted. Surprisingly little is known (Reference 5) in detail about rock thermal properties, particularly the variation, if any, of K with T through the melting transition. Reference 6 gives the measured variation of thermal conductivity of granite with temperature to 350°C. Data given for several types of granite are shown in Figure D.12 along with Blackwell's measured and recommended values. The Rockport 1 data seem appropriate for Marysville because it spans the Marysville measurements and because the quartz content was 25 percent which is the same as the granite for which good C_V data exist (Reference 7), as discussed below. Also shown in Figure D.12 is an extrapolation of the Rockport 1 data to 850°C based on a nearly linear extrapolation of resistivity (Curve 2 of the insert in Figure D.12). The conductivity function was

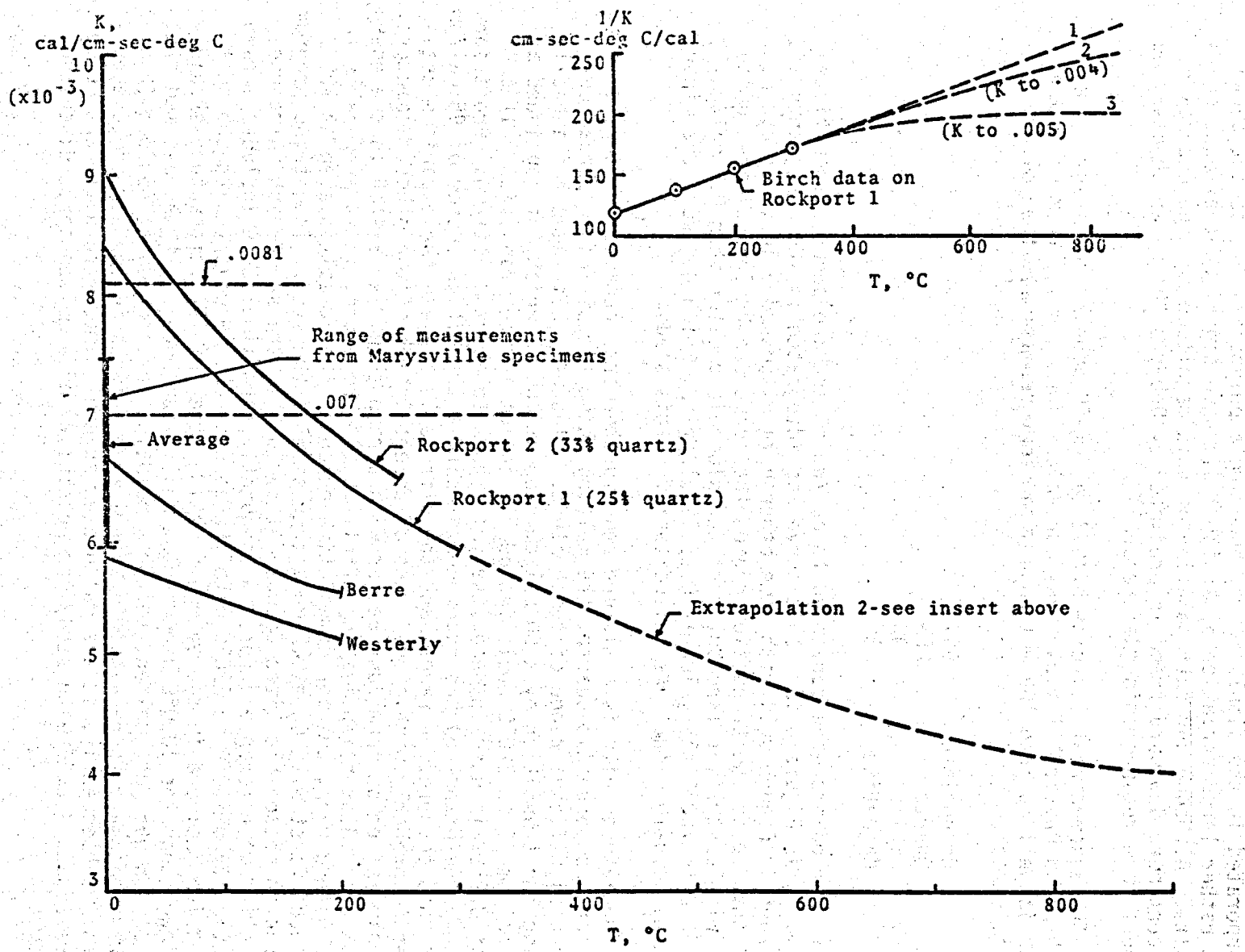

FIGURE D.12. Thermal Conductivity of Granite

incorporated in the simulation by encoding a polynomial fit to the curve. This rather large variation of K with T did have significant effects on the results. Although any extrapolation of this magnitude must be uncertain, the continued downward trend is predicted by Debey's theory which has good support from measurements (Reference 6).

The assumed heat capacity of 0.2 cal/gm-°C appears to be low. The Smithsonian Physical Tables give four values for C_p ($\approx C_v$) from 0° to 800°C, which is well up into the molten region, for granite with the following constituents:

Orthoclase	65%
Quartz	25%
Albite	9%
Magnetite	1%

These four points were converted to cal/gm-°C and are shown with a fitted curve, E, in Figure D.13. This curve was integrated in 100°C segments and is shown in Figure D.14 with some other data discussed below. It can be seen that up to the transition region the curve can be approximated quite well with a straight line but that the slope is greater than 0.2 cal/gm-°C. From 0°C to 700°C the value is 0.2589 cal/gm-°C, which neglects the minor effects below 0°C that are unimportant for this study.

Because granite is a mixture and, furthermore, because the second most abundant component is quartz, the melting phase transition is spread out over a significant range of temperature. Blackwell has suggested approximating the transition by a 50 cal/gm step at 700°C, which, if continued at 0.2 cal/gm-°C to 820°C would include 74 cal/gm in the transition. If a C_v of 0.2589 is used instead, the value goes to about 81 cal/gm. Professor Kennedy (Reference 5) has recommended using a transition energy of 95 cal/gm over this temperature range, and the difference between these various estimates is probably within the range of uncertainties of the other parameters. The simulation program runs better with a ramp than with a step in the energy function. (A step implies an infinite C_v.) Therefore, it is preferable to work with a ramp, but for comparative purposes the 50 cal/gm step at 700°C was used first with C_v = 0.2 on either side of the step. To get the program to run in reasonable times C_v was set to 10.0 in the step which introduces a small, but tolerable error. Subsequently, the simulation included a ramp function from 700°C to 820°C with the correct C_v. However, with the heat of fusion included in the energy function, the initial temperature should be lower than the 1000°C used in the analytical model. It was assumed that the pluton was just molten, so the simulation was started at 850°C. Thus, it was necessary to recalculate Case 1 with T_0 = 850°C for comparative purposes. Subsequently, it was calculated several times with different geometries and C_v = 0.2589 to study the possiblity of a molten core, discussed below.

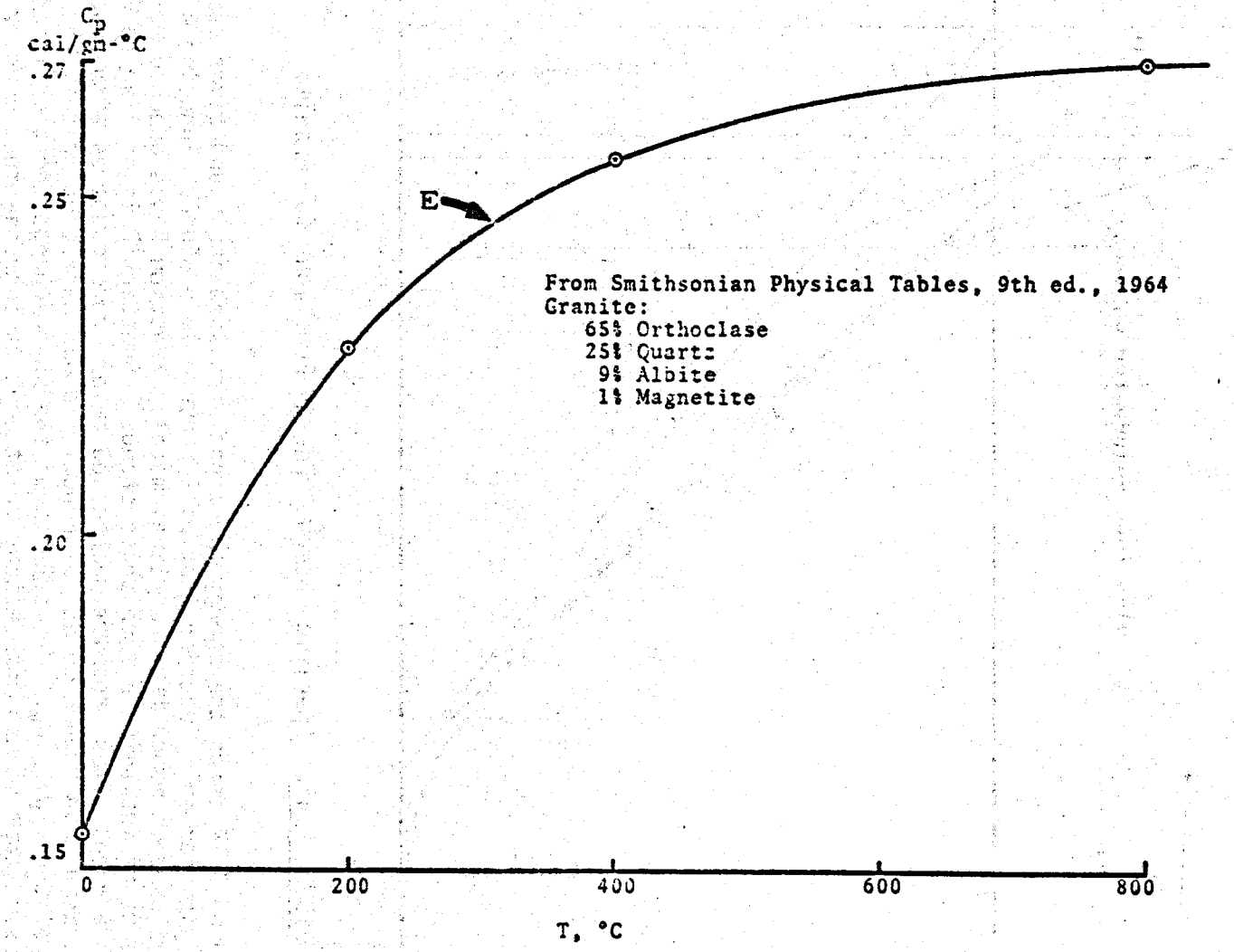

FIGURE D.13. Specific Heat of Granite

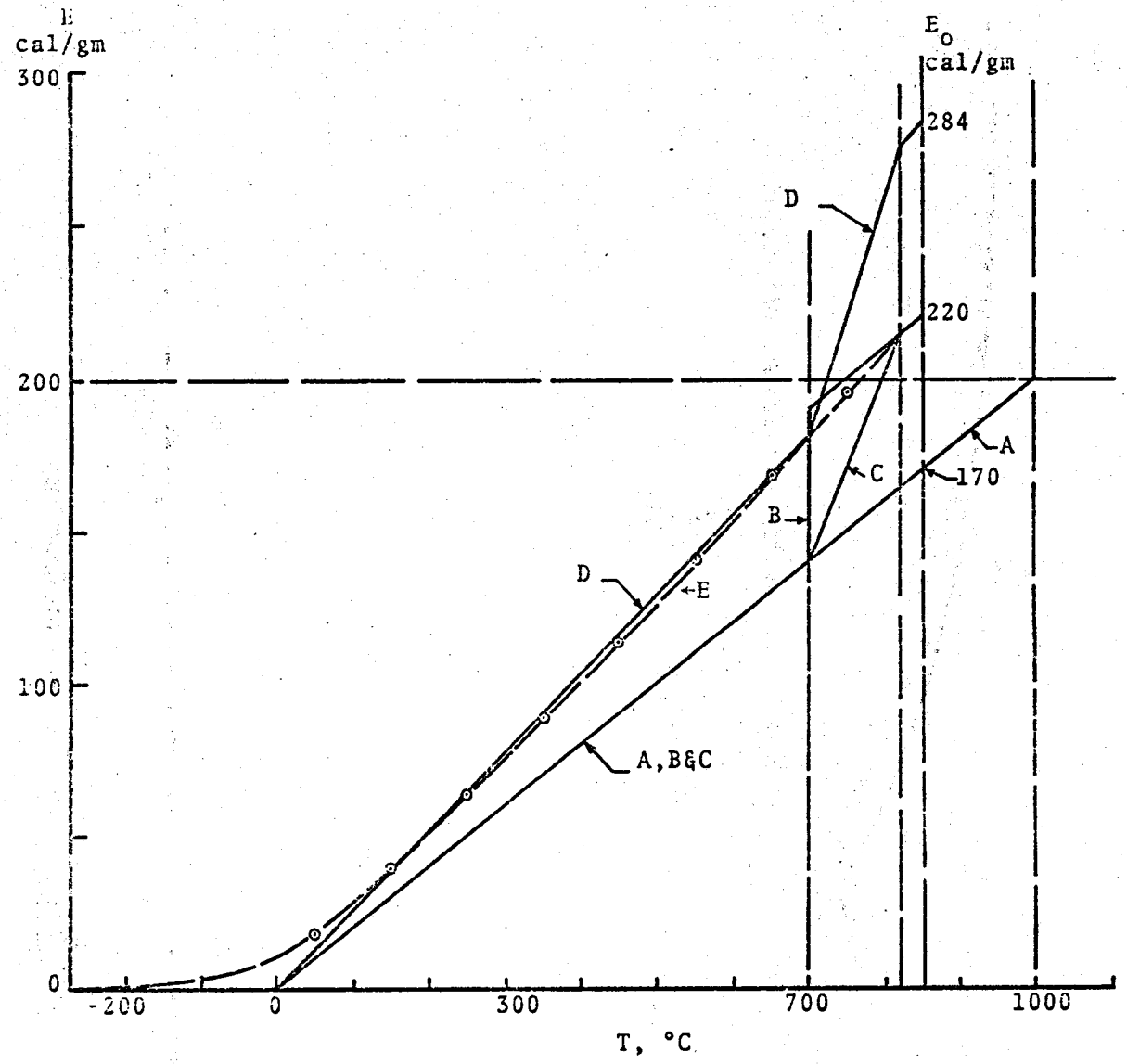

FIGURE D.14. Specific Internal Energy Functions for Granite

Figure D.14 shows the energy functions discussed above and gives starting energies for each function that will produce T_0 = 850°C. Function A to 1000° was used to match the analytical model. Function B was used to test the effects of including a step phase change. Function C is similar to B, but with a ramp. These results, discussed below, were compared with results obtained using Function A to 850°. Function D was then used to test the effects of the higher C_v. The effects of the phase change and the higher C_v indicated that it was unnecessary to attempt to increase the accuracy of this part of the simulation by encoding Function E, especially considering the uncertainties in and sensitivity to the geometry.

Effects of Including the Phase Change

The effects of including the several energy versus temperature functions shown in Figure D.14 will be discussed below. However, in general it appears that the effects on the near-surface temperature gradients are secondary with respect to assumptions concerning depth and initial temperature. The most prominent effect appears in the T versus depth curves in the region of the receding molten core. For the case which employed Function B with the step phase change, the difference in temperature from the linear case at 20 ky exceeds 200°C below 3 km depth (top of hot body is at 2 km, T_0 = 850°C in both cases) (see Figure D.15). At the same time the difference in surface gradient over the center of the body is only 24°C/km (see Figure D.16). If the linear case had been started at about 1070°C, the gradient curves would have to be quite similar, thus supporting Blackwell's assumption that starting a linear case with a high temperature is a good approximation to including the heat of fusion. The gradient curve from linear Case 1, T_0 = 1000°, has been replotted as the upper dashed curve in Figure D.16 for convenient comparison, and the T versus depth curve is also shown in Figure D.15.

Comparative cases for ramp functions C and D were all started at T_0 = 850°C with the hot body depth at 1.7 km, which at the time was believed to be the best depth for the two-dimensional approximation. Function A was recomputed under the same conditions to 20 ky and the three centerline gradients are shown as the upper curves in Figure D.17. Except for the slower rising curve of Function D, due to the higher C_v of all the rock, there appears to be little significant difference between these cases at times of interest. However, the temperature versus depth curves show differences between the linear and nonlinear cases similar to those shown in Figure D.15. In fact, with Function D the body stayed hot in the center long enough to suggest that there still may be a molten core, especially when the conductivity was made a function of temperature.

Possibility of a Molten Core

If the core is still molten, it means that there is a lot of energy still stored in the latent heat of fusion. Whether this energy is practically accessible depends on the thermal conductivity of the hot rock and the technology of energy removal. If the molten core dimensions include only 3 km^3, there is approximately 7.5×10^{17} cal in the transition phase between 700° and 820°C. That is enough energy to keep a 1000-MW power station running for 25 years at a 25 percent overall efficiency. Several cases were computed in the search for a molten core. Some of these used the variable conductivity curve discussed above. The results are discussed below.

In all cases the size and depth of the hot body were kept the same, 2.6 km wide and 1.7 km deep below a flat surface. Two energy functions were used, C and D, and both were calculated in rectangular and axisymmetric geometries. The calculations with Function D were repeated using the

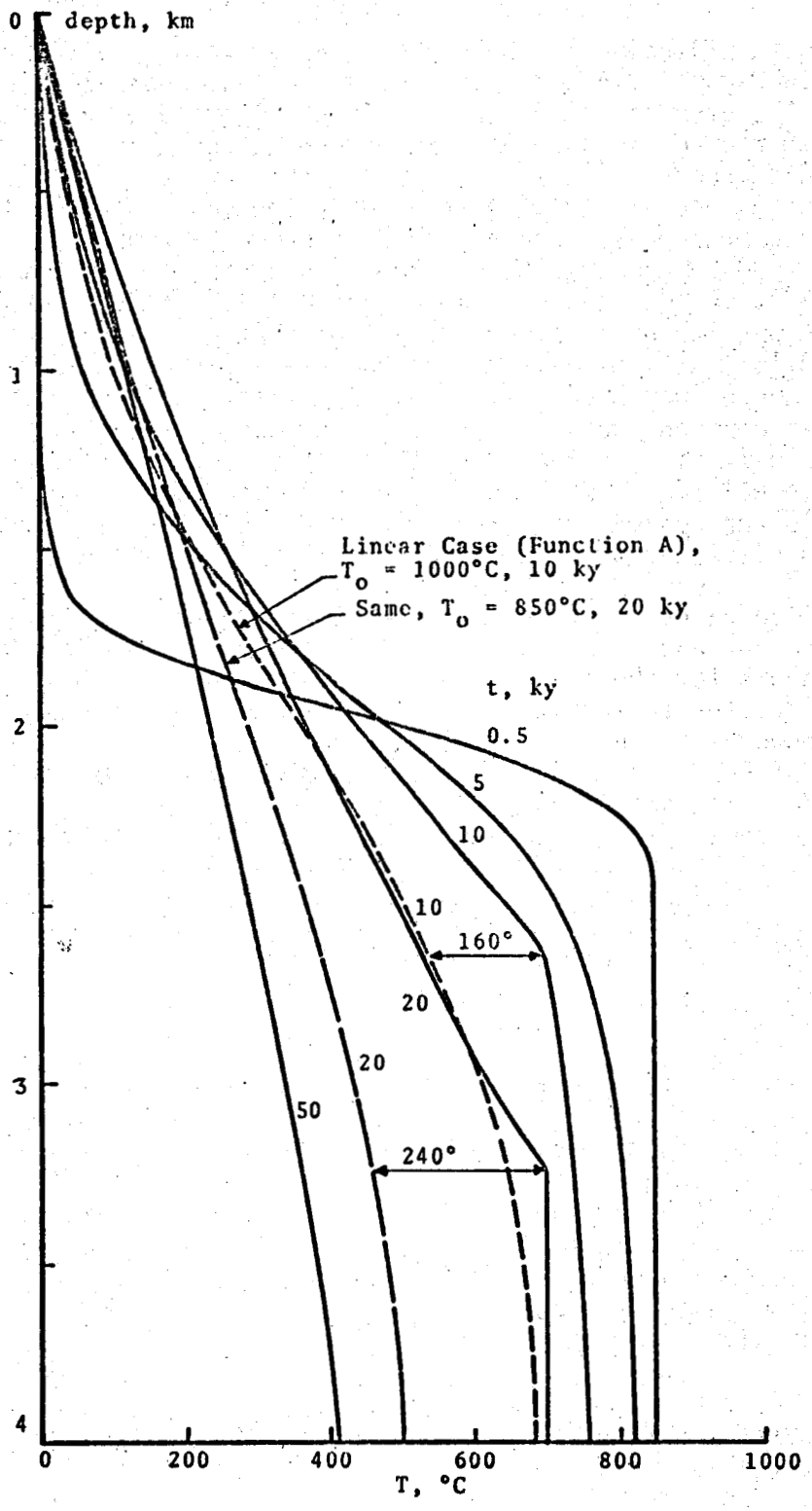

FIGURE D.15. Temperature Versus Depth for Energy Functions A and B on Centerline

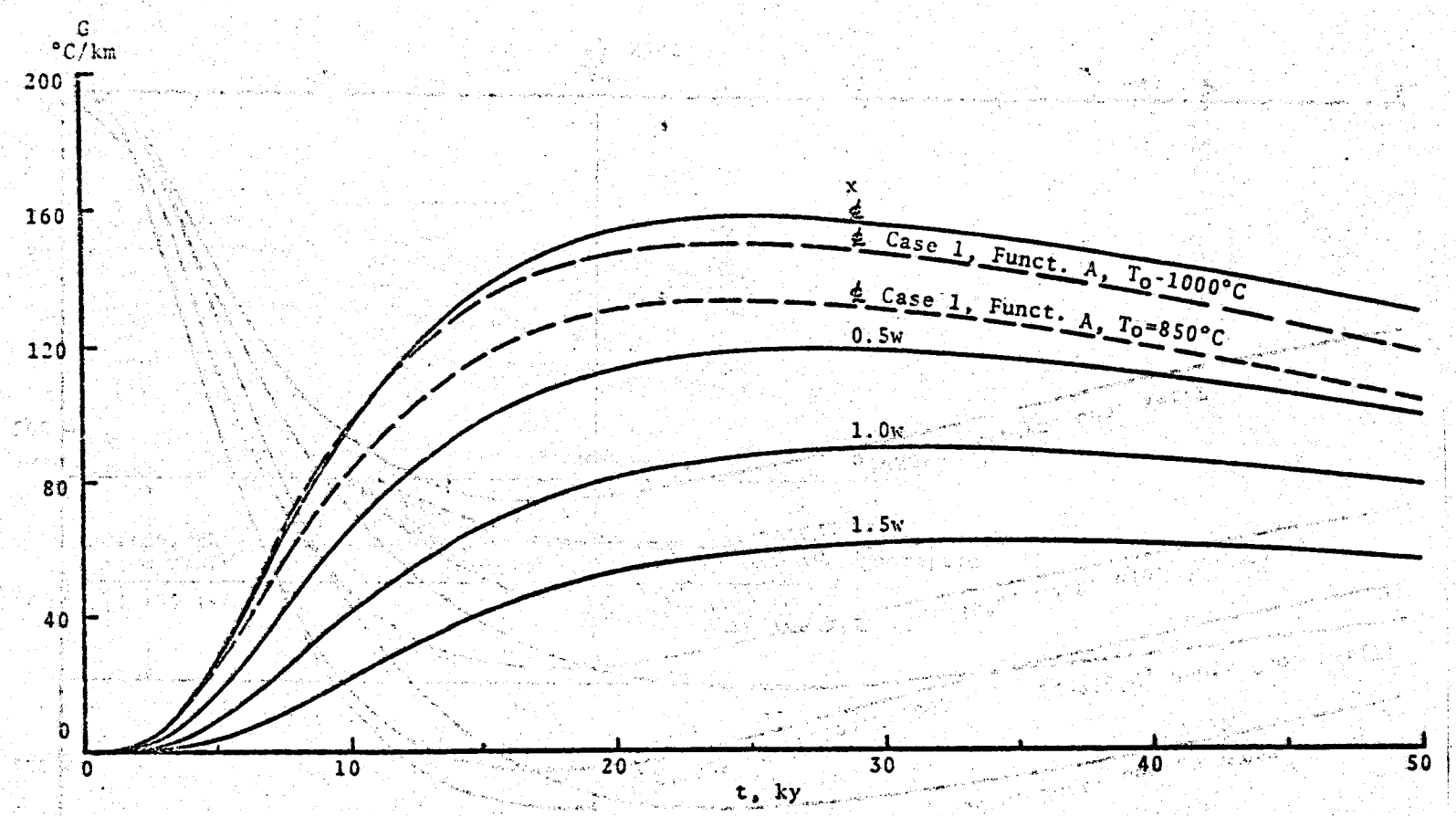

FIGURE D.16. Gradients Versus Time for Energy Functions A and B. Solid lines are all for Function B.

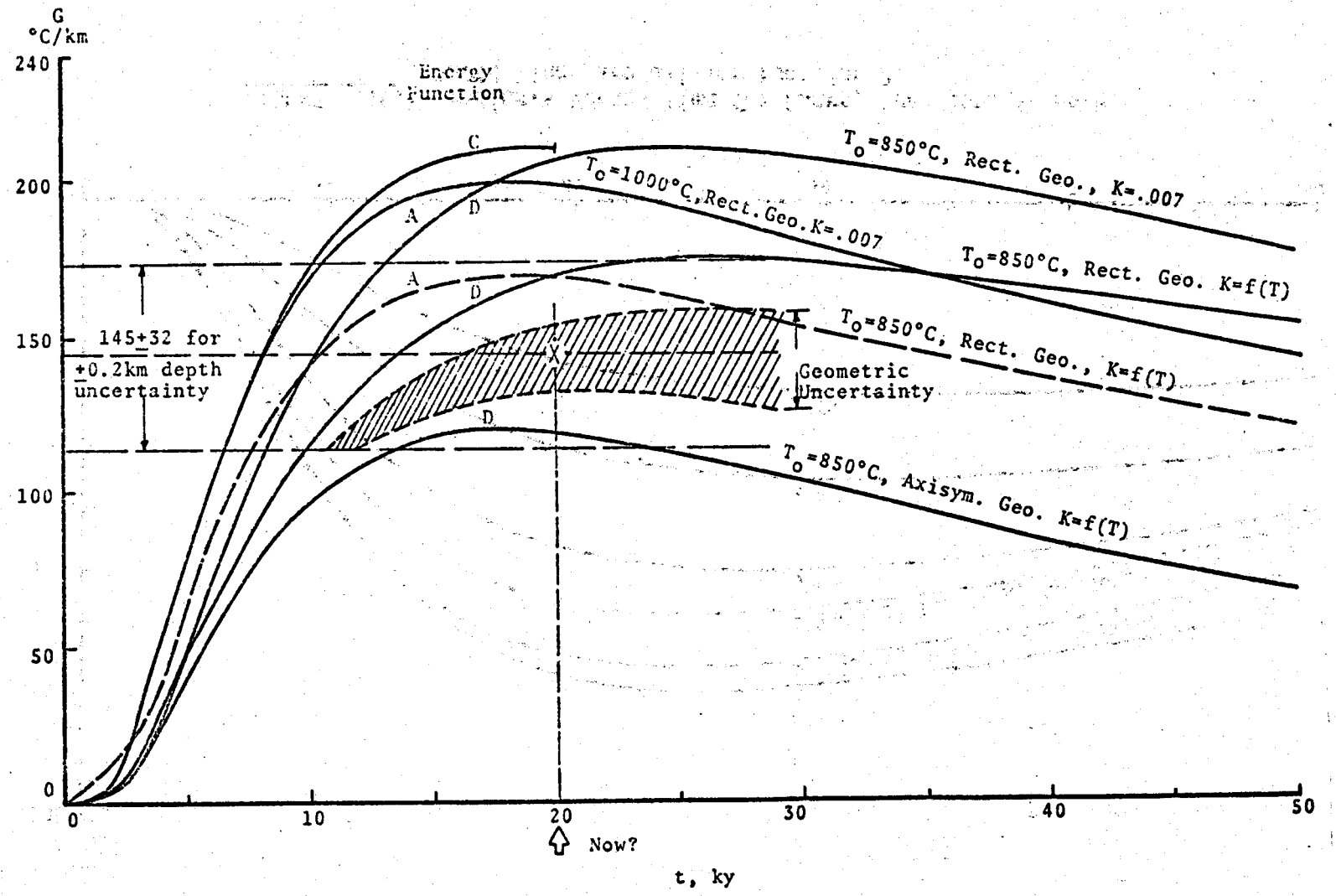

FIGURE D.17. Centerline Gradients Versus Time for Functions A, C and D. Depth = 1.7 km

temperature dependent conductivity function. The gradients for the rectangular cases and one axisymmetric case are shown in Figure D.17. As was discussed above, the rectangular geometry makes the hot body effectively too big (infinitely long) and the axisymmetrical geometry with the same width the hot body is too small. Since the actual hot body is believed to be approximately three times as long as it is wide, the real answers lie between these two cases, probably more toward the rectangular cases. An estimate of the region of the "real" centerline gradients is sketched in Figure D.17. The uncertainty that this places on the age of the hot body is clear when one looks for the measured (corrected anomalous) gradient of 145°C/km of hole DDH30 which is near the center. Remembering the sensitivity of gradient to depth suggested in Figure D.17 by the band around the 145°C/km line, one can see that the age could be almost anything from 10 ky up, but is probably about 20 ky for this set of conditions.

The six curves shown in Figure D.18 are plots of the temperature at one point in the hot body as functions of time. The point is 4 km deep on the centerline (2.3 km below the top of the hot body as shown in the insert). The six curves represent reasonable variations in the heat capacity and conductivity functions and the geometry. When the variation of conductivity with temperature is included, it moves all the curves to the right. The all-molten region may extend to about 15 ky; however, the partially molten region could extend to well beyond 30 ky. Referring again to Figure D.17, if the lower left-hand corner of the uncertainty region is taken, the age is about 11 ky and there may be an all-molten core. If the median point is taken, as indicated by the X, then the age is 20 ky, the temperature at 4 km may be about 800°C and the core is mostly molten. Geometric uncertainties, discussed above, convection effects, not included in our model, and unknown initial temperature may combine to make an all-molten core improbable. However, the possibility is intriguing and a limited search with seismic instruments may be desirable.

If Function D of Figure D.14 does represent the internal energy variation, then the total energy of the original hot body is greater than that based on a linear model with a C_v = 0.2 cal/gm-°C. If 1000°C is taken as the initial temperature to compensate for not including the heat of fusion, the total energy is 200 cal/gm. If Function D is taken to 850°C (just molten), then the total energy is 284 cal/gm or 42 percent more than the linear model would predict.

Spatial Variation of Conductivity

A case was computed that was similar to Case 1, but with the conductivity 0.0081 cal/cm^2-sec-°C in and above the hot body up to 100 m depth. Elsewhere the conductivity was to remain 0.007 cal/cm^2-sec-°C as it was everywhere in Case 1. The results are shown in Figures D.19 and D.20 where the centerline gradients and temperatures are compared with Case 1 and found to be similar with differences in the direction to be expected from higher conductivity. A conductivity of 0.0081 is quite high as was seen in Figure D.12; yet it raised the 10-ky centerline gradient only about 10 percent.

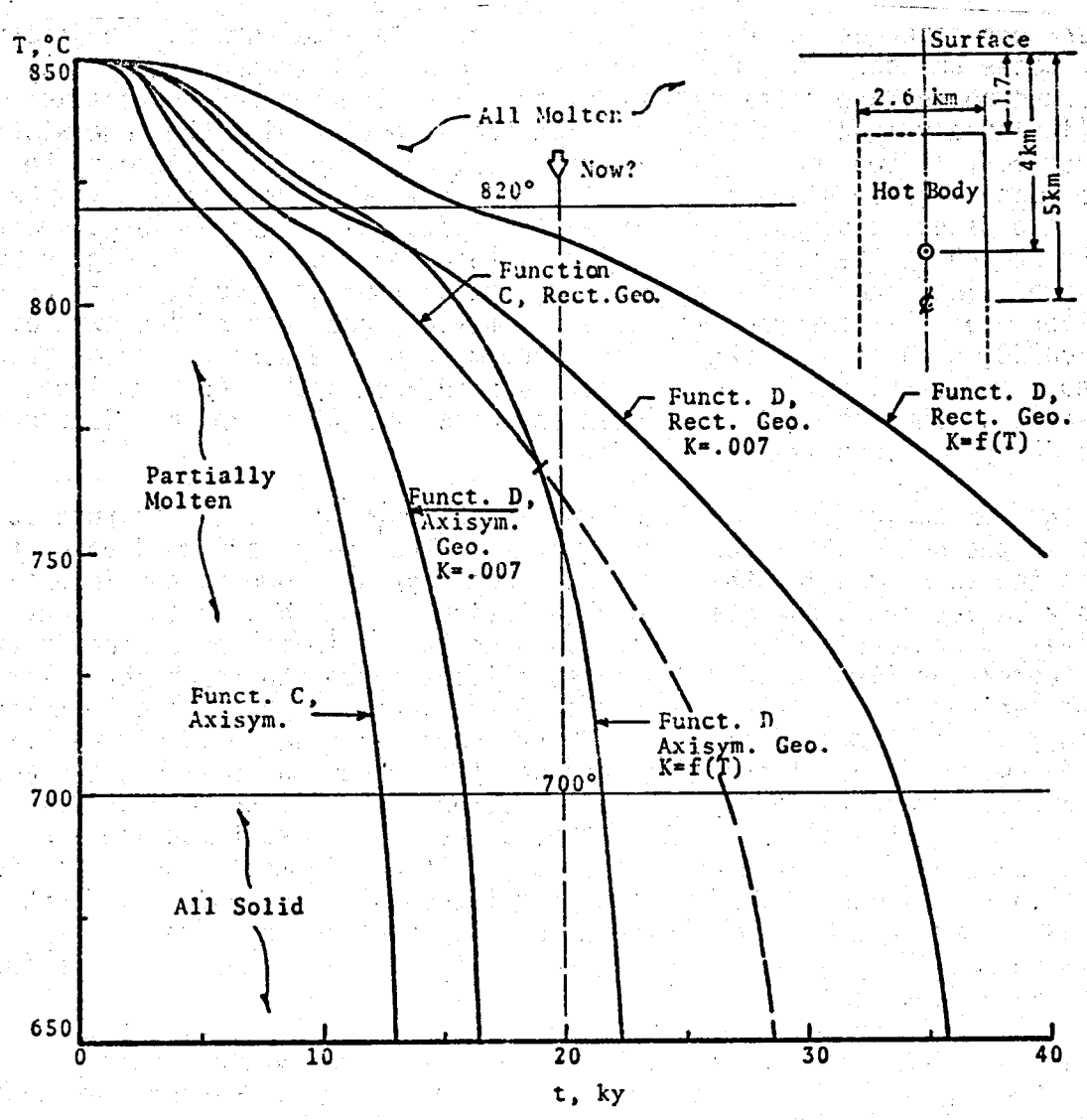

FIGURE D.18. Temperature Versus Time at 4 km Depth on Centerline

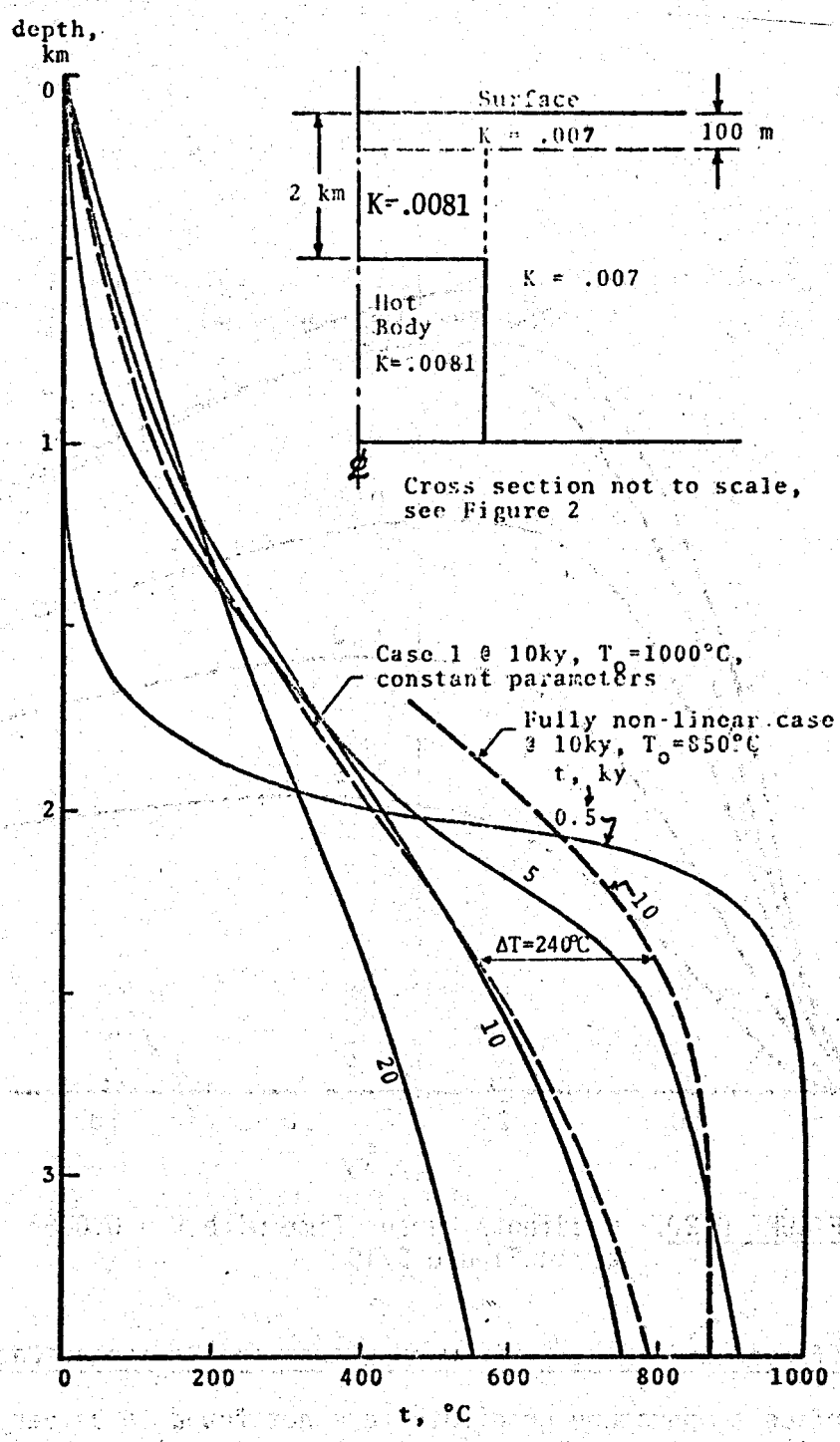

FIGURE D.19. Temperature Versus Depth. Solid lines are for K = 0.0081 cal/cm-sec°C in and above hot body to 100 m of surface, K = 0.007 elsewhere.

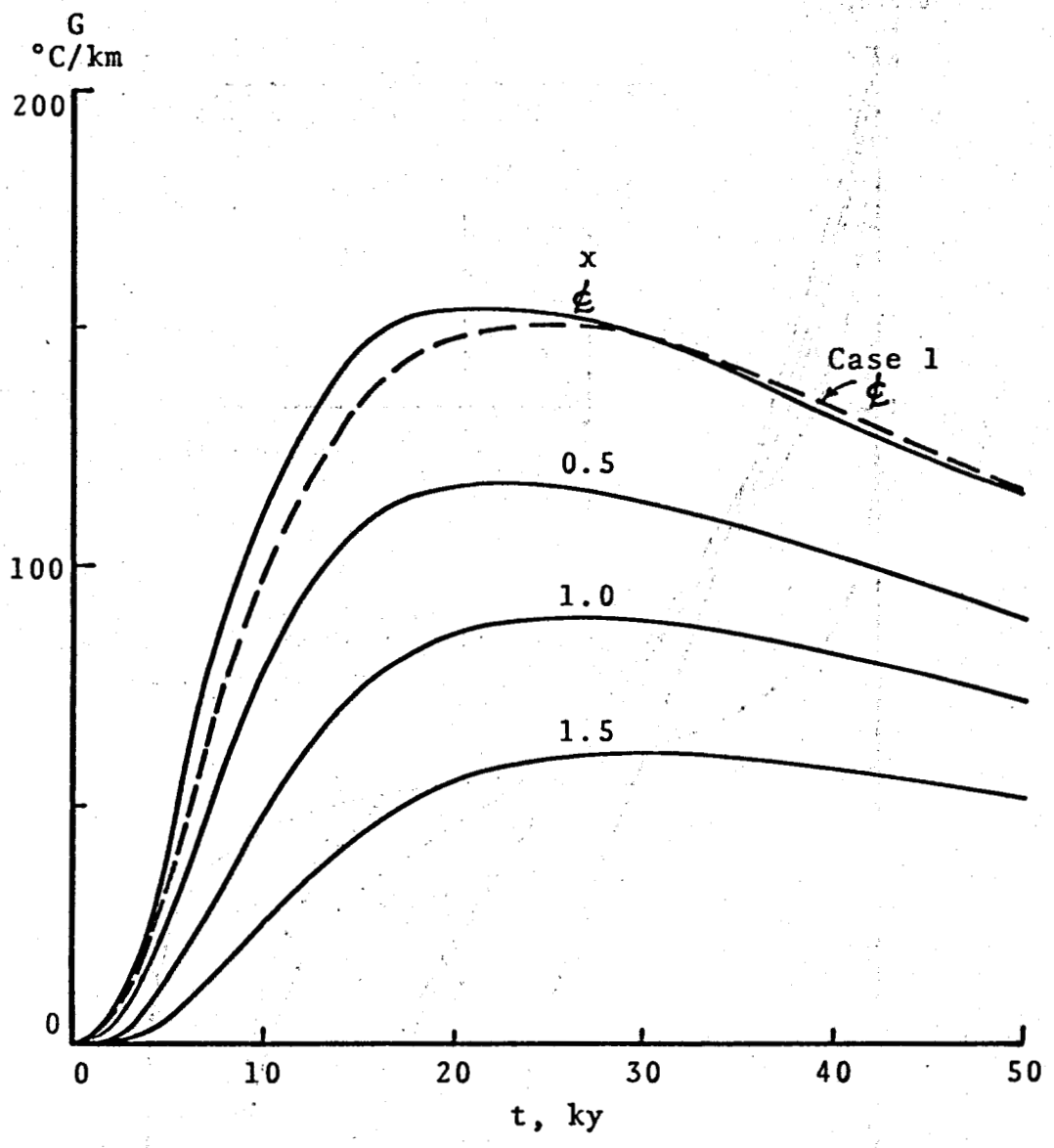

FIGURE D.20. Gradients Versus Time with K = 0.0081 as in Figure D.19

Some Differences in Results Between Linear and Nonlinear Cases

Near surface temperature gradients were not found to be very sensitive to changes in the nonlinear thermodynamic characteristics. However, temperatures within the hot body were found to be quite sensitive to these characteristics, even when the initial temperature of the linear model was raised to compensate for neglecting the phase change of the granite. For example, at 10 ky and 2.4 km depth on the centerline (well within the hot body) the difference in temperature between the linear case, started at

1000°C and the fully nonlinear simulation, started at 850°C is 240°C or about 35 percent. The temperature profile for the nonlinear calculation is shown as a heavy dashed curve in Figure D.19 where the temperature difference from the linear case at the same time and depth is indicated. There was also a minor geometric difference between these cases, but at the depths of interest for these comparisons this difference (in depth to the top of the hot body) is completely insignificant. It did have an effect on the temperature profile above the hot body, so the data from the nonlinear case was omitted from that region.

Grid Size Tests

Reduction in Height

This study was started with a uniform grid of 30 x 50 cells, each 0.1 km on a side. Special cases, like the topographic study reported above, required the use of smaller cells to define the geometry accurately. However, the 0.1-km cells appear to be satisfactory for the heat flow. The size of the grid should be minimized to save computation costs, but not to an extent that distorts the results too much. The first set of tests on grid size was on the height. Briefly, it was found that by changing the lower boundary to a reflective one that 10 rows of cells could be eliminated without changing the results. Most subsequent cases were computed with a 30 x 40 grid.

Grid Width

Figure 3 of Reference 3 hints that the grid may not be wide enough at later times. The original tests, which examined how the temperature approached the right boundary, may not have been entirely adequate. Additional tests were made and an example of the most important result is shown in Figure D.21. These curves show temperature profiles at the depth of the hot body at 20 ky. The solid curve is the reference Case 1. The dashed curve is the same case, but with a 50-cell (5 km) wide grid. Similar profiles were made for other times and other depths. All show that there is no significant difference out to about 1 1/2 body widths and 20 ky. However, the results diverge in a manner typified by Figure D.21 so that near the right boundary of the 30-cell grid the temperatures are a factor of 2 low. Hence, all gradient curves in Reference 3 labeled 2w (cell 28) should be ignored or raised. All of the cases reported here except the molten core study employed the 30-cell grid for the sake of consistency. For the molten core study all grids were at least 40 x 50 cells.

Error in Figure 1 of Reference 3

There is a minor, but unfortunate error in Figure 1 of Reference 3.* This figure was taken from a draft of Blackwell's report that contained a draftsman's error. The gradients on two westerly holes labeled 145 and

* Corrected and included here as Figure D.1.

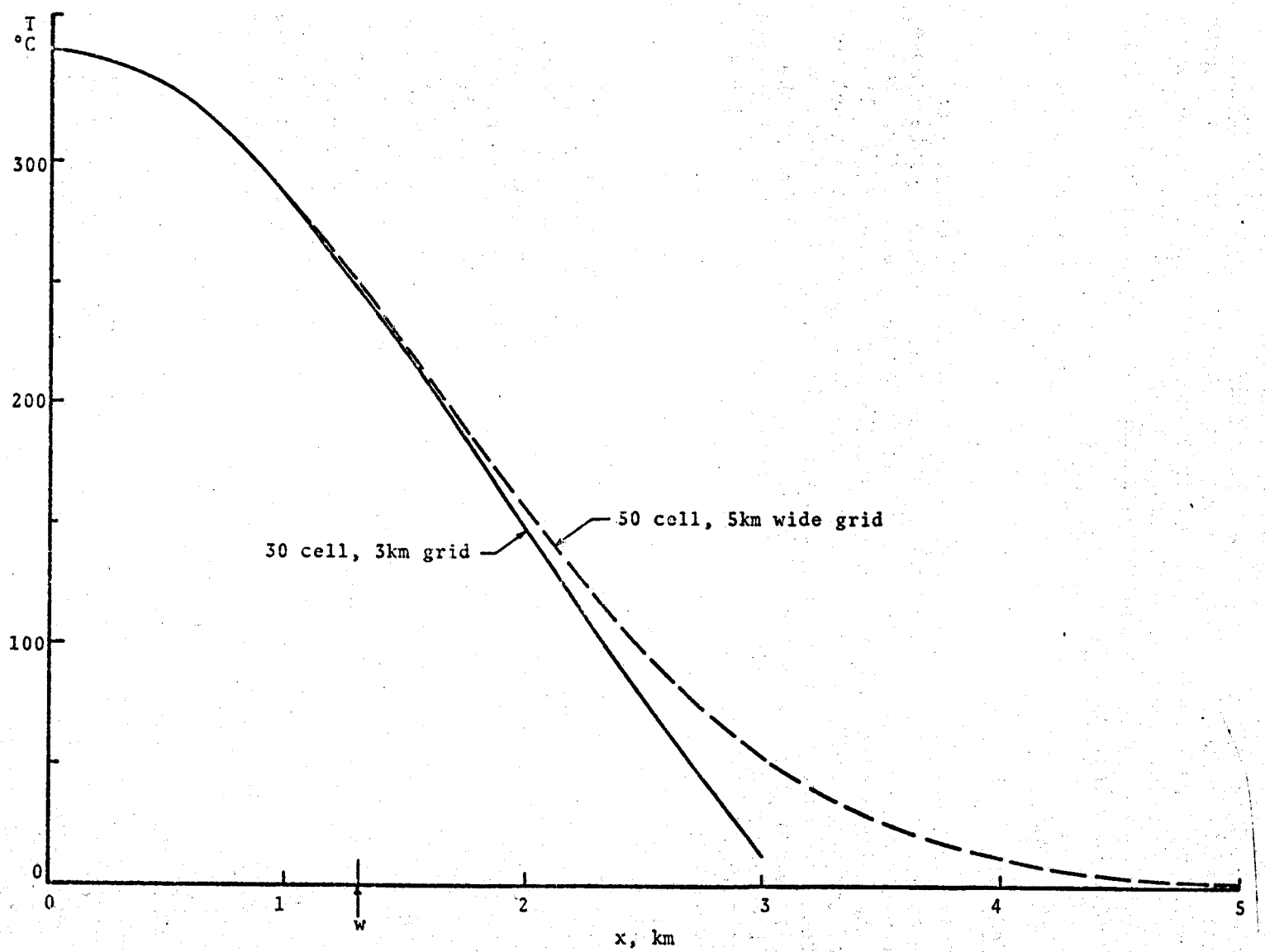

FIGURE D.21. Temperature Versus Grid Width at 2 km Depth

104 (°C/km), were permuted. Unfortunately, the one incorrectly labeled 104 is nearest the center of the model. This is the point labeled 0.0 on Case 1's gradient curve at 10 ky which was taken to indicate good agreement with the first reported results. In order to raise this point to the correct value of 145°C/km, the depth must be 1.7 km (which is why this was chosen for some of the studies reported above) or the age must be about 18 ky. Subsequently, studies have shown such sensitivity to geometry that it is now felt that there is nothing magic about 10 ky or 1.7 km depth. One can get the "correct" gradient by an infinite number of combinations of time, depth, topography and thermodynamic parameters, as was anticipated at the beginning of this study. This fact does not invalidate the results; it merely shows the caution with which the results should be interpreted.

REFERENCES

1. Preliminary Report on the Marysville, Montana Geothermal Project, Battelle-Northwest Report, November 12, 1973.

2. Blackwell, D. D., Draft of a report on the geological studies of the Marysville, Montana Geothermal Project.

3. Hays, S., S^3 letter to Dr. McSpadden, June 7, 1974.

4. Birch, F., Bull. Geol. Soc. Am. 61, 567-630 (1950).

5. Personal communication with Prof. Thomas Shankland of Harvard and Prof. George Kennedy of UCLA.

6. Birch, Francis and Harry Clark, "The Thermal Conductivity of Rocks and Its Dependence Upon Temperature and Composition," Am. J. Sci. 238, Part 1, 529-558, Part II, 613-635 (1940).

7. Smithsonian Physical Tables, Ninth Revised Edition, 1964.

COMPUTER SIMULATION OF DRILLING THERMODYNAMICS

by
C. A. Oster, Battelle-Northwest
Wilbert A. Scheffler, Joint Center for Graduate Study

September 1975

COMPUTER SIMULATION OF DRILLING THERMODYNAMICS

C. A. Oster, Battelle-Northwest
Wilbert A. Scheffler, Joint Center for Graduate Study

INTRODUCTION

The prediction of temperature distributions in rock through which a well is being drilled is an important task. An accurate prediction of the depth at which temperatures are high enough to cause steam flashing permits the driller to safely operate for longer periods with less pressure control and thus with less cost. Because the ambient rock temperature is disturbed by the drilling needs and other fluids flowing in the well, it is difficult to predict accurate temperature changes. Here we present a quasisteady state model for predicting the rock temperature changes caused by the drilling of the well. The depth change in the well is accounted for by adding new layers of rock below the layers used in the previous time period simulation. In this manner the hole is followed down through the rock formations.

The result is a computer code, THERMWEL, in FORTRAN which is simple enough to permit implementation on a minicomputer; hence it has the potential of becoming a field use tool.

MATHEMATICAL MODEL

The temperature distribution in rock surrounding a well is modeled in cylindrical coordinates with axial symmetry. The origin of this coordinate system is located at the earth's surface with the Z axis coinciding with the center of the well. The Z axis is positive in the downward direction, as indicated in Figure D.22. Three regions are assumed. Region one is a pipe of radius r_1 extending to the well bottom with no openings except at the endpoints. Region two is an annulus between the well wall and the pipe. (The well has a constant radius r_2). The well wall may have openings into the surrounding rock. Region three is the surrounding rock. Regions two and three are further divided into "control volumes" or "layers" which may coincide with the various rock layers.

We assume a cooling fluid is pumped through the drill pipe to the hole bottom where it is returned through region two, where it may mix with water from one or more aquifers. The possibility of the coolant being lost into the rock formation is also covered.

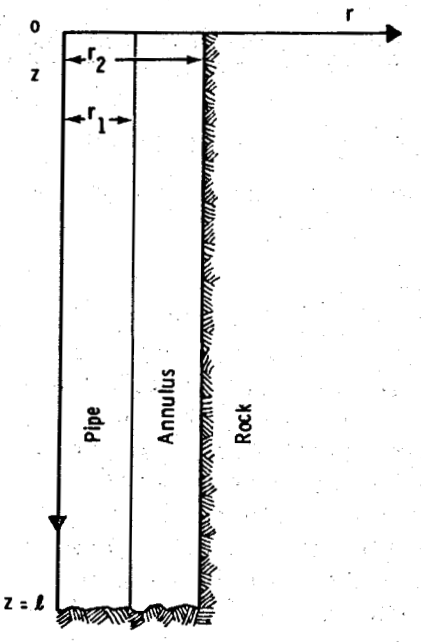

FIGURE D.22. The Well-Rock Formation Geometry

Let the subscripts 1, 2 and R refer to regions one, two and three respectively. The temperature distribution is governed by the following equations: For the pipe (region one),

$$\dot{m}_1 \, C_{pc} \, \frac{dT_1}{dz} = 2\pi r_1 \, h(T_2 - T_1) \tag{1}$$

where $\dot{m}_1$ is the mass flow rate of the coolant, C_{pc} is the specific heat of the coolant, h is a heat transfer coefficient for the pipes, and T_1, T_2 are temperatures in regions 1 and 2.

For the annulus (region two), control volume j with no aquifer flow present:

$$-\dot{m}_j \, C_{pj} \, \frac{dT_{J2}}{dz} = 2\pi r_1 \, h(T_{j2} - T_{j1}) - 2\pi r_2 \, k_j \, \left.\frac{\partial T_{jR}}{\partial r}\right|_{r=r_2} \tag{2}$$

where $\dot{m}_j$ and C_{pj} are the mass flow rate (measured positive downward) and specific heat determined by the mixture of coolant and entrained aquifer water flowing into the control volume j; and where k_j is the thermal conductivity of the rock in the j^{th} layer.

If aquifer flow is present in control volume j, the following relationship is used:

$$\dot{m}_j \, C_{pj} \, T_{j2} = (\dot{m} \, C_p \, T_2)_{upstream} + 1/2(\dot{m}_{hj} + |\dot{m}_{hj}|) C_{pH_2O} \, T_{H_2Oj}$$

where $\dot{m}_{hj}$ is the aquifer mass flow rate, C_{pH_2O} is the specific heat of water, and T_{H_2Oj} is the aquifer water temperature.

For the rock (region three), layer j,

$$\frac{1}{\alpha_{Rj}} \frac{\partial T_R}{\partial t} = \frac{\partial^2 T_R}{\partial r^2} + \frac{1}{r} \frac{\partial T_R}{\partial r} + \frac{\partial^2 T_R}{\partial Z^2} \tag{3}$$

where α_{Rj} is the thermal diffusivity for the $j^{\underline{th}}$ layer.

Boundary conditions are

$$T_R\ (r, Z, 0) = f(Z)$$

T_R is finite as $Z \longrightarrow \infty$, $r \longrightarrow \infty$

$$\left.\frac{\partial T_R}{\partial Z}\right|_{Z=0} = (q/k_R)_{surface}$$

$$T_R\ (r_2, Z, t) = T_2(Z, t)$$

$$T_1\ (Z = 0, t) = T_o$$

$$T_2\ (Z = \ell, t) = T_1\ (z = \ell, t) + \Delta T(\ell).$$

The function of f(Z) is assumed known as are (q/k_R) the surface temperature gradient with Z the surface heat flow, T_0 the temperature of the coolant at the drill pipe inlet, and $\Delta T(\ell)$ the temperature rise due to energy released by the drill bit during drilling. At the bottom of the well the depth is $Z = \ell$.

A numerical solution of the model described above may be obtained by imposing an r-Z grid on the three regions. By specifying T_0, ℓ, $\Delta T(\ell)$ at specific points in time, it is possible to obtain time dependent solutions. At any fixed time the temperatures in regions one and two are obtained iteratively. This then determines the boundary conditions needed to obtain T_R. The rock temperatures are then determined iteratively.

NUMERICAL RESULTS

The numerical procedure described in the previous section has been programmed, and Figures D.23 and D.24 show two example cases processed by the program. In both cases the simulation time was treated in three 12 hour

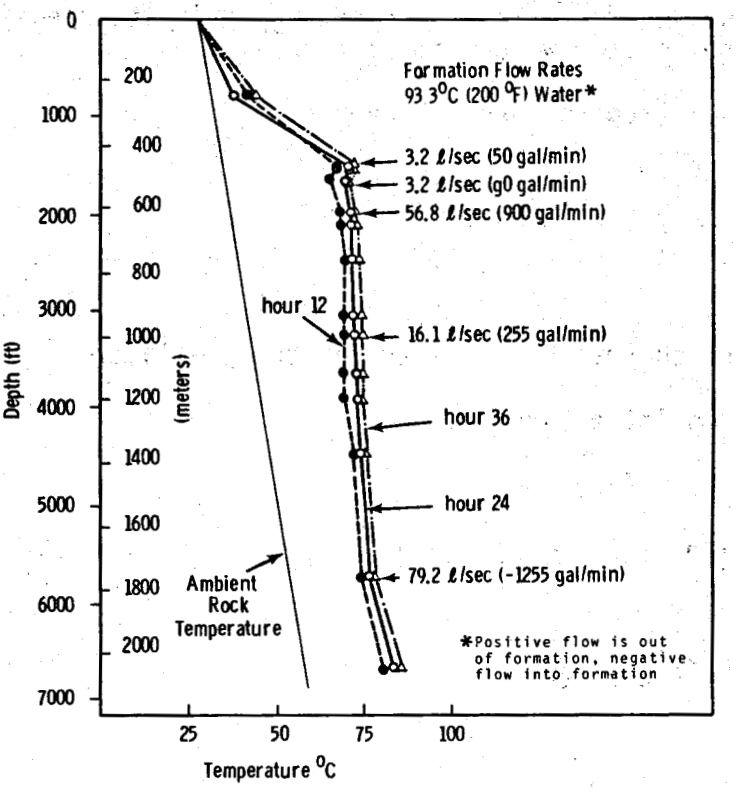

FIGURE D.23. Rock Temperature Adjacent to Well

blocks. The first and third blocks were identical, with 1.26 ℓ/sec (20 gallon/minute) of water (coolant) flowing down the pipe and a like amount flowing out of the annulus. A (5/3)°C temperature (3°F) increase $\Delta T(\ell)$ was added at the well bottom to account for the energy released by the drill bit. The second block had no flow into the pipe or out of the annulus. No temperature increase was made at the well bottom to simulate standby conditions when no drilling is in progress for the second time block.

In both cases inflow of water from the rock formation to the well and outflow from the well to the rock formation were permitted during the entire 36-hour period. The location and flow rates of these aquifer flows are shown in each figure. During the second time block the flow in the annulus is from the top aquifer to the bottom aquifer. This is generally opposite from the flow direction during the first and third time blocks when drilling fluid is being pumped.

Both Figures D.23 and D.24 show the rock temperature adjacent to the well. This temperature is taken at 10.2 cm (4 in.) out from the well wall. In Figure D.23 we have arbitrarily assumed that the formation water is considerably hotter than the ambient rock, which accounts for the continued rise in temperature of the rock adjacent to the well during the second time

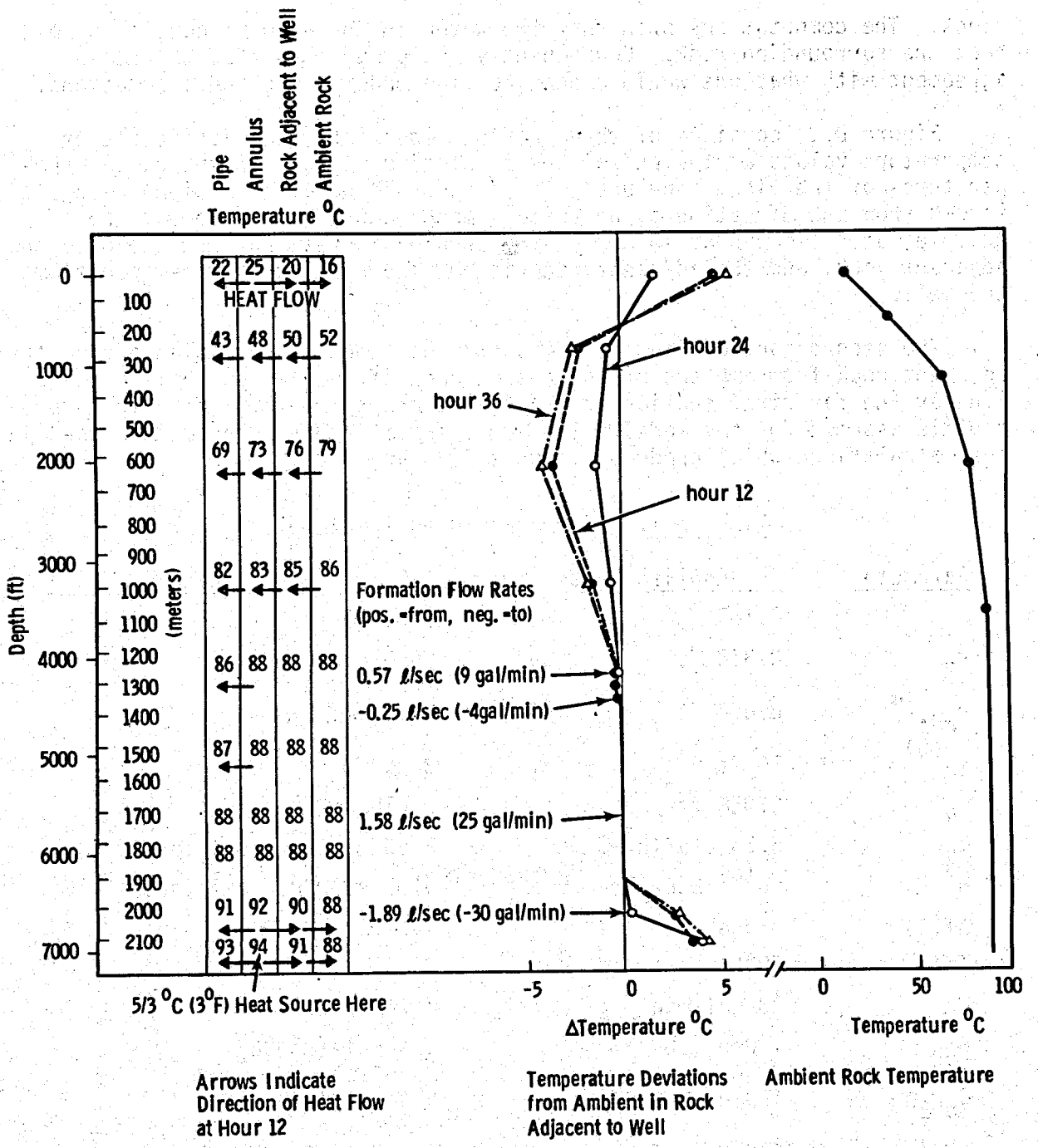

FIGURE D.24. Simulation of Rock Adjacent to Well Temperature Over a 36-Hour Period

block. The computations show that the water in the annulus continues to heat the surrounding rock. Consequently the programmed results are in agreement with what one would expect to find under the given assumptions.

Figure D.24 consists of three parts. The first part is a table of temperature values at the end of the first time block. These are the temperatures of the pipe, annulus, rock adjacent to well and ambient rock. Arrows show the direction of heat flow among each of these zones. For example, at the depth of 15 meters the annulus is heating both the pipe and adjacent rock, and the adjacent rock is heating rock further removed from the well.

The second part of Figure D.24 shows the temperature deviations of the adjacent rock from ambient at the end of each of the 12 hour time blocks. Finally the far right section of the figure graphs the ambient temperature profile assumed for the model. Table D.1 summarizes the parameters used in the calculations which produced Figures D.23 and D.24.

TABLE D.1. Parameters Used in Examples

Parameter	English Units	Metric Units
r_1	0.167 ft	5.09 cm
r_2	0.328 ft	10.0 cm
r_{adj} (a)	0.664 ft	20.2 cm
r_∞ (b)	10 ft	3.048 m
α_R	0.058 ft^2/hr	0.015 cm^2/sec
k_R	6.36 Btu/(hr-ft-°F)	2.63 x 10^{-3} K cal/(sec-m°C)
h	50 (c) Btu/(hr-ft^2-°F)	67.8 x 10^{-3} K cal/(sec-m^2-°C)
$\Delta T(\ell)$	3 and 0°F	1.67 and 0°C
To	70°F	21.1°C
Mo	20 gal/min	1.26 ℓ/sec
C_{pc}	1 Btu/(lb-°F)	1 K cal/(kg-°C)
C_{pH_2O}	1 Btu/(lb-°F)	1 K cal/(kg-°C)
q	0.259 Btu/(hr-ft^2)	0.195 x 10^{-3} K cal/(sec-m^2)

a. Location of adjacent rock temperature shown in Figures D.23 and D.24.
b. Location of ambient rock temperatures in Figures D.23 and D.24.
c. Calculated from the Sieder-Tate turbulent flow correlation.

COMPUTING REQUIREMENTS FOR THERMWEL

The computations discussed in the previous section were made by coding the mathematical model in FORTRAN and executing the resulting program (THERMWEL) on a Systems Engineering Laboratories (SEL) 840A computer. The FORTRAN program required 2838 (decimal) memory locations plus 3155 (decimal) storage locations, for a total of 5993 storage locations. The program currently permits up to 15 radial points and 30 depth points. From these numbers it appears that the current program could be slightly expanded and still fit into a minicomputer with 8K memory locations.

Execution times were not precisely determined but are estimated at 1 minute computer time needed to simulate 12 hours of clock time. Based on this, the model should provide no difficulties in permitting several simulations during a drilling period of several hours.

DIRECT TREE TEMPERATURE SURVEY, AUGUST 1974

by
Jay R. Eliason
Battelle-Northwest

September 1975

DIRECT TREE TEMPERATURE SURVEY, AUGUST 1974

J. R. Eliason and H. P. Foote, Battelle-Northwest

An aerial infrared survey[1] of the terrain surrounding the drill site was made in September 1973. The optical mechanical imaging system used operates in the 3-5μ and 8-14μ wavelength spectral bands and the tests were made at an altitude of approximately 10,000 feet. The temperature rise in the survey area, due to heat flow from the geothermal anomaly, had been estimated at 0.2°C maximum. However, the survey did not directly detect thermal anomalies at the earth's surface, even though the infrared imaging systems were sensitive to changes of ≤0.1°C.

Direct thermal detection of geothermal gradients can be limited by natural effects such as terrain, microclimate, emissivity, and vegetation. Measurements of the magnitude of these effects indicated that they would be on the order of 0.2°C or greater, or approximately the amount of the anticipated surface temperature difference above the predicted geothermal anomaly. Since these natural effects appeared to be inhibiting temperature detection, an attempt was made to delineate the anomaly by carefully comparing data from sparsely vegetated clearings and making temperature corrections for altitude. Using this technique, the natural surface thermal variations were found to dominate the observed temperature patterns in these areas. A significant thermal anomaly (∿1.5°C) was found in tree canopies which appeared to correlate with the mapped geothermal anomaly. This was interpreted as an indication that the trees' root systems were withdrawing soil moisture from the zone of high heat flow. Field surveys were conducted in August 1974 to determine whether the anomaly measured in the tree canopies was in fact related to the area of high heat flow; these studies verified the existence and area of the anomaly.

The thermal anomalies first observed in tree canopies are thought to be an indirect indication of geothermal activity. The root systems of the trees may be tapping warm groundwater from the areas of high heat flow and causing the trees to reflect this temperature rise (which could be 1 to 2°C for a root system 10 to 20 feet deep). Subsequent field measurements of tree temperatures in and near the anomalous area have confirmed the existence of a significant difference in tree canopy temperatures. This does not appear to relate to visible differences in the tree canopies and trees in the anomalous area do not appear to be diseased or infected by insects. Trees in the area of the highest geothermal gradient (as detected by direct thermal measurements) demonstrate the most significant variation in canopy temperatures. Trees west of the Marysville townsite also show significant thermal variations, but this area has not been mapped for heat flow and the source of thermal variation is unknown.

---

(1) First Annual Report, Marysville, Montana Geothermal Project, Part I, Section 7, Battelle-Northwest, NSF-RA-N-74031a, June 1974.

Limited digital computer analyses of the imagery were conducted to enhance the observed anomalies. These analyses show that the anomalies identified in the tree canopies are significant.

The thermal anomalies observed in the 8-14μ infrared imagery collected in September 1973 were verified by field measurements collected in late August 1974. Over a period of several days, measurements of tree temperatures were collected within the anomalous area on Lost Horse Creek and at several locations outside this area. These included radiometric measurements of the bark and canopies with an 8-14μ infrared radiometer and contact measurements of the tree trunks at various depths beneath the bark with a thermistor probe and mercury thermometers. Measurements were made at several times of day, including the diurnal low during which the anomalies were observed in the aerial thermal imagery.

Radiometric measurements made at the diurnal low confirmed that trees in the anomalous area identified in the aerial survey had canopy temperatures approximately 1.5°C above those of trees in surrounding areas. These direct measurements of tree temperatures tend to confirm the existence of the anomaly observed in the aerial infrared imagery. Examples of tree temperature data collected at several locations near the observed anomaly are presented in Table D.2.

No evidence of significant tree disease or insect infestation was observed within the anomalous area during the August 1974 field survey period. If the higher temperatures in anomalous area had been caused by tree disease or insect infestation during the September 1973 survey, these conditions or their results should have been visible.

TABLE D.2 Tree Temperatures°C[a]

	Trunk Temperatures[b]	Canopy Temperatures[c]
Trees on west-facing slope outside the thermal anomaly	10.6	1.9
	10.0	2.0
	10.45	1.9
Trees on west-facing slope outside the thermal anomaly	12.8	3.2
	13.8	3.5
	12.3	3.2

(a) measurements collected predawn August 21, 1974
(b) trunk temperatures at 4 in. beneath the bark of trees ranging from 30 to 40 in. in diameter
(c) tree canopy measurements collected with an 8-14μ infrared radiometer

The results of this study show that variations in geothermal heat flow near the surface may significantly influence vegetation temperatures and thus may provide an indirect indication of anomalous geothermal gradients in vegetated areas. In trees in the Marysville area, surface temperatures have been amplified to a level significantly above the normal background thermal variations. Correlation of these results with final geologic, geophysical, and geochemical studies conducted by D. D. Blackwell et al. was not possible due to termination of the program.

SECTION E

GEOLOGICAL, GEOPHYSICAL AND GEOCHEMICAL STUDIES

Results and Analysis of Exploration and Deep Drilling at Marysville Geothermal Area

D. D. Blackwell et al., Southern Methodist University

Magnetotelluric Sounding-Marysville, Montana

W. J. Peeples, University of Utah and
D. Rankin, University of Alberta

SECTION E GEOLOGICAL, GEOPHYSICAL AND GEOCHEMICAL STUDIES

CONTENTS

CONTENTS (contd)

LIST OF FIGURES

LIST OF FIGURES (contd)

LIST OF TABLES

RESULTS AND ANALYSIS OF EXPLORATION AND DEEP DRILLING AT MARYSVILLE GEOTHERMAL AREA

by
David D. Blackwell, M. J. Holdaway,
Paul Morgan, David Petefish, Thomas Rape,
John L. Steele, D. Thorstenson and
A. F. Waibel
Southern Methodist University

September 1975

RESULTS AND ANALYSIS OF EXPLORATION AND DEEP DRILLING AT MARYSVILLE GEOTHERMAL AREA

David D. Blackwell, et al.

Southern Methodist University

INTRODUCTION

This report contains the results of geological and geophysical studies in the Marysville geothermal area during 1974 and of the geological and geophysical studies both during and subsequent to the drilling of a 2.1 km deep hole in the geothermal area. The report is composed of two parts, the first part dealing with studies carried out at Southern Methodist University and the second part describing detailed magnetotelluric and audiomagnetotelluric studies carried out by University of Utah personnel (Peeples, 1975) and University of Alberta personnel (Randin, 1975) as a subcontract. Other primary sources of material contributing to the studies described here are reports dealing with the drilling of the deep exploration drill hole (Rogers Engineering Company, 1975), a report submitted by Schlumberger concerning results of the well logging (Coates, 1974), and a report dealing with some numerical models of topographic effects on heat flow measurements and of magma chamber cooling histories (Hays, 1975). These reports are also included as part of the project final report. The geological and geophysical background for the 1974/75 studies is contained in the interim technical report submitted in 1974 (Blackwell et al., 1974; Friedline and Smith, 1974) while details of the environmental impact studies and deep well drilling specifications were included in a companion report (McSpadden et al., 1974).

During 1974 the exploration studies included a continuation of geological mapping, sample collection, gravity and magnetic surveys, and heat flow programs begun in 1973. In addition, an extensive magnetotelluric and audiomagnetotelluric survey was carried out in order to determine the subsurface electrical resistivity in the geothermal area. Two heat flow holes were drilled outside the geothermal area in order to investigate the implications of the microearthquake data obtained by Friedline and Smith (1974). In addition, geological and geophysical decisions dealing with the drilling and logging of the 2.1 km deep hole were provided. Special studies dealing with the deep exploration drill hole included temperature logging during drilling, the collection and analysis of fluid samples obtained from the well, studies of the physical and chemical properties of the rock from cuttings and core samples, and analysis of the various geophysical logs obtained. Subsequent to the completion of the field studies extensive laboratory and data analysis have been in progress. The present report is a summary of these studies.

A topographic map of the area is shown in Figure E.1. The area is about 30 km northwest of Helena, Montana and sits astride the Continental Divide. Most of the maps shown in succeeding sections of the report have the same scale as Figure E.1 and cover the same area. The location of the deep exploration drill hole (Marysville Geothermal Exploration Number 1 - MGE #1) is shown in Figure E.1 by the derrick symbol.

The results of the 1973/74 studies were a verification of data obtained by Blackwell (1969), Blackwell and Baag (1973), and Mazzella (1974) with the

Figure E.1 Topographic Map of the Marysville Area. The map is a composite of parts of the Granite Butte, Canyon Creek, Silver 3 Northeast, and Silver 3 Northwest 1:24,000 scale USGS quadrangle maps. The following localities are indicated by numbers: 1. Bald Butte, 2. Ottawa Gulch, 3. Roundtop Mtn., 4. Drumlummon Hill, 5. Mt. Belmont, 6. Towsley Gulch, 7. Woodchopper Gulch, 8. Hope Creek, 9. Spring Gulch. The location of MGE #1 is shown by the derrick symbol.

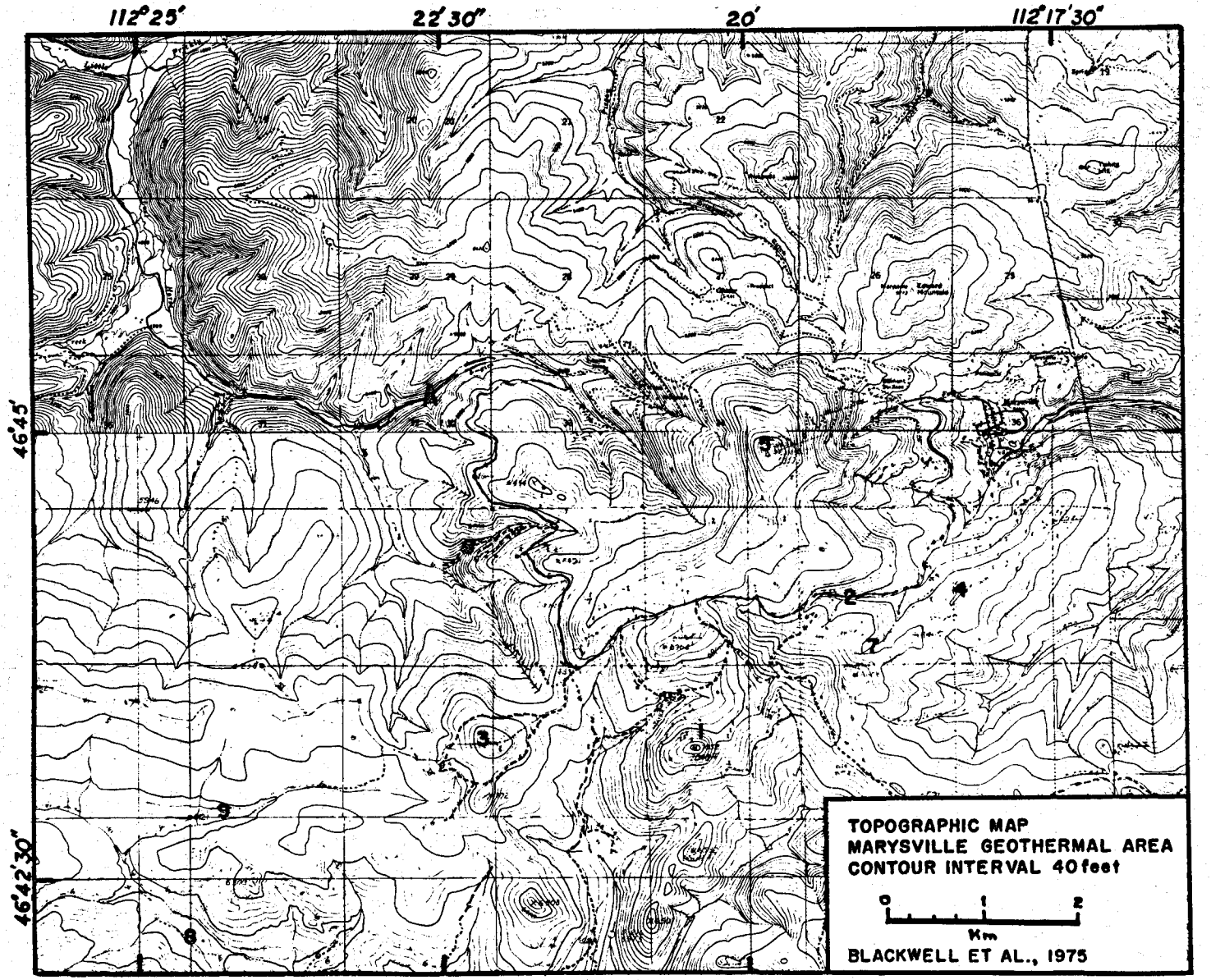
112°25'
22'30"
20'
112°17'30"
46'45'
46'42'30"
TOPOGRAPHIC MAP
MARYSVILLE GEOTHERMAL AREA
CONTOUR INTERVAL 40 feet
0
1
2
Km
BLACKWELL ET AL., 1975

FIGURE E.1

addition of much additional information. The results of these investigations indicated a geothermal area with a surface expression in excess of 50 km^2 with heat flow values as high as 19.5 $\mu cal/cm^2$ sec and geothermal gradients as high as 240°C/km. The geologic section in the area of the geothermal anomaly was found to be a thin cap of highly contact metamorphosed sedimentary rocks overlying a large unexposed Cenozoic granitic pluton. It was predicted that the depth to this pluton would not exceed 300 meters in most of the region of highest heat flow. The two possibilities considered for the source of high heat flow were a shallow cooling magma chamber and a shallow reservoir of circulating hot water. The features of the area are a lack of surface manifestations of hot ground water, high shallow electrical resistivity values, correlation of a negative gravity anomaly with the high heat flow, and a geologic section at depth that included mostly granitic rocks. On the basis of these results authorization was given by the National Science Foundation for drilling of the deep exploration hole in the Marysville geothermal area during the summer of 1974.

The responsibilities for the material in this report rest with a number of different people, primarily as follows: David D. Blackwell, Chief Scientist of the Marysville geothermal project was in overall charge of the scientific aspects of the studies carried out during the project; geologic mapping was carried out by A. F. Waibel, M. J. Holdaway, and David Petefish; M. J. Holdaway and David Petefish continued their study of the metamorphism in the Marysville area and A. F. Waibel continued studies of the chemical composition of the igneous rocks. Both of these studies were broadened to include samples from the deep drill hole as well as those from the surface. Structural analysis and synthesis of the geologic data were prepared by David Petefish and David D. Blackwell. The gravity survey field work was carried out by Tommy Rape and the computer analysis and interpretation were by Paul Morgan. Paul Morgan also interpreted the magnetic data, the microearthquake data, and the temperature logs made during drilling of MGE #1. R. B. Smith of the University of Utah was a consultant for the field and laboratory phases of the microearthquake survey. The heat flow study was directed by D. D. Blackwell and Paul Morgan. Thermal conductivity measurements were made by J. L. Steele and heat flow calculations and interpretation were by D. D. Blackwell, J. L. Steele and Paul Morgan. David Petefish acted as the on site well geologist during the drilling of the deep hole. D. C. Thorstenson analyzed and interpreted the water samples obtained from MGE #1.

The results of the geological and geophysical studies relating to the exploration in the Marysville area and results of the deep well drilling have been discussed extensively in the literature. Papers summarizing interim results have been given at the 9th Intersociety Engineering Conference in San Francisco in August 1974 (Blackwell, 1974), at the National Science Foundation RANN sponsored meeting on geothermal energy in Pasadena, California in September 1974 (Blackwell et al., 1974a), in a publication on Montana energy resources (Blackwell et al., 1975), and in a paper given and to be published in the Proceedings of the Second United Nations Geothermal Symposium, held in San Francisco during May 1975 (Blackwell and Morgan, 1975).

In addition, the results of the research are represented in several thesis studies. The microearthquake survey carried out during 1973 is the subject of a Masters Thesis (Friedline, 1974). The magnetotelluric studies carried out during 1974 will be the subject of a Masters Thesis (Stodt, 1975). Some aspects of the metamorphic and geologic studies of the geothermal area will also form part of a Masters Thesis (Petefish, 1975). In addition, the various aspects of the studies will form portions of at least two Ph.D. theses. These include a detailed study of the distribution of U, Th, and K in the surface rocks and the deep drill hole (Gosnold, 1975) and a study of interpretation techniques applied to heat flow studies in geothermal areas (Brott, 1975).

Interaction with groups outside the project included several cooperative studies with the U.S. Geological Survey which included resistivity measurements in the geothermal area (Jackson, 1972) and two different surveys of soil gases (Craig Rightmire and Margaret Hinkle, personal communications). During the summer of 1974 numerous people and organizations visited the project. Among these were a meeting of the Montana Geological Society which included a field trip to the area on August 26, 1974.

Acknowledgements

Many people have made contributions to the studies described here. Among these to which special acknowledgements are due are R. E. Spafford for assistance in the field in 1973 and for the design, fabrication and maintenance on most of the geophysical equipment used during the field studies. Barbara Doolin typed several versions of the manuscript. Jiaw Chu and David Davies made terrain corrections for the gravity and heat flow surveys and assisted in the laboratory measurements. Charles Brott calculated the continuation model of the geothermal reservoir shown in Figure E.25 and W. D. Gosnold measured U, Th, and K contents of core samples from the deep well. Most of the studies took place on Federal land and John Fields of the Missoula Office of Bureau Land Management and Jim Fishburn of the U.S. Forest Service were most cooperative and helpful during the course of the project. Dr. A. H. Truesdell loaned a drill hole fluid sampler which was used to obtain fluid samples in the well. The gravimeter used during the 1974 field season was loaned by Dr. Charles Whalen at the 1st Geodetic Squadron, U.S. Air Force, Cheyenne, Wyoming. Discussions and/or contributions of various kinds from Dr. E. C. Robertson, Dr. G. D. Robinson, Giles Walker, Ora Rostad, and Marvin Ratcliff are greatly appreciated. Thanks are also expressed to the residents of Marysville for their hospitality.

1974/75 EXPLORATION STUDIES - MARYSVILLE GEOTHERMAL AREA

Most of the studies carried out during 1974 in the immediate area of the geothermal anomaly were the continuation of studies begun in 1973 or before. The most significant efforts were continued geological studies, measurement of additional gravity stations, and the drilling of four additional holes for heat flow studies. The most extensive new study was the combined magnetotelluric and audiomagnetotelluric survey aimed at obtaining data on the subsurface resistivity in the geothermal area. The new results

of the various studies will be described in this section. Since most of these studies are a continuation of the work done in 1973, reference should be made to the 1974 report for more detailed background on the geothermal area for details of the previous results of some of these studies, and for details of previously completed studies (seismic ground noise study, magnetic surveys, and geochemical studies).

Geologic Map and Lithologic Units

In 1974 geologic mapping was carried out by A. F. Waibel, M. J. Holdaway, and D. Petefish. Mapping during 1973 demonstrated certain problems in the available maps of the area, which needed to be resolved in order to adequately understand the geologic framework of the geothermal area. The map resulting from the two years of the studies is shown in Figure E.2. In addition, a summary of the igneous history of the Marysville area is shown in Table E.1. Little new information has been obtained during this year's studies to modify the pre-existing knowledge of the sequence of events. Additional potassium-argon age dating was planned, but funding uncertainties have precluded the obtaining of these data. Regional aspects of the geology and geophysics of the central-western Montana area have been discussed by Ross (1963), Robinson et al. (1968), Tilling et al. (1968), Johnson et al. (1965), Biehler and Bonini (1969), Burfiend (1967), Davis et al. (1963), Kleinkopf and Mudge (1972), Pardee (1950), Blackwell and Robertson (1973) and others. Parts of the geothermal area were first studied by Barrell (1907), who described the Marysville stock and the intruded sedimentary units. Barrell showed that the stock was intruded at a shallow depth (epizonal in terms of the classification of Buddington, 1959), and described the contact metamorphism in an epizonal environment. Knopf (1950) discussed the stock and its relation to gold-bearing veins of the Marysville district and to the Boulder batholith 15 km to the south. He also contributed information on the contact metamorphism. More recently, mapping in the area has also been done by Bierwagen (1964), and Ratcliff (personal communication, 1973). Additional studies in the area have been by Pardee and Schrader (1933), Mantei and Brownlow (1967) and Rostad (1969).

All but the southwestern quarter of the area shown in Figure E.2 has been remapped as part of this project with a particularly detailed emphasis on the dome southwest of the Marysville stock, and the immediate vicinity of the Marysville stock. At the margins of Figure E.2 the mapping has been less detailed. The units shown in the map are listed in the legend of Figure E.2 and some of the sedimentary and metamorphic units are described in more detail below.

An important difference between the map shown in Figure E.2 and the map shown in the 1974 report is a modification of the distribution of the Empire Shale. The exposures of the Empire Shale are now confined to the center of the map where the Empire Shale occurs in the core of a broad dome. Exposures of the Empire Shale, shown by Barrell (1907) and subsequent workers, northeast of the Marysville stock are actually highly contact metamorphosed Helena Formation. Detailed studies suggest that incorrect identification of the Helena

Figure E.2 Geologic map based on maps of Barrell (1907), Bierwagen (1964), Ratcliff (unpublished) and 1973/75 studies by M.J. Holdaway, A.F. Waibel, and D. Petefish. The light lines are formation contacts and the heavy lines are faults. The axes of folds are indicated by heavy lines and arrows showing plunge direction. Question marks indicate the areas of the map where the data are uncertain. The map key is as follows:

Sedimentary rocks

- Qal Quaternary Alluvium
- Dj Jefferson Formation, Devonian
- Ꞓppr Cambrian shales, dolomite and limestones
- Ꞓm Meager limestone, Cambrian
- Ꞓw Wolsey Shale, Cambrian
- Ꞓf Flathead Quartzite, Cambrian
- PꞒb Black Mountain Formation (Quartzite)
- PꞒg Greenhorn Mountain Formation (Quartzite)
- PꞒm Marsh Shale
- PꞒh Helena Formation
- PꞒe Empire Shale
- PꞒs Spokane Argillite (Cross sections only)

Igneous Rocks

- Kgr Cretaceous Granodiorite (Marysville Stock - 79 million years old)
- Kg Cretaceous Gabbroic plugs
- Tv Cenozoic volcanic rocks (37 million years old)

Many dikes and sills have been omitted from the map

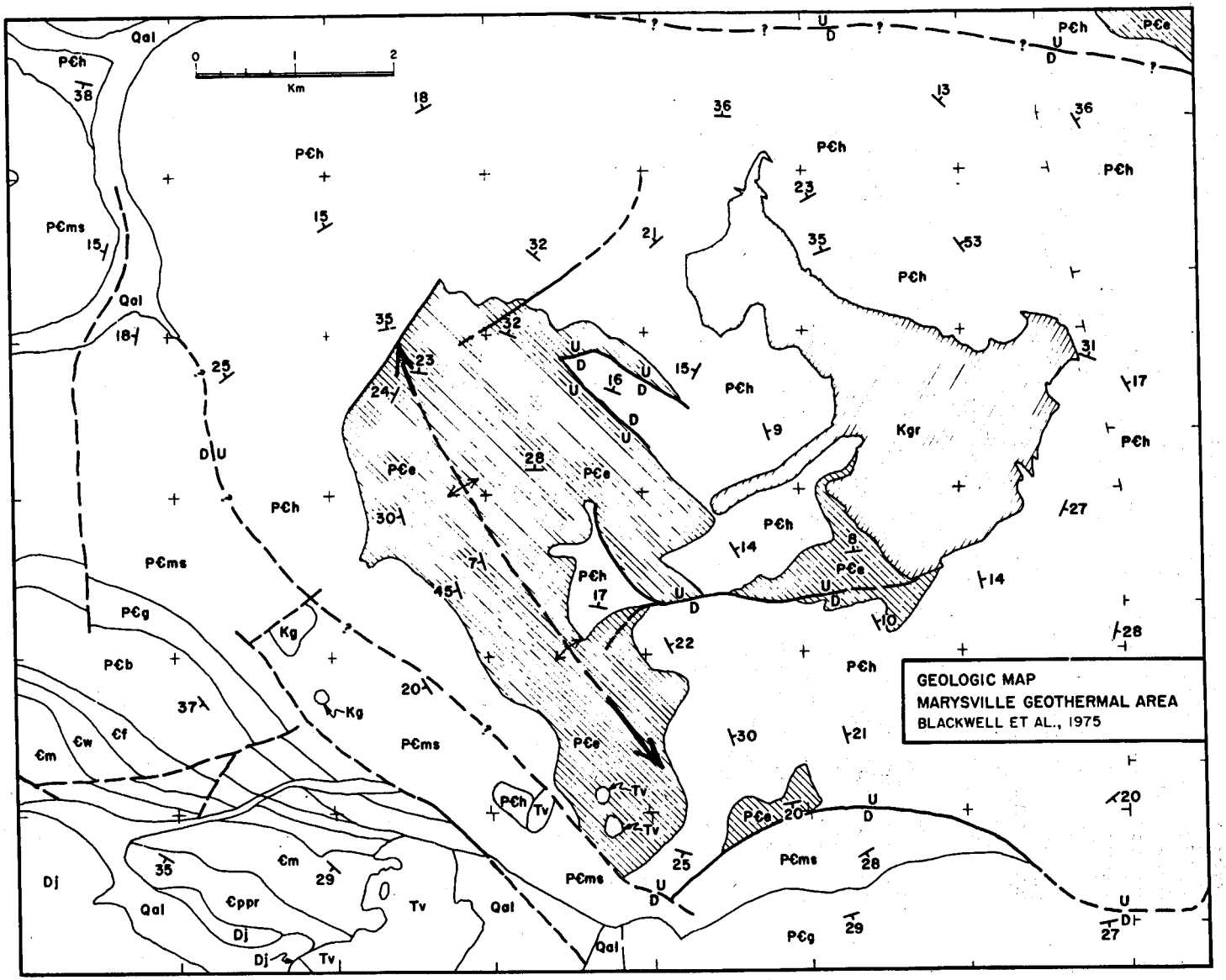
GEOLOGIC MAP
MARYSVILLE GEOTHERMAL AREA
BLACKWELL ET AL., 1975
Km
Qal
PCh
PCe
PCms
PCg
PCb
Kg
Kgr
Tv
Dj
Cm
Cw
Cf
Cppr

FIGURE E.2

Table E.1 History of Major Dated Igneous Events in the Marysville District. The ages of the Cenozoic events are from Ratcliff (personal communication, 1973) and Rostad (personal communication, 1972).

Age	Name and Location	Regional Correlation
Precambrian(?)	Microdiorite Sills, Empire Shale	Regionally developed in upper part of Empire Shale and lower part of Helena Formation
79 M.Y.	Marysville Stock	Same general age and composition as Boulder Batholith
48 M.Y.	Bald Butte Stock	Same age as widespread Lowland Creek Volcanics of Boulder Batholith region
48 M.Y.	Hornblende Diorite Dikes, S.W. of Marysville Stock	
40 M.Y.	Empire Creek Stock	Same age as widespread, but small volume, Oligocene volcanics north of Boulder Batholith
37 M.Y.	Adularia Vein, S.W of Marysville Stock	
37 M.Y.	Hope Creek Rhyolite	

there was probably caused by the inability to differentiate in reconnaissance work between the highly contact metamorphosed Helena Formation and the Empire Shale. Thus doming associated with the Marysville stock is much less pronounced than indicated by Barrell, suggesting even more strongly the role of stoping in the emplacement of the Marysville, as described in classic fashion by Barrell (1907).

The sedimentary and metasedimentary rocks in the Marysville area (Figure E.2) comprise part of the Precambrian Belt Series (Ross, 1963) and lower Paleozoic formations. The units of the Belt Series are the Spokane Shale, the Empire Shale, the Helena Formation, the Marsh Shale, the Greenhorn Mountain Quartzite, and the Black Mountain Quartzite.

Spokane Shale. The oldest formation in the area, the Spokane Shale, is exposed along Prickly Pear Creek in the northern part of the area where it conformably underlies Empire Shale. Metamorphosed Spokane Shale may also occur in MGE #1 on Empire Creek beneath the Empire Shale. The Spokane Shale consists of purple-red siliceous, argillaceous, and arenaceous shale, lacking in calcareous material (Ross, 1963). In the Marysville area the unit consists of quartz, detrital muscovite, hematite, and minor plagioclase.

Empire Shale. The overlying Empire Shale is exposed in the Prickly Pear Creek area and the more extensively as hornfels southwest of the Marysville stock in the Empire Creek and Bald Butte areas. According to Ross (1963), unmetamorphosed Empire is a compact, locally calcareous, light to dark greenish gray shale. In the study area the original Empire sediments were thin-bedded light green dolomitic shale with no limestone. Near igneous bodies the Empire now consists of fine-grained light green, dark green, or black hornfels. Bedding may be preserved as a tendency for the rock to split parallel to slight lithologic differences. Except at the highest grades, most of the Empire hornfels is calcite-bearing. Rarely, the unit consisted of pure shale, as implied by the presence of cordierite in one small area south of the Marysville stock.

Helena Formation. The Helena Formation overlies the Empire Shale and is widely exposed in the project area. It consists of two lithologies interbedded on every scale from 0.5 cm to the scale of an outcrop. Perhaps most common is limestone with traces of quartz and other impurities. The limestone occurs as edgewise conglomerate, "molar tooth" structure (Knopf, 1950), or rarely as oolitic limestone. The grey limestone weathers quickly while the impurities stand out on the weathered surface. A second lithology is dark brown or black, buff weathering siliceous dolomite. The dolomite contains significant amounts of quartz, K-feldspar, and muscovite, and in the lower parts of the formation, increasing fractions in these impurities make the Helena dolomites compositionally similar to the Empire Shale. Contact metamorphism has little effect on the limestones until the highest grades are reached, at which stage they become white and coarse in grain size. Metamorphism of the dolomites produced white, light green, or purple-brown rocks. Commonly the hornfels is banded limestone-siliceous dolomite with bands of white, light green, and brown hornfels 1 to 2 cm thick.

The contact between the Helena and Empire formations is a transition zone about 40 m thick. The map contact is drawn near the middle of this zone where calcite-rich rocks become common. The transitional rocks are commonly banded hornfels containing white and light to dark green bands 1/2 to 1 cm in width. The underlying Empire contains only fine (1 to 3 mm) subtle banding in various shades of green.

Marsh Shale. In the west, southwest, and south part the area the Marsh Shale overlies or is in fault contact with the Helena Formation (Figure E.2). This unit consists of red shale with some calcareous and quartzitic layers. These rocks show no metamorphism because of their distance from the plutons and/or because of modification of the contact zone by faulting.

Greenhorn and Black Mountain Quartzites. The youngest Belt Series rocks of the area occur above the Marsh in the southeast. Greenhorn Mountain Formation is white to pink microcline-bearing quartzite.

Lower Paleozoic Rocks. Southwest dipping Paleozoic rocks unconformably overlie the Belt Series rocks. The formations exposed are the Cambrian Flathead Quartzite, a pure quartzite; the Cambrian Woolsey shale; the Cambrian Meager Limestone; unnamed Cambrian shale, dolomite, and limestone; and the Devonian Jefferson Formation (Bierwagen, 1964).

Metamorphic Petrology

The detailed study of the metamorphic petrology in the area continued during 1974/75. The 1973/74 study was primarily responsible for the conclusion that the Empire Creek stock must be much larger than its known extent at shallow depths and indeed could underlie most of the dome in the Empire Shale southwest of the Marysville stock. The metamorphic data were also primarily responsible for the conclusion that the Empire Creek stock would be encountered within 300 m from the surface in the deep exploration bore hole (the actual contact was at 294 m).

About 400 specimens were collected in the field or from drill cores. Of these 220 were analyzed petrographically and 150 were studied by x-ray diffraction. In many thin sections calcite and K-feldspar were stained to facilitate identification. The only reliable test for dolomite or talc presence was found to be x-ray diffraction. The most intense concentration of samples is from the area of the heat flow anomaly. The area southeast of the Marysville stock was studied the least because that area is the subject of an intensive study in progress by Jack Rice at the University of Washington (personal communication, 1974).

Metamorphic Reactions. Table E.2 shows the sequence of chemical reactions deduced for these rocks with increasing metamorphic grade. Each number designates a reaction zone: for example, 0 designates low grade rocks in which dolomite-microcline-muscovite is a stable assemblage. Each reaction is designated by a pair of numbers: 0,1 refers to the critical reaction separating zone 0 from zone 1. Reactions designated A or B are reactions favored by H_2O-rich metamorphic fluids and are not part of the zone mineral sequence but occur mainly in veins.

The reaction sequence was determined from (1) observations of mineralogical changes with increasing grade, (2) available literature (e.g., Kerrick, 1974), and (3) topological relationships between reactions and assemblages. Positions of some reactions relative to others are imperfectly known. The scapolite-forming reaction is simplified because scapolite presence is partly a function of Cl content, possibly coming from the Marysville stock. Presence of Fe in the rocks will have small effects on the various equilibria. The effect of Fe is greatest on reaction 10,11 where it stabilizes the phlogopitediopside assemblage to lower temperatures than those of the pure Mg reaction. Fe in Empire rocks appears to increase conditions of reaction 7,8

Table E.2 Reactions at Marysville, Montana in Approximate Sequence of Increasing Temperature.

Zone	
	Dolomite Microcline Calcite Phlogopite
0,1	$3CaMg(CO_3)_2 + KAlSi_3O_8 + H_2O \rightarrow 3CaCO_3 + KMg_3AlSi_3O_{10}(OH)_2 + 3CO_2$
	Dolomite Muscovite Quartz Calcite
1,2	$6CaMg(CO_3)_2 + KAl_3Si_3O_{10}(OH)_2 + 1\ 2/3SiO_2 + 2\ 2/3H_2O \rightarrow 6CaCO_3 +$
	Phlogopite Chlorite
	$KMg_3AlSi_3O_{10}(OH)_2 + 2/3Mg_{4.5}Si_{2.5}Al_3O_{10}(OH)_8 + 6CO_2$
	Dolomite Quartz Calcite Talc
2,3	$3CaMg(CO_3)_2 + 4SiO_2 + H_2O \rightarrow 3CaCO_3 + Mg_3Si_4O_{10}(OH)_2 + 3CO_2$
	Calcite Talc Quartz Tremolite
3,4	$6CaCO_3 + 5Mg_3Si_4O_{10}(OH)_2 + 4SiO_2 \rightarrow 3Ca_2Mg_5Si_8O_{22}(OH)_2 + 2H_2O + 6CO_2$
	Calcite Anorthite Clinozoisite
4,4A (5-9,5-9A)	$CaCO_3 + 3CaAl_2Si_2O_8 + H_2O \rightarrow 2Ca_2Al_3Si_3O_{12}(OH) + CO_2$
	Calcite Muscovite Chlorite Quartz
4,5	$2CaCO_3 + KAl_3Si_3O_{10}(OH)_2 + 2/3Mg_{4.5}Si_{2.5}Al_3O_{10}(OH)_8 + 2\ 1/3SiO_2 \rightarrow$
	Anorthite Phlogopite
	$2CaAl_2Si_2O_8 + KMg_3AlSi_3O_{10}(OH)_2 + 2CO_2 + 2\ 2/3H_2O$
	Calcite Chlorite Quartz Anorthite
5,6	$16\frac{1}{2}CaCO_3 + 5Mg_{4.5}Si_{2.5}Al_3O_{10}(OH)_8 + 38\frac{1}{2}SiO_2 \rightarrow 7\frac{1}{2}CaAl_2Si_2O_8 +$
	Tremolite
	$4\frac{1}{2}Ca_2MG_5Si_8O_{22}(OH)_2 + 16\frac{1}{2}CO_2 + 15\frac{1}{2}H_2O$
	Calcite Muscovite Quartz Anorthite Microcline
6,7	$CaCO_3 + KAl_3Si_3O_{10}(OH)_2 + 2SiO_2 \rightarrow CaAl_2Si_2O_8 + KAlSi_3O_8 + CO_2 + H_2O$
	Calcite Phlogopite Quartz Microcline Tremolite
7,8	$6CaCO_2 + 5KMg_3AlSi_3O_{10}(OH)_2 + 24SiO_2 \rightarrow 5KAlSi_3O_8 + 3Ca_2Mg_5Si_8O_{22}(OH)_2$
	$+2H_2O + 6CO_2$
	Calcite Tremolite Quartz Diopside
8,9	$3CaCO_3 + Ca_2Mg_5Si_8O_{22}(OH)_2 + 2SiO_2 \rightarrow 5CaMgSi_2O_6 + H_2O + 3CO_2$
	Clinozoisite Calcite Quartz Grossularite
9A,9B	$2Ca_2Al_3Si_3O_{12}(OH) + 5CaCO_3 + 3SiO_2 \rightarrow 3Ca_3Al_2Si_3O_{12} + 5CO_2 + H_2O$
	Calcite Anorthite Scapolite
9,10	$CaCO_3 + CaAl_2Si_2O_8 \rightarrow Ca_2Al_2Si_2O_8CO_3$

10,11 Microcline + Tremolite → Phlogopite + Diopside + Quartz

$$KAlSi_3O_8 + CaMg_5Si_8O_{22}(OH)_2 \rightarrow KMg_3AlSi_3O_{10}(OH)_2 + 2CaMgSi_2O_6 + 4SiO_2$$

11,12 Chlorite + Muscovite + Quartz →

$$10Mg_{4.5}Si_{2.5}Al_3O_{10}(OH)_8 + 7\tfrac{1}{2}KAl_3Si_3O_{10}(OH)_2 + 31\tfrac{1}{2}SiO_2 \rightarrow$$

Cordierite + Phlogopite

$$11\tfrac{1}{2}Mg_2Al_4Si_5O_{18} + 7\tfrac{1}{2}KMg_3AlSi_3O_{10}(OH)_2 + 4OH_2O$$

12,13 Muscovite + Phlogopite + Quartz → Microcline

$$6KAl_3Si_3O_{10}(OH)_2 + 2KMg_3AlSi_3O_{10}(OH)_2 + 15SiO_2 \rightarrow 8KAlSi_3O_8$$

Cordierite

$$3Mg_2Al_4Si_5O_{18} + 8H_2O$$

to near those of reaction 8.9. Judging by distance from the Marysville stock, the two reactions which produce cordierite in pelitic compositions occur at about the same temperature as reaction 10,11. Cordierite may well be possible at lower temperatures if rocks of the pelitic composition were exposed farther from the pluton or if the rocks contained more Al_2O_3 and less K_2O. Paragenesis diagrams for these mineral zones will be presented in a future publication.

A metamorphic zone map (Figure E.3) shows a sequence of four generalized zones of progressive contact metamorphism. The dolomite zone (reaction zones 0-2) is distinguished by presence of dolomite and quartz. Such rocks commonly appear unmetamorphosed in hand specimen. In thin section they are seen to vary from very low grade regional metamorphic rocks containing dolomite-microcline-muscovite or calcite-phlogopite-dolomite-muscovite[1] to calcite-phlogopite-chlorite-dolomite (zone 2) developed between one and two kilometers from the intrusives. Due to smaller initial amounts of dolomite, the Empire Shale generally loses its dolomite by the time zone 2 is reached and muscovite persists to higher grades.

The boundary of the dolomite zone is marked by the presence of talc in Helena rocks of appropriate composition as indicated by the Ta symbol on the map.

The second major zone, the tremolite zone, includes reaction zones 4-8 and is characterized by tremolite-calcite-quartz in rocks of appropriate composition. However, most of the Empire Shale and much of the lower Helena contain muscovite-bearing assemblages which preclude the formation of dolomite, talc, or tremolite in the interval including zones 2 through 7. The reactions occurring within the tremolite zone involve calcite and phyllosilicates. In muscovite-bearing rocks, tremolite does not appear until calcite reacts with phlogopite (reaction 7,8). Thus, there are more tremolite occurrences at the edge of the diopside zone, and diopside is produced from this tremolite (reaction 8,9) even in the Empire Shale. Calcite-mica-quartz assemblages, shown on the map in areas where dolomite does not occur, serve to distinguish the tremolite zone from the diopside zone but allow grade to be as low as zone 2. Accordingly, rocks between the Marysville and Empire Creek stocks and southeast of the Marysville stock where tremolite is rare, may be in part lower grade than the generalized tremolite zone.

The diopside zone includes reaction zones 9-10. In many rocks of this grade in both formations, calcite or quartz is used up before all the

---

[1]Oxygen isotope studies by Eslinger and Savin (1973) indicate that regionally developed temperatures ranged between 225° and 310°C in correlative Belt Series rocks.

Figure E.3 Contact metamorphism in the Marysville Geothermal Area. Major metamorphic zones are identified by the index assemblage and isograde are drawn between the zones.

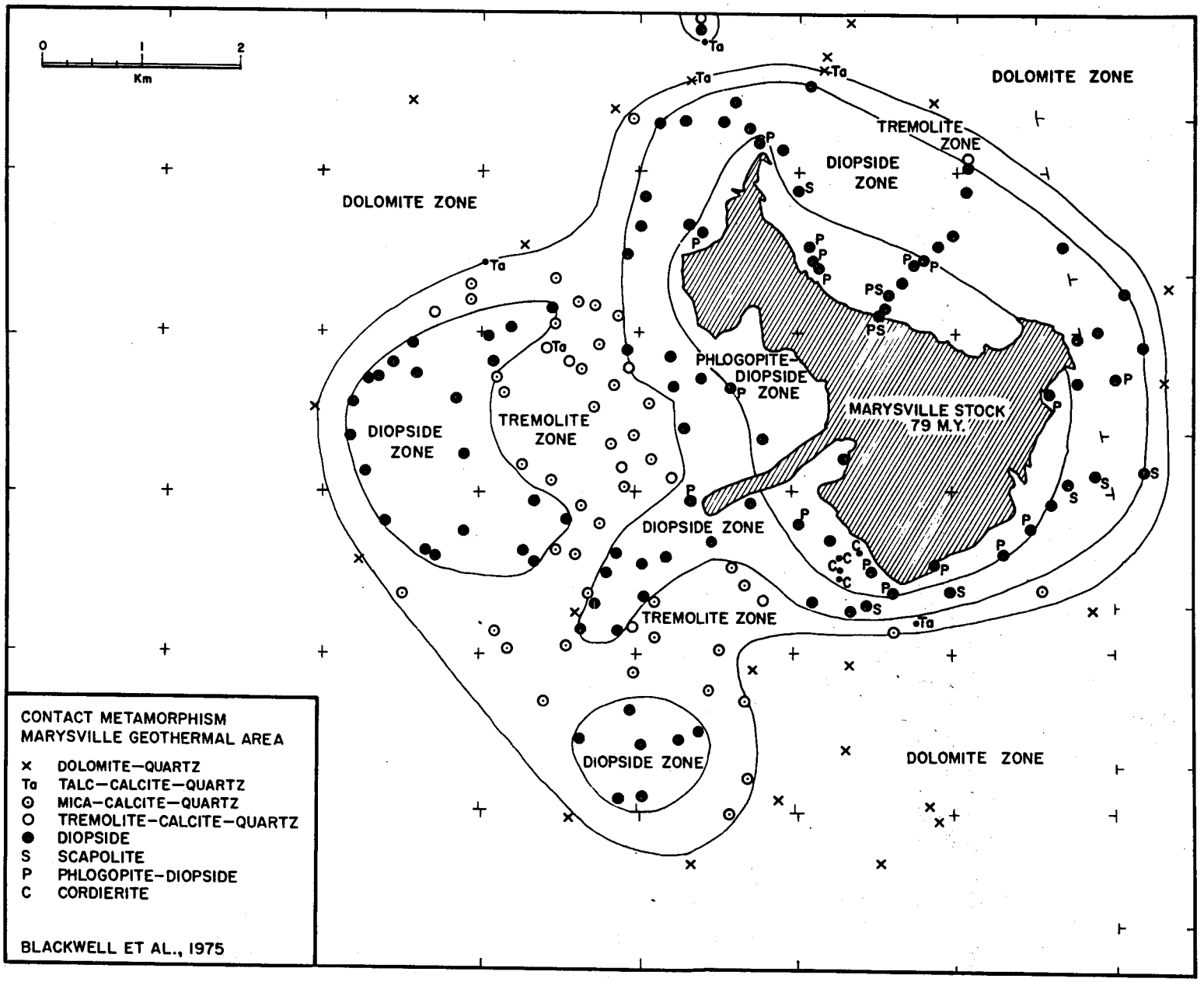
0
1
2
Km
DOLOMITE ZONE
TREMOLITE ZONE
DIOPSIDE ZONE
DOLOMITE ZONE
PHLOGOPITE-DIOPSIDE ZONE
MARYSVILLE STOCK 79 M.Y.
DIOPSIDE ZONE
TREMOLITE ZONE
DIOPSIDE ZONE
TREMOLITE ZONE
DIOPSIDE ZONE
DOLOMITE ZONE
CONTACT METAMORPHISM
MARYSVILLE GEOTHERMAL AREA
× DOLOMITE–QUARTZ
Ta TALC–CALCITE–QUARTZ
⊙ MICA–CALCITE–QUARTZ
O TREMOLITE–CALCITE–QUARTZ
● DIOPSIDE
S SCAPOLITE
P PHLOGOPITE–DIOPSIDE
C CORDIERITE
BLACKWELL ET AL., 1975

FIGURE E.3

tremolite has reacted, leaving a diopside-tremolite assemblage. Scapolite may form in this zone from rocks containing plagioclase and calcite.

Zones 11-13 are grouped as the diopside-phlogopite zone. In calcite-free calcareous hornfels, tremolite and microcline react to form phlogopite and diopside. Cordierite forms from pelitic composition at about the same grade. Some isolated phlogopite-diopside occurrences are outside the zone of common phlogopite with diopside, presumably because the reaction products were stabilized by increased Fe.

It should be emphasized that the control on the isograds is that presented on the map. The zones of tremolite stability are exaggerated somewhat in that the zone is drawn from the last dolomite or talc to the first diopside. Despite this fact, the tremolite zone is narrow in most places.

The still unroofed Empire Creek and Bald Butte stocks produced maximum grades of reaction zone 9 whereas the exposed Marysville stock produced scapolite, phlogopite-diopside, and cordierite as well. These differences are probably due to several factors: (1) the younger plutons are not exposed at the surface; (2) the younger plutons were more acidic and produced more extensive veining, suggesting that they contained more water and were emplaced at lower temperatures; (3) retrogressive effects associated with intense veining, seen especially in the deep exploration hole (see Section on Geological Studies), may have destroyed higher grade assemblages; and (4) scapolite is excluded as a possible phase in the Empire Shale due to rock composition.

The width of contact metamorphism around the intrusions must vary with the dip of the contact and the outcrop pattern of the intrusion. Thus the study of the metamorphic effects supplies important information on the shallow unexposed portions of the stocks. Such inferences, described in this paragraph, can be compared with the results of the geophysical studies. In general the agreement of the geologic model with the calculated models from geophysical data is excellent (see Gravity and Magnetic Studies and SUMMARY AND DISCUSSION). Contact effects are narrowest at the southern tip of the Marysville stock (Figure E.3) possibly due to a near vertical dip combined with an outside corner of the stock. Contact effects are widest on the northeast and southwest sides of the intrusion. Barrell (1907) indicates gently-dipping or flat contacts in these areas with the intrusion passing laterally beneath Mt. Belmont. The thick aureole on the northeast may be partly caused by the focusing effect of heat coming from this reentrant portion of the pluton. In the southwest the contact must not remain flat for a great distance or metamorphism would be still more extensive. The long southwest-trending prong of diopside-zone metamorphism indicates that the dike-like portion of the intrusion is more extensive at depth and may bend toward the south and dip steeply southeast. The diopside isograd over the buried Empire Creek and Bald Butte stocks gives an indication of the limits of these bodies at 300 to 600 m depths.

Metamorphic Conditions. In a carbonate-hydrate terrain with no graphite, one can assume that $P_{fluid} = P_{CO_2} + P_{H_2O}$. For the conclusions which follow it is assumed that P_{fluid} was about 500 bars around the Empire Creek and Bald Butte stocks and 1000 bars around the Marysville stock at time of emplacement,

and that rock pressures were not significantly above the fluid pressures. The Marysville stock is about twice as old as the other two stocks, and is a classic example of epizonal intrusion (Buddington, 1959; Barrell, 1907). The Empire Creek stock has correlative volcanic rocks 3 km to the south. Vertical offset on the fault between the Helena and Marsh formations is on the order of 1 km (Figure E.2). Allowing for probable southward tilting in the area, a depth of emplacement of about 2 km seems reasonable for the Empire Creek and Bald Butte intrusions.

Temperature-fluid composition equilibria for the two pressures are shown in Figure E.4 for several of the reactions listed in Table E.2.

Possible reaction paths for the two formations are given based on relative widths of mineral zones and evidence for closed or open system behavior. Nearly total absence of phases which require H_2O-rich composition of fluid (clinozoisite and grossularite), scarcity of veins, and the especially narrow tremolite zone around the Marysville intrusion suggest that here little fluid was introduced to the rocks externally and the mineral assemblages buffered the H_2O-CO_2 ratio. On the other hand abundance of veins, especially with fluorite and adularia, more common clinozoisite-bearing veins, and a possibly wider tremolite zone are consistent with some external effects on the H_2O ratio for the Empire Creek and Bald Butte aureoles.

Two other effects of importance were noted. When contact metamorphism was directly above a pluton, as over Empire Creek, Bald Butte, and two small buried intrusions north of the Marysville stock, tremolite is more common suggesting an upward rise of water from the intrusive bodies and more external control. Finally, the path of conditions in the Empire Shale must differ somewhat from that in the Helena Formation because in the former reaction 7,8 was important, while in the latter reactions 2,3 and 3,4 were more important.

The six occurrences of talc observed by x-ray diffraction lend support to the conclusion of Slaughter et al. (1975) that talc is stable in low pressure metamorphism of siliceous dolomites. Talc incorporates very little Fe, so that 20 mole % of Fe replacing Mg in dolomite and tremolite would somewhat reduce the field of talc shown in Figure E.4.

Structural Geology

Structural relations in the Marysville area are shown on the geologic map in Figure E.2. The main differences between this map and the map in the 1974 report are the location of several east-west trending normal faults and in modification of the distribution of the Empire Shale.

The dome shown in the center of the map, resulting in exposures of the Empire Shale and Marysville stock in the core, is the most prominent structural feature on the map. The portion of the dome southwest of the Marysville stock appears to be related to the emplacement of the Empire Creek stock as will be shown in a subsequent section. An additional feature of the map which differs from pre-existing maps is the absence of the syncline shown

Figure E.4 Temperature-fluid composition phase diagrams for minerals in the system CaO-MgO-Al_2O_3-SiO_2-CO_2-H_2O at $P_{fluid} = P_{total} = 1000$ bars and 500 bars. Only reactions stable with excess quartz and pertinent to the present study are shown. Solid lines represent reactions of Slaughter, Kerrick, and Wall (1975) or reactions calculated from their data at 500 bars. Long dashed lines represent approximate reactions estimated from Hewitt (1973 and unpublished) or estimated from reaction sequence. Short dashed lines and dots represent typical reaction paths for Empire dolomitic shale and Helena siliceous dolomite respectively. Abbreviations: Do, dolomite; Mi, microcline; Ca, calcite; Ph, phlogopite; Qz, quartz; Ta, talc; Tr, tremolite; Mu, muscovite; An, anorthite; Di, diopside; Wo, wollastonite.

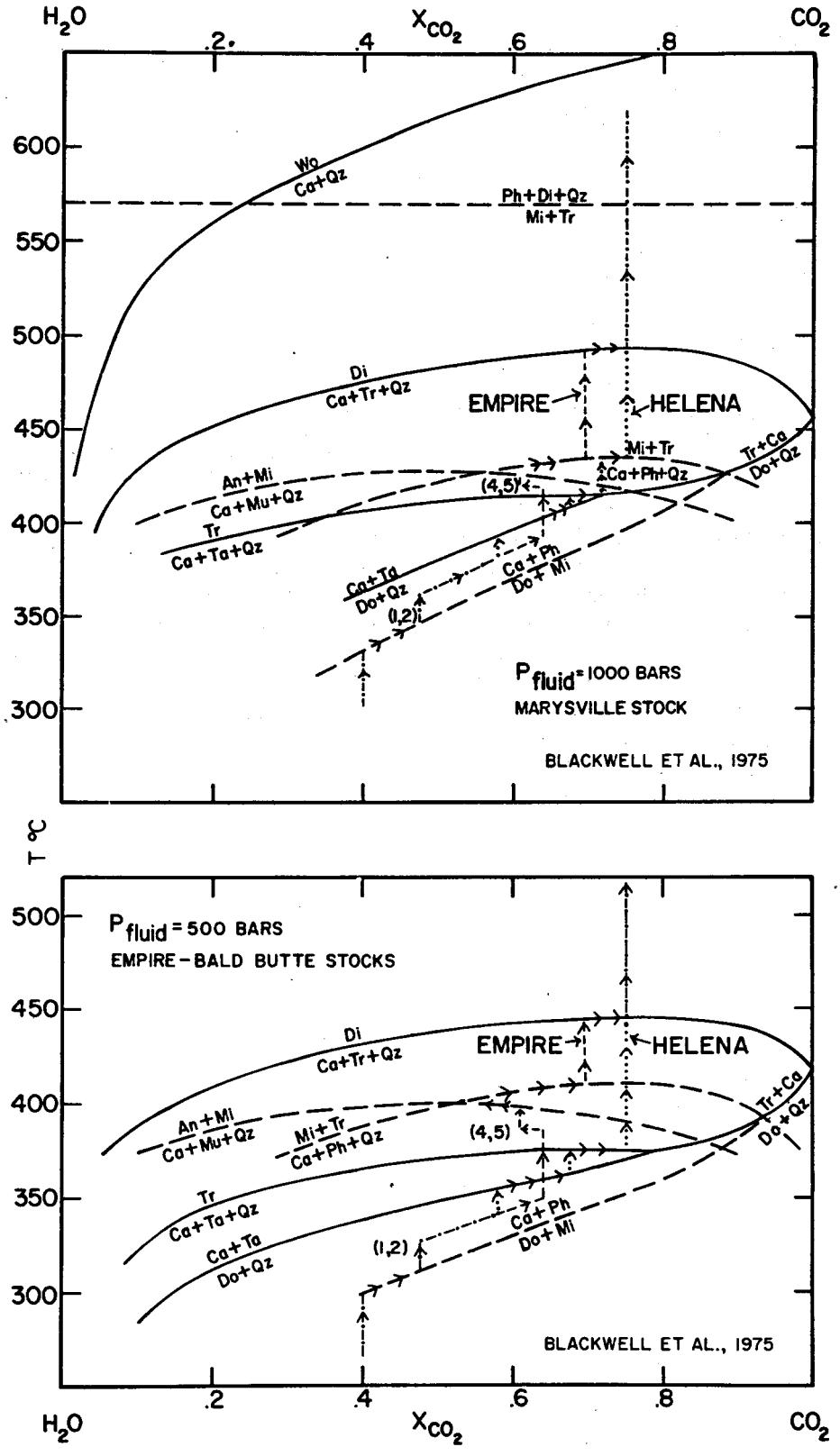
H2O
.2
.4
XCO2
.6
.8
CO2
600
550
500
450
400
350
300
Wo
Ca+Qz
Ph+Di+Qz
Mi+Tr
Di
Ca+Tr+Qz
EMPIRE
HELENA
Mi+Tr
Ca+Ph+Qz
Tr+Ca
Do+Qz
An+Mi
Ca+Mu+Qz
(4,5)
Tr
Ca+Ta+Qz
Ca+Ta
Do+Qz
Ca+Ph
Do+Mi
(1,2)
Pfluid=1000 BARS
MARYSVILLE STOCK
BLACKWELL ET AL., 1975
T °C
500
450
400
350
300
Pfluid = 500 BARS
EMPIRE-BALD BUTTE STOCKS
Di
Ca+Tr+Qz
EMPIRE
HELENA
An+Mi
Ca+Mu+Qz
Mi+Tr
Ca+Ph+Qz
(4,5)
Tr+Ca
Do+Qz
Tr
Ca+Ta+Qz
Ca+Ta
Do+Qz
(1,2)
Ca+Ph
Do+Mi
BLACKWELL ET AL., 1975
H2O
.2
.4
XCO2
.6
.8
CO2

FIGURE E.4

along the north border of the map in the 1974 report. It appears from slightly more detailed mapping that this syncline does not exist except perhaps as drag, and the structure required to expose the Empire Shale along the Prickly Pear Creek road is a fault. The location of this fault is not well determined since the Helena formation is faulted against itself, but it must occur somewhere between the north end of the Marysville stock-Empire dome, and the exposures of Empire Shale along Prickly Pear Creek as shown by Barrell (1907). The fault is assumed to be a south dipping normal fault similar to the one mapped about 1 km to the north by Barrell (1907).

The dip of a large displacement (about 1 km) fault immediately south of the Empire Shale exposures was a subject of some doubt in the 1974 report. Studies during 1974, however, demonstrated that the fault dips south with the Marsh Shale being downdropped against the Helena Formation. Another fault with similar characteristics is mapped along Ottawa Gulch, although the displacement is not great (60-100 m). There must be large displacement along a fault or faults west of the dome, but lack of exposures in this area preclude detailed mapping, and the faulting may be different from that shown on the map. The intersection of this fault or faults and the normal fault cutting off the south end of the dome is also an area of poor exposure and the relationship of the two faults is not known. The Belt Series rocks are highly fractured and jointed and there are many small displacement faults cutting the units. However, because of the very gradational changes in units, the thickness of the units, and the lack of complete exposures, no attempt has been made to map all possible faults. The geologic map shown in Figure E.2 is a "minimum fault" map and undoubtedly detailed mapping would identify many other faults.

Thus most of the major faults in the area are east-west, south dipping normal faults (south side down). There are at least four relatively large faults involved. One just north of the map area, one at the very northern margin of the map area, a third near the south end of the Marysville stock, and a fourth near the south end of the dome in the Empire Shale. These faults appear to have played an important part in emplacement of the Marysville stock, the Empire Creek stock and possibly in localization of the geothermal area.

There appears to be no way with the present data to demonstrate conclusively the age of most of the faults, although several of them appear to block out the dome associated with the Empire Creek-Marysville stocks and thus could have formed during or possibly subsequent to the emplacement of the intrusive rocks. The faults along Empire Creek and its immediate tributary to the south in sections 34 and 33 downdrop a block of Helena Formation. These faults have occurred subsequent to the intrusion of the Marysville stock as the contact metamorphism is offset by the faults and the Marysville stock itself may be offset (based on irregularities in the magnetic map pattern). If the northernmost fault extends along Empire Creek it would appear to predate the intrusion of the Empire Creek stock as the contact metamorphic aureole of the Empire Creek stock does not appear to be offset. Alternatively throw might decrease toward the west so that the offset would be small by the time the metamorphic aureole of the Empire Creek stock is reached.

The important aspects of the geology as related to the heat flow anomaly are summarized in Figure E.5, which shows the outcrop of the Marysville stock in the northwestern and the outcrop of the Empire shale in the southeastern portion of the map. The known locations of the buried porphyry intrusives at the two ends of the Empire Shale outcrop based on drilling are indicated by x's.

Three cross sections (Figure E.6) have been prepared to illustrate the structure of the area. The locations of these cross sections are indicated in Figure E.5. Cross sections AA', BB' and CC' illustrate the domal nature of the area and the extent of the igneous rocks. These cross sections are essentially identical to those of Figure 2.10 in the 1974 report with the exception that in cross section CC' a much more extensive subcrop of the Empire Creek stock is indicated. The shape of the stock at depth is based on the analysis of the gravity data. In addition the fault pattern has been modified based on the additional mapping. The offset of the Empire Creek stock along the fault at a horizontal distance of 3.5 km (the Ottawa Gulch fault) is inferred. If the offset is actually present it can be due either to the fault influencing the emplacement of the Empire Creek stock, or the subsequent offset of the stock by the fault. The Bald Butte and Empire Creek stocks are shown to merge at depth to a single body in cross section CC' in spite of their apparent age difference. Additional age dating of the igneous rocks is necessary, however, for more definite conclusions on the temporal relationship of the Bald Butte and Empire Creek stocks. In any event, the geometric relationship shown appears to be required by the gravity data. Finally it appears that the southern edge of the Empire Creek body is controlled by or associated with the large normal displacement fault between the Helena Formation and the Marsh Shale-Greenhorn Mountain Quartzite units.

Gravity and Magnetic Studies

In the 1974 report the conclusion was reached that the geothermal anomaly was associated either with fracture porosity in the Empire Creek stock or with a recent intrusive below the Empire Creek stock and conductive heat flow through the stock to the surface. In the favored model (Figure 3.10, 1974 report) the gravity anomaly was interpreted as due to the heat source body below the Empire Creek stock; however, with the data available in the 1974 report there still remained a gravity anomaly south of the geothermal area after interpretation of the combined heat flow and gravity anomaly (see Figure 3.11, 1974 report). In order to investigate the existence and significance of this gravity anomaly south of the geothermal area in more detail, 53 additional gravity stations were occupied during the summer of 1974 (most involving detailed surveying). The contour map of the gravity anomaly in the geothermal area itself is scarcely changed with the addition of the new data and reference is made to the 1974 report for a detailed contour map in the geothermal area.

In addition to the new gravity data obtained, a reconnaissance ground magnetic survey was carried out south of the map area shown in Figure E.1 in order to investigate the possibilities that a buried intrusive similar to the Marysville stock might be causing the observed gravity anomaly there.

Several small but lithologically similar bodies of granodiorite have been mapped in the area (Bierwagen, 1964; Ratcliff, 1973), but the bodies shown on these maps appear to be steep sided and of limited lateral extent because they have only very local magnetic anomalies. Thus no magnetic anomaly was observed that could come from a body similar to the Marysville stock which might cause the gravity anomaly. Measurements of magnetic susceptibility of five core samples from MGE #1 average 4.6 x 10^{-5} cgs (Table E.3), two orders of magnitude less than the Marysville stock. The low susceptibility is due to the acidic composition of the Empire Creek stock, and possibly to hydrothermal alteration as well. Thus no magnetic anomaly is to be expected from the Empire Creek stock.

For the gravity data, terrain corrections were calculated and added to the simple Bouguer values. The strong regional gravity gradient present on the complete Bouguer gravity map was removed by a simple one-dimensional equation. The equation used for regional removal was $R_{grav} = .161.2 + 0.77 \times +0.015 x^2$ (with x in km). The strike of the surface generated by this equation is N41°W and the zero point (x=0) is 46°45'N lat and 112°15'E long. The complete set of gravity data for the whole area is shown in the form of a residual gravity map in Figure E.7. These data are used for the interpretation in following sections. Assuming such a simple surface for the regional anomaly is probably not satisfactory over such a large area, the residual gravity map thus generated (Figure E.7) may include effects on too broad a scale to relate to anomalous densities in the local area of interest. Of most interest to the study here, however, are mass anomalies in the uppermost 1-3 km, which will result in rather sharp gradients on the scale of Figure E.7 and can be easily identified.

The gravity map shown in Figure E.7 includes the gravity effect of the Marysville stock. This effect was removed from the gravity map used for interpretation of the Empire Creek body by using the shape of the Marysville stock deduced from analysis of the magnetic data (1974 report, with minor modifications based on the ground magnetic data). A density contrast between the stock and the country rocks of 0.1 gm/cm^3 was assumed with the bottom of the body at sea level. The maximum subcrop extent of the Marysville stock used in the interpretation is shown in Figure E.8. The gravity models were calculated using the technique of Talwani and Ewing (1960). The source of most of the gravity anomaly north of the southernmost normal fault shown on Figure E.2, remaining after the effect of the Marysville stock is removed, is presumed to be due to the Empire Creek stock. The mean in situ density of the Empire Creek stock to a depth of at least 2 km is 2.54 gm/cm^3 with a resulting density contrast of approximately 0.2 gm/cm^3 with respect to the surrounding country rocks (see Table 3.1, 1974 report and Table E.8 this report). The contact metamorphism associated with the Empire Creek and Bald Butte stocks gives some evidence of their lateral extent while the deep drill hole furnishes evidence on the vertical extent of the Empire Creek stock. If the combination of the Empire Creek and Bald Butte stocks must satisfy all of the gravity anomaly present in the map area (Figure E.1) then the intrusives must have a lateral extent similar to that of the geothermal anomaly. The inferred top of the reservoir, assuming it has a temperature of 95° becomes slightly deeper to the south (see Figure E.23) as apparently must the top of the Empire Creek stock because of the lower grade of contact

Figure E.5 Geological Index Map. The outcrop of the Marysville stock is indicated by a diagonal line pattern. The outcrop of the Empire Formation in the core of the dome is indicated by a second diagonal line pattern. The locations of drill holes which intersect the two unexposed Cenozoic stocks are indicated by the x's. The locations of the cross sections AA', BB' and CC' shown in Figure E.6 are also indicated.

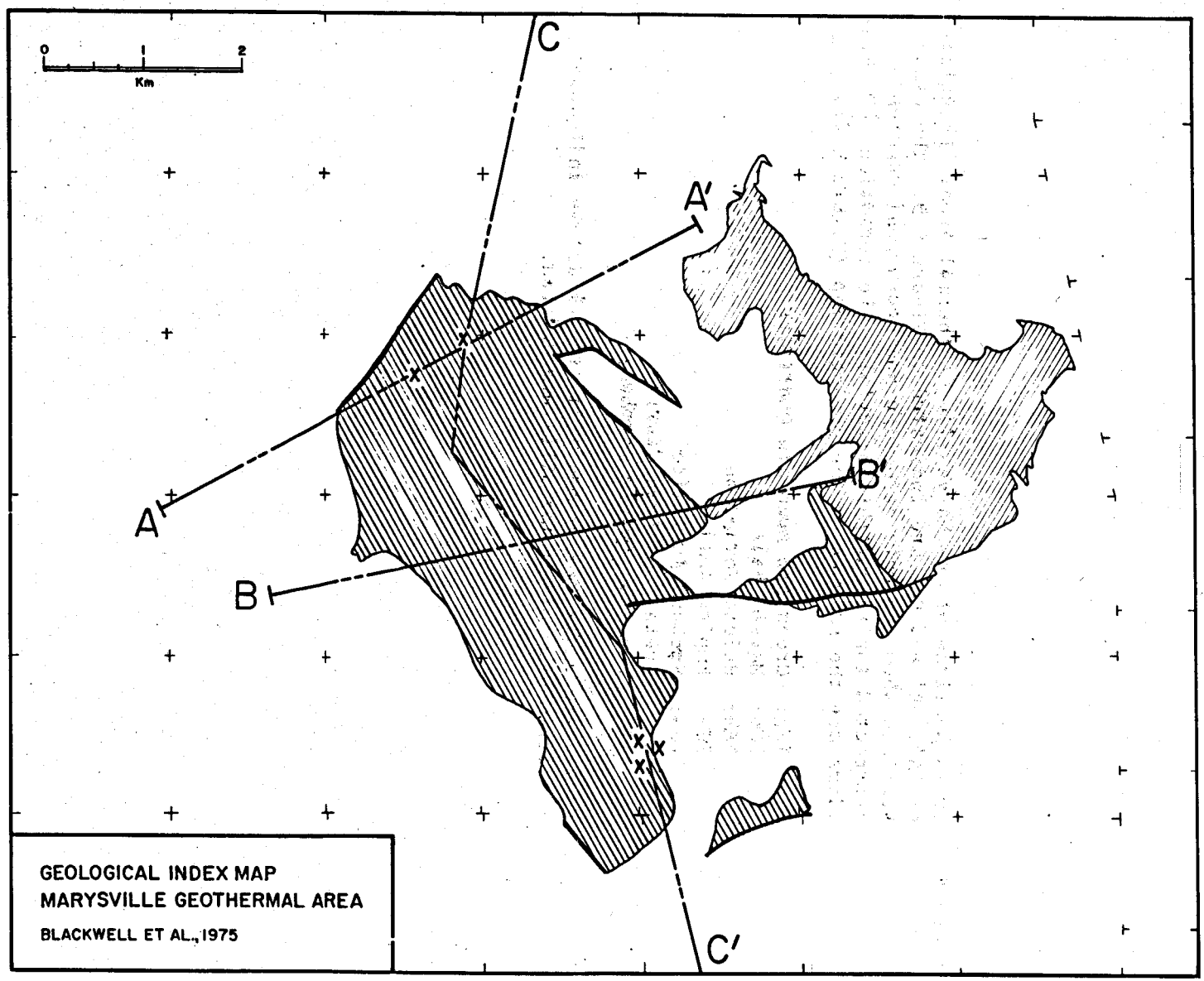
0
1
2
Km
C
A'
A
B'
B
C'
GEOLOGICAL INDEX MAP
MARYSVILLE GEOTHERMAL AREA
BLACKWELL ET AL., 1975

FIGURE E.5

Figure E.6 Cross sections of the Marysville Geothermal Area. Locations of AA', BB' and CC' are indicated in Figure E.5. The cross sections show geologic structure and geothermal gradients (corrected for topographic effects). The formation abbreviations are the same as on the geologic map (Figure E.2):

P€g: Greenhorn Mountain Quartzite
P€m: Marsh Shale
P€h: Helena Formation
P€e: Empire Shale
P€s: Spokane Argillite
Kgr: Cretaceous Granodiorite
Ti : Cenozoic Quartz Porphyry

Faults are indicated by heavy lines with arrows indicating displacement. Dikes and sills are omitted.

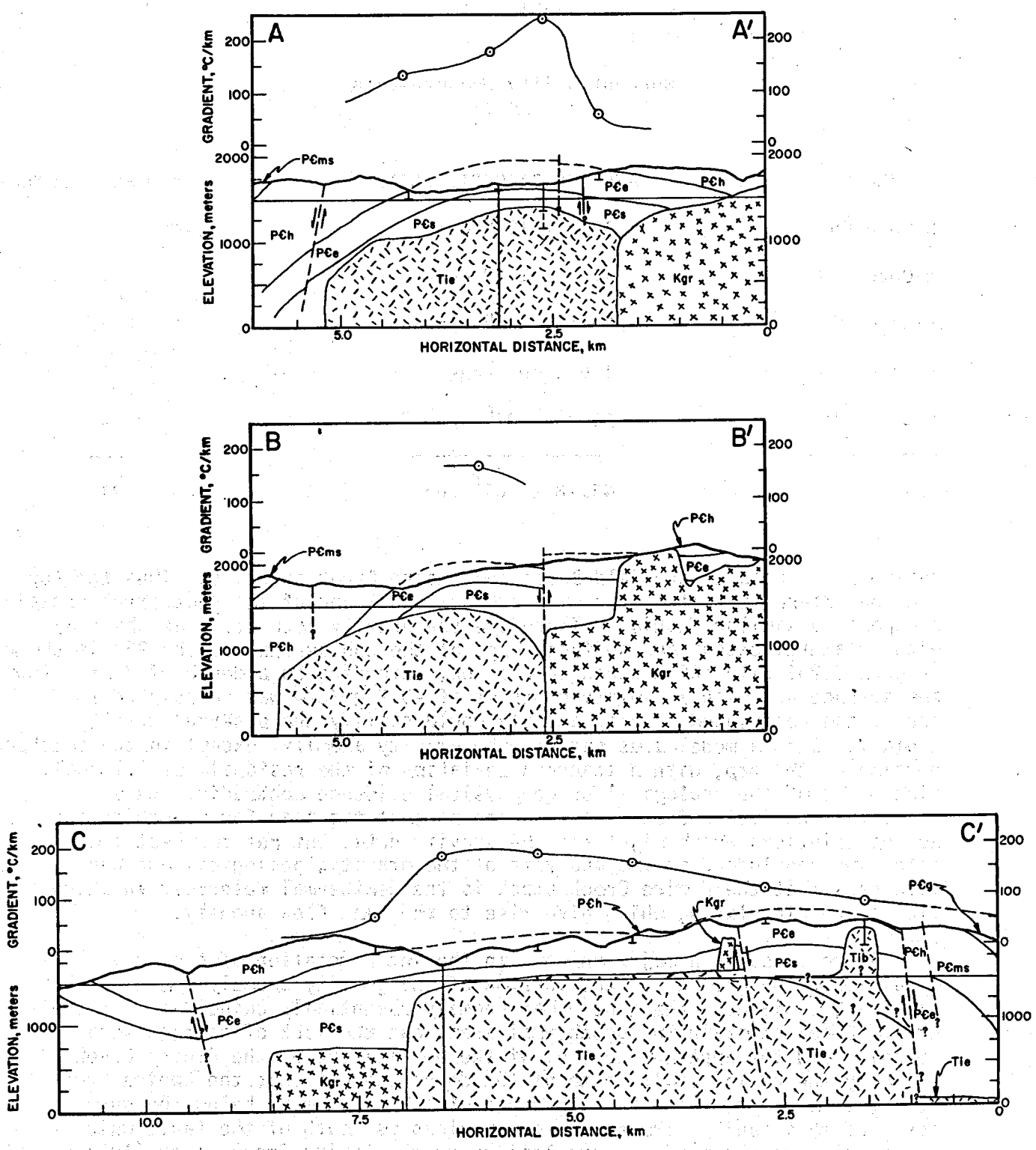
A
A'
B
B'
C
C'
GRADIENT, °C/km
ELEVATION, meters
HORIZONTAL DISTANCE, km
PCms
PCe
PCh
PCs
Tie
Kgr
Tib
PCg

FIGURE E.6

Table E.3

Susceptibility Measurements
MGE #1

SAMPLE #	AVERAGE SUSCEPTIBILITY	# OBSERVATIONS
M-Core #6	13.8×10^{-6} cgs	3
M-Core #10	17.8×10^{-6} cgs	4
M-Core #12	20.1×10^{-6} cgs	3
M-Core #13	126×10^{-6} cgs	7
M-Core #14	51.2×10^{-6} cgs	4
MEAN	45.78×10^{-6} cgs	21

metamorphism between the Bald Butte and Empire Creek aureoles. Thus the top and the lateral extent of the Empire Creek stock and of the geothermal anomaly behave in a similar fashion. Therefore the gravity attraction of the body with a lateral extent and surface shape of the contour map of the 95° isotherm (Figure E.25) with 100 m added to the top, extending to a depth of 3 km below the surface and with a density contrast of -0.2 gm/cm^3 was calculated to see if the calculated gravity anomaly would satisfy the observed gravity anomaly. Such a model does satisfy the gravity anomaly, except in the southern portion of the map, with a standard deviation of the residuals of 1.1 mgal. Since none of the geological or geophysical evidence contradicts this model for the Empire Creek stock we see no justification for searching for ad hoc solutions which might fit the gravity data, but not the heat flow data. We conclude from the analysis of the gravity, geological and heat flow data that the Empire Creek stock is the geothermal reservoir in which fluids are circulating which give rise to the heat flow anomaly.

There is still a major unknown in the interpretation of the gravity data, i.e., the origin for the portion of the gravity anomaly south of the Continental Divide. The geothermal anomaly essentially coincides with the Empire Creek stock in the geothermal area, but the lack of contact metamorphism and the apparent control of the emplacement of the Empire Creek stock by the normal fault south of the dome, suggest that the Empire Creek stock, if present, must lie at a depth of 1.2 km or more below the surface south of this fault. The exposure of volcanics south of the fault which apparently are the surface correlatives of the Empire Creek stock (1974 report), also suggests deeper burial for the Empire Creek stock, if present. Further structural information on the presence or absence of the Empire stock south of the fault and the presence or absence of any geothermal anomaly south of the fault are extremely important to obtain and would require further drilling.

The anomaly south of the map has been interpreted in two parts. The central portion of the anomaly has the steepest gradients in the map area (excepting the anomaly associated with Silver Valley, well to the east of the geothermal anomaly) and is attributed to a mass deficiency associated with a shallow, possibly fault bounded, sediment filled trough underlying an area immediately south of Figure E.1. The area, Thompson Flats, is mapped as Tertiary gravel by Bierwagen (1964) and Rafcliff (personal communication, 1973). Exposures of the Hope Creek volcanics also occur in the general area of the gravity low. The density contrast associated with the basin is -0.4 gm/cm^3. The shape of the basin was obtained by separating the part of the anomaly with sharp gradients from the more gentle gradient anomaly by hand and fitting the resulting anomaly with a basin using the technique of Cordell and Henderson (1968). The maximum gravity anomaly is 6 mgal and the maximum thickness of the resulting basin is 570 meters. It is emphasized that the existence and density contrast of the basin are purely speculative.

The remainder of the gravity anomaly south of the geothermal anomaly, having a maximum amplitude of 3 to 5 mgal is attributed to a more deeply buried portion of the Empire Creek stock. The plan shape of this portion of the body is shown in Figure E.8. The top of the body, basically a slab, is at 2.0 km while the bottom is at 3.0 km, and in the north a section of the body is brought up to a depth of 1.4 km.

The audiomagnetotelluric data suggest some possible constraints on the bottoms of the various igneous units; these results are discussed in more detail in the section on Heat Flow Study. Again it is emphasized that the interpretation of the gravity data south of Figure E.1 is speculative and the real cause of the anomaly may be much different than the model. The Paleozoic and Mesozoic rocks that occur in this area may be the origin of part of the anomaly. However, the possible occurrence of the Empire Creek stock south of the known geothermal anomaly suggests that heat flow drilling might indicate a large extension of the geothermal anomaly in an area having much different geologic characteristics from the area described in detail here.

Heat Flow Study

The heat flow data available in the geothermal anomaly area through 1973 were discussed in the 1974 report. During the summer of 1974 six additional shallow holes were drilled for heat flow studies. Four of these holes were located in the immediate vicinity of the geothermal anomaly while two of the holes were located between Marysville and Helena along the trend of the microearthquake activity. The results of all six holes drilled in 1974 are listed in Table E.4 and temperature-depth curves are shown in Figure E.9. Three of the holes were drilled to a depth of 64 meters and three went to 120-135 meters. Hole RDH-32 had to be deepened as it appeared that 60 meters was too shallow to obtain a true geothermal gradient. Drill holes RDH-35 and 36 were drilled to 135 meters because they were in an area where the heat flow could not be anticipated and thus deeper holes were felt necessary. The results from RDH-35 and 36 will be discussed in a subsequent section.

Figure E.7 Residual gravity anomaly map of the Helena-Marysville area, Montana. The anomaly values are based on removal of assumed regional gravity from complete Bouguer gravity map. The area of Figure E.1 is indicated by the northernmost of the two dashed boxes. The area of Figure E.8 is indicated by the sum of the two dashed boses.

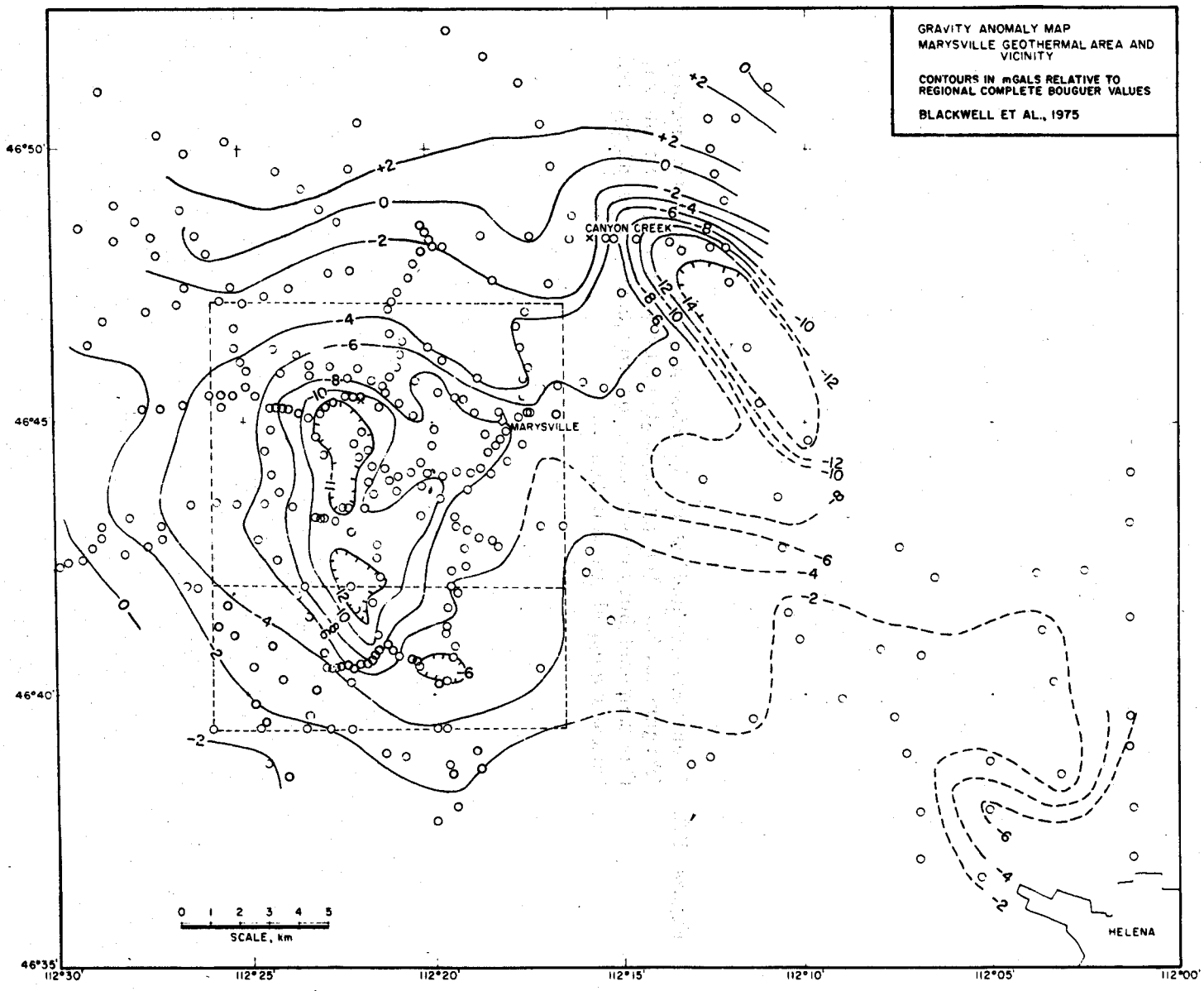
GRAVITY ANOMALY MAP
MARYSVILLE GEOTHERMAL AREA AND VICINITY
CONTOURS IN mGALS RELATIVE TO REGIONAL COMPLETE BOUGUER VALUES
BLACKWELL ET AL., 1975
CANYON CREEK
MARYSVILLE
HELENA
SCALE, km
0 1 2 3 4 5
46°50'
46°45'
46°40'
46°35'
112°30'
112°25'
112°20'
112°15'
112°10'
112°05'
112°00'

FIGURE E.7

Figure E.8 Plan view of bodies satisfying residual gravity anomaly (Figure E.7). The assumed density contrasts are shown. The top and bottom surfaces of the bodies are discussed in more detail in the test.

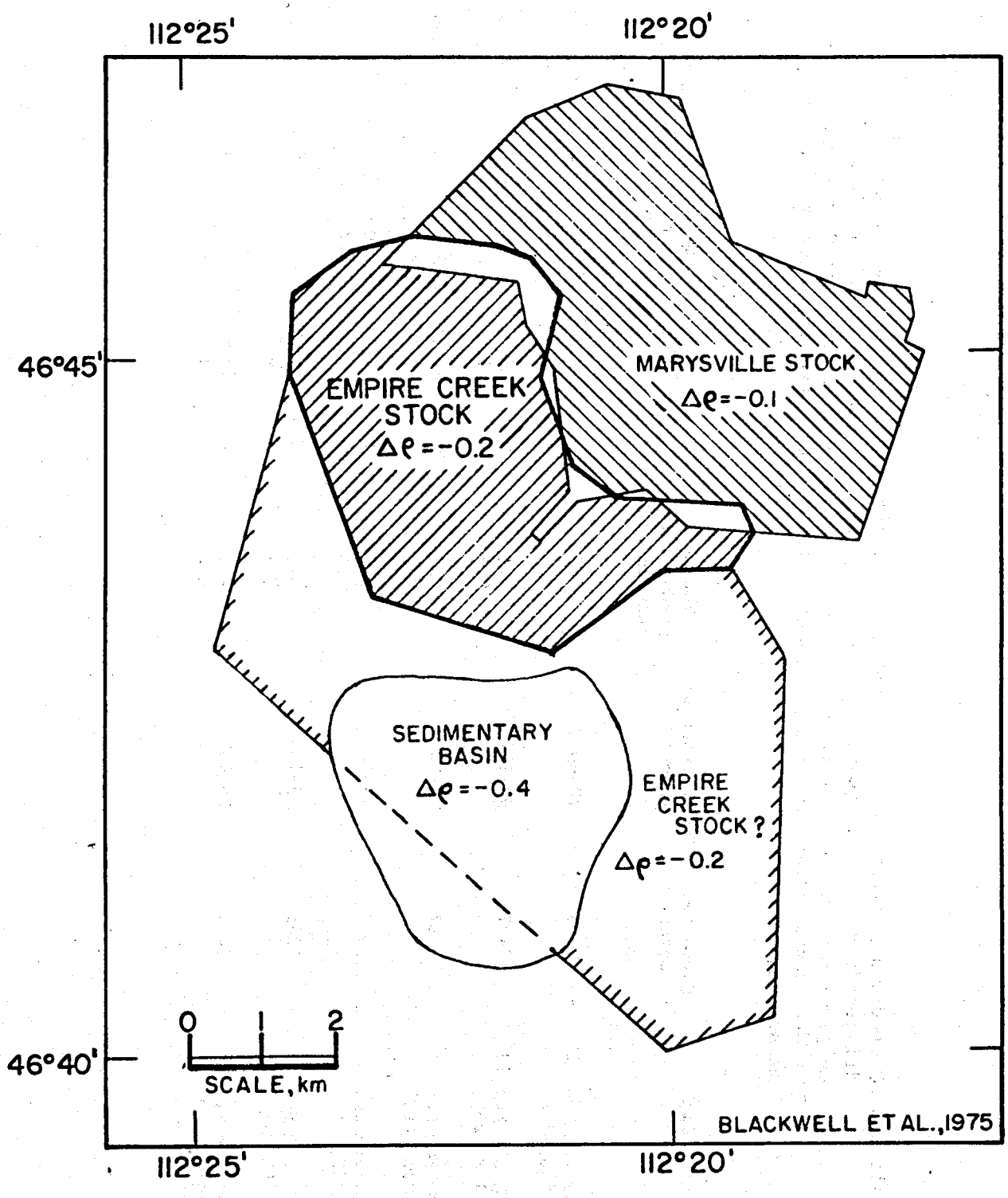
112°25'
112°20'
46°45'
46°40'
EMPIRE CREEK STOCK
Δρ=-0.2
MARYSVILLE STOCK
Δρ=-0.1
SEDIMENTARY BASIN
Δρ=-0.4
EMPIRE CREEK STOCK?
Δρ=-0.2
0 1 2
SCALE, km
BLACKWELL ET AL., 1975

FIGURE E.8

Table E.4 Geothermal gradient, thermal conductivity, and heat flow for shallow holes drilled in 1974. The quantities G* and Q* are the gradient and heat flow respectively, after topographic corrections. The second quantity in the row in the Thermal Conductivity, G, and G* columns is the standard error of the measurement.

Drill Hole	Location	Elevation meters	Depth Interval meters	Thermal Conductivity mcal/cmsec°C	N	G °C/km	G* °C/km	Q μcal/cm²sec	Q*
RDH-31	NW¼ SE¼ Sec 11 T11N, R6W	2003	30-60	7.7 0.3	5	28.3 1.3	31.8 1.5	2.2	2.5
RDH-32	NW¼ NE¼ Sec 13 T11N, R6W	2027	90-120	8.8 0.3	5	22.0 1.8	25.7 2.2	2.0	2.3(5)
RDH-33	SW¼ NE¼ Sec 7 T11N, R6W	1987	25-60	8.9 0.3	11	32.3 2.8	38.3(5) 3.5	2.9	3.4(5)
RDH-34	SE¼ SE¼ Sec 8 T11N, R6W	1975	25-60	13.3 0.3	8	31.4 2.0	34.0 2.2	4.3	4.6
RDH-35	NE¼ SE¼ Sec 17 T10N, R4W	1295	25-135	8.6 0.3	12	21.0 0.5		1.8	
RDH-36	NW¼ NE¼ Sec 26 T11N, R5W	1439	25-130	7.8 0.4	10	23.0 1.6		1.8	

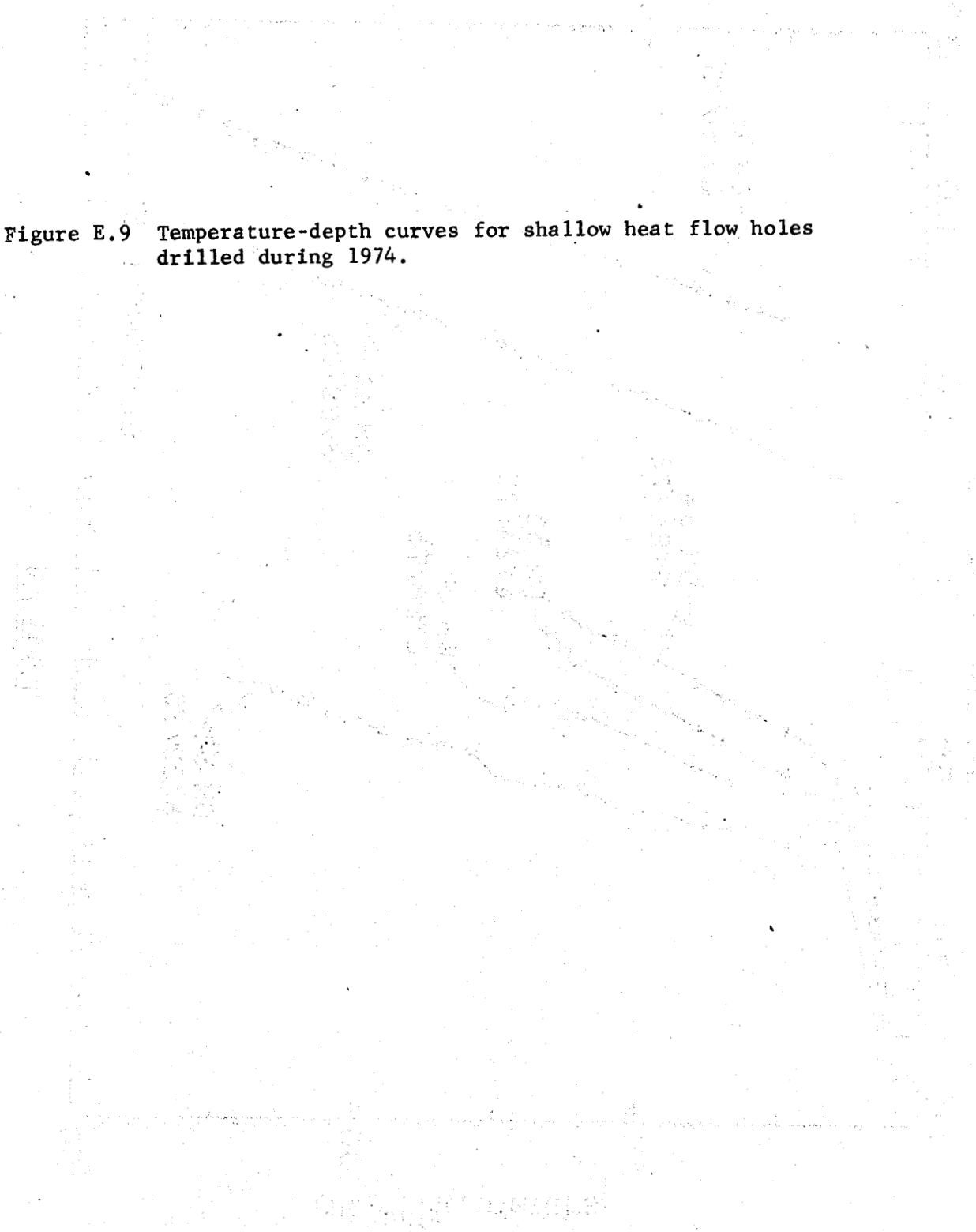

Figure E.9 Temperature-depth curves for shallow heat flow holes drilled during 1974.

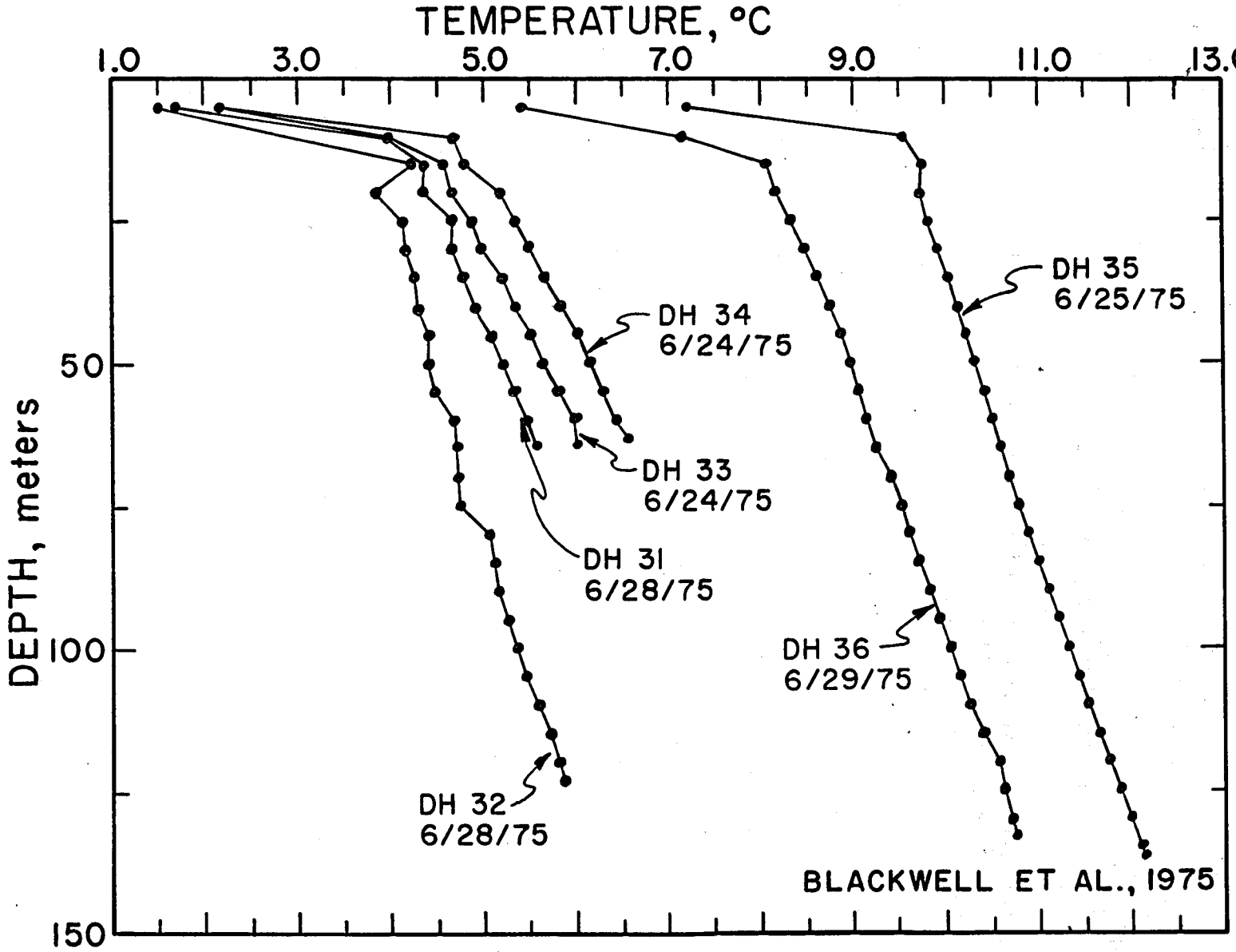
TEMPERATURE, °C
1.0
3.0
5.0
7.0
9.0
11.0
13.0
DEPTH, meters
50
100
150
DH 34
6/24/75
DH 33
6/24/75
DH 31
6/28/75
DH 32
6/28/75
DH 35
6/25/75
DH 36
6/29/75
BLACKWELL ET AL., 1975

FIGURE E.9

The topography in the vicinity of the geothermal anomaly is mountainous and the heat flow determinations required significant terrain corrections. These terrain corrections were calculated using the technique suggested by Birch (1950), but include topography only to a distance of 2 km from the drill hole. The lateral variation of geothermal gradient in the Marysville district makes calculation of distant terrain corrections suspect using this technique since a uniform gradient everywhere is assumed in the correction. The largest source of error in the heat flow measurements comes from uncertainties in the terrain correction (estimated to be 50% of the correction). The terrain corrected gradients and heat flow values are listed in Table E.4 as are the uncorrected data. The thermal conductivity values shown in Table E.4 were obtained from measurements on cutting samples (see Sass et al., 1971, for a description of the technique) because the wells were drilled with rotary equipment and no core samples were obtained. All of the heat flow data available, including those data previously discussed, are shown in Figure E.10. The geothermal gradient (corrected for topography in the manner discussed above) and the heat flow are listed below each measurement point. The anomalous gradient due to the heat source would be the measured gradient minus approximately 30°C/km. The gradient of 30°C/km is the gradient that would be observed in rock with the average thermal conductivity of the rocks in the Marysville district (6.8 mcal/cm sec °C) and a regional heat flow of about 2 μcal/cm^{2}sec (Blackwell and Robertson, 1973).

During the preparation of the 1973 report an inadvertent error crept into the map of heat flow shown in Figure 3.9. On this map the results from DDH-29 and DDH-30 were interchanged. The result of this error is that the anomaly appeared to have an almost triangular shape. The correct shape of the anomaly is more nearly rectangular with a long axis oriented north-south as shown in Figure E.10. The holes and their corresponding results were correctly identified in Table 3.2 in the 1974 report, however.

The importance of measuring thermal conductivity values as part of the heat flow survey rather than using geothermal gradients alone is illustrated by the results from drill holes RDH-33 and 34. Both of these drill holes have thermal conductivities higher than those observed elsewhere in the geothermal area. In contrast to the other heat flow values the holes are drilled in geologic units other than the Empire Shale and Helena Formation (the Marsh Shale and Greenhorn Mountain Quartzite respectively). The actual thermal conductivity of the rocks cut by RDH-34 averages 13.3 mcal/cmsec°C, almost twice the average of the Marysville district in general. Therefore, in order to have an equal base for comparing the geothermal gradients shown in Figure E.10, the heat flow calculated by the product of the observed conductivity times the observed gradient was divided by the average thermal conductivity for the Marysville district to obtain the gradient shown in parentheses. Thus the equivalent geothermal gradient for RDH-34 is approximately 65°C/km as opposed to the observed value of 33.5°C/km, and the equivalent gradient for RDH-33 is 40°C/km. For this reason the geothermal gradient values shown for RDH-33 and 34 are shown in parentheses in Figure E.10.

Figure E.10 Heat Flow and Geothermal Gradient Map. The location of holes available for gradient and heat flow studies are indicated on the map and the symbol key is identified in the upper right hand corner of the figure. The upper number of each pair is the terrain corrected geothermal gradient in $^{o}C/km$. The lower figure is the terrain corrected heat flow value in $\mu cal/cm^2sec$. The average background for the area is approximately 30 and 2.0 for the geothermal gradient and heat flow respectively. Gradient values for RDH-33 and 34 are shown in parenthesis as these have been adjusted for thermal conductivity variations (see text).

The anomaly pattern in the geothermal area is relatively well determined except in the southern part of the map and along Ottawa Gulch. Both areas are relatively important in the interpretation of the implications of the geothermal anomaly as will be clear in the detailed discussions and interpretation described in the Summary and Discussion Chapter.

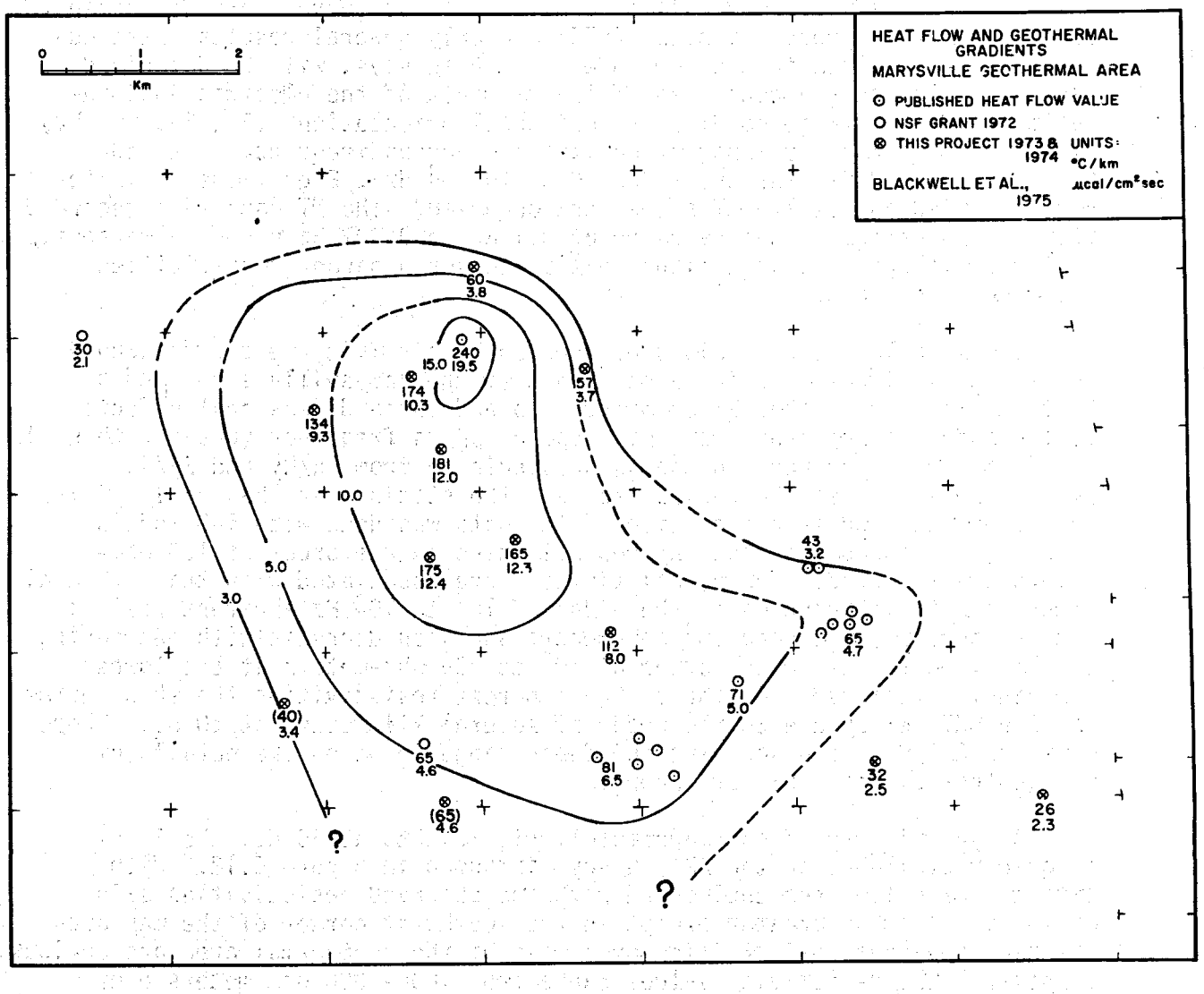

FIGURE E.10

Magnetotelluric Survey

In order to obtain more information on the depth and lateral variations of electrical resistivity in the Marysville geothermal area a magnetotelluric (MT) survey and an audiomagnetotelluric (AMT) survey were carried out during the summer of 1974. The detailed results of these surveys are discussed in an accompanying report (Peeples, 1975) and only general results, particularly as they relate to the remainder of the surveys, will be described here. The AMT survey consisted of measurements of the electric and magnetic fields in two perpendicular horizontal orientations (Ex, Ey, Hx, Hy) each. Calculations of apparent resistivity versus frequency were made based on these data over the range 20 Hz to 10^4 Hz. Eighty-one AMT sites were occupied and twelve MT sites were occupied. The MT data were recorded digitally over the frequency range of 0.1 Hz to 0.001 Hz and simultaneously in three orthogonal orientations so that tensor apparent resistivities could be calculated.

Sample bilogarithmic plots of apparent resistivity versus frequency are shown in Figure E.11 for a station over the Marysville stock and a station over the geothermal anomaly. Two and three dimensional effects on the data are apparent from the slope of ρ_a vs frequency (greater than 1) and from the differences in the ρ_a's calculated from Ex/Hy and Ey/Hx pairs. Nevertheless the curves from all the stations are basically similar to those shown and interpretation of the data was done with 1-D models. At highest frequencies apparent resistivities on the order of 100 ohm-meters are recorded. These resistivities are associated with the surficial material. At frequencies on the order of 10^2 to 10^3 Hz apparent resistivities approach or exceed 10^4 ohm-meters and then decrease with decreasing frequency to values on the order of 10^2 to 10^3 ohm-meters at the lowest frequencies recorded. At these high apparent resistivities the skin depths for the AMT survey are on the order of several kilometers at 20 H_z. Therefore the AMT data are sounding the depth range in which the details of the geothermal reservoir are known.

A synoptic map of the magnetotelluric results at 20 Hz, the lowest frequency available on the AMT survey, is shown in Figure E.12. With data at these low frequencies and with the observed resistivities skin depths are 1 km or greater except in the southwest corner of the map area. The high apparent resistivities over most of the geothermal area are obvious. In general the resistivity values range from 1000-3000 ohm-meters over the geothermal anomaly. Over the Marysville stock the resitivity values are in the range 3000 to 10,000 ohm-meters.

Unfortunately, due to the nature of the two types of equipment used, there is a two decade gap between 20 Hz, and 0.1 Hz in the apparent resistivity data available and therefore it is impossible to follow with detail the nature of the variations at frequencies between the AMT and MT apparent resistivity curves. There does not appear, however, to be evidence for very low resistivities in this period range which would be expected if a still molten intrusive body is present in the area at relatively shallow depths in the crust. In view of the general high resistivity at the longest period, the crust is probably not abnormally hot in this

locality, suggesting that the source of the high temperature water may be deep circulation rather than a young intrusive rock. If a recent intrusive is responsible for the heat it must be essentially solidified so that its presence is no longer obvious on the electrical sounding curves, or outside the area of the survey. The lowest resistivities at long period (less than 50 ohm-meters at 10 sec) occur southwest of the anomaly near the corner of the map area. The significance of the lower resistivity at depth is not known. There is no gravity anomaly where the resistivities are lowest and thus their origin due to a magma chamber at some distance from, but driving the hot water convection system seems unlikely. The low resistivities may be due to the deep sedimentary basin in that direction.

Detailed measurements of resistivity on core samples are discussed by Peeples (1975). It is apparent from modeling the data that the details of the resisitivity structure associated with fracture zones in the drill hole would not be detected by the AMT survey. Evidence for the extensive zone of low resistivity between 100 and 400 meters is not present on apparent resistivity curves and it is concluded that the low values shown are artificially low due to fluid invasion from the drilling (Peeples, 1975).

Although the survey appears to give little evidence of the shallow geothermal reservoir, 1-D interpretation does give information on the geologic structure and evidence of a horizon at depth beneath the map area. The AMT data at all frequencies delineate the faults along the south and west margins of the geothermal anomaly because the Marsh Shale apparently has a much lower resistivity than the older formations and the intrusive rocks. However, the lower shallow resistivities result in smaller skin depths and thus no deep resistivity information is obtained for comparison with the results in the geothermal area. This result is unfortunate in view of the gravity anomaly south of the known extent of the geothermal area. The results from the geothermal area suggest an interface at depths ranging from about 1.5 to 7 km. The interface is at a depth of 1.5 to 2.9 km beneath the geothermal anomaly and 5 to 7 km beneath the Marysville stock. It has a depth of 2.1 $\pm$ 0.2 km at the site of the deep drill hole. Such depths are consistent with the gravity data although the interpretation favored has a slightly deeper extent for the Empire Creek stock and a shallower bottom for the Marysville stock. The depth to the bottom of the Marysville stock, based on gravity data, could be easily varied as the density contrast could be much less than assumed (as low as 0.08 gm/cm^3). The results of core analysis from the deep drill hole do not suggest rapid changes in chemistry or physical characteristics which might be expected if the bottom of the intrusive were close by. Thus the significance of the low resistivity layer remains enigmatic. The implications of the data will be discussed in the Summary and Discussion Chapter and a more detailed discussion may be found in the AMT-MT report (Peeples, 1975).

DEEP EXPLORATION TEST WELL

Subsequent to the studies of the summer of 1973, funding was approved for the drilling of a deep exploration test well, Marysville Geothermal Exploration Number One (MGE #1), in the geothermal area during the summer of

Figure E.11 Type apparent resistivity (ρ_a) curves. Station MT 12/AMT 71 was over the Marysville stock and station MT 5/AMT 31a was over the geothermal anomaly. Symbols: MT 5/AMT 31a, open circles and closed triangles, E-W electric; crosses and closed circles, N-S electric field; MT 12/AMT 71, open circles and closed circles, E-W electric; crosses and closed triangles, N-S electric field (see Peeples, 1975, for details of antenna orientation etc.).

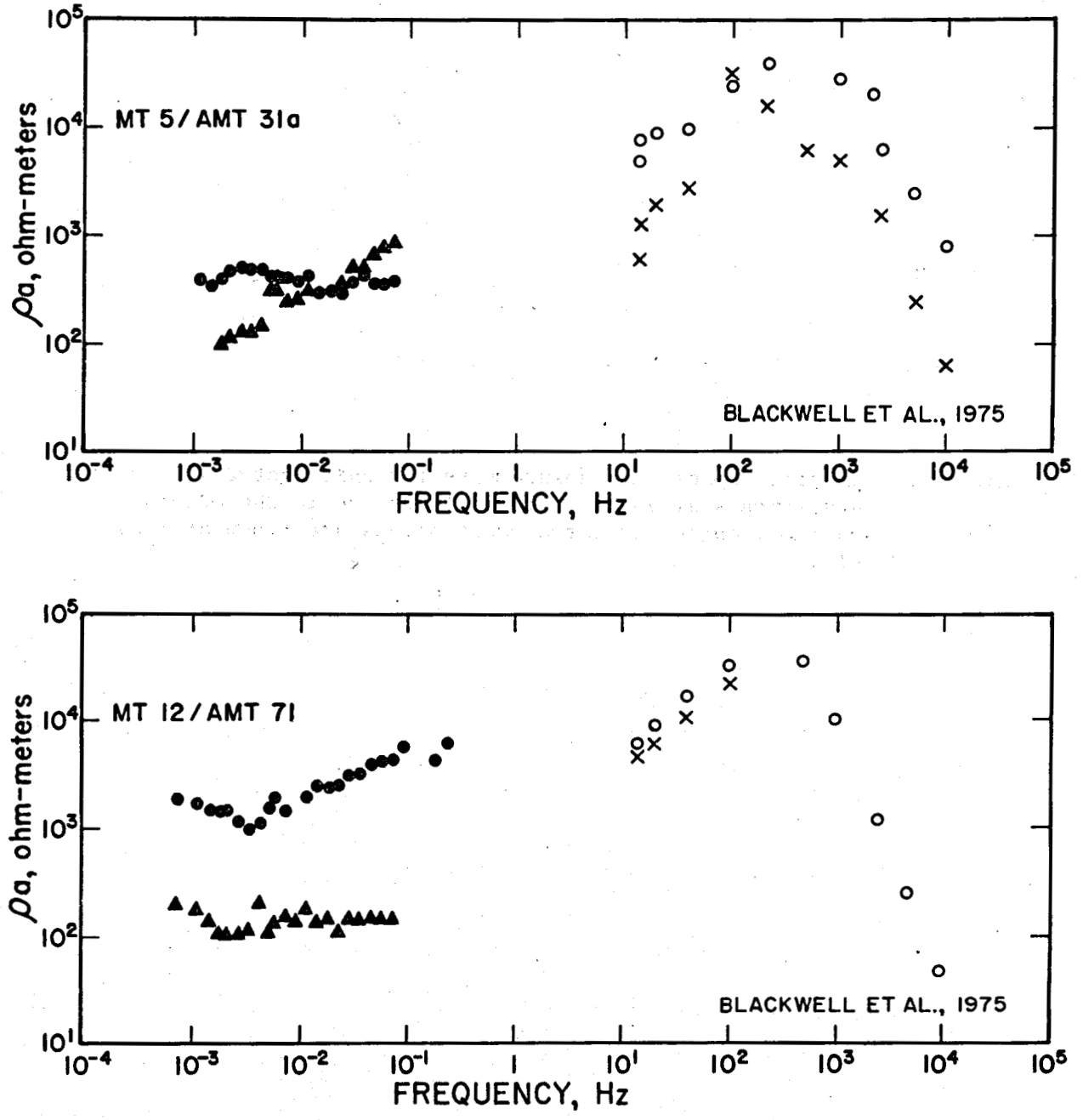
MT 5/AMT 31a
BLACKWELL ET AL., 1975
ρa, ohm-meters
FREQUENCY, Hz
MT 12/AMT 71
BLACKWELL ET AL., 1975
ρa, ohm-meters
FREQUENCY, Hz

FIGURE E.11

Figure E.12 Synoptic map of AMT measurements for east-west telluric measurements at 20 Hz. The contours are in ohm-meters and the location of measurement points are shown as small dots.

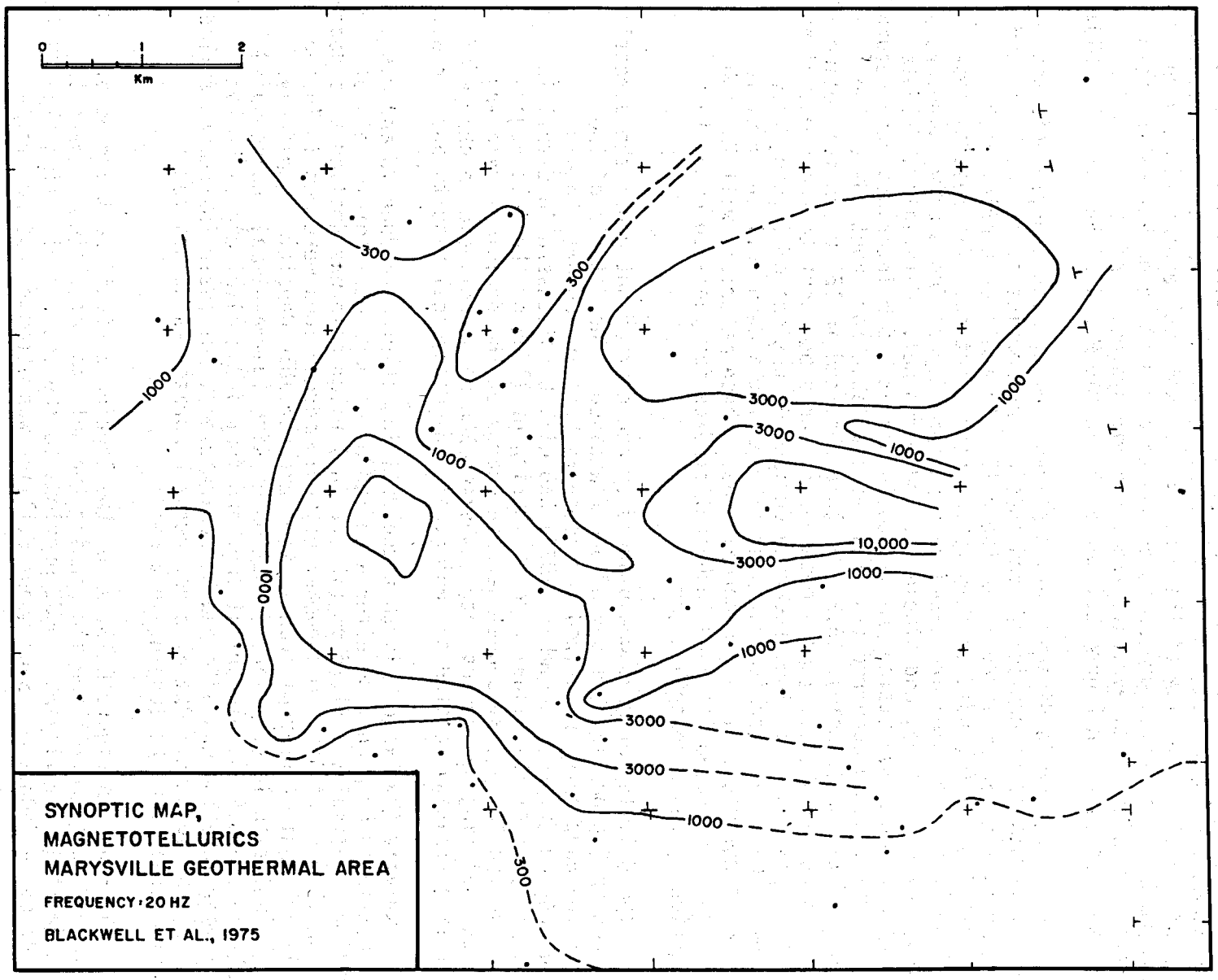
0
1
2
Km
300
300
1000
1000
3000
3000
1000
1000
10,000
3000
1000
1000
3000
3000
1000
300
SYNOPTIC MAP,
MAGNETOTELLURICS
MARYSVILLE GEOTHERMAL AREA
FREQUENCY: 20 HZ
BLACKWELL ET AL., 1975

FIGURE E.12

1974. The object of the drill hole was to explore at depth the implications of the surface exploration data. If the area turned out to be due to conductive heat flow from a shallow magma chamber, then tests to evaluate the possibilities of use of the area for dry hot rock exploitation were proposed. If the area proved to be due to circulation of hot water, then tests were planned to evaluate the reservoir system. The location of the well is shown on Figure E.1 and E.25 (in the NE1/4 of Sec 32, T12, R6W).

This chapter is divided into sections dealing with the geologic setting, temperatures, fluid chemistry, and physical properties of the geologic and hydraulic regimes encountered in the well. In addition a brief history of the drilling is included in this introductory section. The results described in this chapter are based on data from Rogers Engineering Company, Schlumberger Limited, and studies by SMU personnel. Materials available for study included cutting samples collected at 1.5 m intervals when return fluid circulation occurred (samples are available for about 50% of the depth of the drill hole), 25.2 m of core obtained in 15 successful coring runs, water samples collected both during and subsequent to the completion of the well, and well logs recorded during two periods of logging (see below). Such an extensive data set is rare for a deep well in granitic rocks, particularly in a geothermal area. These materials will furnish the basis for scientific and technical studies for years to come, in addition to those described here.

The drilling program was planned by and carried out under the direction of Rogers Engineering Company of San Francisco. The details of the drilling have been summarized (Preliminary Drilling Report, Rogers Engineering Company, November, 1974) and will be discussed in detail in another part of this final report. During drilling of the hole Rogers Engineering Company personnel were in charge of the decisions relating to the drilling procedures, etc., whereas SMU personnel were in charge of drilling strategy related to geological and geophysical results and coring.

Briefly the history is that the drilling started on June 10 and was discontinued on August 30 after a period of 81 days at a total depth of 2070 m. Initially a 31.75 cm (12-1/2 in.) pilot hole was drilled to a depth of 466.3 m.* At 466.3 m a number of Schlumberger logs were run including caliper, sonic (interval transit time and variable density), gamma-ray, dual induction lateral log, formation density (gamma-gamma), compensated neutron (porosity), electrical log, and four arm digital dip meter log. A temperature log was attemped by Schlumberger, but their instrument failed during the logging. Battelle Northwest Laboratories contracted to Schlumberger for the logging services.

As shown in Figure E.13, after the logging a significant period of time was spent redrilling and reaming the hole to set casing. The hole was drilled primarily with mud, previous to the setting of casing (13-3/8 in., 33.97 cm) at 404.2 m. Subsequent drilling was attempted using air.

---

*Depths used throughout this report when referring to MGE #1 are depths from Kelly Bushing, approximately 6.1 m above ground level.

Figure E.13 MGE #1 drilling record (Rogers Engineering Co., November, 1974). The sequence of events is (1) air drilling and reaming to 44.45 cm (17½ inches) and 66.04 cm (26 inches); (2) 50.8 cm (20 inches) casing set to 35.1 m; (3) coring at .3-.6 m/hr and mud drilling at 1.2-2.4 m/hr.; (4) logging and reaming to 44.45 cm (17½ inches); (5) 33.97 cm (13 3/8 inches) casing set to 404.2 m; (6) coring (.3-.6 m/hr) and drilling with water in a 31.12 cm (12¼ inch) hole at 5.5-7.6 m/hr; (7) drum shaft repair and (8) coring and drilling with water in 20.0 cm (7 7/8 inch) hole below 1300.0 m and 24.45 cm (9 5/8 inch) casing set to 1300 m.

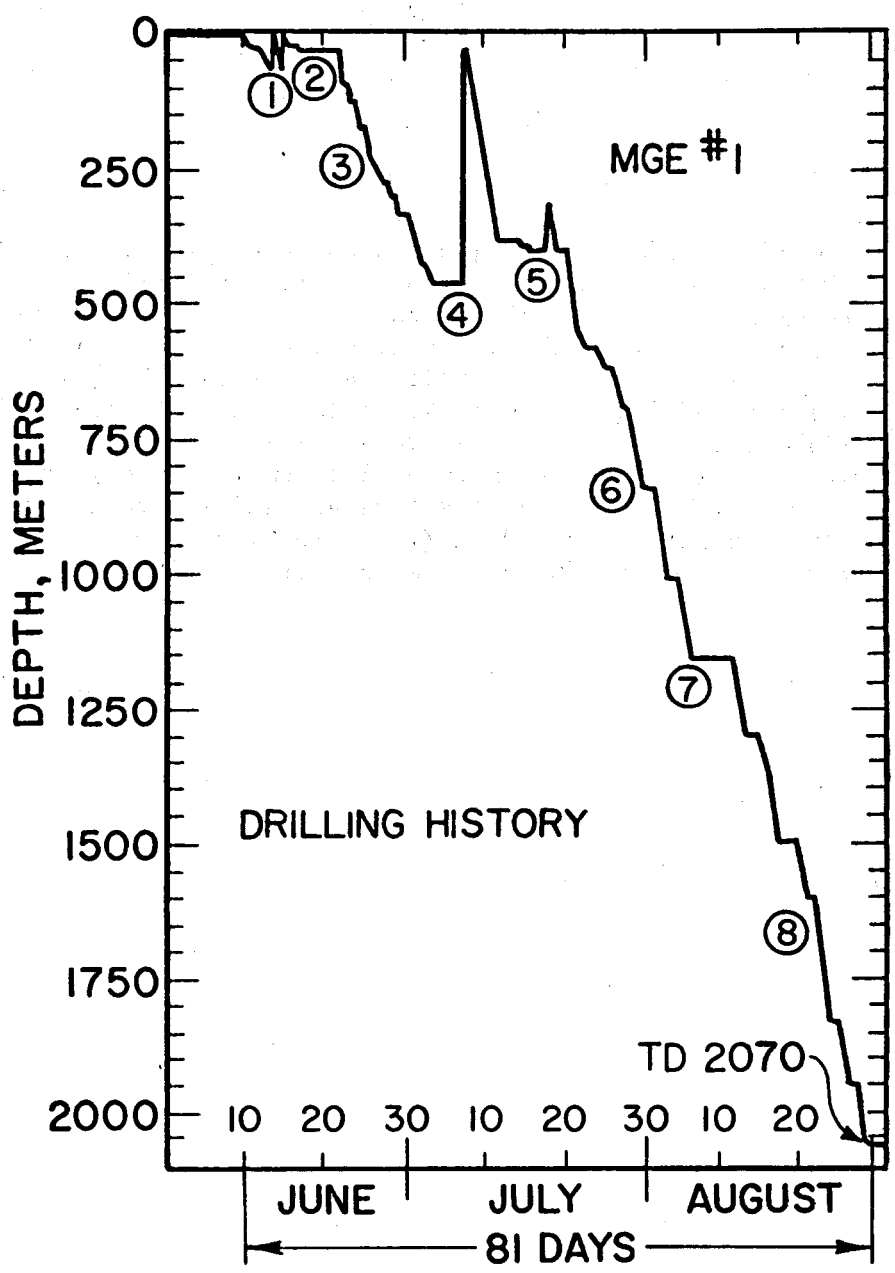
0
250
500
750
1000
1250
1500
1750
2000
DEPTH, METERS
MGE #1
DRILLING HISTORY
①
②
③
④
⑤
⑥
⑦
⑧
TD 2070
10 20 30 10 20 30 10 20
JUNE
JULY
AUGUST
81 DAYS

FIGURE E.13

Within the span of a hundred meters large amounts of hot water began to be encountered in the hole and at a depth of 582.8 m the hole was producing so much water that air drilling had to be discontinued. Below this depth the hole was drilled using an aerated water column. The hole diameter was reduced from 31.12 cm (12-1/4 in.) to 20.0 cm (7-7/8 in.) at a depth of 1300 m on August 15. Several temperature logs were obtained during this period with SMU equipment which had a maximum depth capability of 840 m.

During drilling of the hole several fracture zones were encountered although no serious hole stability problems developed until a depth of 2070 m was reached. At this point caving from a large fracture zone below 2048 m made it impossible to reach the drilled depth with the drill string. It was decided to stop drilling at this point because not enough money was available to stabilize the hole for continued drilling.

On completion of the well a number of Schlumberger logs were run including most of the types of logs run previously at 466.3 m. Subsequent to the logging, 24.45 cm (9-5/8 in.), casing was set in the hole to a depth of 1300 m and an attempt was made to cement the casing into the hole. This cement job was only partially successful, and subsequent flow meter logs in the well indicated continuing circulation, as discussed in the following section. At the same time a concrete plug was placed in the bottom of the well between 1954 m and 2030 m in order to eliminate the possibility of water flow into the bottom fracture zone encountered during drilling.

The results of the logging, including various computed logs and interpretations, are discussed in a report submitted by Schlumberger (Coates, 1974) included as part of this final report. Reference to that report is made for a synthesis of the logs run, cross calculations of porosity using the various logs, fracture analysis, etc.

After the rig was removed from the site several types of logs continued to be run. These included various types of flow meter logs and temperature logs. The final Schlumberger temperature and flow log was recorded on 11/16/74.

Geological Studies

During drilling of the well SMU personnel were on site in order to supply geological input to the drilling decisions and to monitor geologic results. The services of a mud logger had been obtained as part of the drilling contract, but the mud loggers were not in general familiar with igneous and metamorphic rocks and most of the lithologic descriptions in the mud logger's report were based on discussions with Dave Petefish of SMU.

The metamorphic and igneous rocks encountered by the well are the hornfelsed Empire and possibly Spokane Formations, a metamorphosed dacite porphyry dike or sill, and the Empire Creek stock which grades from granite porphyry at shallow depth to equigranular granite at greater depth. Based on the 1973 studies it was anticipated that the Empire Creek stock would be encountered at a depth on the order of 300 m or less (1974 report, p. 74).

The actual contact occurred at 294.1 m. Rock descriptions were obtained by optical microscope study of the cuttings, petrographic studies of thin sections of the cores, x-ray diffraction analyses and analysis of the electric logs and drilling records. Fracture zones were located by comparison and analysis of drilling records, cores, study of cuttings, and well logs. The depth intervals cored, lengths recovered, and detailed descriptions of the cores are shown in Table E.5. Recovery of cutting samples from the bottom third of the hole was poor as returns were obtained only about half the time. Thus this critical part of the well is not as well known as might be desirable. The generalized lithologic information for the well is shown in Figure E.14.

The metamorphism of the Empire and possible Spokane Formations in the well has been to tremolite or higher grade. No diopside-bearing rocks are found in the well core, but 100 m northwest of the well, diopside grade rocks occur at the surface. The scarcity of calicte and the high K_2O in the well cores produced tremolite-phlogopite-quartz assemblages which are stable over a wide range of temperatures including those of the diopside zone. Little coarsening of grain size was noticed as either igneous body was approached. The Empire Shale consists of a K_2O-bearing dolomitic shale which forms tremolite and phlogopite when metamorphosed, while the Spokane Argillite contains very little or no dolomite, and would form muscovite, biotite, and quartz when metamorphosed. Presence of phlogopite and tremolite in cores 2 and 3 imply that most of the cored metasedimentary rocks are metamorphosed Empire Shale. Absence of tremolite in core 4 (Table E.5) suggests a transition towards Spokane Argillite. More details on the metamorphic assemblages may be found in Table E.5 and in the Section on Metamorphic Petrology.

Between 88.4 and 121.9 m a metamorphosed dacite porphyry was cut by the well. This porphyry contains phenocrysts of plagioclase and biotite and possibly some hornfels xenoliths of the Empire Formation. Many of the biotite phenocrysts were recrystallized and the plagioclase phenocrysts were partially replaced by sericite.

The Empire Creek stock was reached at 294.1 m and was found to be a granite porphyry containing phenocrysts of orthoclase, plagioclase, quartz, and biotite. Orthoclase and quartz make up the sugary ground mass. The plagioclase phenocrysts are highly, and orthoclase phenocrysts slightly, altered to kaolinite and montmorillonite, and replaced by sericite. Fluorite, sphene, zircon, and pyrite were also identified in the porphyry. Veins include fluorite, calcite, and sericite. Most of the contacts in the igneous body are gradational with the grain size and degree of crystallization increasing with depth. The uppermost rock is a light gray granite porphyry (or quartz-feldspar porphyry). This unit grades into a greenish to whitish-gray granite porphyry.

At greater depths the light pink to greenish-gray Empire Creek granite porphyry grades into a more equigranular pink granite as typified by core 15. The orthoclase and plagioclase are less altered at greater depths although the plagioclase is still rather highly altered to kaolinite with minor montmorillonite. Identifiable plagioclase throughout the hole remained of albite composition. Fluorite was observed in most of the cores, including a fluorite vein at 1835.5 m.

Table E.5 Core location, recovery and description, MGE #1

Core 1: 99.1-102.1 m (325-335') 3.0 meters of core was recovered. The core consists of a dark gray to greenish gray, metamorphosed dacite porphyry containing phenocrysts of biotite and plagioclase. The rock in thin section has approximately 25% plagioclase phenocrysts up to 0.7 cm, 25% plagioclase in the groundmass, 15% biotite in phenocrysts up to 0.2 cm and groundmass, 25% quartz, and less than 1% unaltered pyrite. Xenoliths of up to 2.5 cm in length from the Empire or Spokane Shale are found in the core. The rock displays several fracture systems with the last system vertical. The fractures are filled with calcite, quartz, fluorite, and pyrite and have associated 4.0 cm wide alteration zones of chlorite. Other alteration includes plagioclase to sericite and biotite to chlorite. Accessory minerals in the rock are apatite, zircon, and leucoxene (in recrystallized, biotite phenocryst sites).

Core 2: 132.9-135.9 m (436-446') 2.1 m of core was recovered. The core consists of a dark green to brownish gray, hornfelsed dolomitic Empire Shale which has been strongly veined and fractured. The rock as seen in thin section and by x-ray diffraction contains in order of abundance: quartz, phlogopite, tremolite, and green biotite. Veins up to 3.0 cm wide contain quartz, adularia, calcite, fluorite, chlorite, and muscovite. Accessory minerals include apatite, zircon, tourmaline, pyrite, hematite, and leucoxene. Late vertical and inclined (60°) fractures filled with montmorillonite and calcite (identified by x-ray diffraction) developed horizontal slickensides as healing occurred.

Core 3: 177.0-180.1 m (581-591') 3.0 m of core was recovered. The core consists of a dark green to brownish gray, hornfelsed dolomitic Empire Shale, which has been strongly veined and fractured. The rock as seen in thin section and by x-ray diffraction contains in order of abundance: quartz, phlogopite, tremolite, and very light green biotite. Veins up to 1.0 cm wide and generally dipping 60-90° contain quartz, fluorite, calacite, adularia, chlorite, albite or oligoclase, tremolite, phlogopite, green biotite, and leucoxene. Some slickensides may be found along fractures dipping at 60° and coated with a clay-like mineral. Accessory minerals include apatite, zircon, sphene-leucoxene, pyrite and rutile.

Core 4: 280.7-283.8 m (921-931') 3.0 m of core was recovered. The core consists of a dark greenish-gray to brown, hornfelsed shale which has been strongly veined and fractured. This core could possibly represent a transitional zone between the Empire Shale and the Spokane Argillite. The rock as seen in thin section contains in order of abundance: quartz, phlogopite or light brown biotite, tremolite, plagioclase in various stages of alteration to sericite, and a small amount of orthoclase. Veins up to 0.7 cm wide and generally oriented vertically contain quartz, fluorite, calcite, dolomite, chlorite, adularia, phlogopite, green biotite, and plagioclase. Some horizontally oriented slickensides may be found along fractures dipping at 30°. The more recent fractures also contain montmorillonite identified by x-ray diffraction analysis. Accessory minerals include apatite, zircon,

sphene-leucoxene, sphalerite, pyrite, and tourmaline.

The hornfels in the contact zone with the Empire Creek stock show slightly enlarged crystals of phlogopite or light brown biotite and tremolite. The cuttings in thin section contain quartz, phlogopite or biotite, olive brown biotite, tremolite, and pyrite in the hornfels. Veins contain fluorite, chlorite, quartz, and pyrite in various stages of alteration to hematite. The igneous rock contains quartz, orthoclase, biotite, fluorite, muscovite or sericite, pyrite, hematite, highly sericitized plagioclase, and chlorite.

Core 5: 303.9-306.9 m (997-1007') 3.0 m of core was recovered. The core consists of a very light gray, altered, granite porphyry containing phenocrysts of plagioclase up to 0.6 cm, biotite up to 0.5 cm, quartz up to 1.0 cm, and orthoclase up to 1.4 cm. The rock has approximately 15% orthoclase microperthite, 10% quartz, 2% biotite, and 5% plagioclase phenocrysts. The groundmass of the rock in thin section is made up of quartz, orthoclase, plagioclase, biotite, fluorite, and pyrite. Plagioclase has been altered to sericite, kaolinite, and montmorillonite, while the biotite has been partially altered to chlorite. Vertical, 35° and 65° veins with alteration zones of up to 3 cm width contain quartz, orthoclase, sericite or muscovite, fluorite, calcite, pyrite, and molybdenite. Some horizontal movement is indicated by the horizontal striations or slickensides along fractures. Accessory minerals include zircon and sphene.

Core 6: 464.5-466.3 m (1524-1530') 1.8 m of core was recovered. The core consists of a pinkish gray granite porphyry containing phenocrysts of biotite 0.7 cm, plagioclase 0.7 cm, orthoclase 1.7 cm, and quartz 1.0 cm. The rock in hand specimen has approximately 20% quartz, 10% orthoclase, 10% plagioclase, and 3% biotite phrnocrysts. The groundmass of the rock is composed of quartz, biotite, plagioclase, and orthoclase. Plagioclase has been strongly kaolinized, while the orthoclase has only been slightly altered. The biotite has been partially altered to chlorite with some pyrite and other sulphides being located in some of the crystal sites. Vertical, 20° and 60° veins up to 0.4 cm wide are filled with quartz, pyrite, molybdenite, and other sulphides.

Core 7: 590.1-593.3 m (1936-1940') 0.2 m of core was recovered. The core consists of a light greenish-gray, altered, granite porphyry containing phenocrysts of biotite (0.6 cm), plagioclase (0.7 cm), orthoclase (1.4 cm), and quartz (0.9 cm). The rock in hand specimen has approximately 40% quartz, 5% plagioclase, 50% orthoclase, and 5% altered biotite. The feldspars in the rock have been highly altered to kaolinite, montmorillonite, and possibly other clay minerals. The biotite has been altered mainly to chlorite. A vein dipping at 45° approximately 0.5 cm wide contains quartz with altered feldspar and biotite.

Core 8: 699.5-701.0 m (2295-2300') 1.5 m of core was recovered. Core 8 in hand specimen is similar to core 7, but with slightly less feldspar and biotite alteration. The fractures are from 0.5 to 0.6 m wide and only partially healed with quartz, molybdenite, etc. The voids still seem to be linked along the fracture zones.

Core 9: 848.0-849.2 (2782-2786') 0.9 m of core was recovered. The core consists of a light gray to light greenish-gray, highly altered granite porphyry containing phenocrysts of biotite (0.6 cm), plagioclase (0.7 cm), orthoclase microperthite (1.4 cm), and quartz (1.3 cm). The relative percentages of the minerals remain the same in thin section as core 7 and 8. The composition of measurable plagioclase is An_5. 55° and 75° veins from 0.2 to 1.0 cm wide in the core contain quartz, chlorite, pyrite, and molybdenite. These fractures have been almost totally healed, with some having 1.0 cm alteration zones. Accessory minerals include fluorite, pyrite and zircon.

Core 10: 1009.5-1010.7 m (3312-3316') 0.9 m of core was recovered. The core consists of a brecciated, highly altered, light gray granite porphyry containing phenocrysts of biotite (0.9 cm), orthoclase (1.4 cm), plagioclase (0.7 cm), and quartz (1.1 cm). The rock in hand specimen has approximately 25% orthoclase, 20% quartz, less than 5% plagioclase, and less than 5% biotite phenocrysts. The groundmass consists of these same minerals. Brecciation fractures have been totally healed by cryptocrystalline quartz and feldspars. Later 10°, 60° and 80° fractures have only been partially healed by cryptocrystalline quartz and other minerals. These fractures contain openings 0.1 to 0.5 cm wide.

Core 11: 1163.4-1165.9 m (3817-3825') 1.6 m of core was recovered. The core consists of a light gray, altered granite porphyry containing phenocrysts of biotite (1.0 cm), plagioclase (0.9 cm), orthoclase (1.3 cm), and quartz (1.1 cm). The rock in hand specimen has approximately 5% biotite, 50% orthoclase, 5% plagioclase, and 40% quartz. The feldspars have been strongly kaolinized, but the biotite has been only moderately altered to chlorite. Veining in the core has mostly a 55° to 75° orientation with the veins being 0.5 to 1.0 cm wide. The veins are filled predominantly with cryptocrystalline quartz and have zones of alteration containing orthoclase and green biotite surrounding them.

Core 12: 1297.2-1299.7 m (4256-4264') 1.7 m of core was recovered. The core consists of a light gray to purplish-gray, altered porphyritic granite containing phenocrysts of biotite (1.0 cm), plagioclase (1.2 cm), orthoclase (1.4 cm), and quartz (1.2 cm). The rock in hand specimen has approximately 5% biotite, 5% plagioclase, 50% orthoclase, and 40% quartz. Plagioclase has been strongly kaolinized, while the orthoclase has only been moderately altered. The biotite has been partially altered to hematite, chlorite, etc. Some mineralized veins containing cryptocrystalline quartz and kaolinite are found in the core. Late 85° veins up to 0.3 to 0.5 cm wide contain mylonite zones. Horizontal fractures 3.0 to 5.0 cm apart may be found in a 15 cm section of the core.

Core 13: 1606.3-1608.1 m (5270-5276') 1.0 m of core was recovered. The core consists of a light pink, altered porphyritic granite containing phenocrysts of orthoclase (1.3 cm), plagioclase (0.7 cm), and quartz (0.9 cm). The rock in hand specimen has approximately 5% biotite, less than 5% plagioclase, 50% orthoclase, and 45% quartz. The groundmass of the rock in this

core is more equigranular with fewer phenocrysts. Plagioclase is highly altered to clay minerals, while the orthoclase has only been slightly altered. The biotite has been moderately altered to chlorite. There are few if any veins in the core, but there are horizontal fractures every 3 cm or closer. The core has also been fractured vertically with little or no veining associated with the fractures. Miarolitic cavities up to 0.3 to 0.5 cm in diameter can be found in the core. (A fine grained granite porphyry sample containing phenocrysts of quartz, biotite, and orthoclase and a quartz vein 1.5 cm wide was retrieved at the top of the core. It is not considered to have originated at this depth).

Core 14: 1835.5-1837.6 m (6022-6029') 1.5 m of core was recovered. The core consists of a dark pink, altered porphyritic granite containing phenocrysts of orthoclase microperthite (1.4 cm), plagioclase (0.8 cm), and quartz (1.0 cm). The rock in thin section has approximately 5% or less biotite, 5% plagioclase, 45% orthoclase, and 45% quartz. The plagioclase is highly altered to clay minerals, while the orthoclase is only slightly altered. The composition of measurable plagioclase is An_{5-7}. The biotite has been slightly altered to chlorite. The groundmass is easy to see in hand specimen and equigranular. Horizontal fractures occur every 8 to 10 cm with little or no alteration along them. 80° fractures 0.2 to 0.3 cm wide contain cryptocrystalline quartz, orthoclase, plagioclase, fluorite, and limonite. Accessory minerals include apatite, sericite, zircon, pyrite, and hematite. Miarolitic cavities of up to 4 x 1.5 x 1 cm are found in the core (containing euhedral crystals of orthoclase and quartz).

Core 15: 1953.8-1955.0 m (6410-6414') 0.6 cm of core was recovered. The core consists of a pink, altered equigranular granite. The rock in thin section has approximately 5% or less biotite up to 0. 9 cm, 10% plagioclase (0.8 cm),55% orthoclase microperthite 1.2 cm, and 35% quartz (1.0 cm). The plagioclase is less altered in this core than in previous cores, but is still highly altered to kaolinite and lesser amounts of montmorillonite as identified by x-ray diffraction. The composition of measurable plagioclase is An_{5-7}. Orthoclase in the core has only slightly altered to clay. The biotite is still replaced partially by chlorite (brunsvigite). There are some horizontal fractures 8 to 20 cm apart and diagonal fractures with little or no alteration, except for a thin film of clay or a dull appearance along the fractures. Miarolitic cavities can be found in the core with dimensions 1 x 2 cm.

Figure E.14 Lithology, location of fracture zones determined by drilling, hole casing sizes and core locations versus depth in the deep exploration test (MGE #1).

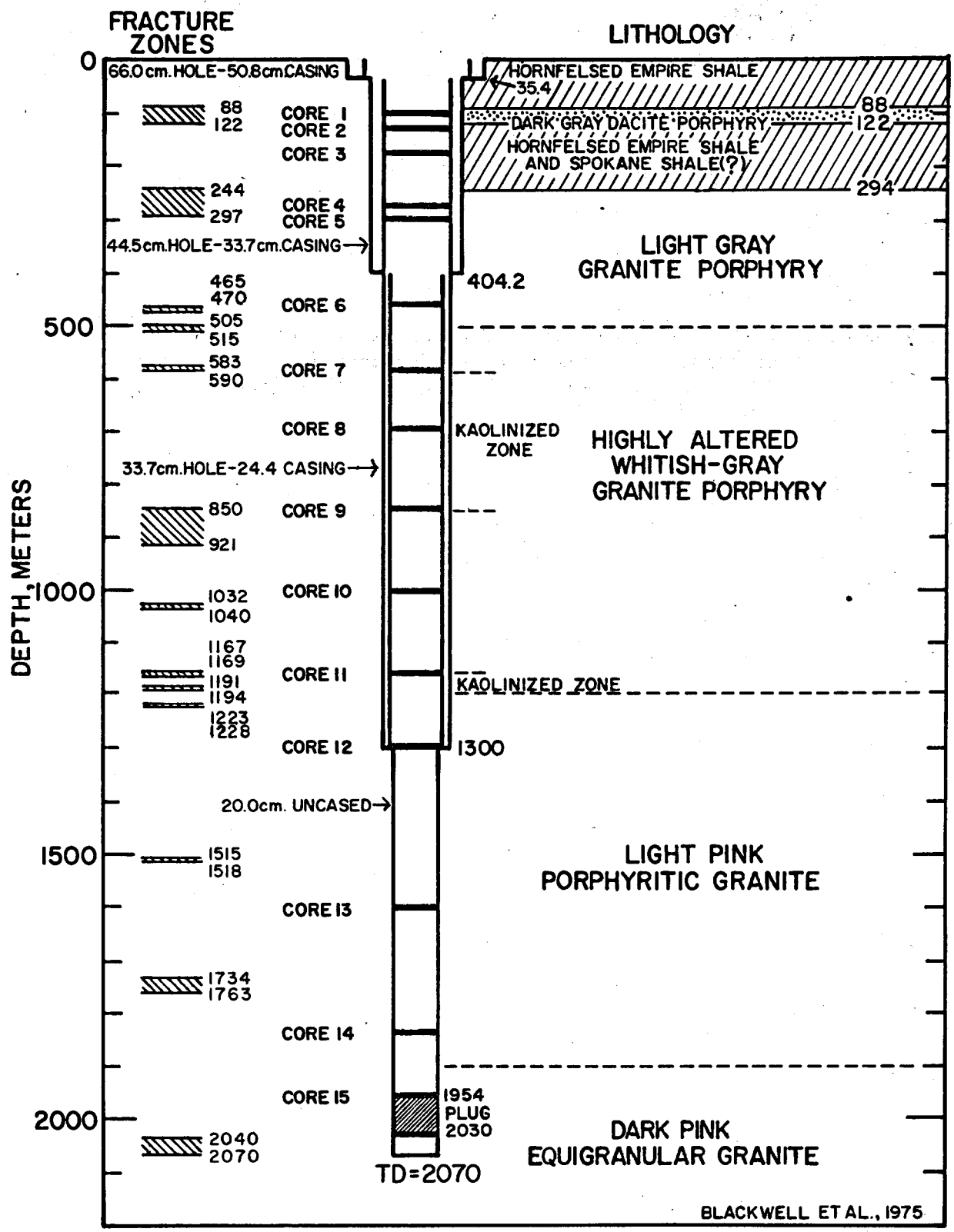
FRACTURE ZONES
LITHOLOGY
0
66.0 cm. HOLE-50.8 cm CASING
88
122
CORE 1
CORE 2
CORE 3
244
297
CORE 4
CORE 5
44.5 cm. HOLE-33.7 cm. CASING
HORNFELSED EMPIRE SHALE
35.4
DARK GRAY DACITE PORPHYRY
88
122
HORNFELSED EMPIRE SHALE AND SPOKANE SHALE(?)
294
LIGHT GRAY GRANITE PORPHYRY
404.2
465
470
505
515
CORE 6
500
583
590
CORE 7
CORE 8
KAOLINIZED ZONE
HIGHLY ALTERED WHITISH-GRAY GRANITE PORPHYRY
33.7 cm. HOLE-24.4 CASING
850
921
CORE 9
DEPTH, METERS
1000
1032
1040
CORE 10
1167
1169
1191
1194
1223
1228
CORE 11
KAOLINIZED ZONE
CORE 12
1300
20.0 cm. UNCASED
1500
1515
1518
LIGHT PINK PORPHYRITIC GRANITE
CORE 13
1734
1763
CORE 14
CORE 15
1954
PLUG
2030
2000
2040
2070
DARK PINK EQUIGRANULAR GRANITE
TD=2070
BLACKWELL ET AL., 1975

FIGURE E.14

Veins in the well cores, oriented both diagonally and vertically, contain a variety of minerals. These minerals include quartz, calcite, dolomite, adularia, fluorite, tremolite. phlogopite, green biotite, muscovite or sericite, montmorillonite, chlorite, clinozoisite, plagioclase, pyrite, limonite, hematite, sphalerite, galena, and molybdenite as well as rock chips. There were at least two stages of veins: high and low temperature. The high temperature veins consist of most of the above minerals, generally with an outer zone of adularia on the country rock followed by quartz and pyrite. Low temperature veins are composed of the assemblage dolomite-quartz which would break down at temperatures above 300°C to talc (Figure E.4). Some open fractures were encountered in the hornfels as shown on the well diagram (Figure E.14, between 243.8 and 297.2 m).

A generalized summary of the geologic history in the well area includes deposition of sediments, minor deformation, intrusion of the Marysville stock which slightly metamorphosed the sediments, intrusion of the dacite porphyry, intrusion of the Empire Creek stock with considerable high temperature veining, later low temperature veining and formation of slickensides along fractures, and development of open, disking fractures in the Empire Creek stock.

After the intrusion of the Marysville stock, the dacite porphyry was intruded above the present position of Empire Creek stock. The intrusion temperature of the dacite was about 700 to 800°C as implied by titanium presence in the biotite phenocrysts. These biotite phenocrysts were recrystallized to phlogopite, leucoxene, and ore during the metamorphism associated with the Empire Creek stock. The Empire Creek stock followed the dacite porphyry by enough time to allow the hardening of the dacite porphyry so it could be fractured and altered by the later intrusion.

The Empire Creek stock was then intruded with considerable associated high temperature veining. The main minerals are adularia, calcite, quartz, and fluorite. These veins may be seen with little variation from the surface to the Empire Creek stock contact. The quartz and fluorite veins continue at depth to the deepest core, and are presumed to have continued forming while the rock was cooling. Galena, sphalerite, and molybdenite veins are also found above the contact, with the molybdenite veins continuing several hundred meters below the contact.

Late veins associated with the Empire Creek intrusion contain dolomite, calcite, and quartz. The temperature of these veins was probably below 300°C. These veins might also be associated with some later event.

Finally, open fractures and those containing montmorillonite may represent events late in the cooling process of the intrusion. Some of these fractures and vein fillings show slickensides and striations indicating horizontal movement. Other horizontal fractures with little or no alteration or fillings in the Empire Creek intrusive are later and may be related to final cooling or to release of stress by unloading during drilling. Unloading is suggested as an origin for these fractures since at least one of the cores was audibly crackling when it was retrieved at the surface.

Temperature Measurements

An extensive series of temperature measurements was made both during and subsequent to drilling of MGE #1. The drill hole was sited near the location of one of the shallow heat flow holes drilled during the summer of 1973 (DDH-23). The observed geothermal gradient in that drill hole corrected for topography is 174°C/km with an uncertainty of 10-20°C because of a large terrain correction. None of the geophysical data, including the two types of resistivity surveys, furnished any definite idea as to how far this geothermal gradient might be extrapolated. Drilling proceeded to 466,3 m on 7/6/74. At this depth the Schlumberger logs were run in the 31,75 cm hole because reaming was planned to such a large diameter that use of some of the Schlumberger tools would be precluded. During this logging the Schlumberger temperature tool failed and no reliable information was obtained on temperatures in the drill hole except from the mercury maximum thermometers run slightly above each tool during the logging (presumably recording average near bottom hole temperatures). When it was recognized that the Schlumberger log could not be obtained, a series of temperatures were measured using SMU equipment of the type used in obtaining temperatures in the shallow holes. These data were obtained without difficulty except that, because of the heavy mud in the hole, the probe had to be weighted for penetration and the resulting increased resistance upon retrieval stretched the logging cable by almost 5%. Thus depth corrections had to be applied to the rest of the data obtained with that particular set of instrumentation.

Of the series of mercury maximum thermometer readings and two maximum depth temperature readings obtained during SMU loggings, the measured maximum hole temperature was 86°C at 457.2 m during the last logging run. The data fit no reasonable extrapolation formula and so no equilibrium temperature can be calculated. Subsequent to the logging the hole was reamed and cased. This job required about two weeks. At that point the drill hole was cleaned out to total depth and a period of 24 hr (7/20/74) was available for temperature logging in the bore hole during make up of the drilling rig for the deeper drilling. The extrapolated equilibrium temperatures based on this set of measurements are shown as the +'s in Figure E.15. Each of these plotted points is based on a series of temperature versus time measurements with the temperatures extrapolated to the estimated equilibrium temperature. The points at 424.5, 435.0, 445.1 and 465.3 m fall close to an extrapolated geothermal gradient curve with the slope of 174°C/km observed in the shallow measurements (light line in Figure E.15). The temperature at 455.3 m falls below the extrapolated curve which suggests local downward flow of water between 445 and 465 m or unsatisfactory equilibrium extrapolations.

Drilling began with air and very shortly thereafter the drill hole began to make copious quantities of hot water. Several sets of temperature measurements were made on 7/23/74 while preparations were in progress to switch from air to water drilling and while haulage of fluid from the mud pit was in progress. Hole depth was 590.1 m. The temperature measurements obtained in the bottom part of the hole approximately reflect equilibrium conditions as the temperatures were changing very slowly, if at all, at

Figure E.15 Selected temperature logs in the depth range 0-1 km during and subsequent to drilling in MGE #1. An X at the end of the temperature-depth curve indicates total depth at that particular time. The log b on 8/1/74 was taken about 2 hours after log a. The log on 8/29/74 was first log taken after completion of drilling. Equilibrium temperatures extrapolated from measurements on 7/20/74 are shown by +'s.

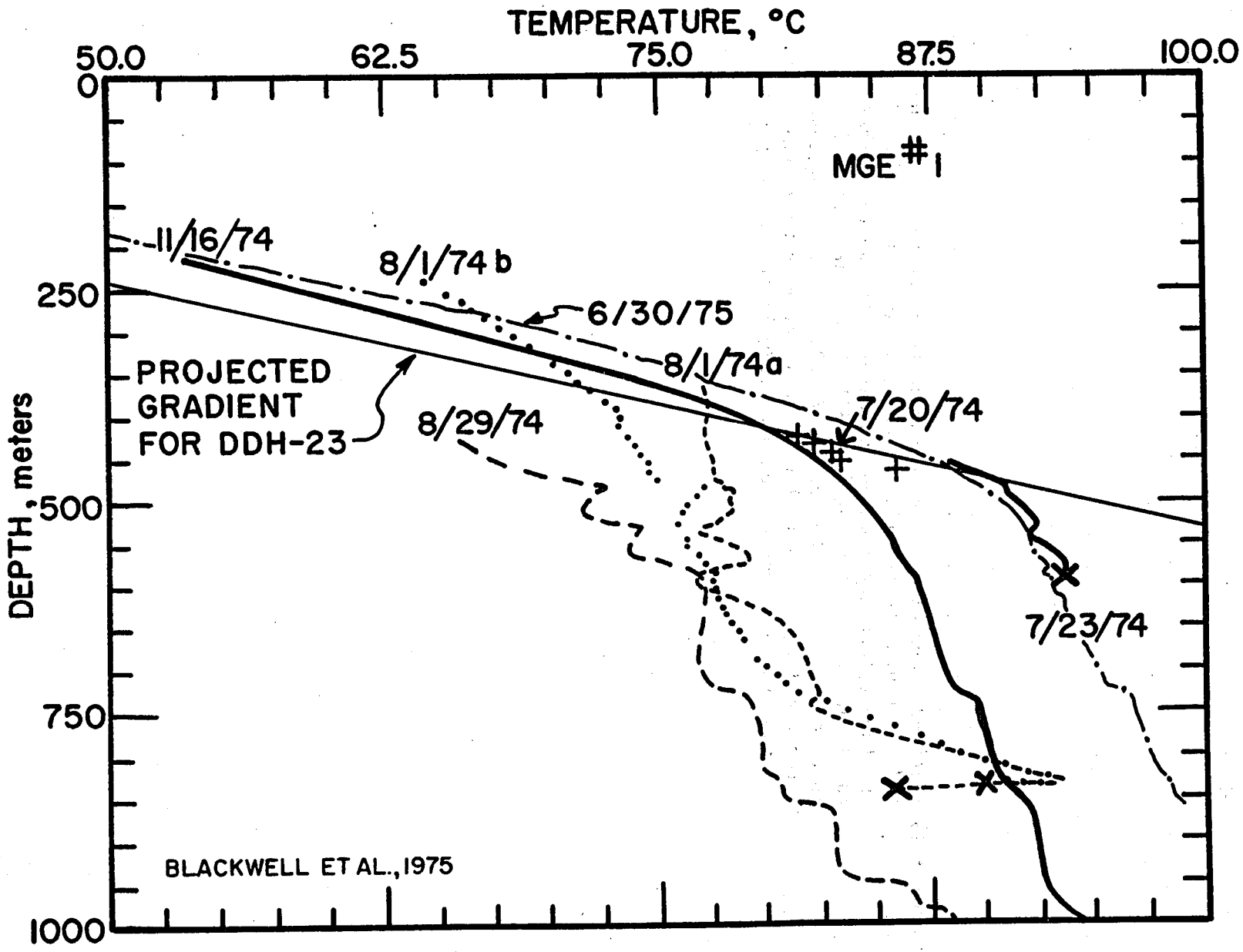
TEMPERATURE, °C
50.0
62.5
75.0
87.5
100.0
0
250
500
750
1000
DEPTH, meters
MGE #1
11/16/74
8/1/74 b
6/30/75
8/1/74a
7/20/74
PROJECTED
GRADIENT
FOR DDH-23
8/29/74
7/23/74
BLACKWELL ET AL., 1975

FIGURE E.15

the end of the logging period. The results of the last measurement (12 hr after circulation stopped) are shown in Figure E.15 (the 7/23/74 curve). It is clear that in this depth interval there is a distinct departure from the projected geothermal gradient from the shallow holes, apparently characteristic of the hole down to a depth of approximately 475 m. The maximum observed temperature was 93.8°C at the bottom hole with a maximum temperature of about 90°C along the extrapolated temperature-depth curve at a depth of 475 m. Above the contact of the extrapolated equilibrium curve and the curve measured on 7/23/74, the temperatures shown are not equilibrium values. This temperature curve shows irregularities which may be correlated with some of the fracture zones. It cannot be determined definitely from the temperature data whether the fluid column was static or was moving within the bore hole.

Drilling proceeded with a mixture of air and water as described earlier. Another opportunity for temperature logging occurred on 8/1/74 at 848 m. These results are also shown in Figure E.15. Two curves are plotted. The curve marked 8/1/74a was measured first and the curve marked 8/1/74b was measured about 2 hr later. The temperature curve at this point has the typical sigmoidal shape due to the effects of drilling with a fluid at lower temperature than in situ temperatures. There is a sharp reversal of temperature in the bottom of the hole, apparently due to a thief zone at that point. The problem with this simple interpretation of the temperature-depth curve is that the temperatures below 400 m were actually decreasing with time rather than increasing toward the previously measured values at those depths. This strange behavior can be explained either by an unusual history of drilling fluid temperature, not observed, or by colder water flowing slowly down the bore hole gradually cooling off the hole before exiting somewhere between 700 and 800 m. The maximum temperature observed was 93.8°C at 833.5 m.

The final logging obtained with the SMU temperature equipment used in the shallow part of the hole was on 8/10/74. The hole was at 1155 m, however, only 850 m of cable was available. The observed temperatures are almost isothermal with a maximum temperature of 89.6°C at 848.5 m. Maximum reading mercury thermometers were run at a depth of 1025 m and 1150 m. These recorded maximum temperatures ranging from approximately 96°C to 102.5°C, thus showing slightly higher temperatures than observed at shallower depths in the well, but far below the projected curve based on the shallow hole data. The most extensive series of fracture zones (except possibly for the bottom zone) in the well was encountered between 800 and 1100 m and strong flow of water into the bore hole was observed during drilling.

It was clear at this point that a hydrothermal convection cell had penetrated; however, its significance, depth of influence, etc., were unknown. The geochemical analyses (section on Water Chemistry) indicated higher temperatures than those observed in the well, but it was possible that the drill hole temperatures were modified by communication of fracture zones in the bore hole. The interpretation of the audiomagnetotelluric data (see Magnetotelluric Survey Section and Peeples, 1975), indicated a decrease

in resistivity by an order of magnitude at approximately 2 km. Such a decrease implies a large change in temperature or porosity of the reservoir. Thus the decision was made to continue drilling to at least 2 km since this depth was within the target depth planned for the original hole. Drilling to such a depth would test the vertical extent of the hydrothermal convection cell, the temperatures in that cell, and the implications of the resistivity change at about 2 km.

From this time drilling proceeded for approximately another 2 weeks until a total depth of 2070 m was reached. At this point the most extensive fracture zone yet encountered caused caving and hole accessibility problems. These problems required suspension of drilling at this depth. At some depths between 1 and 2 km drill hole temperatures as high as 115.5°C were measured with mercury maximum thermometers at the bottom hole; however, the most frequent bottom hole temperature measured was 90 to 95°C. It appears on reconstructing the conditions of these measurements that the highest temperatures (above 100°C) occurred at random and were apparently only obtained when the maximum thermometers were run in pressure containers which were not sealed with teflon tape. There have been no measured temperatures of similar magnitude since completion of the well. Therefore, it seems possible that these high temperature readings were the result of pressure effects on the thermometers rather than actual bottom hole temperatures.

Subsequent to completion of the well a series of Schlumberger temperature logs were made, successfully this time, to a total depth. Several of these logs are shown in Figure E.16 and the detailed results of the first and last logs to 1000 m are shown in Figure E.15. In general the upper parts of the hole show a more or less consistent recovery with time as would be expected, while the loggings between 450 to 1100 m show a rather complex temperature-time behavior. Below 1100 m temperatures are very nearly isothermal although there are some small but significant low temperature zones. Continued modification of temperatures in the upper part of the bore hole has occurred, however, as the temperatures observed at the logging of 11/16/74 still differ from the estimated in situ temperature (based primarily on the logging of 7/23/74) by 5°C or more, although almost complete recovery of the upper hole temperatures had occurred by the last SMU logging on 6/30/75.

The features of the temperature-depth curves shown in Figures E.15 and E.16 are a high, linear segment of gradient to about 400 m, a stairstep temperature-depth curve between 400 and 1000 m, and a slightly negative gradient with even more negative local zones below 1000 m. The recovery from the drilling and/or natural circulation effects in the bore hole appeared (see below) to be complete as the 11/16/74 log barely differs from the log on 10/21/74, but significant further recovery was seen in the last log on 6/30/75. In general three types of temperature behavior are associated with the fracture zones encountered during the drilling. The fracture zone may show a positive temperature spike, a negative spike, and a positive step. The positive and negative temperature spikes probably represent zones of potential source and thief fluid zones, respectively. The temperature step

Figure E.16 Temperature and flow logs in MGE #1. The logs of DDH-23, and of MGE #1 on 7/23/74 and 6/30/75 were made with SMU equipment while the logs of 8/29/74, 9/21/74, 10/21/74, and 11/16/74 were measured by Schlumberger.

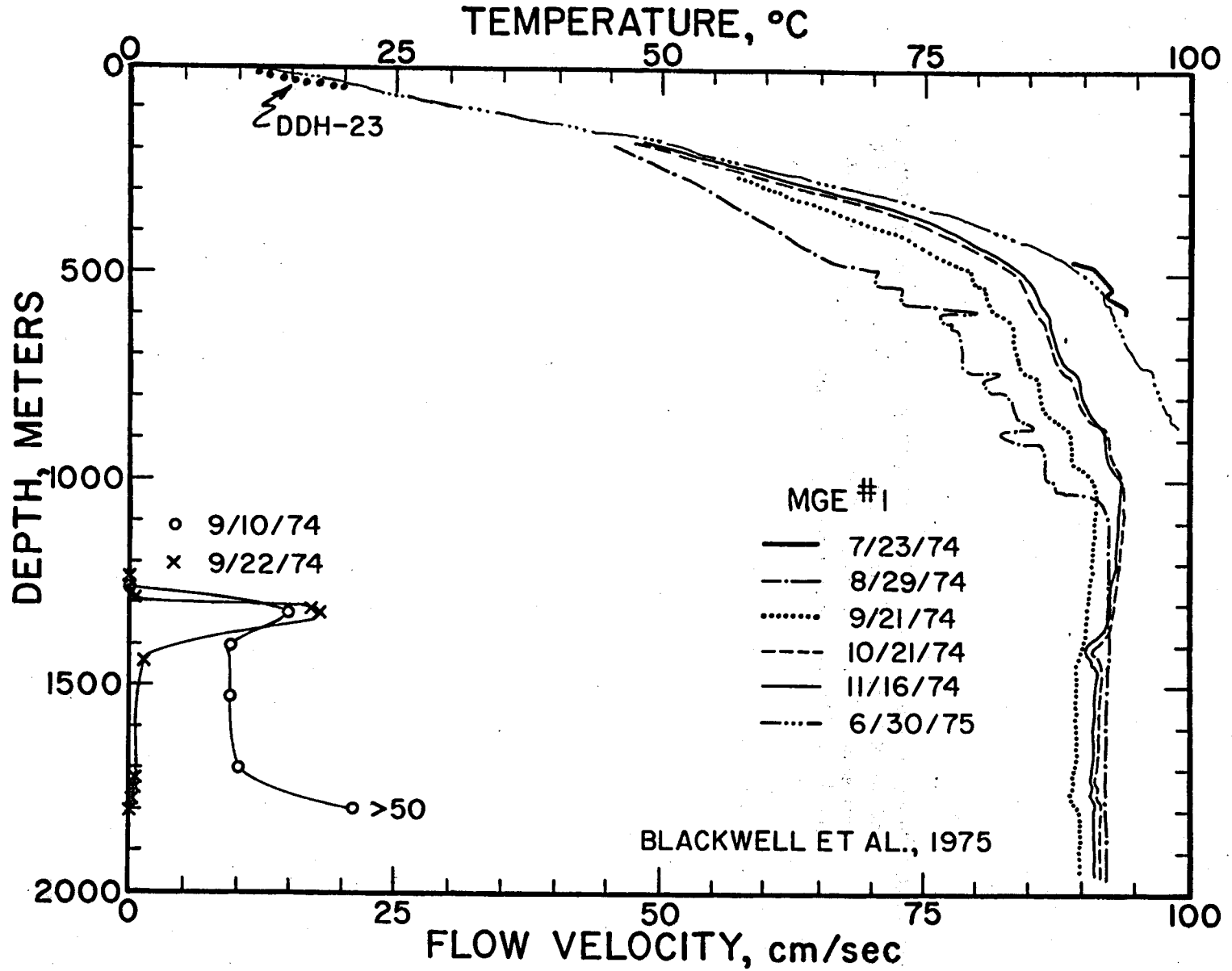
TEMPERATURE, °C
0
25
50
75
100
DDH-23
DEPTH, METERS
500
1000
1500
2000
9/10/74
9/22/74
>50
MGE #1
7/23/74
8/29/74
9/21/74
10/21/74
11/16/74
6/30/75
BLACKWELL ET AL., 1975
0
25
50
75
100
FLOW VELOCITY, cm/sec

FIGURE E.16

zones represent either thief zones, below which flow decreases and the hole temperatures approach in situ temperatures more closely, or source zones of warmer fluid which increase the temperature of fluid moving down the bore hole. The zones of potential water influx heat up more quickly as the hot water in the fracture zone rapidly displaces the cooler drilling fluid and thus positive temperature spikes are observed (see temperature log on 8/29/74). The negative spikes during drilling indicate thief zones while the negative spike zones on the 11/16/74 log probably represent fracture zones with access to colder fluid which is being forced along them since disturbance of the hydraulic regime by drilling.

Thus the temperature logs indicate the general nature of flow as seen during the drilling of the bore hole; the shallow fracture zones have, in general, a higher piezometric level than the deeper zones and are commonly source zones for fluid while the deeper zones act as fluid sinks. On 11/16/74 there was still a 5°C discrepancy between the in situ temperatures and the actually measured temperatures in the 400 to 600 m depth range but this was almost fully recovered by 6/30/75. This discrepancy suggests that fluid was still moving behind the casing from a source zone between 400 to 450 m. Flow logs (see below) suggest that the fluid flow is very small or absent below the casing, at 1300 m, however.

As part of the completion procedure casing was set at 1300 m and a cement job was attempted. This cement job was not completely successful, however, as can be seen from the flow velocity logs obtained after cementing, the results of which are shown in synoptic form in Figure E.16. Previous to setting the casing the observed flow velocity using an open hole flow meter in the well increased from 50 cm/sec downward above 1 km to over 400 cm/sec downward below 1300 m. Subsequent to cementing of the casing various kinds of flow logs were obtained. These show a much reduced but still high velocity of flow immediately below the casing, the first measurement on 9/10/74 in general showing increasing flow velocity with depth. The second logging on 9/22/74 shows a high velocity immediately below the casing with a rapid decrease to a velocity of approximately 3 cm/sec and finally a decrease to immeasurable velocity below 1770 m. A final velocity log obtained on 10/21/74 showed that flow had stopped (to the level of detection) in the bottom part of the hole. As mentioned above the temperature data imply that flow behind the casing still existed between 400 and 1000 m.

Water Chemistry

No matter which of the hypotheses for the origin of the geothermal area was valid, it was anticipated that geochemical studies of any fluids encountered during the drilling would be very important. Therefore preparations were made during the spring of 1974 to collect water samples from the drill hole and to obtain water chemistry data both on site and by analysis at SMU as quickly as possible so that the data would be available for drilling decisions. In geothermal areas characterized by circulation of hot water,

some of the most important information about the system comes from study of the geochemistry of the fluids involved (White, 1970; White et al., 1971; Sigvaldson, 1973; and others). Thus a number of different studies of water chemistry were carried out on the samples. Data which can be most rapidly obtained and which furnish important information on the temperatures of the system are the concentrations of sodium, potassium, calcium and silica in the geothermal fluids.

When the first water flow to seriously affect the air drilling was encountered in fracture systems while drilling at 551 m, samples were immediately collected from the flow line. A water sampler was flown in (borrowed from Dr. A. H. Truesdell at the U.S. Geological Survey, Menlo Park) and subsequent samples were obtained in the well using the water sampler. Finally, after completion of drilling, several water samples were obtained during drill stem tests.

The samples were collected in polyethylene bottles. During the first few weeks of collection the samples were shipped directly to SMU. Immediately upon arrival (24 to 48 hr after collection), the water samples were pressure filtered through 0.45 micron membrane filters. These samples were collected in pairs which were treated differently; one sample was prepared for cation analysis by addition of a few drops of concentrated HCl. The second sample was untreated and used for HCO_3 (at Marysville) and SiO_2 determinations. During the latter part of the project, samples were filtered immediately after collection through Whatman #42 filter paper. Upon arrival at SMU (after filtering, if done at SMU) a 10 ml aliquot of sample was added to a 10 ml of 1 N NaOH solution, and the resulting solution used for SiO_2 analysis. Cation analyses were performed on the acid treated samples as soon as was convenient.

Cation analyses were performed by atomic absorption spectroscopy. Bicarbonate was determined on a few samples (at Marysville) shortly after collection by tritation of a 10 ml aliquot of sample with 0.001 N HCl. In addition pH's were measured on some samples shortly after collection. Silica was determined by the method of Mullin and Riley (1955), with appropriate dilution of the samples. The major analytical concern was the possibility of polymerization of SiO_2 during the time interval between collection of samples at Marysville and analysis at SMU. As a means of checking this possibility, the earlier samples were subjected to the following procedures. Both the acid treated and untreated samples were analyzed for SiO_2. In addition a 10 ml aliquot of each sample was added to a 10 ml of 2 N NaOH and allowed to stand overnight before SiO_2 analysis. As a final check, additional aliquots of one sample were treated with NaOH and boiled for 1 hr. These results were compared for the same samples. Only one sample (579 m) showed greater than 10 percent variation in SiO_2 between any of these procedures. Most other samples agreed within 2 to 3 percent. Thus, probably because of the relatively low concentrations of SiO_2 present, polymerization did not appear to be a problem. The later samples obtained during the series of drill stem tests were subjected to the overnight NaOH treatment, and replicate analyses were not run.

The results of all the partial chemical analyses are shown in Table E.6. For the samples collected during drill stem tests the depths shown are the positions of the packers and the depth below the derrick floor from which the samples were collected from the drill pipe. Zones for testing were determined based on site log analyses. It would have been desirable to have obtained additional tests, but time and money ran out. None of the zones flowed water at the surface and the static head for each zone was at a depth of about 180 m. Thus it is not known for sure whether the packers leaked and only the fluid in the bore hole was obtained, or the packers held and true samples of formation fluid were obtained.

As can be seen from Table E.6 the cation concentrations show little variation from sample to sample. Temperature estimates were calculated for the water based on the Na-Ca-K geothermometer of Fournier and Truesdell (1973). The predicted temperatures are remarkably uniform and range only from 165°C to 180°C. The uniformity of cation concentraiton suggests that major contamination by drilling fluids is not a problem.

If the gradient from the most recent temperature log (6/30/75) can be extrapolated below the deepest measurement point in the log (855 meters), it is possible that temperatures of the order of 110°C may be reached in the bottom of the hole. These temperatures are consistent with the estimated SiO_2 temperatures shown in Table E.6.

However, most of the samples were collected during or shortly after drilling; the possibility of contamination by drilling fluids is a definite possibility. In this respect a brief digression to discuss the manner of drilling of the well is in order. Below the 403.6 m casing depth the hole was open to the depth of drilling. After encountering the fracture zones, it was found that in general the fluid in the fracture zones would not support a column of fluid equal to the depth of the drill hole. Thus if the drilling medium was water and the hole was filled, the water would be lost in the formation and makeup fluid required. On the other hand it was found that if drilling was attempted with air only, the fracture zones would flow and the hole would produce large quantities of hot water, which represented a disposal problem. Therefore during drilling from approximately 610 m to bottom hole, a system of drilling was used in which the water column in the bore hole was lightened by the addition of air to the fluid column and in such a way the weight of the total column was adjusted as closely as possible to the average pressure of the fracture zones so that no fluid was lost or gained. This balance was approximate, however, and from 610 m to total depth the hole alternatively made and took water. The drilling fluid consisted of water and air with small amounts of a soapy material (ADOFOAM) added, as well as, on occasions, small amounts of antirust agents to prevent oxidation of the drill rods. Subsequent to completion of the well, flow meter tests indicated large flow velocities down the bore hole. Therefore it is likely that there was extensive flushing action from the fracture zones affected by drilling. Thus the drill stem tests should represent a somewhat different regime than that sampled during drilling.

Table E.6 Chemical analyses of water samples from Marysville Geothermal Test #1. The drill stem tests were conducted after completion of drilling. The concentrations are in ppm.

Sample Collected from Drill Site Water Well

Depth (m)	Date Collected	pH	HCO_3^-	SiO_2	Na	K	Ca	Est. Temperature T_{SiO_2}	Est. Temperature $T_{Na-K-Ca}$
100	6/10/74			20	8.5	2.4	53	40°C	174°C

Samples Collected During Drilling

Depth (m)	Date Collected	pH_{25}	HCO_3^-	SiO_2	Na	K	Ca	Est. Temperature T_{SiO_2}	Est. Temperature $T_{Na-K-Ca}$
551.1	7/23/74	8.4-9.2	395	90	225	13.5	9.8	125°C	165°C
551.1	8/21/74			79	217	19.6	18.5	120°C	180°C
579.1	8/12/74	9.08	170	162	237	19.9	8.3	155°C	185°C
585.2	8/21/74			97	221	19.8	15.6	130°C	180°C
1150.6	8/12/74	8.38	180	98	227	17.1	7.6	130°C	180°C
1606.3	8/21/74			84	217	19.4	17.7	120°C	180°C

Samples Collected During Drill Stem Tests*

Sample No.	Depth coll.(m)							
	Test A - Packers at 1996 - 2070 m							
51	183	8.36	59	235	17.5	19.3	100°C	172°
52	640	8.29	67	219	15.1	16.8	110°C	167°
53	1219	8.10	77	209	15.3	15.4	120°C	169°
54*	tool water sampler		27	221	12.1	12.8	50°C	159°
	Test B - Packers at 1500 - 1527 m							
55	191	8.07	74	222	15.7	13.5	115°C	171°
56	tool water sampler	7.90	41	224	14.6	12.1	80°C	167°
	Test C - Packers at 1721 - 1771 m							
57	192	8.23	69	235	17.5	9.8	110°C	175°
58	1579	7.36	74	233	15.8	12.0	115°C	169°
59	tool water sampler	7.0-7.8	34	244	15.9	17.6	60°C	165°
	Test D - Packers at 1020 - 1050 m							
510	549	7.4-7.8	86	219	14.6	12.7	125°C	170°
511	856	7.5-8.0	93	220	14.1	11.6	125°C	167°
512	tool water sampler	7.5-8.5	81	220	14.2	9.3	120°C	169°

* results listed are from Table E.7.

Whether or not separate horizons were actually sampled or whether the packers failed and the drill stem was filled up with the fluid available in the bore hole is not presently certain. In any event the remarkable similarity of the chemical analyses argues against a number of very different fluid regimes penetrated by the bore hole, and it appears that the results might apply to a single fluid system, not too highly disturbed by the drilling effects. As a further check on the problem of contamination, a sample of the most common additive to drilling fluid (ADOFOAM) was analyzed for Na, K, Ca, and SiO_2. The ADOFOAM is high in Na, but contains no K, Ca, or SiO_2. Since Na is the most abundant species in the water, the Na-K-Ca temperature estimates would be least sensitive to contamination by Na, providing further indirect evidence for lack of serious contamination effects in the Na-K-Ca temperature estimates.

Silica temperatures were estimated on the basis of quartz solubility, from a graph based on the work of Fournier and Rowe (1966). The SiO_2 temperatures are consistently lower than the Na-K-Ca temperatures, and show more variability from sample to sample. The anomalously high value of SiO_2 at 579 m was obtained on a sample that was shipped unfiltered, and appeared to be particularly contaminated in that the sample contained approximately 5 percent solids by volume. Thus it may be that solution of SiO_2 from rock powder might be responsible for the observed high SiO_2 content.

Subsequent to the analyses described above, which were carried out within a few days after collection of each sample, three samples were selected for more complete chemical analysis. The analyses were performed by the water quality laboratory at New Mexico State University. The results of these three analyses are shown in Table E.7. Two of the samples (511 and 512) were chosen from the drill stem test that attempted to test the fracture zone in the vicinity of 1040 m. It is near this zone that the highest temperatures are presently observed in the drill hole. The third sample (54) was chosen because it represents the last sample taken during the deepest drill stem test and thus presumably the most representative of the formation fluid, although as noted above it is not known for sure whether the packers leaked during the tests or not. Furthermore this sample was not analyzed immediately following collection. The total dissolved solids content of the three samples average 787 ppm so the formation waters are fairly dilute. The silica and cation analyses agree within ±5 percent of those listed in Table E.6.

The water is basically a dilute sodium bicarbonate-sulfate water. The chlorine content is relatively low while HCO_3^- is 50 percent more abundant than SO_4^-. The most unusual feature of the water is the high content of fluorine. However, the ubiquitous occurrence of fluorite in the metamorphic aureole of the Empire Creek stock and in the rock itself (1974 report, Figure 2.9; Geological Studies Section, this report) is undoubtedly the explanation for the high values. The similar high fluorine contents for the samples suggests that the waters are representative of formation conditions since the fluorine is not a contaminant in the drilling additives and can be explained by in situ conditions. In turn the major and minor components are similar in all the samples and are similar to those shown in Table E.6, again suggesting a minimum of contamination of formation fluid. The only other comparable

Table E.7 Chemical analyses of three selected drill stem test water samples, MGE #1. Analyses performed by New Mexico State University, Agronomy Department, Water Quality Laboratory. Concentrations in ppm. Electrical conductivity in millimoles/liter.

Sample No.	Drill stem Test	Total Dissolved Solids	SiO_2	Na	K	Ca	Mg	Cations	$CO_3^=$	HCO_3^-	Cl^-	$SO_4^=$	Anions	Fe	F	B	Electrical Conductivity
54	A	787	27	221	12.1	12.8	1.0	274	0	250	43	180	513	<.12	19.6	.87	1.07
511	C	782	94	214	9.8	10.2	0.6	329	16.8	226	43	168	454	.49	19.0	.93	0.99
512	C	792	84	223	11.3	8.4	0.7	327	0	262	43	160	465	<.12	19.0	1.03	1.06

samples are numbers 56 and 59. All the samples with low silica contents, and thus low estimated silica temperatures are the deepest samples from each of the first three drill stem tests. Unless the packers leaked, these samples thus represent the deepest formation fluid sampled, and thus possibly the least contaminated. However, only the last sample of each test gives the low SiO_2 values, and the Na-K-Ca contents do not vary significantly from the other fluid samples. Therefore it appears that: 1) some systematic affect on SiO_2 content is associated with the tool water sampler fluid sample (except 512); 2) the fluid in the fracture zones below 1500 m has in situ temperatures lower than those actually measured; 3) the fluid fracture zones below 1500 m come from a lower temperature regime than that in the fracture zones above 1100 m although its in situ temperature is near 90°C. If the difference in SiO_2 contents is real, the results also suggest that the packers did not leak during the drill stem tests, and the measured pressures in the various fracture zones, which were almost the same, are valid estimates of the in situ pressures.

In addition to variations in the chemical constituents of the water, another type of evidence bearing on the underground flow regime is the distribution of oxygen isotopes. The variations of oxygen isotopes in fluids in geothermal systems have been described by Craig (1966), White et al. (1971), and Copeland and Kolesar (1975). Craig (1966) found that the hydrogen and oxygen isotopic composition of precipitation differs from one locality to another mainly due to differences in temperature. He obtained a linear correlation between δD and δO^{18} for meteoric water samples of the form $\delta D = 8\ \delta O^{18} + 10$. This curve predicts the variation of the oxygen and hydrogen isotopes due to precipitation. In general the geothermal systems will have a small effect on the hydrogen isotopic composition of the water flowing through the system because there is very little hydrogen in the rocks and thus the hydrogen isotopic composition of precipitation which enters the ground water system and flows through a geothermal system remains relatively unchanged. On the other hand the oxygen isotopic composition will change during transit through a geothermal system, if the temperature is sufficiently hot (on the order of 150°C or greater), because of the exchange of the oxygen in the water with the oxygen in the rock. The effect of this exchange is to increase the O^{18} content in the water and to decrease the O^{18} abundance of the rock. Thus O^{18} "shifts" are characteristic of geothermal areas. With this possibility in mind several samples from the Marysville area were analyzed for their isotopic content.

The samples were analyzed by Dr. Lynton Land at the University of Texas at Austin using a CO_2 exchange technique with an estimated precision of $\pm 0.05\ ^o/_{oo}$. The results are shown in Table E.8. In view of the constancy of hydrogen it was not determined, but (in this area) would be approximately $150\ ^o/_{oo}$. The results of these analyses are that the waters from the drill hole are essentially identical in isotopic composition to the waters from the surface. The only significant exception to this conclusion is the 579 m sample which has an isotopic shift of approximately 1/2 unit. It is interesting to note that this sample had the highest silica temperature, which was thus the one most similar to the calculated Na-K-Ca temperatures.

Table E.8 Oxygen isotope determinations on spring and MGE #1 waters. The spring identified as Dry Gulch is located in section T 12N, R6W Sec 31

Locality	Sample No.	δO^{18} ,°/oo
Dry Gulch		19.05
Water Well		19.23
MGE-1	579.1 m	18.58
"	53	19.04
"	59	18.93
"	512	19.02

The results of the water chemistry are shown in Figure E.17. The depth and estimated geochemical temperature for each sample from Table E.6 are shown on the figure as an interpretive generalization of the in situ temperatures. Temperatures based on the SiO_2 geothermometer are shown as circles and temperatures based on the Na-K-Ca geothermometer are plotted as boxes. The discrepancy between the two types of geothermometers is obvious as the general agreement between samples with the same geothermometer. The only exceptions to this general consistency are the high values of the SiO_2 temperature at 579 m and the low values of the SiO_2 temperatures in the deepest samples from drill stem tests A, B, and C. These temperatures seem to be well below the formation temperature based on the temperature logs, and their significance has been discussed above. A curve has been drawn connecting the various SiO_2 geochemical temperatures assuming that the samples collected during drilling and drill stem test D represent SiO_2 temperatures between 500 and 1200 m and the deepest samples from drill stem tests A, B, and C represent SiO_2 temperatures below 1500 m. The curve (1) may be a figment of the sampling in some manner or the other; (2) may represent in situ temperatures before drilling; (3) may indicate that the fluid in the upper and lower portions of the drill hole comes from different locations in the geothermal area. Hypothesis (2) seems unlikely although there is still evidence in the temperatures bore hole for communication of the fracture zones behind the casing. The third hypothesis seems the most likely, but the similarity of all the other chemical constituents is difficult to explain with this hypothesis. Further temperature and flow tests are necessary to determine with certainty the temperatures in the well in this zone.

In conclusion the results of the chemical analyses can be summarized as follows: in general the waters obtained from MGE #1 are extremely uniform in Na, Ca, K and SiO_2 content with depth and the fluid is a dilute

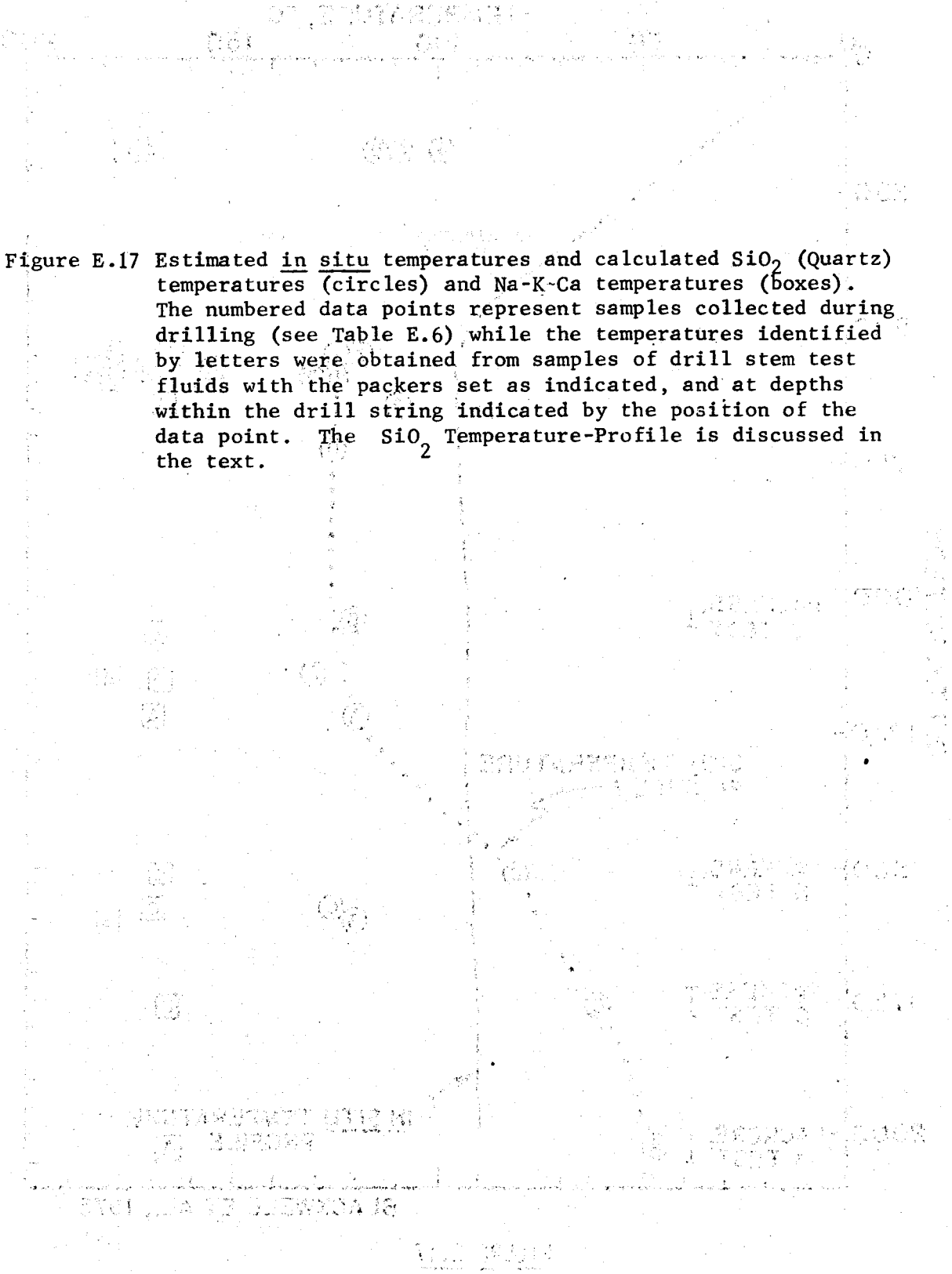

Figure E.17 Estimated in situ temperatures and calculated SiO_2 (Quartz) temperatures (circles) and Na-K-Ca temperatures (boxes). The numbered data points represent samples collected during drilling (see Table E.6) while the temperatures identified by letters were obtained from samples of drill stem test fluids with the packers set as indicated, and at depths within the drill string indicated by the position of the data point. The SiO_2 Temperature-Profile is discussed in the text.

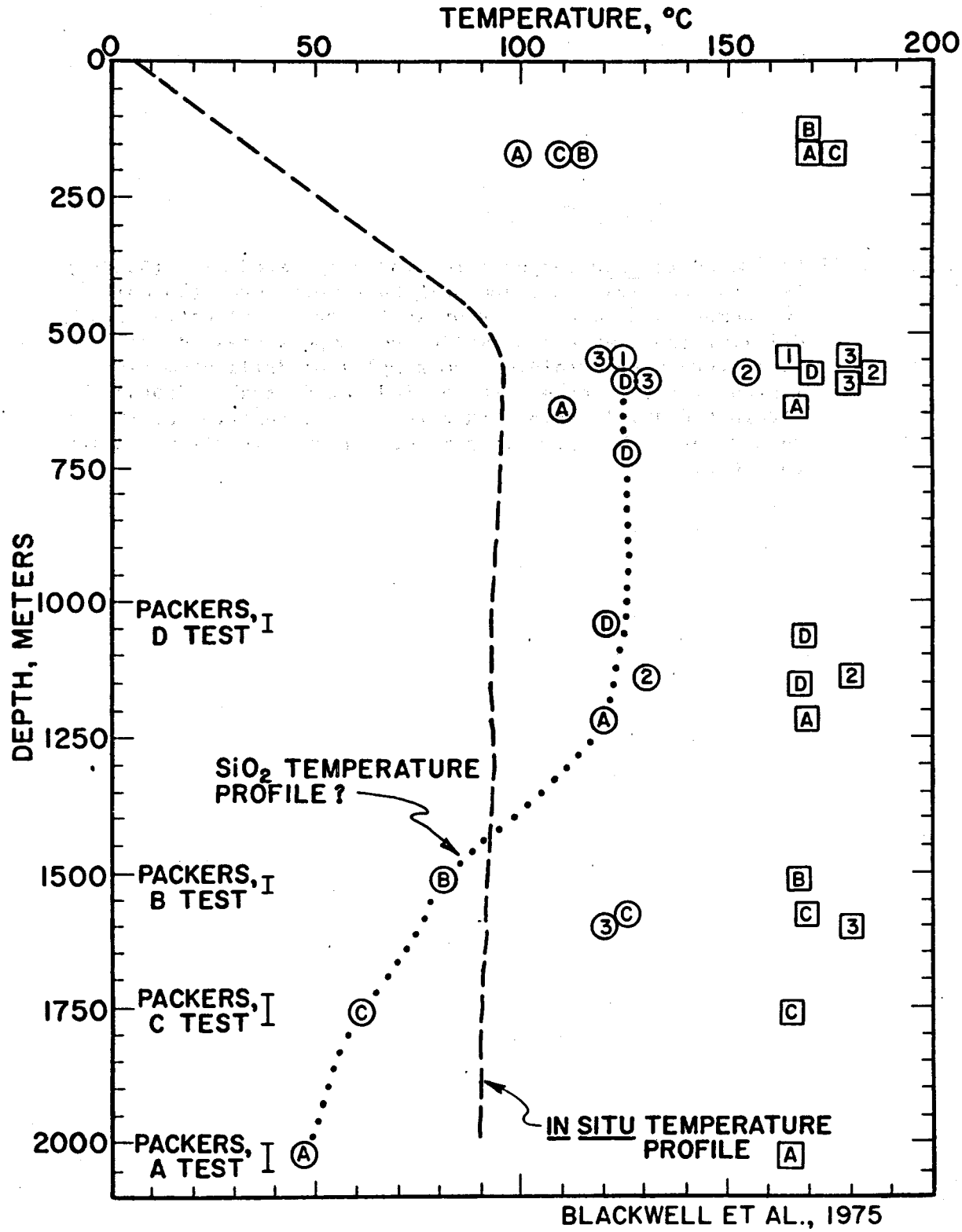
TEMPERATURE, °C
0
50
100
150
200
250
500
750
1000
1250
1500
1750
2000
DEPTH, METERS
PACKERS, D TEST
PACKERS, B TEST
PACKERS, C TEST
PACKERS, A TEST
SiO2 TEMPERATURE PROFILE?
IN SITU TEMPERATURE PROFILE
BLACKWELL ET AL., 1975

FIGURE E.17

sodium bicarbonate-sulfate water. Calculated temperatures based on the SiO_2 geothermometer are between 110 and 130°C except below 1500 m while those based on the Na-K-Ca geothermometer are between 165 and 180°C. The waters show little O^{18} shift except for the sample from 579 m which also had the highest SiO_2 temperature. On the basis of these data it thus appears that somewhere in the geothermal system temperature must be on the order of 120°C+, with some evidence of temperatures in excess of 150°C somewhere in the system that feeds the fracture zone(s) at or above 579 m. The SiO_2 temperatures may indicate a much greater temperature between 500 and 1200 m and a much greater drop in temperature with depth below 1500 m than actually observed by the temperature logs.

Well Log and Core Studies

Measurements of in hole physical and chemical properties by the logs in MGE #1 serve two important functions: they furnish ground truth for the inferred subsurface conditions based on the surface geophysical investigations, and they furnish important information on the location and description of important lithologic and physical parameters of the rock cut by the well bore. In this section both of these applications will be briefly discussed. An interval summary of the logging results is shown in Figure E.22 and discussed in the section on Summary of Deep Drilling Results. The studies on core samples recovered from the hole will be briefly described. Other similar data sets of the quantity and quality available for MGE #1 are virtually nonexistent in the public domain. Such data sets are rare enough for deep holes in basement rocks and do not exist for other holes in basement rocks in geothermal areas. Detailed studies of the results briefly described here will continue for years. Unfortunately the appropriate studies could not be carried out in a completely satisfactory way due to manpower limitations. Therefore the results described here represent just a beginning of the utilization of the collected data. The studies described here will be continued and expanded in the future.

The types of logs run in MGE #1 and their application have been discussed in the Schlumberger report included with this final report (Coates, 1974). Therefore this detailed information will not be repeated here. Briefly the types of logs run measured formation resistivity, P wave velocity, density, porosity, natural gamma activity, structural information (dip meter log) as well as temperature, hole size and fluid flow. Coates (1974) included as well a log of computed porosity from the sonic log and of computed porosity from the resistivity log. The application of all the data to the location of fracture zones was discussed.

A general summary of some of the logging results and of their implications is presented in a later section. The average values of some important physical parameters are shown in Table E.9. This table shows average P wave velocity, density and porosity for the drill hole. The interval 50 to 300 m includes the dacite dike and hornfelsed sedimentary rocks above the Empire Creek stock. This interval also includes a thick zone of fracturing associated with the contact of the stock. Thus the 50 to 250 m interval was

Table E.9 Some interval average properties from MGE #1 Logging results. Standard deviation of property is shown below average.

Depth Range meters	P wave Velocity km/sec	Density gm/cm^3	Porosity %	Lithology
50-250	5.6	2.67	19.0	Pred. Empire Shale
	0.1	0.02	7.0	
50-300	5.2	2.65	20.1	" " "
	0.7	0.04	7.0	
300-TD	5.3	2.51	3.4	Empire Creek granite porphyry
	0.1	0.03	1.8	
1800-2000	5.6	2.54	2.0	Empire Creek granite porphyry
	0.1	0.01	0.3	
304-1954*		2.57	1.0	Empire Creek granite porphyry
		0.02		

* 11 core samples

chosen to avoid the fracture zone. The effect of the fracture zone is most obvious on the average sonic velocity, which varies by 8 percent between the two interval averages. The average porosity is very high, about 20 percent, and must consist mostly of fracture porosity as the intrinsic porosity of the hornfelsed sedimentary rocks is essentially zero. The interval from 300 m to total depth includes the Empire Creek stock, while the interval 1800 to 2000 m was chosen as most representative of the least fractured portion of the stock, based on log analyses. The sonic velocities are similar to those in the rock above the stock, but there is a 0.08 to 0.16 gm/cm^3 density contrast across the contact. The density calculated in the 1800 to 2000 m interval and that measured in the lab on saturated core samples are very close, particularly when the difference in porosity is taken into account. It appears that the Empire Creek stock has an average of about 2.5 percent fracture porosity and about 1 percent intrinsic porosity (mostly in the form of miarolitic cavities).

Thus the high observed resistivities are not entirely due to lack of porosity as might be inferred without well information. The laboratory and log measurements of resistivity are discussed in more detail by Peeples (1975). In spite of the overall porosity figure of 3.4 percent, a well integrated (on the scale of 100's of meters) hydrothermal convection cell exists, implying high permeability along the fracture systems.

REGIONAL EXPLORATION STUDIES

Microearthquake Studies

Microearthquake studies carried out during 1973 and discussed in the 1974 report indicated a zone of microearthquake activity between the area of the Marysville geothermal anomaly and the town of Helena, approximately 30 km southeast of the geothermal anomaly. The results of the 1973 microearthquake study have been previously discussed (Friedline and Smith, 1974; Friedline et al., 1974, 1975). An additional 2 months of recordings were obtained during 1974 in order to evaluate more completely the seismicity of the general area. Observed microearthquake rates at arrays in the Marysville-Helena area are highly irregular, but average one to two events per day. The microearthquakes located during the 2 years of recordings are shown in Figure E.18. The approximate focal depths of located earthquakes are indicated in Figure E.18 as are their epicenters. More detail of the location procedure and data reduction techniques are given by Friedline and Smith (1974). The accuracies of the locations and epicentral determinations are discussed in more detail in Friedline et al. (1975), but are in general ±1 to 2 km for focal depth and epicenter for events located within an array. All of the events plotted in Figure E.18, with the exception of a few near the margin of the area, were within one array diameter or less from the array locations.

There is diffuse activity over most of the map area and the activity appears to decrease away from the map area shown. Very few events were located in a 50 km band around the map area shown in Figure E.18 even though they should have been detectable if they had occurred. Figure E.18 shows a cluster of events approximately 5 km northeast of Helena (Scratch Gravel Hills) and a second cluster of events approximately 5 km southeast of the geothermal anomaly near Three Mile Creek and Greenhorn Mountain. There are no recorded events in the immediate vicinity of the geothermal anomaly and there is a second seismic gap between the Scratch Gravel Hills and Three Mile Creek groups of microearthquake events. Composite fault plane solutions for the 1973 data are shown in Figure E.19. Data from the 1974 survey indicate at least two different composite fault plane solutions in the Scratch Gravel Hills area as did the 1973 data, and the 1973 data are taken to be representative. Very few epicenters were located in the Three Mile Creek area during 1974 and the composite fault plane solution from this area could not be verified. The composite fault plane solutions are consistent with northwest-southeast striking normal faults or east-west, north-south striking strike slip faults.

The possible interrelationships of the heat flow and seismic data are discussed in the Heat Flow section and in the section, Nature of the Geothermal Area.

Figure E.18 Microearthquake location and heat flow in the Marysville-Helena region. The line bordering the Marysville geothermal anomaly is the 3.0 $\mu cal/cm^2 sec$ contour line. The area of Figure E.1 is shown by the dashed box. Outcrops of large granitic intrusives are shown by the solid lines, except for the geothermal anomaly. The remainder of the symbols are identified on the figure.

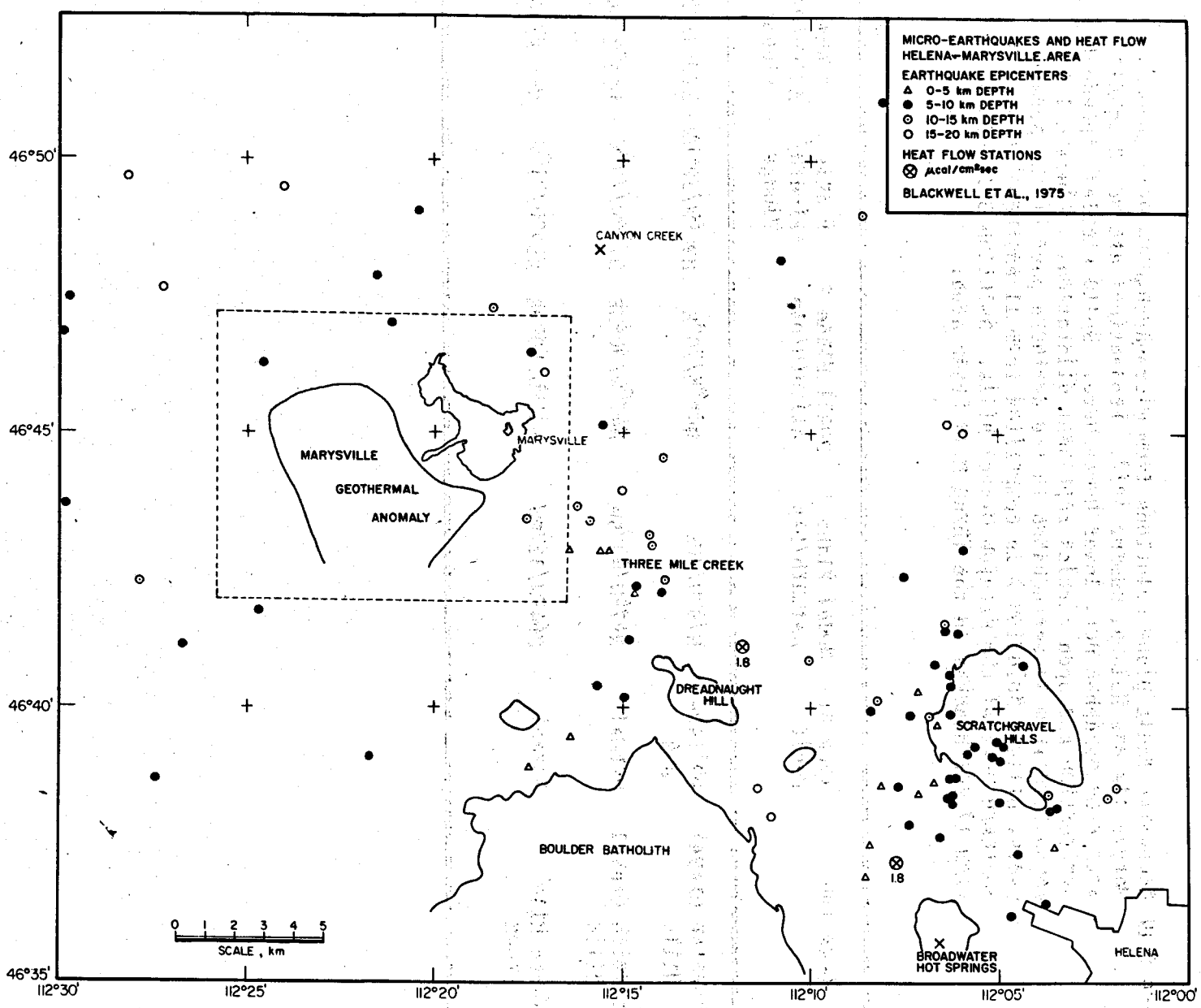
MICRO-EARTHQUAKES AND HEAT FLOW
HELENA-MARYSVILLE AREA
EARTHQUAKE EPICENTERS
0-5 km DEPTH
5-10 km DEPTH
10-15 km DEPTH
15-20 km DEPTH
HEAT FLOW STATIONS
μcal/cm²sec
BLACKWELL ET AL., 1975
CANYON CREEK
MARYSVILLE
MARYSVILLE GEOTHERMAL ANOMALY
THREE MILE CREEK
1.8
DREADNAUGHT HILL
SCRATCHGRAVEL HILLS
BOULDER BATHOLITH
1.8
BROADWATER HOT SPRINGS
HELENA
0 1 2 3 4 5
SCALE, km
46°50'
46°45'
46°40'
46°35'
112°30'
112°25'
112°20'
112°15'
112°10'
112°05'
112°00'

FIGURE E.18

Figure E.19 Composite fault plane solutions from microearthquake data between Marysville and Helena, Summer 1973. Projections are on an equal-area stereographic net, lower hemisphere. Solid circles represent compression and open circles represent dilatation. Solution 1 is composited from 11 earthquakes in the northern part of the Scratch Gravel Hills. Solution 2 is composited from 11 earthquakes in the southern part of the Scratch Gravel Hills. Solution 3 is composited from 12 earthquakes in the Three Mile Creek area.

CFPS	Location	Type of Fault	Nodal Plane 1 Azimuth/Dip	Nodal Plane 2 Azimuth/Dip	P axis Azimuth/ Plunge	T axis Azimuth/ Plunge
1	Scratch Gravel Hills	Oblique S-S	N76°W/70S	N06°E/70°E	N34°W/30°NW	S55°W/02°SW
2	Scratch Gravel Hills	Normal	N67°W/42°SW	N47°W/50°NE	N78°W/79°W	N35°E/04°NE
3	Three Mile Creek	Normal	N64°W/32°SW	N34°W/60°NE	N89°W/71°W	N45°E/14°NE

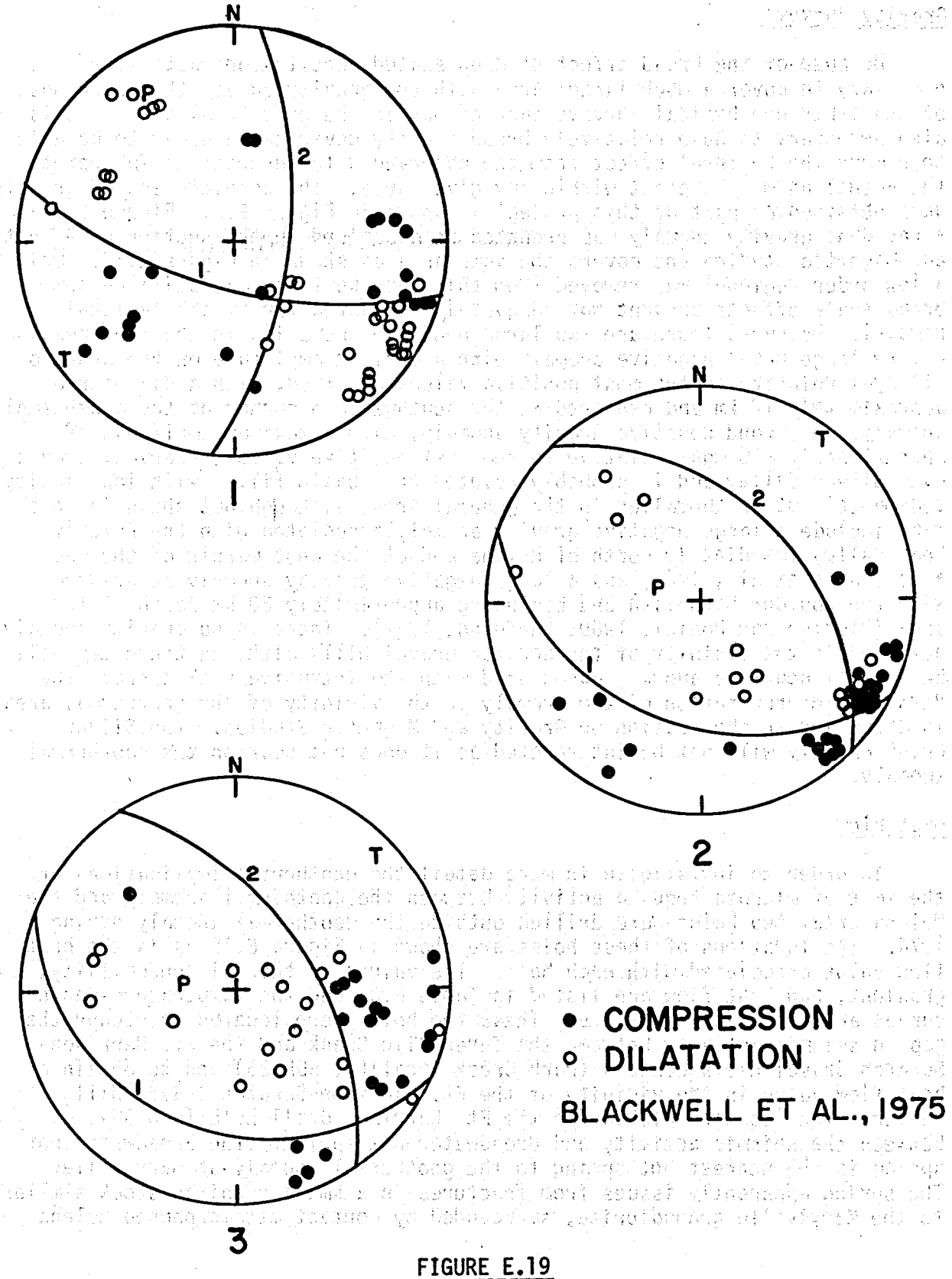
N
P
2
1
T
1
N
T
2
P
1
2
N
T
2
P
1
3
• COMPRESSION
○ DILATATION
BLACKWELL ET AL., 1975

FIGURE E.19

Gravity Surveys

Because of the broad effect of deep seated density contrasts it was necessary to cover a much larger area with the gravity survey than with most of the other geophysical surveys carried out in the geothermal area. It is also necessary to have relatively broad gravity coverage in order to be able to remove the regional effect from the observed data in order to interpret the actual anomaly present within any given area. The complete set of gravity data obtained as part of this project is shown in Figure E.7. Figure E.7 is a residual gravity anomaly map prepared as described in the section on Gravity and Magnetic Studies and covers the same area as shown in Figure E.18. Only a low order regional was removed from this data so there may still be some broad scale effects present not adequately accounted for by the regional removal. However, there are two large negative anomalies in the map area, a very large broad negative anomaly with a maximum amplitude on the order of -14 mgal relative to the most positive values observed, with a diameter of approximately 12 km and centered at the southwestern corner of the geothermal anomaly. A second negative gravity anomaly, with a maximum amplitude of approximately -16 mgal relative to the most positive values observed, occurs over Silver Valley and is probably related to a basin filled with low density sediments. Other anomalies in the general area, although not shown in this map, include a large negative gravity anomaly associated with the Prickly Pear Valley immediately north of Helena and at the west margin of the map area (Davis et al., 1963) and a large negative gravity anomaly associated with the Boulder batholith and beginning approximately 20 km south of the area (Biehler and Bonini, 1969; Burfeind, 1967). There is no gravity anomaly detected in the vicinity of the Scratch Gravel Hills although there may well be a small negative anomaly associated with the intrusive rock there. The detailed interpretation of the anomaly in the vicinity of the geothermal area is discussed in the section on Gravity and Magnetic Studies. The Silver Creek anomaly will not be interpreted as it does not bear on the geothermal anomaly.

Heat Flow

In order to investigate in more detail the geothermal implications of the zone of microearthquake activity between the geothermal anomaly and the Helena area, two holes were drilled outside the geothermal anomaly during 1974. The locations of these holes are shown in Figure E.18 as is the heat flow value associated with each hole. The values of thermal conductivity, gradient, and heat flow are listed in Table E.3, and the temperature-depth curves are shown in Figure E.9. These two holes were located to occupy the gap in seismic activity between the Three Mile Creek and the Ft. Harrison-Scratch Gravel Hills centers (Park Creek locality, RDH-36) and to obtain a heat flow value in the vicinity of the Ft. Harrison-Scratch Gravel Hills center. The location picked for the Ft. Harrison drill hole (RDH-35) was between the seismic activity and Broadwater hot spring. The Broadwater hot spring is the nearest hot spring to the geothermal anomaly at Marysville. The spring apparently issues from fractures in a small granitic stock similar to the Marysville granodiorite, surrounded by contact metamorphosed Helena

and Empire formations (Knopf, 1963). There is a north trending dome in the Empire shale extending from the Broadwater hot spring intrusive toward the Scratch Gravel Hills intrusive which occupies an area at the southeastern margin of the seismic activity. The location of both of these intrusives are shown in Figure E.18. Drill hole RDH-35 was located between these two areas of granite outcrop, near the zone of microearthquake activity, on an outcrop on the Empire shale in the dome.

Before drilling the heat flow holes a reconnaissance ground magnetic survey was carried out over the zone of microearthquake activity in order to locate possible buried intrusives similar to the Marysville stock. Such a survey indicated no large unexposed pluton in the area mapped by Knopf (1963).

The results of both drill holes were negative with respect to discovery of geothermal anomalies in spite of the structural resemblance to the Marysville geothermal area of the site of RDH-35.

The heat flow values were not corrected for topography because both sites were selected in areas of low relief within 1 to 2 km from the bore hole so that the topographic correction will be small. A maximum effect of -5 percent is estimated for the topographic correction at each site. The observed heat flow values, 1.8 $\mu cal/cm^2sec$ at Park Creek (RDH-36) and 1.8 $\mu cal/cm^2sec$ at Ft. Harrison (RDH-35), are typical of heat flow values in Belt Series rocks in west-central Montana (Blackwell and Robertson, 1973). On the basis of these data there appears to be no simple relationship, if any, between the geothermal anomaly and the microearthquake activity. The regional association of the two, however, is very interesting and worthy of additional study. The question of the exact correspondence between geothermal features and microearthquake activity is a general one, and this area seems to be an ideal test example of the association because of the geographic association and the large body of geophysical, geological and hydrological information already available for the area.

SUMMARY AND DISCUSSION

Summary of Exploration Results

During the geological and geophysical exploration of the Marysville geothermal anomaly all the standard exploration techniques were used, as well as several less commonly used techniques. Each individual geothermal prospect at the present time seems to require separate design of an exploration flow path because of the extremely variable conditions of the geothermal occurrences; the Marysville geothermal area is no exception to this rule. The geological techniques that were used included geologic mapping, various kinds of geochemical analyses, mapping of the metamorphic mineral assemblages, and analysis of the structural geology. Geophysical techniques included two different kinds of electrical resistivity techniques (roving dipole and magnetotelluric-audiomagnetotelluric), gravity, airborne and ground magnetics, drilling for heat flow determinations, microearthquake and seismic ground noise surveys, and airborne infrared sensing.

Almost every one of the geological and geophysical techniques has furnished important data relating to the setting and controls on the geothermal anomaly. Some of the techniques have furnished information more directly related to the geothermal anomaly than others, but almost all furnished important background information for the interpretations. The uniqueness of each particular exploration target is exemplified by the results from the Marysville geothermal anomaly. For example, analysis of metamorphic assemblages in rocks is not commonly included in flow charts for geothermal exploration; however, the metamorphic study has furnished critical information for interpreting the geophysical data.

The interrelationship and results of the various exploration techniques and their input into the exploration program as applied to the geothermal area will be summarized in this section. In the following section the results of the deep exploration drill hole (MGE #1) will be discussed, and in the section, Nature of the Geothermal Area, the results of the deep drilling and surface exploration will be combined into a preliminary interpretation of the nature of the geothermal area. In spite of the tremendous amount of data available there are still a number of important unknowns. These will be addressed in more detail in the last two sections of this chapter.

The results of the geological studies are shown in Figure E.20. The parameters illustrated on Figure E.20 include the outcrop of the Empire shale, the outcrop and subcrop extent of the Marysville granodiorite, the outcrop of the metamorphic zones, the outline of the heat flow anomaly, and the surface location of several mapped faults. It is apparent from this data that there is a high degree of correlation between the outcrop of the Empire shale, the metamorphic zones not associated with the Marysville stock and the geothermal anomaly. It also appears that the subcrop extent of the Marysville stock bears a very close relationship to the northeastern boundaries of the heat flow anomaly. As discussed in previous sections and in the 1974 report, the existence of isolated high grade diopside zone contact metamorphic rocks southwest of the Marysville stock implies the existence of a buried igneous body(s) of rather large size beneath these metamorphic zones. Based on the magnetic data discussed in the 1974 report, rocks similar in magnetic susceptibility to the Marysville stock cannot underly (and thus cause) these zones. It is known from exploration drilling that at least parts of both of these contact metamorphic aureoles are underlain by Cenozoic quartz porphyry stocks (Rostad, 1969; Blackwell and Baag, 1973; Ratcliff, 1973). The known subcrop of these quartz porphyries in each area (Bald Butte and Empire Creek) previous to these studies consisted of no more than a few hundred square meters, however.

The correlation between the metamorphic zones and the dome as outlined by the outcrop of the Empire shale is also obvious. It would appear that the dome in the Empire shale is caused by these underlying quartz porphyry bodies. The age of these intrusive rocks is 40 and 49 M.Y.B.P. for the Empire and Bald Butte stocks respectively. The extensive set of feldspar porphyry dikes southwest of the Marysville stock probably has equivalent ages. One of these dikes was dated at 48 M.Y. (Ratcliff, 1973). The

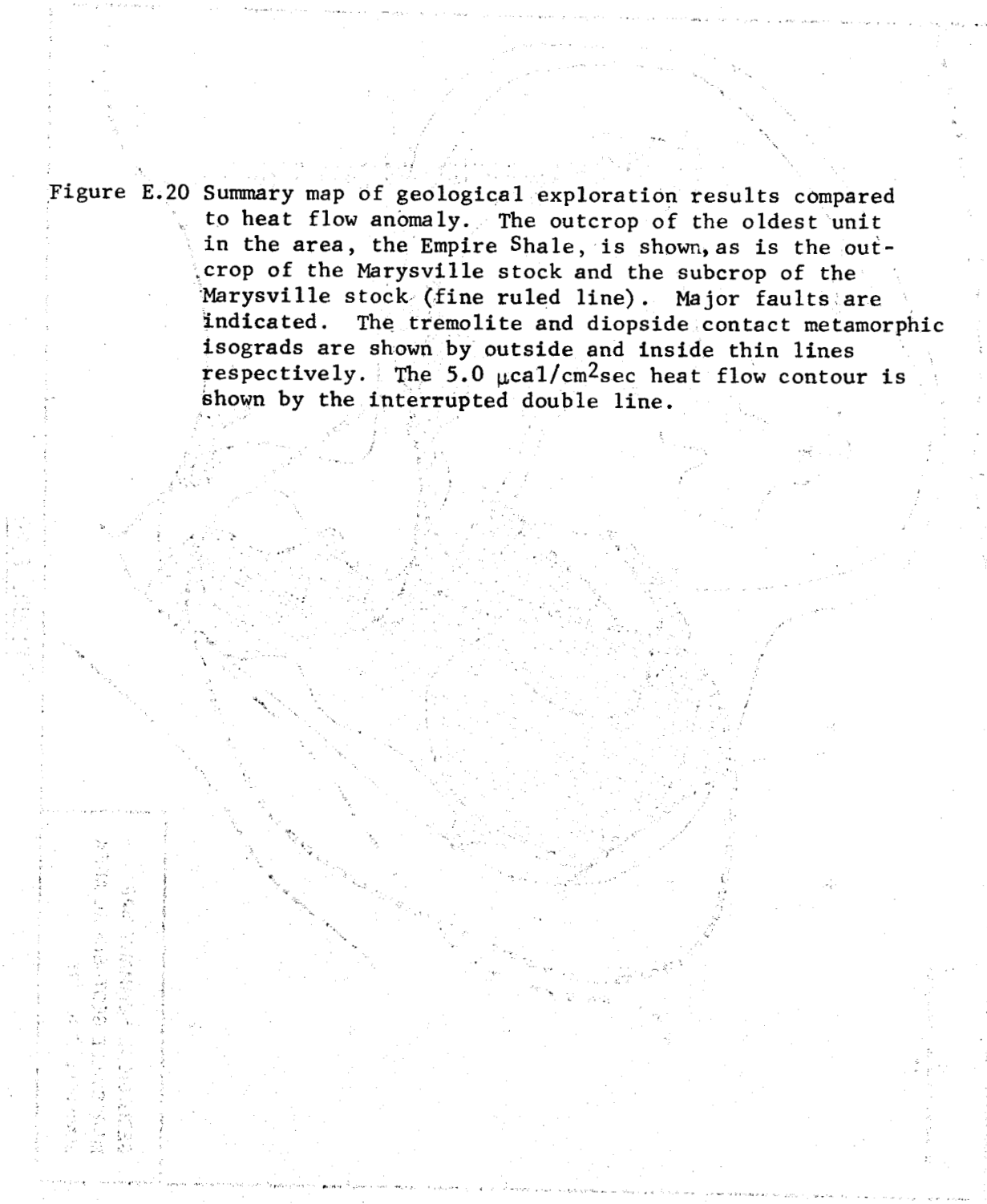

Figure E.20 Summary map of geological exploration results compared to heat flow anomaly. The outcrop of the oldest unit in the area, the Empire Shale, is shown, as is the outcrop of the Marysville stock and the subcrop of the Marysville stock (fine ruled line). Major faults are indicated. The tremolite and diopside contact metamorphic isograds are shown by outside and inside thin lines respectively. The 5.0 $\mu cal/cm^2 sec$ heat flow contour is shown by the interrupted double line.

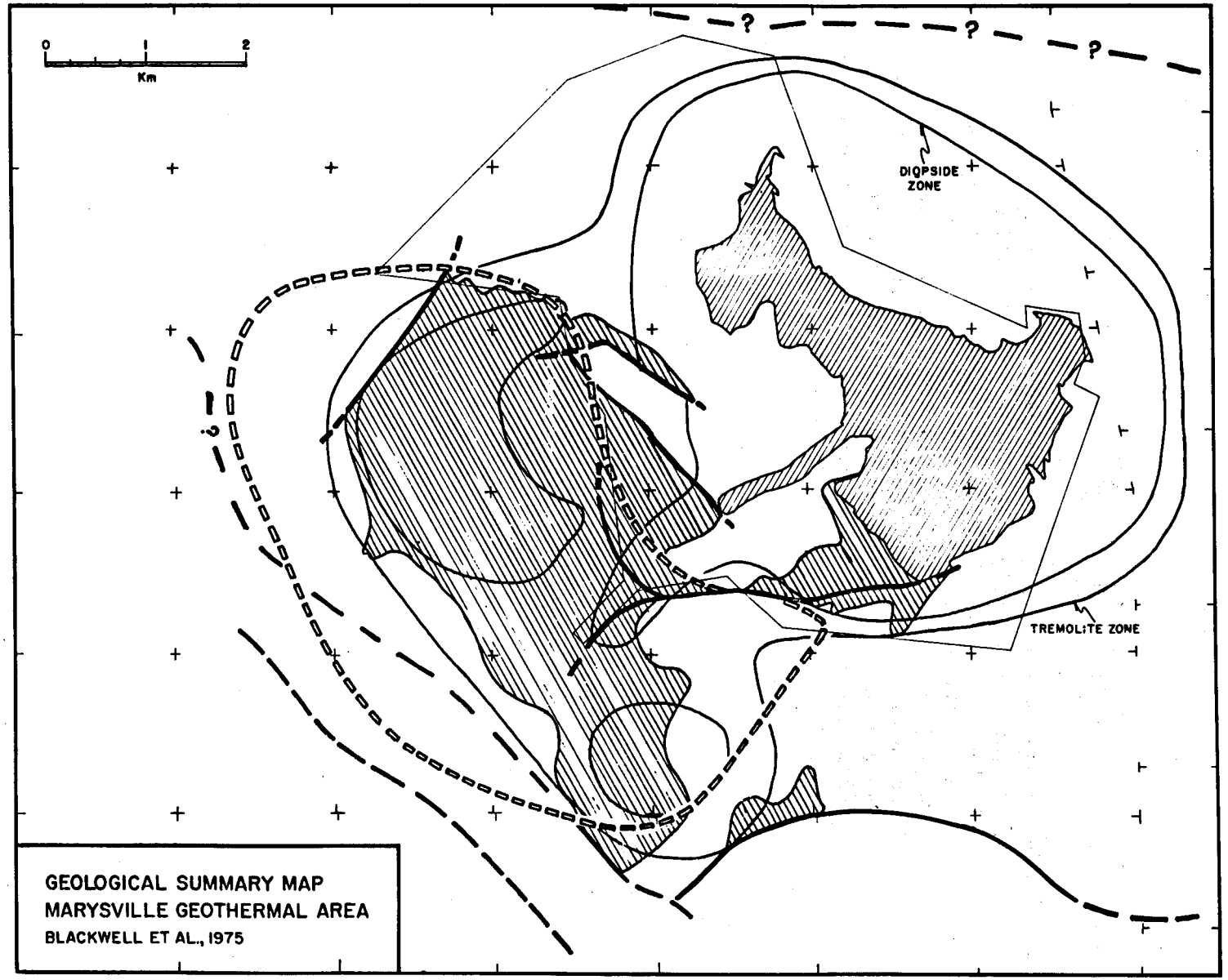
0
1
2
Km
DIOPSIDE ZONE
TREMOLITE ZONE
GEOLOGICAL SUMMARY MAP
MARYSVILLE GEOTHERMAL AREA
BLACKWELL ET AL., 1975

FIGURE E.20

relationship at depth between the Empire Creek and Bald Butte stocks is still unknown. Thus on the basis of the geological studies the source of the geothermal anomaly must be at least partially located in or below Cenozoic quartz porphyries. The quartz porphyry bodies themselves cannot be the source of the heat because the cooling time for a body with a size of many cubic kilometers is on the order of 1 to 2 M.Y.

For subsurface extrapolations of the geological data the geophysical techniques are important, and a synthesis of the geophysical information obtained during exploration studies is shown in Figure E.21. Shown in synoptic form are the results of the gravity, magnetic, heat flow, resistivity, and ground noise surveys. The data on which these figures are based are discussed in the 1974 report and in this report and reference should be made to the individual sections for detailed discussions of the data.

Results of the microearthquake survey are discussed in the section on Microearthquake Studies. The microearthquake zone is closest to the southeastern corner of the map area and two or three of the located earthquakes fall on the map area in that vicinity. The area of the geothermal anomaly itself appears to be aseismic, based on 5 months of recordings.

The interrelationships of the geophysical data are less obvious than those of the geological data and their interpretation is not so straight forward. The gravity data appear to correlate with the heat flow anomaly and with the geological data shown in Figure E.20 because part of a residual gravity low is associated with the heat flow anomaly. The negative gravity anomaly correlates well with the geothermal anomaly except that the gravity anomaly extends south off the map area, while the heat flow anomaly decreases rapidly in amplitude to the south. As usual, however, the gravity data are ambiguous because the gravity anomaly could arise from mass differences not associated with the Empire Creek stock or the geothermal anomaly. The detailed interpretation of the gravity data is discussed in a previous section.

Electrical resistivity is one of the most important exploration techniques in geothermal areas because resistivity is a strong function of some of the properties which are most likely to vary in a geothermal area, i.e., temperature, fluid salinity, and porosity. In general relatively low values of electrical resistivity are generally associated with geothermal areas; however, it is clear from the previous results (Jackson, 1972; Peeples, 1975), as shown in Figure E. 21, that the electrical resistivity values are very high in the geothermal area and that there is no consistent association of low resistivity with the high geothermal gradients. The roving dipole technique on which the original resistivity map was based (1974 Report; Jackson, 1972) has a very shallow penetration, perhaps even as shallow as a few tens of meters, because of the extremely high resistivity of the surface rocks. In order to obtain deeper penetration the audiomagnetotelluric survey was carried out. However, interpretation of the results of that survey show no significant variation in resistivity until depths of many hundreds of meters (2 to 6 km) are reached. Furthermore resistivity values were extremely high

Figure E.21 Summary map of geophysical exploration results. The ground noise lows and highs are indicated as are the -6 and -10 mgal residual gravity contours. The units of ground noise shown are the integral of the power density between 1 and 2 Hz (see 1974 report). The gravity contours are based on the data shown in Figure E.7 except that the effect of the Marysville stock has been removed. One heat flow contour (5.0 $\mu cal/cm^2 sec$) is shown and the apparent resistivity contours at 20 Hz are also shown.

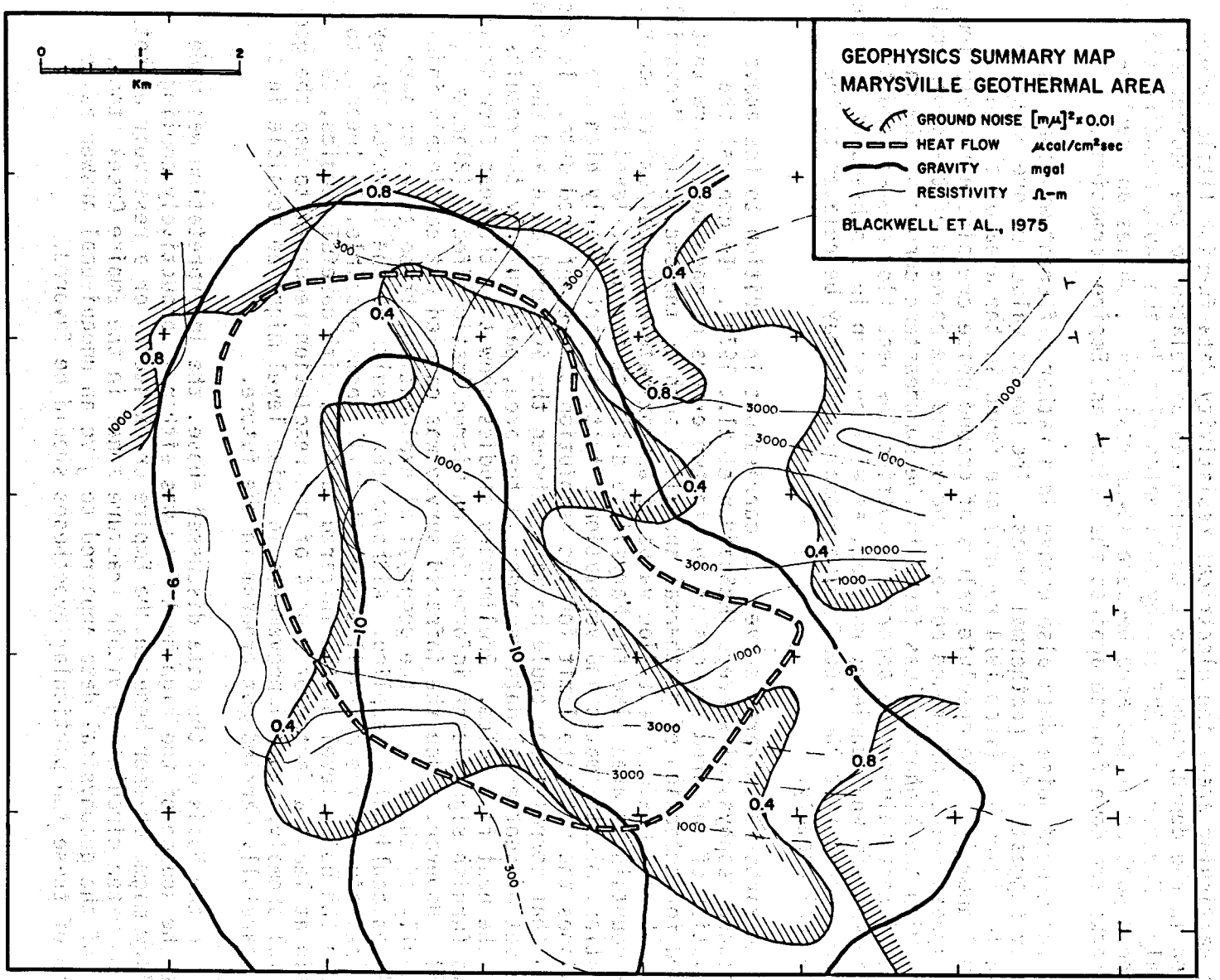
GEOPHYSICS SUMMARY MAP
MARYSVILLE GEOTHERMAL AREA
GROUND NOISE [mμ]² x 0.01
HEAT FLOW μcal/cm²sec
GRAVITY mgal
RESISTIVITY Ω-m
BLACKWELL ET AL., 1975
0
1
2
Km
0.8
0.4
300
1000
3000
10000
-9-
-10-

FIGURE E.21

at high frequencies and rather high at the longer frequencies (minimum resistivity values were on the order of 100 ohm-meters). In any event, in this particular area, the electrical resistivity data furnish little information in the depth range 0 to 2 km which can be related to the geothermal anomaly. However, the AMT survey delineates clearly the fault bounding the southern portion of the area because lower resistivity shales and carbonate rocks are down faulted against the Helena and Empire formations.

The ground noise data also behave in a rather different way than is usually suggested for geothermal areas. The lowest values of ground noise shown in Figure 5.2 (from 1974 report) are found in the area of the geothermal anomaly. The absolute values of ground noise are also extremely low. The highest values of ground noise occur around the borders of the geothermal area, with the highest values found in the southeastern corner of the map. These highest values were apparently outside the heat flow anomaly and their origin was somewhat unclear; however, as will be seen in a subsequent section it now appears that the ground noise anomaly there may be related to the geothermal anomaly.

An airborne infrared survey was carried out in addition to the above mentioned geophysical surveys (McSpadden et al., 1974). In general the resolution of infrared surveys is one to two orders of magnitude below that needed for detection of geothermal anomalies such as the one in the Marysville area, where a maximum heat flow value of approximately 20 $\mu cal/cm^2 sec$ occurs. In a mountainous area like the Marysville district the noise level from elevation, microclimatic and vegetation effects is particularly high and furnishes the ultimate limit for the resolution of the infrared data. It was hoped that correlations could be made between the infrared data and the extensive set of geothermal data recorded in the area, particularly the results from the heat flow holes. Preliminary studies show that the heat flow drill holes furnish significant information on microclimatic effects (Blackwell, 1973). However, since the infrared survey was carried out completely independently of the rest of the geophysical exploration, these types of data analyses could not be applied. Although the results of the infrared survey were negative in the Marysville area it still seems possible, in theory, to reduce the noise level of the infrared surveys, with careful studies, to within at least a factor of 2 or 4 of the resolution required to map the geothermal anomaly. Such improvements in noise level might be possible in a more carefully carried out program in the future.

On the basis of the data discussed above, the interpretation was made that the source of the high heat flow was either a conductively cooling shallow magma chamber beneath the Empire Creek stock, or a reservoir of hot ground water circulating within fracture zones in the Empire Creek stock. None of the geophysical data appeared to give an unequivocal answer as to which of these two particular hypotheses should be favored.

Summary of Deep Drilling Results

The drilling history and the detailed results of the deep exploration drill hole (MGE #1) have been discussed earlier. The purpose of this section is to summarize these results and to present synthetical data dealing with the drill hole. The hole was drilled to a total depth of 2070 m. It penetrated the Empire Creek stock at a depth of 294 m and remained in the Empire Creek stock for the remainder of the drill hole. The maximum temperature measured in the drill hole during 1974 was 94°C at a depth of 500 m. At the temperature logging approximately 2 months after completion the maximum temperature was about 94°C at 1000 m. The temperatures decreased slightly with depth from that point to 91.3°C at 1950 m. A new temperature log in 1975 (6/30/75) indicated a temperature of 99°C at 855 m (the maximum depth that it was possible to log with the equipment available) and the temperatures were still increasing with depth at approximately 10 to 20°C/km. Significant flows of water were encountered during drilling with the average piezometric level in the bore hole of about 180 m below ground level. Thus the source of the geothermal anomaly is a hydrothermal convection cell circulating along the fracture zones in the Empire Creek stock, consistent with one of the two hypotheses of the 1974 report. The temperature of the water is somewhat lower than was anticipated, although based on the exploration data there was no firm evidence for the temperatures.

The results of the deep exploration drill hole are shown in Figure E.22 in a form of synoptic results from the logging program. This figure includes a bar graph of the *in situ* electrical resistivity, seismic P wave velocity, density, and gamma-ray activity based on simple 25 m averages of digitized well log data. In addition the temperature-depth curves from the 8/29/74 and 11/16/74 loggings are shown. For comparison with the logs the positions of fracture zones based on the drilling history are also shown.

The gamma-ray log is most sensitive to variations in lithology as reflected in K, U, and Th content and it most clearly shows the contact between the metamorphic rocks and the Empire Creek stock. There is some effect of hole rugosity on the gamma-ray log and most of the large deviations to values below 340 in the depth interval below 450 m are due to the combined effect of increased hole size and/or fracture zones rather than to variations in the properties of the granite porphyry. The distinct change in gamma activity at about 450 m corresponds to a joining of two different logs and is not a function of lithologic changes in the porphyry.

The density log is based on the gamma-gamma log. The main change in density occurs at the lithologic contact at 294 m between the Empire Creek stock and the metasedimentary rocks. Smaller variations are due to porosity variations related to fractures, the content of microlitic cavities and to variations in bore hole rugosity. The bore hole rugosity effect on the density log is probably responsible for the measured densities below 2.45 gm/cm^3.

The resistivity log is very sensitive to the fluid content and to the fracturing (porosity) if the fracture zones are at high angles to the bore

Figure E.22 Bar graphs of interval (25 m) average data density, relative gamma-ray intensity, travel time, and resistivity, from MGE #1. Also included are fracture zones (from drilling) and temperatures measured during the 8/31/74 and 11/16/74 loggings.

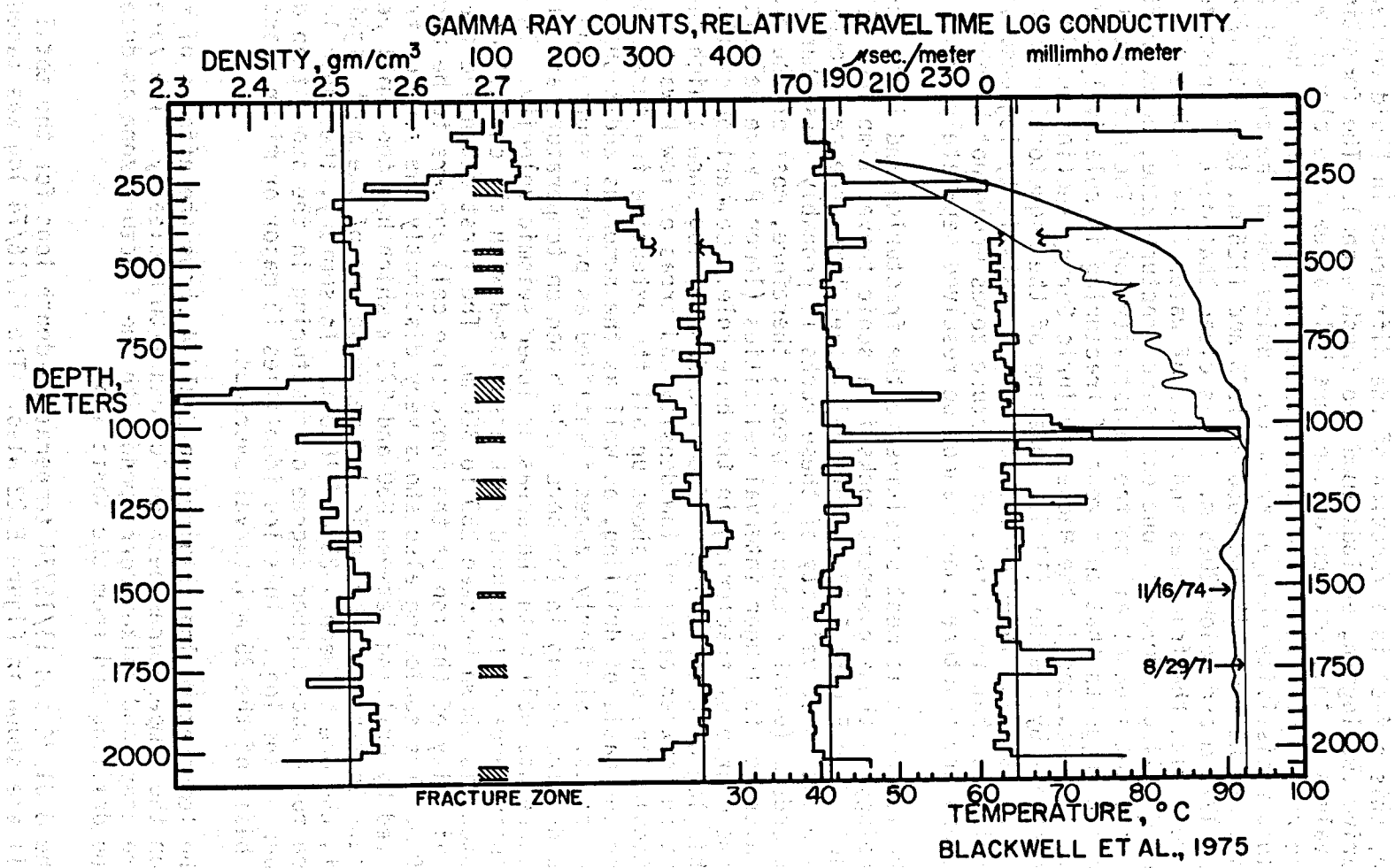
GAMMA RAY COUNTS, RELATIVE TRAVEL TIME LOG CONDUCTIVITY
DENSITY, gm/cm³
2.3 2.4 2.5 2.6 2.7
100 200 300 400
μsec./meter
170 190 210 230
millimho / meter
0 1
DEPTH, METERS
250 500 750 1000 1250 1500 1750 2000
11/16/74
8/29/71
FRACTURE ZONE
30 40 50 60 70 80 90 100
TEMPERATURE, °C
BLACKWELL ET AL., 1975

FIGURE E.22

hole. The resistivity values plotted are uniformly high to a depth of 450 m. However, this effect is a function of the difference in fluid content of the hole during two logging periods (mud and fresh water). The formation resistivity values in that section of the bore hole agree more closely with the fracture zones interpreted from the seismic log if variations due to bore hole fluid resistivity changes are made. Below 450 m the zones of high conductivity are between 975 and 1050 m, 1075 and 1125 m, 1200 and 1250 m, 1700 and 1775 m and below 2025 m. It is clear that most of these zones correlate well with the fractures and zones of water flow as determined on the basis of drilling. However, one extensive fracture zone, between 850 and 925 m, does not show at all on the resistivity log. The apparent lack of correlation suggests that this zone of fracturing is relatively flat (see below). As discussed in the Magnetotelluric Survey section and in the accompanying report by Peeples (1975), modeling of the magnetotelluric response due to a resistivity layering similar to the resistivity log observed in the well indicates that the effect of fracture zones would not be observed at the surface and the fracture zones cannot be resolved separately from each other.

The log which is most sensitive to the fracturing and least sensitive to lithology in these basement rocks is a sonic travel time log. The quantity plotted in Figure E.22 is interval travel time, the reciprocal of velocity. The intrinsic velocity of these rocks is probably less than 180 microseconds/m (greater than 5.6 km/sec); therefore, most of the excursions of the averages to longer interval velocities (lower P wave velocities) suggest some degree of fracturing in the bore hole. Comparison of the averages from this log with the averages from the density log show a high degree of correlation between areas of low density and areas of low P wave velocity. In particular the sonic log shows up all the extensive fracture zones indicated on the basis of drilling, as well as the numerous additional possible fracture zones. Similarly, zones identified as primary source and sink zones for fluids circulating in the bore hole based on temperature and flow velocity logs, correlate well with the areas of lower seismic velocity. In particular an extensive area of fractured rock associated with the contact of the Empire Creek stock is shown between 250 to 300 m. The first extensive fracture zone in the vicinity of the top of the convective cell appears to be between 425 and 450 m. The sonic log also shows very distinctly the zone of fracturing identified by drilling between 850 and 925 m which has the small resistivity response. In terms of the sonic log response one of the most significant zones is the one between 1025 and 1050 m. In summary, the sonic log shows evidence for a much higher degree of fracturing in the stock than do the remainder of the logs. This log identifies 15 major or minor fracture zones on the basis of the 25 m interval averages.

The temperature log obtained on 8/31/74 shows the effects of fracture zones on the temperatures between 400 and 1100 m clearly. The zones of temperature steps and spikes correspond with the fracture zone as determined from the drilling and from the sonic log.

The 8/31/74 and 11/16/74 temperature-depth logs for the total depth of the well are shown in Figure E.22 also. The 11/16/74 log was taken long enough following completion of drilling for the dissipation of the drilling

effects. The log shows a conductive gradient of about 150°C/km above 400 m, a decreasing gradient between 400 m and the maximum temperature at about 1040 m, and a slightly decreasing temperature between 1040 and TD. There is fully cemented casing to 424 m, partially cemented casing between 424 and 1300 m, and an open hole below 1300 m. On the basis of flow logs made during the last temperature logging, there is no vertical flow (or very small flow) within the bore hole, although very large vertical flows were present at one time. The lack of approach of the interval between 400 and 1000 km to the predrilling temperatures is apparently due to flow behind the casing. The developing reintrants in the temperature-depth curve suggest that fracture zones at those depths (about 1415, 1720, and 1760 m) have connections to colder fluid and that flow along these zones might have been initiated by the drilling. The last temperature log (6/30/75) indicates that these flows have ceased. The relatively constant temperatures below 1000 m (except for the fracture zones), if not due to downward flowing water, imply that the fracture flow system is acting as a homogeneous permeable medium in a gross average way.

The average data discussed are intended merely as a summary of conditions in the bore hole. More complete interval-by-interval discussion of the data is required for detailed correlations and comparisons of the different parameters. The result of the analysis of information regarding the state of the geothermal system based on bore hole data is that the Empire Creek stock is a large fracture aquifer. The aquifer is inside the stock and extends to a depth of at least 2100 m. The fracture zones which transfer fluid within the aquifer in general have a higher piezometric level at shallower depth. The permeability within the stock is primarily fracture permeability although the granite has a rather high intrinsic porosity of 2 to 5 percent, due mostly to microlitic cavities. The temperature of the aquifer where cut in the bore hole is 90 to 99°C although it may be 120 to 180°C at other locations in the convective system.

Nature of the Geothermal Area

Based on the results of the surface exploration and the deep drill hole, a preliminary model of the geothermal system is proposed in this section. The area appears to be unique in several respects. The most unusual aspect of the geothermal area is that the reservoir for hot water is a granite stock. It is generally supposed that circulation of fluids in granitic rocks is confined to a discrete fault or fracture system as contrasted to a diffuse set of fractures. Secondly, based on the data summarized in Summary of Exploration Results it is clear that the northeast limits of the heat flow anomaly are associated with the southwest subcrop extent of the Marysville granodiorite. Thus one granite body serves as a reservoir, while another acts apparently as a boundary to the circulation system. Thirdly, no resistivity anomaly is associated with the geothermal anomaly even though significant hydrothermal convection is present.

Even in geothermal areas characterized by hydrothermal circulation, conductive heat flow measurements may be used to estimate the shape and depth of the geothermal reservoir if the reservoir, fault zone, etc. is capped or

bounded by impermeable zones, and the temperature of the hydrothermal cell, or its depth at one point, is known. In the case of the Marysville geothermal area none of the geophysical data furnish evidence on the depth to which the temperature gradients can be extrapolated. Furthermore, there are no surface manifestations of geothermal fluid which can be geochemically analyzed and the estimated reservoir temperatures calculated. However, as measured in MGE #1, at least in the northern extremity of the geothermal area the base temperatures in the reservoir are 90 to 99 °C. Based on these data an extrapolation to the depth of the 95° isotherm using the surface gradient can be made in order to investigate the depth and shape of the reservoir in the remainder of the area. The results of a qualitative extrapolation of the data are shown in Figure E.23. It is to be emphasized that this figure is qualitative, and does not represent a mathematical solution for the isothermal surfaces. However, particularly at the northern end of the anomaly the geometric constraints on the temperatures are strong and the reversal in temperature gradient is actually observed in MGE #1. The southern border of the geothermal anomaly as drawn is much more qualitative. An approximate position of the possible 120° isotherm is also drawn, based on the geochemical evidence that the base temperatures in the reservoir may be as high as 120°C. It is possible, but speculative, that drill holes on the order of 700 to 900 m deep, south of MGE #1 might encounter higher temperatures. Based on this geometric construction, however, it is clear that the temperatures of 170 to 180°C implied by the Na-K-Ca geothermometer cannot occur over a very broad region in the geothermal area, and if such temperatures are present in the convection cell they must be confined to a thin plume somewhere in the system, the location of which is presently unknown.

In the previous models of the geothermal area (Blackwell et al., 1974; 1974 Report, etc.) the geometric constraints of the heat flow data were resolved by the interpretation of the source of the anomaly as a very recent shallow intrusive. In this case the time lag for heat flow through rocks allows a considerably different isothermal section than the one shown in Figure E.23 to satisfy the heat flow data.

In order to illustrate the correlation of the geothermal reservoir with geologic structure, the 95° and 120° isotherms have been superimposed on the geologic cross section CC' (Figure E.6) in Figure E.24. The geological and geophysical (primarily gravity) constraints on the top of the Empire Creek stock are discussed in more detail in the section on Gravity and Magnetic Studies. The correlation of the geothermal reservoir with the Empire Creek stock is clear. Also the association of the north boundary of the reservoir with a boundary of the Marysville granodiorite is illustrated. The apparent occurrence of the top of geothermal reservoir at an almost constant depth of 100 to 200 m below the reconstructed top of the Empire Creek stock is consistent with either of two hypotheses for the containment of the geothermal reservoir. The first hypothesis is that the highest piezometric levels reached anywhere in the reservoir correspond to an elevation of approximately 1463 m, the average fluid level in MGE #1. Therefore the reservoir fluid would not have enough pressure anywhere throughout the geothermal area to reach the surface, and indeed as shown in Figure E.24, the apparent altitude of the top of the reservoir remains almost constant from the north to south

end of the geothermal anomaly (it becomes deeper because of the change in elevation). However, none of the surface springs show evidence of mixing with warm water at depth which would seem likely if the geothermal reservoir is actually connected to the surface. In particular the water from a well 100 m deep at the site of MGE #1 has fluid which cannot be derived from the geothermal reservoir at 450 m by simple dilution (Table E.6). The second hypothesis is that the water is confined to the stock by a relatively unfractured chilled contact zone and thus the Empire Creek stock acts as both the reservoir and its cap. This hypothesis is speculative, but seems to be consistent with the data. In either case these results seem to imply a different type of geothermal reservoir than any other known. The results and implications shown in Figure E.24, it must be emphasized, are speculative and confirmation can only come from further drilling and testing.

In general the calculation of the location of subsurface isotherms in geothermal areas has been based merely on extrapolation as in the above discussion; however, the appropriate solution to the problem involves the theory of downward or sourceward continuation (Grant and West, 1965 and many others). At the present time no general technique for downward continuation of temperature data has been presented. Bodvarsson (1973) has considered some one-dimensional problems and presented downward continuation results. A technique for downward continuation of heat flow data has been developed for other purposes, but has been applied here to a digitized representation of the heat flow map (Figure E.10). The technique will be described elsewhere but the results of the application of the technique are shown in Figure E.25 as a contour map of the depth to the 95° isotherm below a hypothetical plane surface at approximately mean surface elevation. In order to calculate the contour map shown in Figure E.25 it was assumed that the thermal conditions above the reservoir are steady state, that the reservoir temperature everywhere at its top is 95°C, and that the heat flow data are measured on a plane surface. Also shown for reference are the outcrop and maximum subcrop extent of the Marysville stock. It should be emphasized that these contours (in contrast to those shown in Figures E.23 and E.24) represent an actual solution to the Laplace equation for the location of the 95° isotherm which would give the surface heat flow data. These data do not represent a mere extrapolation of the surface data downwards as is clearly seen by comparing the shape of the contours in Figure E.25 to the shape of the heat flow anomaly (Figure E.9).

This contour map shows very steep sides to the reservoir on the north and northeast, relatively steep sides on the west and a complicated shape in the south and southeast portions of the anomaly. In particular the broad lobe along Ottawa Gulch immediately south of the Marysville stock as contoured on the heat flow map becomes a narrow east-west salient of the reservoir at right angles to the main trend of the reservoir. The shape of this portion of the anomaly suggests that the fluid may be moving along a very narrow zone such as a fault, and either is flowing eastward away from the main reservoir, or less likely, is flowing up into the main reservoir. A small displacement fault has been mapped along Ottawa Gulch and, as shown in Figure E.6, this fault could dip toward the south, with a dip in the range of 45 to 90°. If the dip were 60°, its location at 1 km depth would be displaced

Figure E.23 Cross section CC' (see Figure E.5) showing extrapolated isotherms at depth below the topographic surface. The isothermal surfaces shown are diagrammatic. The geothermal gradient is shown as the top curve. The possible location of the 120° isotherm if present at shallow depths is shown as the dashed line. The 95° isotherm, approximately the reservoir base temperature based on the results from MGE #1 is shown as the heavy line..

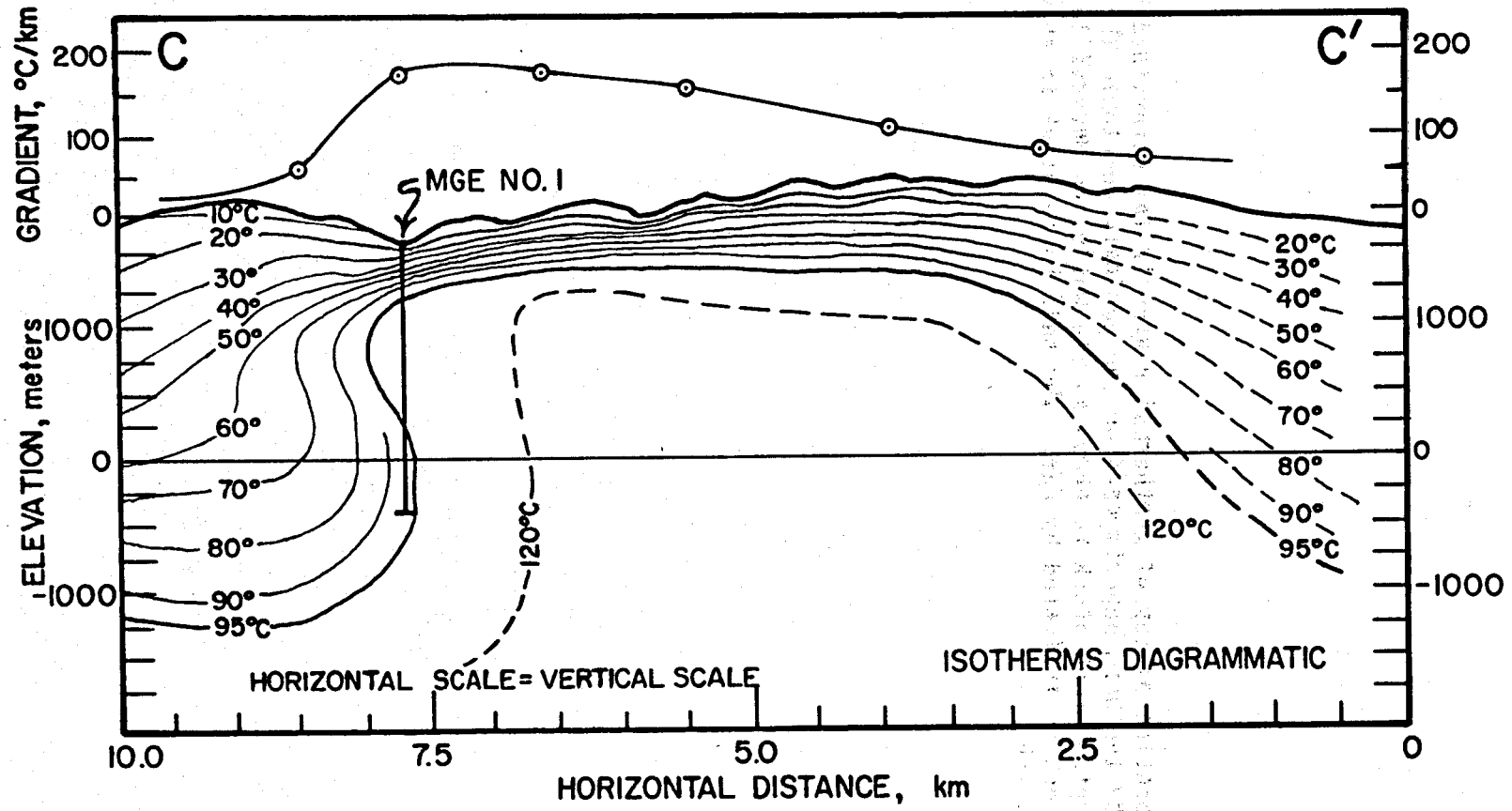
C
C'
GRADIENT, °C/km
200
100
0
-1000
ELEVATION, meters
MGE NO. 1
10°C
20°
30°
40°
50°
60°
70°
80°
90°
95°C
120°C
20°C
30°
40°
50°
60°
70°
80°
90°
95°C
120°C
HORIZONTAL SCALE= VERTICAL SCALE
ISOTHERMS DIAGRAMMATIC
10.0
7.5
5.0
2.5
0
HORIZONTAL DISTANCE, km

FIGURE E.23

Figure E.24 Location of top of geothermal reservoir (as determined by 95° isotherm superimposed on the geologic section). The Empire Creek stock is shown as Tie while the Marysville stock is indicated by Kgr. The Bald Butte stock is shown as Tib.

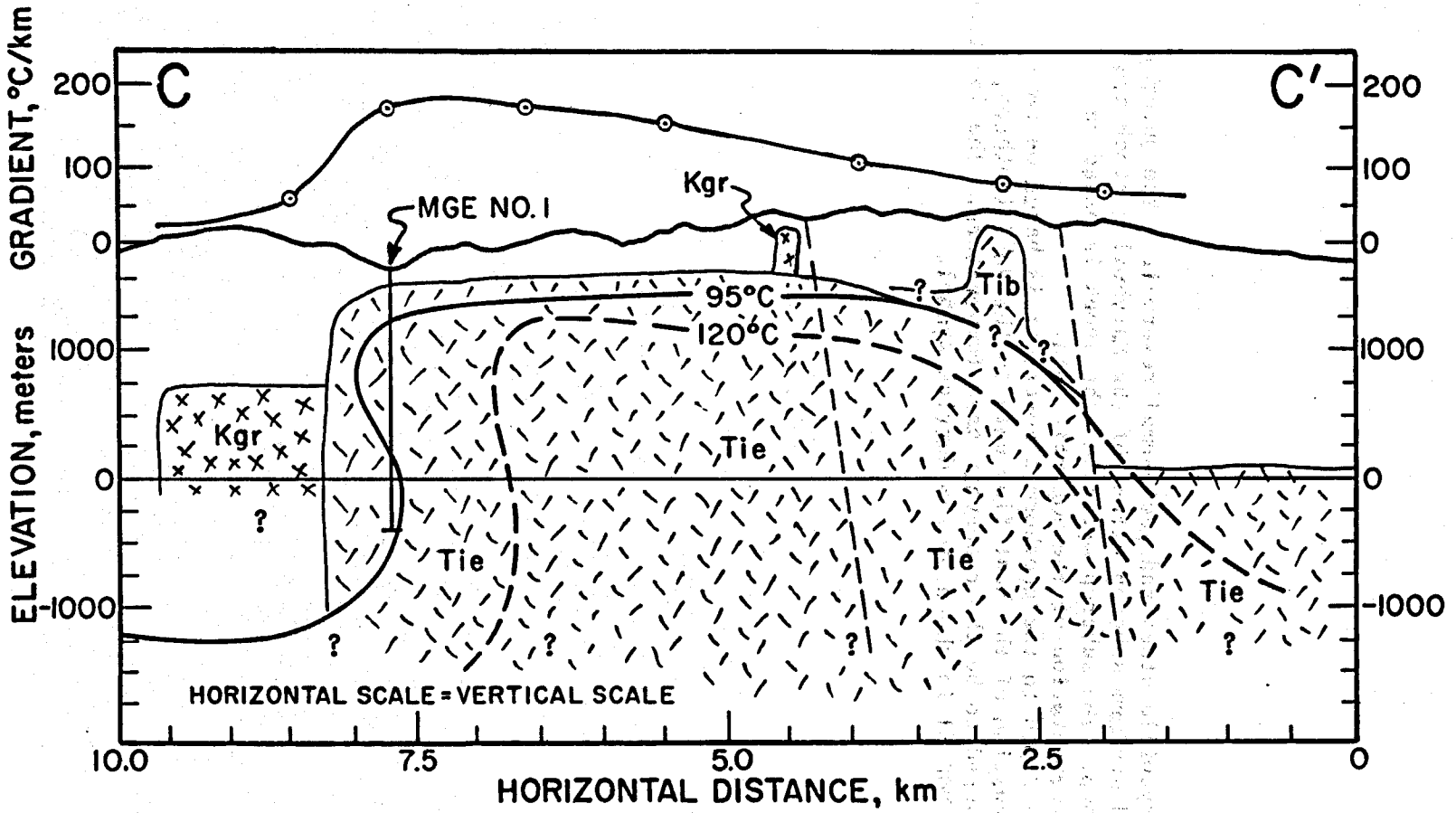
C
C'
GRADIENT, °C/km
200
100
0
ELEVATION, meters
1000
0
-1000
MGE NO. 1
Kgr
95°C
120°C
Tib
Tie
HORIZONTAL SCALE = VERTICAL SCALE
10.0
7.5
5.0
2.5
0
HORIZONTAL DISTANCE, km

FIGURE E.24

Figure E.25 Marysville stock and geothermal reservoir. The outcrop and maximum subcrop extent of the Marysville stock are shown. The subcrop extent of the stock is based on interpretation of the magnetic data.
The depth to the geothermal reservoir is based on continuation of the heat flow data to the 95°C isotherm, assumed to be the reservoir base temperature. The location of MGE #1 is shown by the derrick symbol.

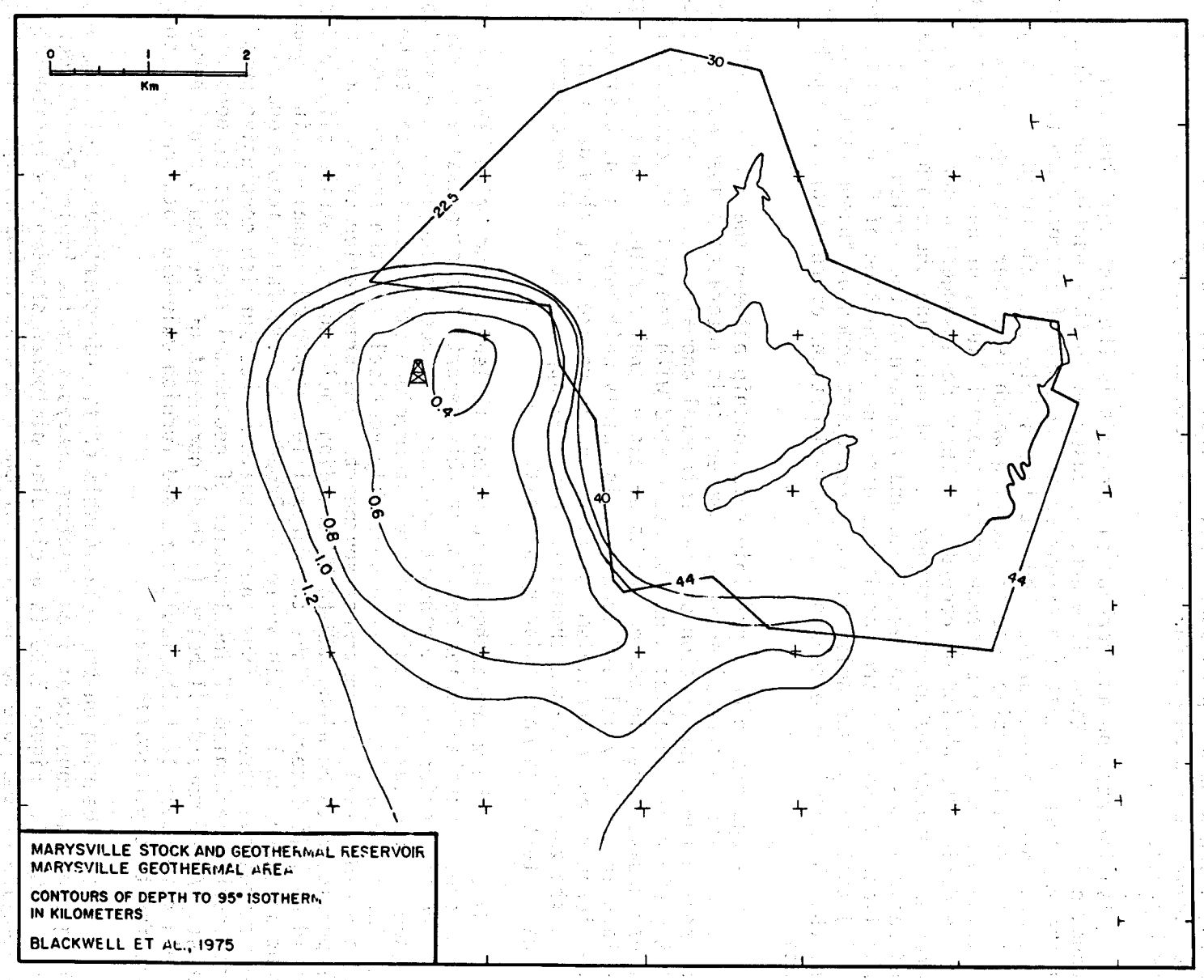
0
1
2
Km
30
22.5
0.4
0.6
0.8
1.0
1.2
40
44
44
MARYSVILLE STOCK AND GEOTHERMAL RESERVOIR
MARYSVILLE GEOTHERMAL AREA
CONTOURS OF DEPTH TO 95° ISOTHERM
IN KILOMETERS
BLACKWELL ET AL., 1975

FIGURE E.25

approximately 600 m to the south of its surface location. This position is near the location of the reservoir salient. Alternatively the fluid may be moving along some unmapped structure, or even along a shattered margin between the Marysville pluton and the surrounding metasedimentary rocks or Empire Creek stock.

Also interesting and perhaps significant is the fact that the highest ground noise in the Marysville area is observed in this particular quadrant of the map area and that the extension of the zone of microearthquake activity projects into the same area. Thus it is possible that the fluid is moving along a currently active zone of faulting which is either not represented by activity because of the presence of the thermal fluid, or has merely not been active during the period of recording. These data suggest a correlation, moreover, between the microearthquake ground noise and the geothermal data, and rational basis for the existence and location of the various types of anomalies. These data are consistent with the suggestion of Combs and Hadley (1975) that the ground noise data may represent zones of "nanoearthquakes" and thus be merely an extension of the implications of the microearthquake data.

There appears to be a possible relationship between the zone of earthquakes and the geothermal anomaly; however, this interaction does not appear to explain the major portion of the geothermal anomaly. It has been suggested that geothermal anomalies might be associated with the ends of active fault or earthquake zones in the quadrants of extensional strain. Since the stress pattern in the Marysville-Helena area is fairly well known on the basis of the microearthquake mechanism solutions and there are heat flow determinations along the zone of microearthquakes, this area appears to be an excellent place to test this particular hypothesis.

Based on the microearthquake solutions (Friedline and Smith, 1974 report, and Microearthquake Studies section in this report) the compressive stress axis in the region has a northeast-southwest surface projection and a shallow plunge. The dilatation axis and the intermediate stress axes appear to be similar in magnitude with one essentially vertical, and the surface projection of the other striking northwest-southeast. The orientation of the faulting is predicted to be along NNW to NW trending fault zones. Strike slip motion would be left lateral. Thus the Marysville geothermal anomaly is in a quadrant of extensional strain while the Broadwater area falls into a quadrant of compressive strain. Thus these results do not furnish conclusive proof that such a mechanism of localization of geothermal areas does or does not exist. A few more drill holes (3 to 4) northeast of the fault zone, however, would completely test the fault zone and furnish valuable data on the hypothesis for this particular area.

Further bearing on the relationship of the microearthquake activity and the geothermal zone comes from fracture analysis of the Empire Creek stock cut by MGE #1. Figure E.26 is a circular histogram showing the horizontal projection of the pole to the plane of the fractures in MGE #1 that gave the most distinct response on the dip meter log (Coates, 1974). These fractures have an average dip of 60°. Also plotted are the horizontal projections of

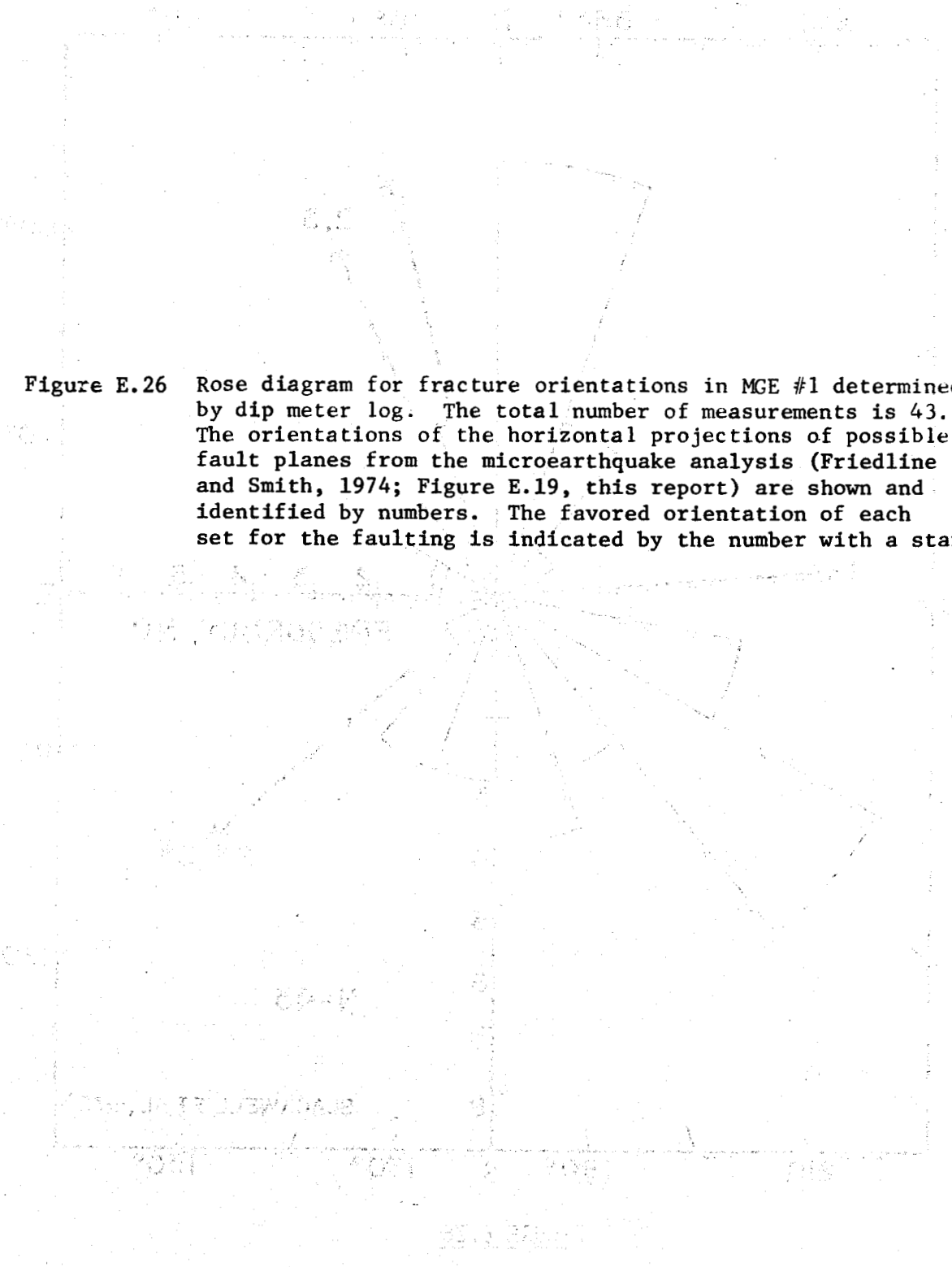

Figure E.26 Rose diagram for fracture orientations in MGE #1 determined by dip meter log. The total number of measurements is 43. The orientations of the horizontal projections of possible fault planes from the microearthquake analysis (Friedline and Smith, 1974; Figure E.19, this report) are shown and identified by numbers. The favored orientation of each set for the faulting is indicated by the number with a star.

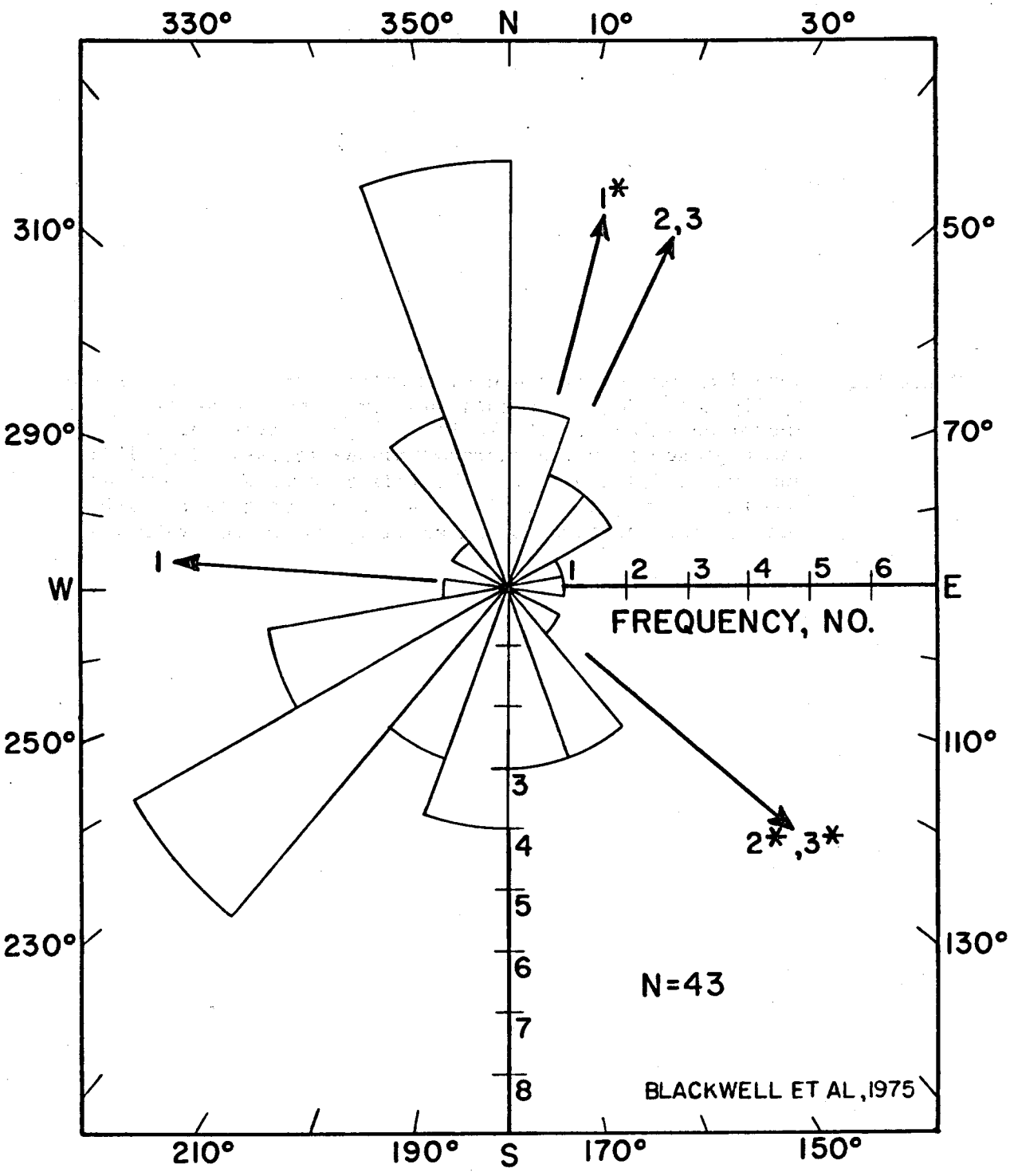
330°
350°
N
10°
30°
310°
50°
290°
70°
W
E
250°
110°
230°
130°
210°
190°
S
170°
150°
1*
2,3
1
1
2
3
4
5
6
FREQUENCY, NO.
2*,3*
3
4
5
6
7
8
N=43
BLACKWELL ET AL, 1975

FIGURE E.26

the poles to the possible fault planes which are the loci of the microearthquake activity. The most likely fault plane of each pair of arrows representing one solution is indicated by an asterisk. It is obvious that the fractures in MGE #1 are not shear fractures related to the present regional stress distribution. The system with the 350° pole azimuth could possibly be an extension fracture system related to the present stress distribution, however, although the orientation is wrong by about 20°. More likely the two sets of joints or fractures are related to thermal stresses generated during cooling of the Empire Creek body. The drill hole is nearest the north end of the body and the fractures are located approximately parallel and perpendicular to that margin suggesting origin by thermal contraction during cooling.

In spite of all these studies and the extensive amount of data available for geothermal area, the origins of geothermal fluids are not at all clear. If the maximum temperature in the system is 99°C then, on the basis of the regional heat flow, the fluid could come from a depth of only 1 km below the depth reached by MGE #1. None of the results of MGE #1 indicate any changes in the Empire Creek body with depth that would suggest a significant boundary near the bottom of the drill hole. The resistivity data have been interpreted in terms of a two layer model with the lower half space having a lower resistivity than the intervening rocks. This model implies a significant boundary at depths ranging from 2 to 6 km in the immediate area of the geothermal anomaly. The gravity data also are consistent with a 2.4 km vertical extent of the density contrast between the 2.55 gm/cm^3 stock and the 2.75 gm/cm^3 surface sedimentary rocks. However, if the geochemical temperatures are valid and higher reservoir temperatures exist at some location in the system, then it is possible that the circulation system could extend to depths of 4 to 6 km depending on the maximum temperature of the system (120 to 180°C).

The two hypotheses that seem most likely for the control on such deep circulation are motion along fracture porosity generated by the active faulting associated with the microearthquakes, deep circulation along fracture porosity and/or intrinsic porosity associated with a regional scale low angle thrust faulting (Blackwell and Baag, 1973), typical of the faulting exposed about 40 km to the east of the Marysville area (Robinson et al., 1968; Schmidt, 1963), or some combination of the two hypotheses.

Discussion of Exploration Results and Recommendations for Future Studies

Each of the exploration techniques carried out in the geothermal area provided information useful in the interpretation of the total data set. In summary a list of the exploration techniques will be given along with their contribution to the exploration results and questions which their implications may raise which have not been resolved at the present time.
(1) Geologic Mapping: Geologic mapping outlined the structure of the area including the dome in the Empire Shale southwest of the Marysville stock and the general fault pattern of the area. The geothermal anomaly seems to be structurally controlled, either because the Empire Creek stock is structurally controlled, and/or because of direct effects of faulting on the

reservoir, thus the structural data has been very important to the interpretation of the geothermal reservoir. (2) Metamorphic Petrology: Although an unusual technique in geothermal areas, the metamorphic petrology furnished the important information that the dome southwest of Marysville must be underlain by one or more relatively large bodies of intrusive rock. Unfortunately the metamorphic effects are only sensitive within a distance of a kilometer or so from the body and therefore do not furnish information on the shapes of the intrusive bodies at depth. (3) Geochemistry: Rock geochemistry has furnished information on the correlations of the igneous rocks in the general area, furnished information that indicates the Empire Creek stock is a large highly differentiated body, and suggests a correlation between the Empire Creek body and the Hope Creek rhyolites. Thus the data suggest a rather extensive period of volcanism and intrusion associated with the Empire Creek stock, and suggest that the Empire Creek stock extends south of the map area. (4) Magnetic Survey: The magnetic surveys did not furnish direct information on the geothermal reservoir; however, interpretation of the data furnishes the shape of the Marysville stock, and since the Marysville stock appears to have exerted control on the north and east sides of the geothermal anomaly, the magnetic data have thus indirectly contributed important information to the knowledge of the controls on the reservoir. There appears to be no magnetic anomaly associated with the Empire Creek stock because of its very low susceptibility. (5) Gravity Data: The gravity data furnish information on the size and distribution of the intrusive rocks in the area. Without independent information on the Marysville stock, however, there would be no way to separate the Marysville gravity anomaly from the other anomalies, and because of the uncertainty of the structural situation south of the map area, a large part of the gravity anomaly is ambiguous. The gravity data do serve to give limits on the shape and size of the Empire stock in the map area which are consistent with the thermal, electrical resistivity and geologic data. (6) Heat Flow: Heat flow data furnish the only direct evidence on the geothermal character of the anomaly area. When combined with the knowledge of the reservoir temperature, they allow calculation of the position of the reservoir. Without information on the temperature of the reservoir, the heat flow data are ambiguous and other interpretations are possible. (7) Resistivity Data: The resistivity data indicate high resistivity values in the area of the geothermal anomaly in sharp contrast to low values usually found in other geothermal areas. The resistivity data would not appear to be sensitive in the type of situation encountered in the Marysville area. Thus it would appear that in a reservoir consisting of fracture porosity the resistivity data may not be capable of detecting the existence of convection in a reservoir. (8) Seismic Ground Noise: The seismic ground noise response of the area is also inconsistent with typical responses proposed for geothermal areas. The lowest values of ground noise were found over the highest values of heat flow; however, there may be a connection between the high ground noise in the southeast quadrant of the anomaly, microearthquakes, and a salient of the geothermal anomaly along what appears to be a fault zone. (9) Microearthquakes: Microearthquakes do not furnish any positive evidence on the existence of geothermal anomaly or its location or nature. The only tentative connection between the two sets of data is with the high ground noise and possible subsidiary fluid circulation mentioned previously. The fracture systems in the reservoir do not appear to be consistent with the stress

distribution inferred from the present day microearthquake distribution, although further work is recommended to investigate the relationship. (10) Infrared Survey: Infrared data were successful in finding two groves of "hot" trees, one associated and one not associated with the geothermal anomaly. It appears that the infrared survey as carried out here is not capable of locating a geothermal anomaly such as the Marysville anomaly.

The exploration results in the Marysville geothermal anomaly have important consequences to other geothermal exploration projects. It appears that distributed fracture systems in granitic rocks can indeed function as rather effective circulation reservoir system for geothermal fluids, but one which might be very difficult to detect, even if reservoir temperatures are higher than those observed in the Marysville area. Unfortunately it is not known whether the permeability and porosity in the Empire Creek stock is sufficient to sustain production of commercial quantities of geothermal fluids. Such knowledge is very important to the national program of geothermal development. An extensive series of reservoir tests in a situation such as the Marysville area should be conducted in order to investigate hydraulic properties of a fracture flow system. Since it appears that one of the major problems in many geothermal exploration projects is the lack of techniques successful in finding sufficient permeability for production, even though high temperatures may be found, research directed toward locating subsurface zones of permeability based on surface data is of greatest importance. In this respect there are several areas in the Marysville geothermal area that might warrant additional deep drilling to clarify the fault zone extension, e.g., along Ottawa Gulch where the high ground noise and microearthquake activity are observed. Furthermore, the Marysville area represents the place where more information could be obtained on exact relationship of seismicity in geothermal areas, since it appears there are two geothermal areas associated geographically with the zone of active seismicity. Further exploration along the zone of microseismic activity should make an important contribution to the understanding of the relationship between seismicity and geothermal areas.

An unexpected bonus obtained in the Marysville geothermal area was the discovery of the Empire Creek stock. Based on the petrologic information the emplacement of this stock was at a depth of about 2 km, and thus the body is a cooled, exhumed example of the body which could have satisfied the conductive heat flow model for the geothermal area. Therefore study of the contact effects associated with the Empire stock, the nature of fracture formation in the Empire Creek stock, and its interaction with the wall rocks, should furnish a model for such interaction of presently existing shallow magma chambers of the type postulated as a source for several geothermal areas. Therefore the nature of the fracturing associated with emplacement, and particularly the origin and significance of the apparent reservoir cap along the chilled margin should be investigated.

Conclusions and Recommendations

An extensive suite of geological and geophysical exploration investigations has been carried out in the Marysville geothermal area. The results were ambiguous and deep drilling was required to distinguish between two models for the geothermal source: a cooling magma chamber or a convecting hot fluid system. The interrelationships of the geological and geophysical data have been extensively discussed in the first two sections of this chapter. Deep drilling proved the source of the geothermal anomaly to be a convecting hot water system.

Perhaps the most significant geophysical result of the exploration is the discrepancy between the electrical resistivity results and the heat flow data. Even with higher fluid temperatures and lower resistivity, the geothermal area would not be located by electrical studies. Unfortunately, because the flow properties of the system were not tested, little is known of the permeability or production capacity of the system, so the economic potential of a similar system, at higher temperatures, cannot be assessed. Nevertheless, it is clear that electrical techniques cannot distinguish a fluid convection system, such as the one at Marysville, from a dry system with no fluid convection. Thus the use of electrical exploration techniques in exploration for dry hot rock systems will be limited.

The knowledge of the reservoir conditions and geometry have been summarized in this chapter. The most serious data missing from the study is that dealing with the reservoir properties. Lack of information regarding the significance of the reservoir makes conclusions on the results of the various exploration techniques tenuous. Therefore it is strongly recommended that further reservoir studies be carried out. The conditions allowing circulation of fluid in the granite are of importance both to the potential of dry hot rock exploitation, and to the limits on natural convection systems in granite rocks, or any fracture type of reservoir.

The exploration data set collected for the Marysville geothermal area is fairly complete, except that there are significant uncertainties on the southern limits of the heat flow anomaly. Two or three holes south of the presently explored area would furnish the data necessary to complete the analysis of the areal extent of the reservoir. Since the exploration data are reasonably complete and, except to the south, the limits of the geothermal anomaly are well defined, the geothermal area can continue to serve as a test area for new exploration techniques.

The existence of the geothermal anomaly near an area of regional seismicity is interesting, and two holes described previously (RDH35 and RDH36) were drilled in order to investigate the relationship between the heat flow and seismicity. Heat flow values from these holes are near the regional average heat flow. The total above normal heat loss for the Marysville geothermal area is about 2×10^6 cal/sec, equivalent to the total regional heat flow from an area of 100 km^2. Since the earthquake zone has only about this area, and this heat loss figure does not include the Broadwater Hot Springs, if deep circulation along the zone of seismicity is the geothermal

source, then a measurable decrease in heat flow should be found along this zone. Because of the large amount of data available for the area and the well known extent of the microseismic activity, additional regional heat flow drilling is recommended.

Although economic exploitation of the Marysville geothermal system is unlikely, the geological, geophysical and deep drilling exploration in the Marysville geothermal area has revealed a geothermal system of a type previously unknown. The economic potential of a similar system at higher temperatures cannot yet be assessed as it depends on the reservoir properties of the system, which have not yet been tested. It is highly likely, however, that similar systems do exist in the western United States and in other areas of the world, and the Marysville geothermal area will act as a model for exploration in these areas. In addition, the extensive suite of data available for the Marysville area makes it an ideal proving ground for new exploration techniques, and flow tests on the reservoir would provide valuable information on the properties of fracture porosity reservoirs, including dry hot rock systems. The discovery of the Empire Creek stock has provided a well studied example of a body that would provide a conductive heat flow source for a dry hot rock system if the time of emplacement was of the order of 1 to 2 million years or less. Geological, geophysical and deep drilling exploration in the Marysville geothermal area has therefore made a valuable contribution to the knowledge of geothermal systems and the exploration of these systems, and will provide useful data and a testing ground for future studies.

REFERENCES

Barrell, J., Geology of the Marysville Mining District, Montana (A study of igneous intrusion and contact metamorphism), U.S.G.S. Prof. Paper 57, 182 pp., 1907.

Biehler, S. and W. E. Bonini, A regional study of the Boulder batholith Montana, in Igneous and Metamorphic Geology, ed. L. Carsen M. Prinz, and V. Manson, Geol. Soc. Amer. Mem. 115, 401-427, 1969.

Bierwagen, E., Geology of the Black Mountain area, Lewis and Clark and Powell Counties, Montana, Ph.D. Thesis, Princeton Univ., 1964.

Birch, F., Flow of heat in the Front Range, Colorado, Bull. Geol. Soc. Amer., 61, 567-630, 1950.

Blackwell, D. D., Heat flow determinations in the northwestern United States, J. Geophys. Res., 74, 992-1007, 1969.

Blackwell, D. D., Surface ground temperature variations in mountainous regions and a new topographic correction technique for heat flow measurements, EOS, 54, 1207, 1973.

Blackwell, D. D., Geothermal Resources at Marysville, Montana, Proceedings of 9th Intersociety Energy Conv. Eng. Conference, 1974.

Blackwell, D. D. and C. G. Baag, Heat flow in a "blind" geothermal area near Marysville, Montana, Geophysics, 38 941-956, 1973.

Blackwell, D. D., and P. Morgan, Geological and geophysical exploration of the Marysville Geothermal Area, to be published in Proceedings of the Second United Nations Symposium on the Development and Use of Geothermal Resources, San Francisco, California, May 20-29 1975.

Blackwell, D. D. and E. C. Robertson, Thermal studies of the Boulder batholith and vicinity, Montana, in Guidebook for the Butte Field Meetings of Soc. Econ. Geol., ed. R. N. Miller, Butte, Montana, 1973.

Blackwell, D. D., C. A. Brott, T. T. Goforth, M. J. Holdaway, P. Morgan, D. Petefish, T. Rape, J. L. Steele, R. E. Spafford, and A. F. Waibel, Geologic and geophysical exploration at Marysville Geothermal Area: 1973 Results, Technical Report, NSF-RA-N-740316, 104 pp., 1974.

Blackwell, D. D., C. A. Brott, T. T. Goforth, M. J. Holdaway, P. Morgan, D. Petefish, T. Rape, J. L. Steele, R. E. Spafford, and A. F. Waibel, A brief description of geological and geophysical exploration of the Marysville geothermal area, Proceedings of Conference on Research and Development of Geothermal Energy Resources, Pasadena, California, Sept. 23-25, 98-110, 1974a.

Blackwell, D. D., C. A. Brott, T. T. Goforth, M. J. Holdaway, P. Morgan, D. Petefish, T. Rape, J. L. Steele, R. E. Spafford, and A. F. Waibel, The Marysville Geothermal Area, Montana, in Montana Energy Resources, Montana Bureau of Mines and Geology, 1975.

Bodvarsson, G.,Downward continuation of constrained potential fields, J. Geophys. Res., 78, 1288-1292, 1973.

Brott, C. A., The interpretation of heat flow data, Subject for Ph.D. Thesis, Southern Methodist University, Dallas, Texas 75275, 1975.

Buddington, A. F., Granite emplacement with special reference to North America, Geol. Soc. Amer. Bull., 70, 671-747, 1959.

Burfiend, W. J., A. gravity investigation of the Tobacco Root Mountains, Jefferson Basin, Boulder batholith, and adjacent areas of southwestern Montana, Ph.D. Thesis, Indiana Univ., Bloomington, Indiana, 1967.

Coats, Results and interpretation of Schlumberger well logging in MGE #1, Marysville Project Final Report, 1975.

Combs, J., and D. Hadley, Microearthquake investigation of the Mesa geothermal anomaly, Imperial Valley, California, submitted to Geophysics, 1975.

Copeland, T. B. and P. Kolesar, Part A: Geochemistry, geophysical, geochemical, and geological investigations of the Dunes geothermal system, Imperial Valley, California, in press, 1975.

Cordell, L., and R. G. Henderson, Iterative three-dimensional solution of gravity anomaly data using a digital computer, Geophysics, 33, 596-601, 1968.

Craig, H., Isotopic composition and origin of the Red Sea and Salton Sea geothermal brines, Science, 154, 1544-1548, 1966.

Davis, W. E., W. T. Kinoshita and H. W. Smedes, Bouguer gravity, aeromagnetic, and generalized geologic map of East Helena and Canyon Ferry quadrangles and part of the Diamond City quadrangle, Lewis and Clark, Broadwater and Jefferson Counties, Montana, U.S.G.S. Map GP-444, 1963.

Eslinger, E. V. and S. M. Savin, Oxygen isotope geothermometry of the burial metamorphic rocks of the Precambrian Belt supergroup, Glacier National Park, Montana, Geol. Soc. Amer. Bull., 84, 2549-2560, 1973.

Fownier, R. O., and J. J. Rowe, Estimation of underground temperatures from the silica content of water from hot springs and wet-steam wells, Am. J. Sci., 264, 687-697, 1966.

Fownier, R. O., and A. H. Truesdell, An empirical Na-K-Ca geothermometer for natural waters, Geochim. Cosmochim Acta, 37, 1255-1276, 1973.

Friedline, R. A., Contemporary seismicity in the Helena, Montana, region, Master's Thesis, University of Utah, Salt Lake City, Utah 84112, 1974.

Friedline, R.A., and R. L. Smith, Contemporary seismicity in the Helena, Montana, region, in Blackwell et al., Technical Report, NSF-RA-N-740316, 84-99, 1974.

Friedline, R. A., R. B. Smith, and D. D. Blackwell, Seismicity and contemporary tectonics in a region of high heat flow near Helena, Montana, Geol. Soc. Am. Abs. With Programs, 6, 292, 1974.

Friedline, R. A., R. B. Smith, and D. D. Blackwell, Contemporary seismicity of the Helena, Montana, region, submitted to J. Geophys. Res., 1975.

Gosnold, W., The distribution of K, U, Th in and around granitic bodies, subject for Ph.D. Thesis, Southern Methodist University, Dallas, Texas 75275, 1975.

Grant, F. S., and G. F. West, Interpretation theory in applied geophysics, McGraw-Hill, New York, 583 pp., 1965.

Hays, Numerical models of topographic effects on heat flow measurements and of magma chamber cooling histories, Marysville Project Final Report, 1975.

Hewitt, D. A., Stability of the assemblage muscovite - calcite - quartz, Am. Mineralogist, 58, 785-791, 1973.

Jackson, D., Apparent resistivity map, Marysville Geothermal Area, U.S. Geol. Surv., 1972.

Johnson, R. W., J. R. Henderson, and N. S. Tyson, Aeromagnetic map of the Boulder Batholith area. southwestern Montana, U.S. Geol. Surv., Map GP-538, 1965.

Kerrick, D. M., Contact metamorphism in some areas of the Sierra Nevada, California, Geol. Soc. Amer. Bull., 81, 2913-2938, 1970.

Kleinkopf, M. D. and M. R. Mudge, Aeromagnetic, Bouguer gravity, and generalized geologic studies of the Great Falls - Mission Range area, Northwestern Montana, Geol. Prof. Paper 726-A, 19 p., 1972.

Knopf, A., Marysville granodiorite stock, Montana, Am. Mineralogist, 35, 834-844, 1950.

Mantei, E. J. and A. H. Brownlow, Variation in gold content of minerals of the Marysville quartz diorite stock, Montana, Geochim. Cosmochim. Acta, 31, 225-235, 1967.

Mazzella, F. E., A. thermal and gravity model of a geothermal anomaly near Marysville, Montana, M.S. Thesis, Southern Methodist University, 1974.

Mullin, J. B., and J. P. Riley, The colorimetric determination of silicate with special reference to sea and natural waters, Analytica Chimica Acta, 12, 162-176, 1955.

McSpadden, W. R., J. R. Eliason, J. Kuwada, and W. Bott, The Marysville, Montana Geothermal Project, First Annual Report, NSF-RANN Grant No. GI-38972, 1974.

Pardee, J. T., Late Cenozoic block faulting in western Montana, Geol. Soc. Amer. Bull., 61 359-406, 1950.

Pardee, J. T. and F. C. Schrader, Metalliferous deposits of the greater Helena mining region, Montana, U.S. Geol. Surv. Bull. 842, 1933.

Peeples, W. J., Magnetotelluric Sounding - Marysville, Montana, Final Contract Report, Dept. Geology and Geophysics, University of Utah, Salt Lake City, Utah 84112, 1975.

Petefish, D., The geology of the Marysville Geothermal Area, Subject for Master's Thesis, Southern Methodist University, Dallas, Texas 75275, 1975.

Rankin, D., Magnetotelluric Sounding - Marysville, Montana, Subcontractors Report, in W. J. Peeples, Magnetotelluric sounding - Marysville, Montana, Final Contract Report, Dept. Geology and Geophysics, University of Utah, Salt Lake City Utah 84112, 1975.

Robinson, G. D. M. R. Klepper, and J. D. Obradovich, Overlapping plutonism, volcanism and tectonism in the Boulder Batholith Region, western Montana, in Studies in Volcanology, R. R. Coats, R. L. Hay and C. A. Anderson, eds. Geol. Soc. Am. Mem. 116, 557-576, 1968.

Rogers Engineering Co., Marysville geothermal project, drilling report (not final), Rogers Engineering Co., San Francisco, California, Nov. 1974.

Rogers Engineering Co., The Marysville, Montana Geothermal Project, Final Contract Report, Rogers Engineering Co., San Francisco, California, 1975.

Ross, C. P., The Belt series in Montana, U.S. Geol. Surv. Prof. Paper, 346, 1963.

Rostad, O. H., The use of geochemistry at the Bald Butte molybdenite prospect, Lewis and Clark County, Montana, Quart. Colo. School Mines, 64, 437-449, 1969.

Sass, J. H., A. H. Lackenbruch, and R. J. Monroe, Thermal conductivity of rocks from measurements on fragments and its application to heat flow determinations, J. Geophys. Res., 76, 3391-3401, 1971.

Schmidt, R. G., Preliminary geologic map and sections of the Hogan 4 and Southeast quadrangle, Lewis and Clark County, Montana, U.S. Geol. Surv. Map I-379, 1963.

Sigvaldson, G. E., Geochemical methods in geothermal exploration, in Geothermal Energy, UNESCO, Paris, France, 49-60 1973.

Slaughter, J., D. M. Kerrick, and V. J. Wall, Experimental and thermodynamic study of equilibria in the system $CaO-MgO-SiO_2-H_2O-CO_2$, Am. J. Sci., 275, 143-162, 1975.

Stodt, J., Magnetotelluric studies in the Marysville Geothermal Area, Subject for Master's Thesis, University of Utah, Salt Lake City, Utah 84112, 1975.

Talwani, M. and M. Ewing, Rapid computation of gravitational attraction of three-dimensional bodies of arbitrary shape, Geophysics, 25, 203-225 1960.

Tilling, R. I., M. R. Klepper, and J. D. Oradovich, K-Ar ages and time span of emplacement of the Boulder Batholith, Montana, Am. J. Sci., 266, 671-689, 1968.

White, D. E., Geochemistry applied to the discovery, evaluation, and exploitation of geothermal energy resources, Geothermics, Sp. Issue, 2, 1, 58-80, 1970.

White, D. E., L.P.J. Muffler, and A. H. Truesdell, Vapor dominated hydrothermal systems compared with hot-water systems, Econ. Geol., 66, 75-97, 1971.

MAGNETOTELLURIC SOUNDING - MARYSVILLE, MONTANA

by
Wayne J. Peeples
University of Utah

September 1975

MAGNETOTELLURIC SOUNDING - MARYSVILLE, MONTANA

Wayne J. Peeples
University of Utah

INTRODUCTION

During the summer of 1974, extensive magnetotelluric and audio magnetotelluric (MT/AMT) measurements were carried out in the Marysville, Montana area under the direction of W. J. Peeples as part of a 1 year contract SMU 86-80 to the University of Utah (UU) from Southern Methodist University. The object of this investigation was to outline the electrical properties through magnetotelluric (MT) and audio magnetotelluric (AMT) measurements of the Marysville, Montana geothermal anomaly discovered by Blackwell (1969). This final contract report summarizes the field and laboratory investigations and their interpretation.

W. J. Peeples was in charge of the MT/AMT data collection and subcontracted the magnetotelluric work to the University of Alberta (UA) under the direction of D. Rankin (see Appendix E.1). J. Stodt collected most of the AMT data in the field with the interpretation carried out by W. J. Peeples and J. Stodt as part of Mr. Stodt's Masters Thesis project. We wish to thank Dr. C. M. Swift, Jr., and Kennecott Exploration, Inc., Salt Lake City, Utah for the use of their AMT instrumentation and technical help during this project.

PREVIOUS GEOLOGICAL AND GEOPHYSICAL STUDIES IN THE MARYSVILLE, MONTANA AREA

The mountainous Marysville geothermal area is located in the Northern Rocky Mountain physiographic and structural province (Eardley, 1962) about 30 km northwest of Helena, Montana and 4 km west of Marysville, Montana.

The country rocks of the district are Precambrian sedimentary rocks of the Belt Series. The two formations of the Belt Series which occupy most of the area of the geology map (Figure E.27) are the Helena limestone and Empire shale. Lower Paleozoic to Cretaceous units unconformably overlie the Belt rocks in a major syncline southwest of the geothermal area.

The oldest igneous rocks of the Marysville area are microdiorite sills in the upper part of the Empire and are dated as Precambrian. The Marysville granodiorite (Marysville stock) was emplaced at approximately 79 M.Y.B.P. (Baagsaard et al., 1961). The intrusion of the Bald Butte quartz porphyry has been dated at 49 M.Y.B.P. and further extensive activity occurred between 37 M.Y.B.P. and 40 M.Y.B.P. The numerous emplacements during this episode were concentrated southwest of the Marysville stock and include a large quartz feldspar porphyry body (the Empire stock) which is presently unexposed.

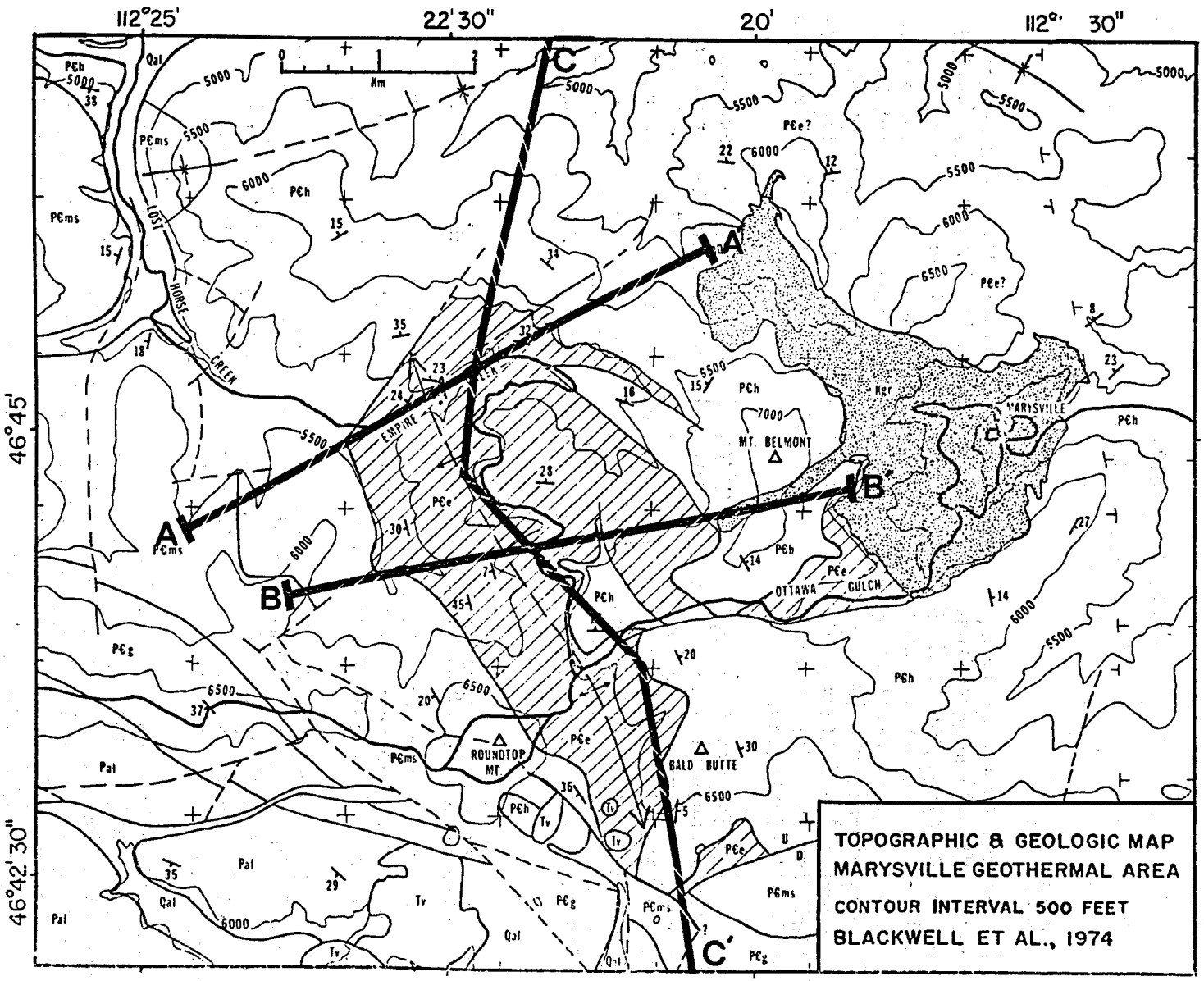

FIGURE E.27. Geology Map of the Marysville, Montana Area

Several episodes of deformation have occurred in western Montana and it is difficult to sort out the relative ages of folds and faults in the Marysville area. The basic structure shown in Figure E.27 is a dome in the sedimentary rocks. The core of this dome is shown by the exposures of Empire shale and Marysville stock. The Marysville stock occupies the northeastern portion of the dome.

Measurements by Blackwell (1969) from the Marysville area indicate heat flow values ranging from 3.3 to 20 $\mu cal/cm^2sec$ (western Montana average is approximately 2.0 $\mu cal/cm^2sec$) while a detailed gravity survey by Mazzella (1974) indicated a negative residual gravity anomaly associated with the area of the high heat flow values. Heat flow corrected for topography and regional gradient of 30°C/km and terrain corrected Bouguer gravity values are shown in Figure E.28 (the effect of the Marysville stock has been removed from the gravity data). Although the geothermal gradient is as high as 240°C/km, there are no surface manifestations of abnormal heat production. Magnetic surveys indicate that the only anomaly in this area is associated with the Marysville stock. Roving dipole surveys by the USGS in 1972 indicated that resistivities of 150 to 1000 Ω M were associated with the geothermal anomaly. A seismic ground noise survey indicated lowest noise values associated with the highest heat flow while a microearthquake survey indicated no microearthquakes were located in the geothermal anomaly region.

A deep exploration hole (2.4 km) was drilled in 1974 at the site indicated on Figure E.27. The drill encountered argillite to a depth of 294 m. The drill then entered the Empire stock (quartz-feldspar porphyry, quartz monzonite or monzonite depending on depth). At approximately 500 meters the first of several fracture zones with extensive fluid movement were encountered. At approximately 500 meters the temperature reached 95°C and remained essentially constant until the total depth was reached.

MAGNETOTELLURIC STUDIES IN MARYSVILLE, MONTANA

MT/AMT Measurements in Marysville, Montana

During the summer of 1974, 6 weeks were spent in the Marysville, Montana region acquiring field data for 12 magnetotelluric (MT) sites (10^{-3} Hz to 10 Hz) and 81 audio magnetotelluric (AMT) (14 Hz to 10^4 Hz) sites. Figure E.27 shows a general geology map for the Marysville region from Blackwell et al. (1973), and Figure E.29 shows the spatial location of the MT and AMT field sites.

The digitally recorded MT data were returned to the University of Alberta, Edmonton, Alberta, Canada (UA) where the data was selected, processed and tensor apparent resistivity versus frequency curves were obtained. Copies of the processed results were then returned to the University of Utah (UU) to be folded in with the AMT results and interpretations.

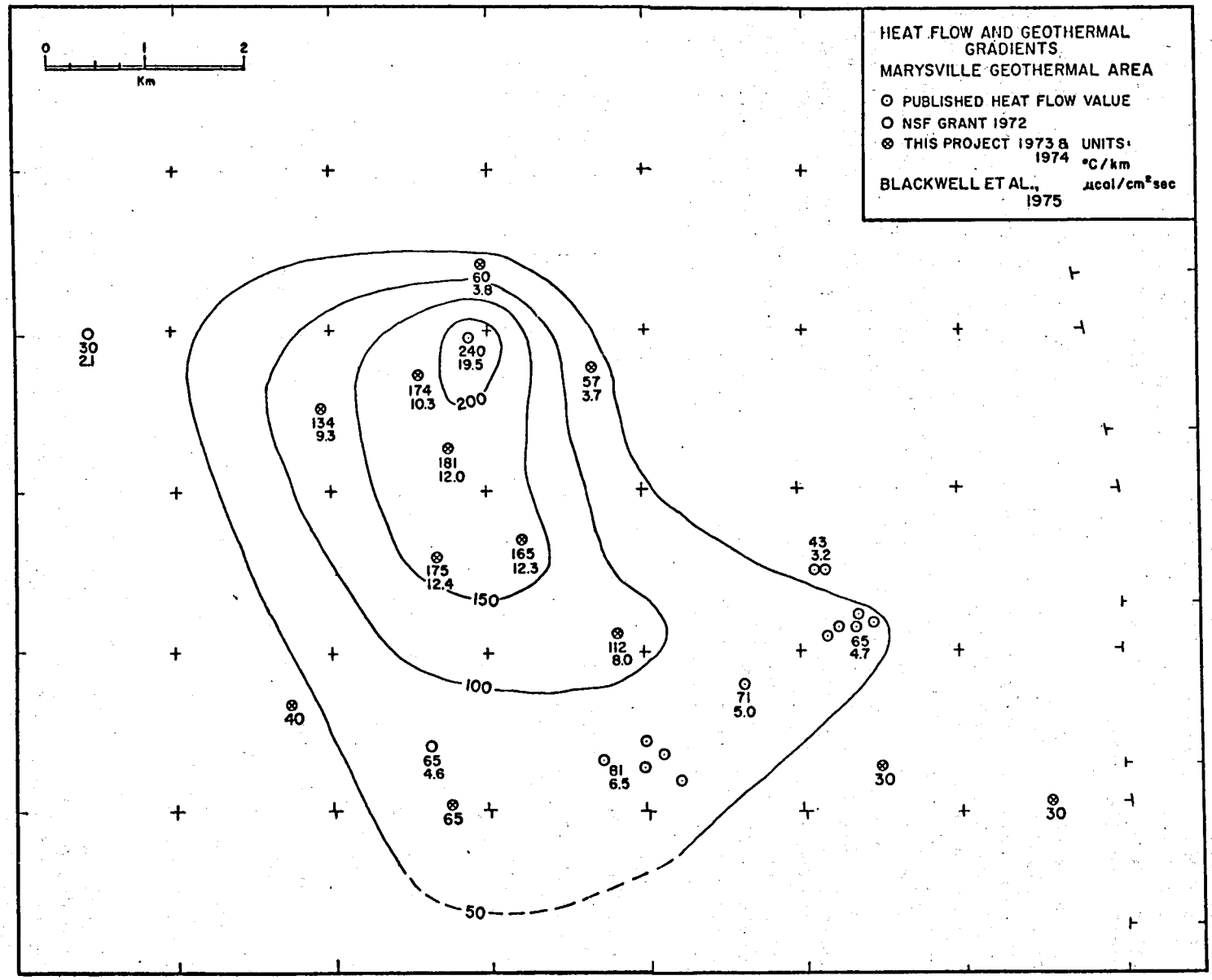

FIGURE E.28. Heat Flow and Bouguer Gravity Values for the Marysville Area

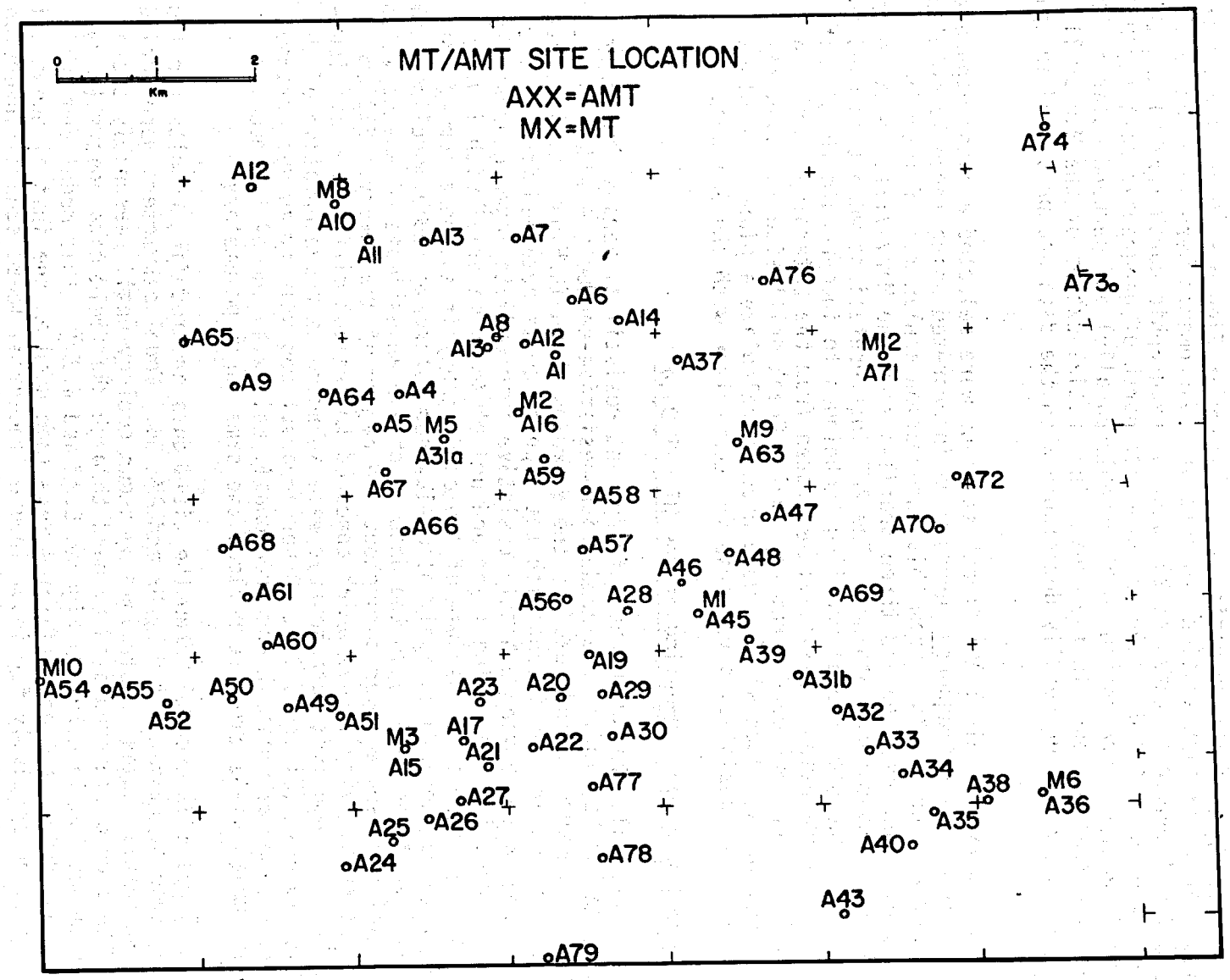

FIGURE E.29. MT/AMT Site Locations at Marysville, Montana

The hand recorded AMT results were returned to UU immediately after the field season and synoptic maps of apparent resistivity for each frequency and each measuring direction were made.

An example of the synoptic maps is shown in Figure E.30 for the 20 Hz measurement. At each station two sets of measurements were made, one with the $\vec{E}$ field sensor oriented at 20° west of geographic north (Ex/Hy) and the other with the $\vec{E}$ field sensor oriented 20° north of geographic east (Ey/Hx). These directions were chosen to be roughly parallel and perpendicular to the gross structural trends in the area. The spatial extent of the Marysville and Empire stocks are readily detectable when the data are presented in this form.

A number of typical AMT "type" stations were selected and the apparent resistivity versus frequency curves were interpreted using three layer plane wave plane layer models. From this information a plan map of interface depths has been prepared and three profiles from the Marysville stock to the Empire stock have been obtained. The AMT interpretations were then used as a basis for two-dimensional modeling techniques to incorporate the MT data in the interpretation. Resistivities taken from the Laterolog 7 and lab measurements on rock cores from the Empire Creek drill site and casually collected surface rock samples were used to calculate a plane wave plane layer apparent resistivity response for comparison with the AMT data.

One-Dimensional Modeling of the MT-AMT Data

In general, the AMT curves of apparent resistivity versus frequency (14 Hz to 10^4 Hz) indicate a conductive-resistive-conductive model for near surface structure as indicated by the examples shown in Figure E.31. That is, the curves are consistent with the type of curve obtained from a three layer earth model having a highly resistive intermediate layer overlain by a thin conductive weathering layer and underlain by material with lower resistivity at depths. Because of the consistency in the behavior of the curves, it was decided to apply plane-layered isotropic media modeling techniques (see Appendix E.2) to the data to obtain an estimate of the depth to the basal half space layer throughout the region of the survey. Eleven apparent resistivity curves which appeared to reflect differences attributable to more than just data scatter were selected as representative of the Marysville area (Figure E.31). Other apparent resistivity curves obtained during the survey which matched reasonably well with one of the modeled "type" curves are assumed to reflect the same earth parameters.

Figures E.32 and E.33 show the field data and modeling results for two of the type stations, AMT 9 Ey/Hx and AMT 54. Model parameters were varied from an initial guess constrained by known geology until reasonably close fit with a curve interpolated by hand through the field data points (x,o) was obtained (solid curve in Figures E.32 and E.33). This model and the interpolated apparent resistivities were then used as the initial guess and field data respectively for input into a linearized least squares inversion program. The large circles and the earth model in the figures are the results from the inversion program.

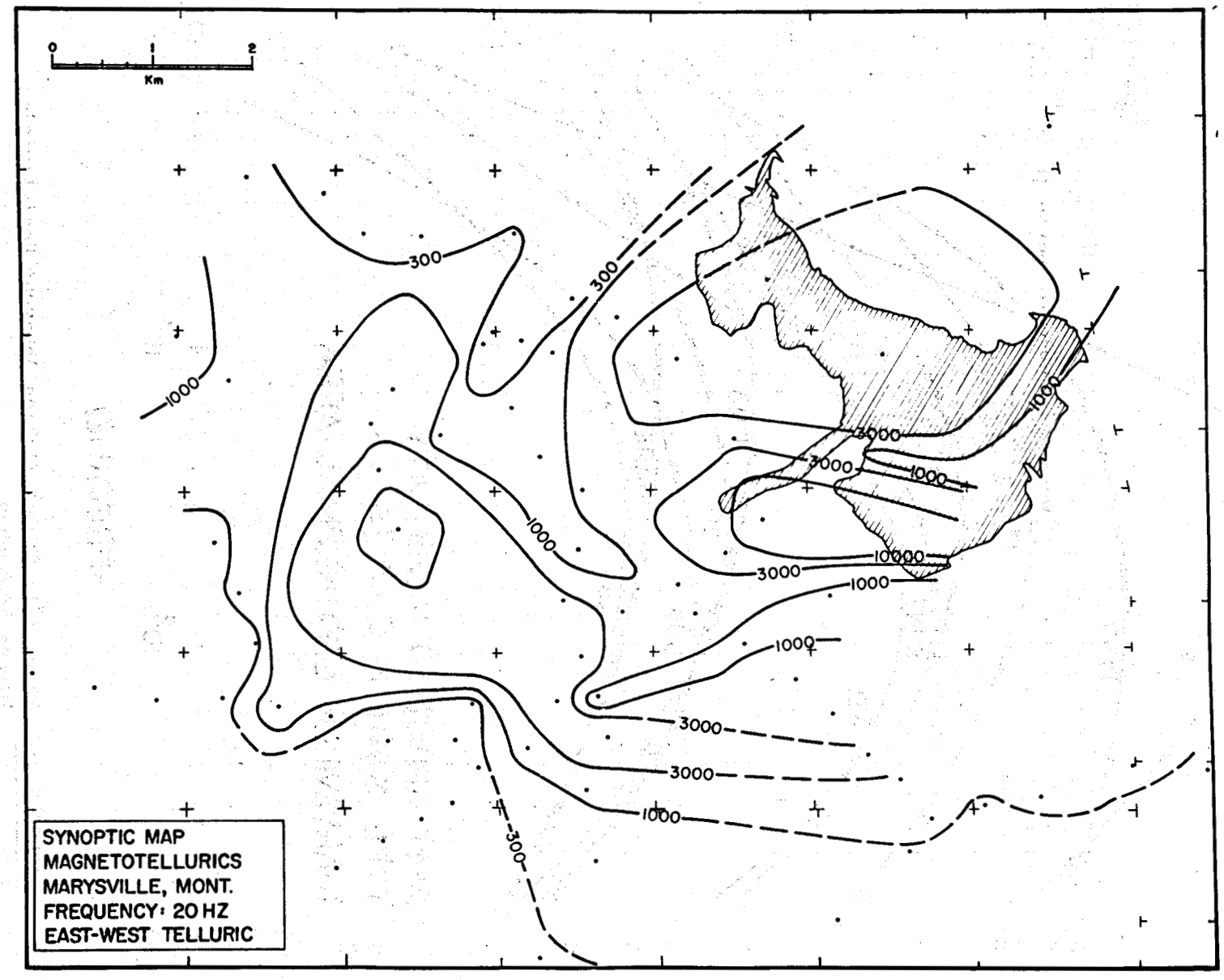

FIGURE E.30. Synoptic Map of 20 Hz AMT Measurements at Marysville, Montana for East-West Telluric Measurements

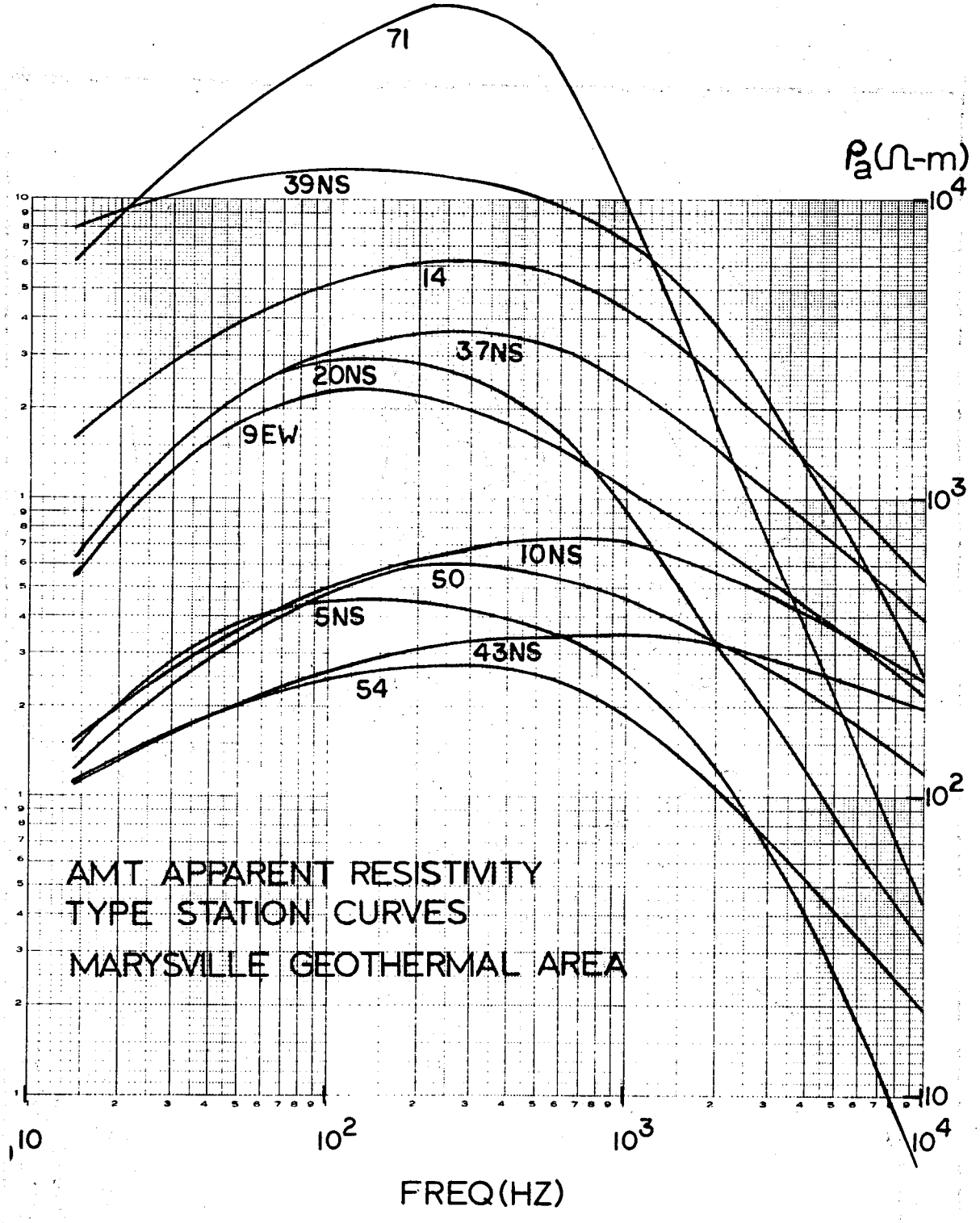

FIGURE E.31. Marysville "Type" Station Apparent Resistivities Versus Frequency

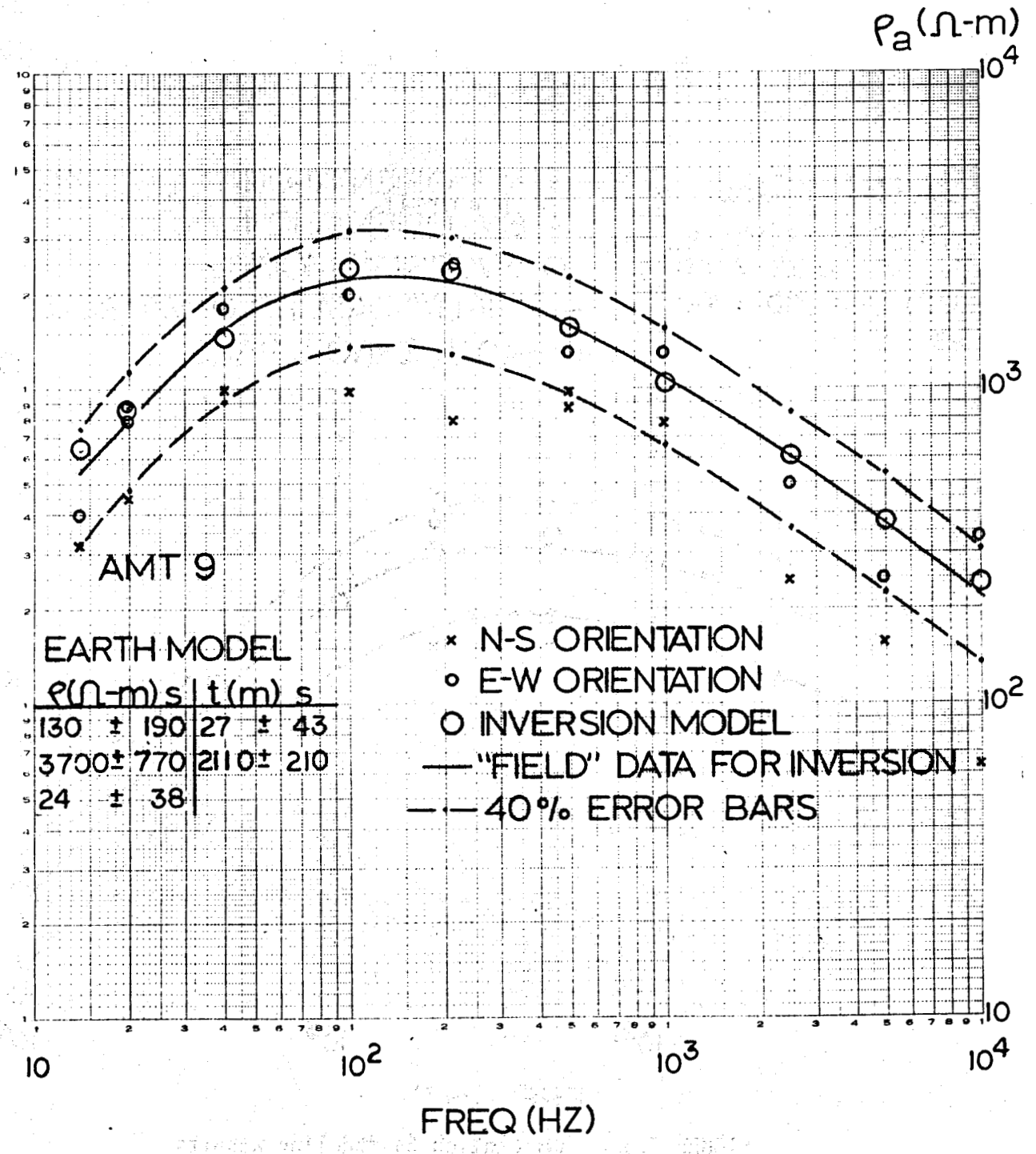

FIGURE E.32. AMT Station 9 Modeling Results

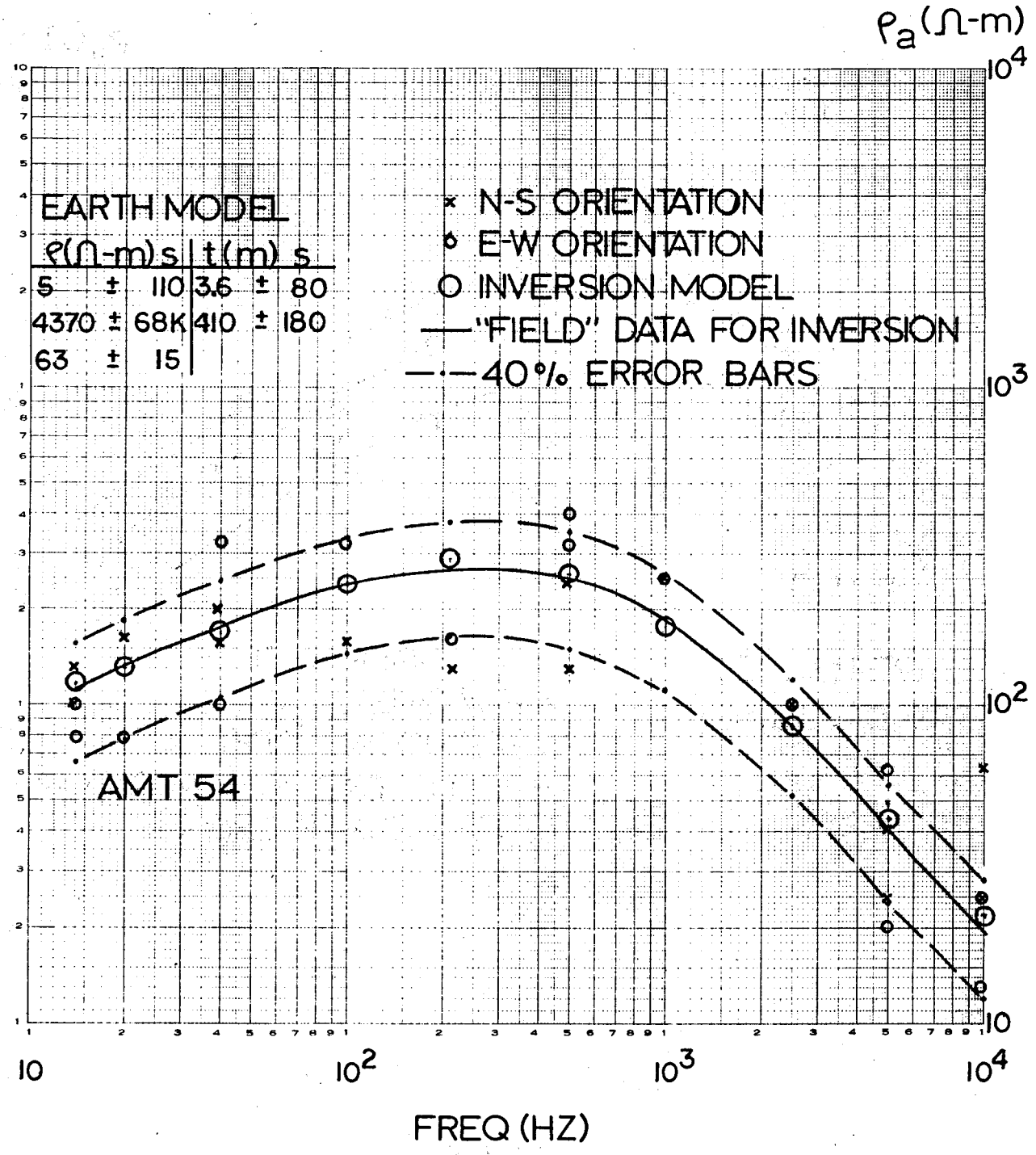

FIGURE E.33. AMT Station 54 Modeling Results

In general, the conductivity and thickness of the surficial layer were highly correlated in all models. Attempts at unconstrained inversion would not converge to an earth model giving a minimum value of the least square error (objective function). A method developed by Marquardt (1963) was used to constrain the inversion process thereby allowing iteration to a minimum of the objective function (see Appendix E.3 for discussion). The resulting earth models were then examined in view of current geological and geophysical information from the Marysville area.

The standard deviations (linear statistics) presented for the parameters represent propagation of normally distributed random error from data space to parameter space through the matrix $[A^TA]^{-1}$. (See Equation A3.15, Appendix E.3). Claimed repeatability of measurements with available instrumentation was to within 3dB. Since 6dB corresponds to a doubling in amplitude, this corresponds to $(2)^{1/2} = 1.414$ or approximately 40 percent expected variation in readings at a particular frequency, due to instrument error. The dashed lines in Figures E.32 and E.33 are 40 percent error bars on the solid curve. In calculating the parameter standard deviations, a standard deviation of ±20 percent about the interpolated field data was assumed.

Two-Dimensional Modeling of the MT/AMT Data

Upon completion of the one-dimensional modeling of the AMT data, profiles across the Marysville region were chosen for two-dimensional MT/AMT modeling. The modeling technique used was the transmission line analogy technique originally developed by Madden and Thompson (1965) and programmed by Peeples (see Peeples and Rankin, 1973).

The results of the one-dimensional modeling were used to construct a two-dimensional model of the Marysville area which also incorporated as much geological and geophysical information about the Marysville area as was possible. The two-dimensional modeling allowed us to bridge the data gap in frequency between the MT and AMT data and to construct a profile which apparently satisfies both data sets.

Criticisms of the Modeling

In examining the drawing conclusions from the above work, one must be cognizant of the following facts. The AMT gear used was not capable of simultaneous phase sensitive recording of both Ex, Hy and Ey, Hx pairs so that coherence tests to determine data reliability could not be performed nor tensor impedances calculated. Narrow band-pass filters at ten selected frequencies were applied to the amplified signal from the orthogonal E and H sensors and the output fed into integrating circuits. The Ex/Hy ratio used in the apparent resistivity calculations was formed electronically. This method of measurement cannot discriminate signal from noise at the same frequency nor does it provide enough information to allow tensor impedance calculations. This last point becomes significant when the earth contains a material anisotropy and/or lateral inhomogeneity, and measuring

sensors do not lie parallel and perpendicular to the directions of the conductivity anisotropy. There will then be a component of the E field induced by the component of H field parallel to it which will give rise to some error in the apparent resistivity estimate if only scalar impedances are calculated.

Two and three dimensional effects manifest themselves in bilogarithmic plots of apparent resistivity versus frequency in two ways. Theoretically, for plane waves incident normally on a homogeneous, isotropic layered earth, the maximum slope of ρ_a versus frequency on a bi-log plot is ±1 and the calculated apparent resistivities are independent of both the orientation of the orthogonal measuring axes, and the polarization of the incident field. Therefore, slopes greater than ±1 and/or differences in apparent resistivity curves calculated from the Ex/Hy and Ey/Hx pairs indicate 2-D or 3-D geometry, source effects, noise in the data, miscalibration of the instruments, anisotropy in earth materials, or a combination of these factors. A large number of the AMT stations produced apparent resistivity curves with these effects, (as could be expected, from an examination of the local geology) so that the assumption of uniform plane layers in the modeling is a fairly gross assumption. It is felt, however, that the local nature of an AMT sounding at these high frequencies and the uniformity in behavior of the apparent resistivity curves from station to station warranted an attempt at one dimensional interpretation of the data to obtain gross estimates of both the depth of penetration of the signal in the survey area, and an idea of the depth to the low resistivity layer at depth indicated in the AMT data.

The two-dimensional modeling allows us to explain some of the lateral inhomogeneity effects in our data sets as well as connecting the MT/AMT data sets with a model that appears to satisfy both data sets. It is readily apparent from a cursory inspection of the known geology that even two dimensional modeling is inadequate to fully predict the response of a region as three dimensional and complex as the Marysville area. However, the two dimensional modeling does allow us to determine model responses which appear to approximate the inhomogeneities appearing in the data sets.

LABORATORY ROCK RESISTIVITY MEASUREMENTS

Ten casual surface samples representing the major formations in the area were collected and cored for the purpose of making laboratory resistivity measurements. The following formations were sampled:

Pεe	Empire Shale (Precambrian)
Pεh	Helena Limestone (Precambrian)
Kgr	Cretaceous Granodiorite (Marysville stock)

In addition, 14 core samples from various depths at the drill site were available for measurement.

Sample Preparation

The main problem in sample preparation lies in saturation of the core with electrolyte of the desired resistivity, particularly when porosity of the sample is low (Brace, et al., 1965). The samples were vacuum pumped 8-12 hours and then electrolyte was drawn into the system utilizing the vacuum created to saturate the cores. Cores were then weighed daily to determine when they quit taking on significant amounts of electrolyte. Generally, after 2-3 days, there was little change in saturation. The electrolyte used was de-ionized water, with NaCl added to bring the resistivity of the solution to 10 Ω-m. This value was chosen by relating salinity to resistivity. Water at the drill site had a salinity of approximately 1000 ppm which corresponds to a resistivity of 10 Ω-m. This same electrolyte was used in the sample holder in making the four terminal resistivity measurements.

Measurement Apparatus

The configurations of the measurement apparatus are shown in Figure E.34. As is shown, four terminal measurements were made, current being applied to the outer electrodes, and voltage being measured across the inner pair. In making an A.C. measurement, voltage is measured across the core sample and across a calibration registor R_c. The resistance of the rock sample, R_r, can then be calculated;

$$R = \frac{R_c V_c}{V_c}$$

and the resistivity of the sample can be obtained if the dimensions of the core are known. R_c is chosen by experiment to $\approx R_r$, and R_b, a ballast resistor, is chosen $\approx 15 \times R_c$ in order to maintain proper signal level for input into the pre-amplifier.

The signal was first fed into a band-pass filter in an attempt to cut down the noise level in the measuring circuit. Measurements with the system were attempted at 5.46, 17.8, 54.6, 178, . . . 17800, 54600 Hz. A similar apparatus was used on two of the samples to extend the measurements from 5 Hz down to 0.1 Hz. A Phase Sensitive Detection (PSD) amplifier was available so that coupling in the circuit with industrial noise could be further filtered out in making the measurements. Its use requires an additional reference signal to be drawn from the oscillator input into the PSD (not shown in the figure). However, particularly for frequencies near 60 Hz and its harmonics the pre-amp was overdriven so that measurements could not be made. If measurements could be made at all, the difference between using and not using the PSD capability was <10 percent, except at high frequencies on some of the more resistive samples. Its use was therefore discontinued as a time saving measure in taking measurements on an oscilloscope placed in the circuit as shown to monitor the quality of the signal. Noisy signals

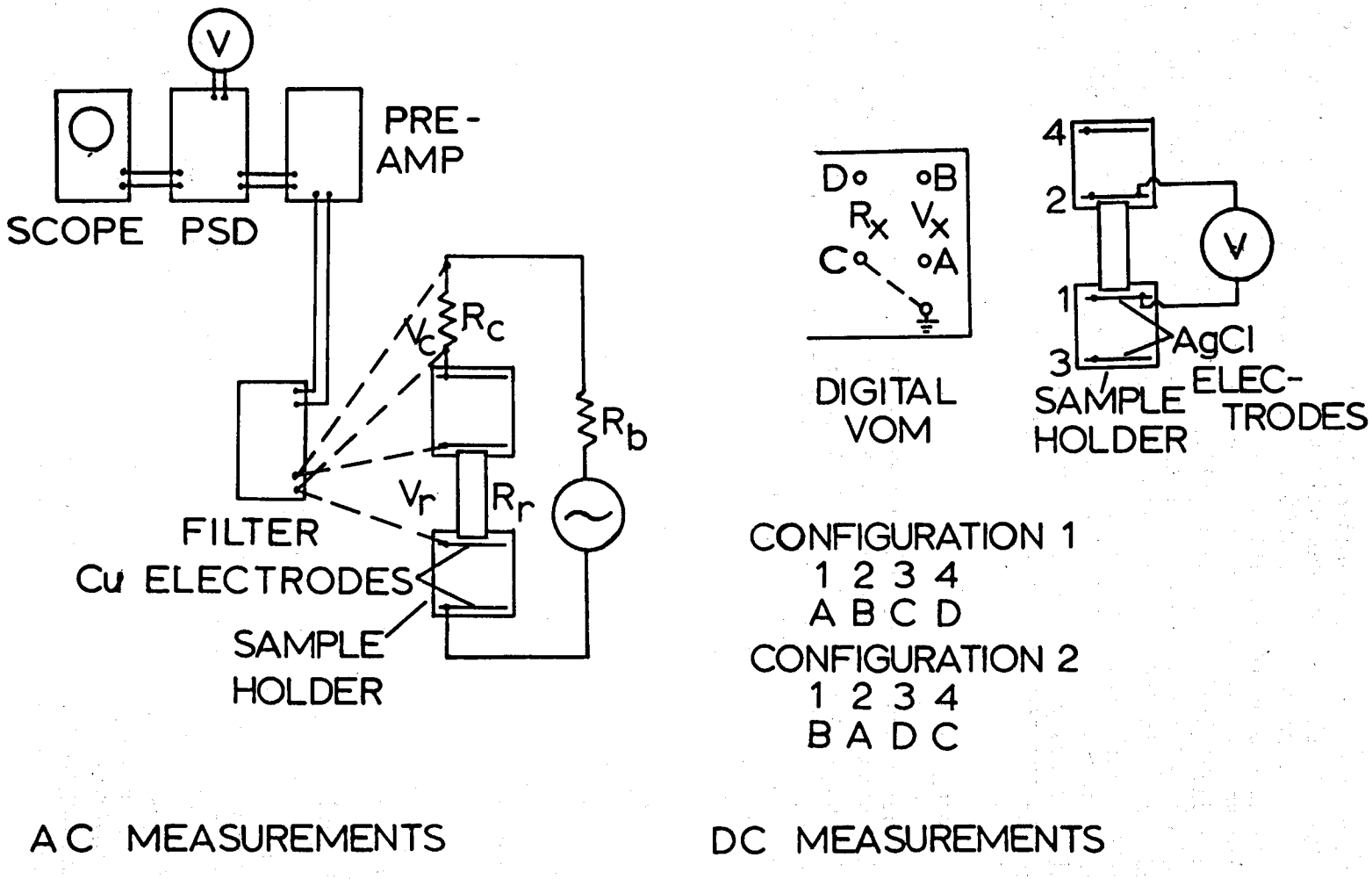

FIGURE E.34. Laboratory Resistivity Measurement Apparatus Schematic

were easily recognized. Coupling problems with industrial noise in the system arose whenever $R_b + R_c + R_r$ exceeded approximately 1 Meg. ohm. A.C. measurements could only be made on samples with resistance low enough so that coupling with industrial noise in the circuit did not overdrive the pre-amp.

A four terminal digital ohm-meter was also available for making D.C. measurements. This instrument was useable on cores with resistances too high to allow A.C. measurements with the available apparatus. The values given correspond as closely as instrument readings would allow to the resistivity of the sample at the onset of current flow. The instrument used had five scale ranges, each range utilizing a different voltage applied to the two current electrodes in obtaining a measurement. Potentials at the current electrodes ranged from 10 mV to 900 mV depending on the resistance of the sample and the instrument scale range used to obtain a reading. Problems arise in making D.C. measurements since voltages at potential electrodes from a variety of causes (concentration gradient in the electrolyte, chemical reactions at the electrode-electrolyte interfaces, etc.) are present even with no voltage applied to the current electrodes. These voltages were often as high as a few mV and caused significant differences in the readings from scale range to scale range on the instrument. These were lessened somewhat by the use of AgCl rather than Cu electrodes, but still had to be accounted for.

These potentials were accounted for by applying a correction factor to the raw resistance measurements as follows. Voltage was measured at the potential electrodes both during and immediately on cessation of application of voltage to the current electrodes. A correction factor $CF = -R_m(\frac{V_{EL}}{V_m})$ was then added to the raw resistance measurement R_m, to obtain a corrected value, where

V_{EL} = Voltage at the potential electrodes with no voltage applied at the current electrodes

V_m = Voltage at the potential electrodes during a measurement

A set of four readings was taken on each sample, representing measurements at two scales on the instrument (corresponding to two different applied voltages at the current electrodes) for two different measurement configurations, corresponding to a change in direction of current flow through the sample (see Figure E.34). Corrected values of resistance agreed to within 5 percent.

Laboratory Resistivity Measurement Results

Results of the measurements are summarized graphically in Figures E.35 and E.36. Figure E.35 shows results of the A.C. measurements. Deviations from flat response are attributed to cultural noise contamination in the measuring circuits. Peh 2 is not represented because of its high resistance which precluded making A.C. measurements; its D.C. resistivity was 4750 Ω-m.

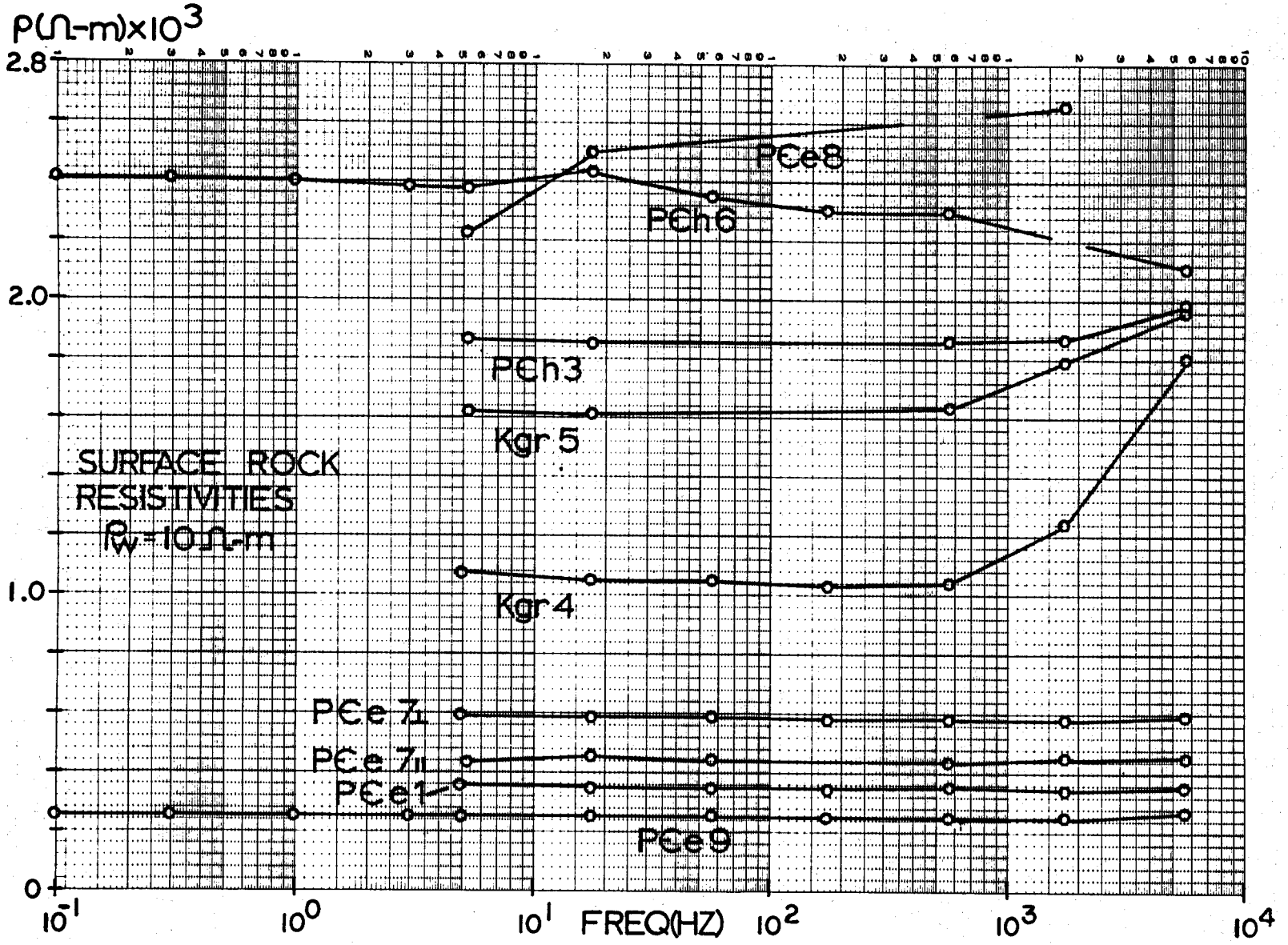

FIGURE E.35. A.C. Measurements of Resistivity from Marysville Samples Using 10 Ω-m Water

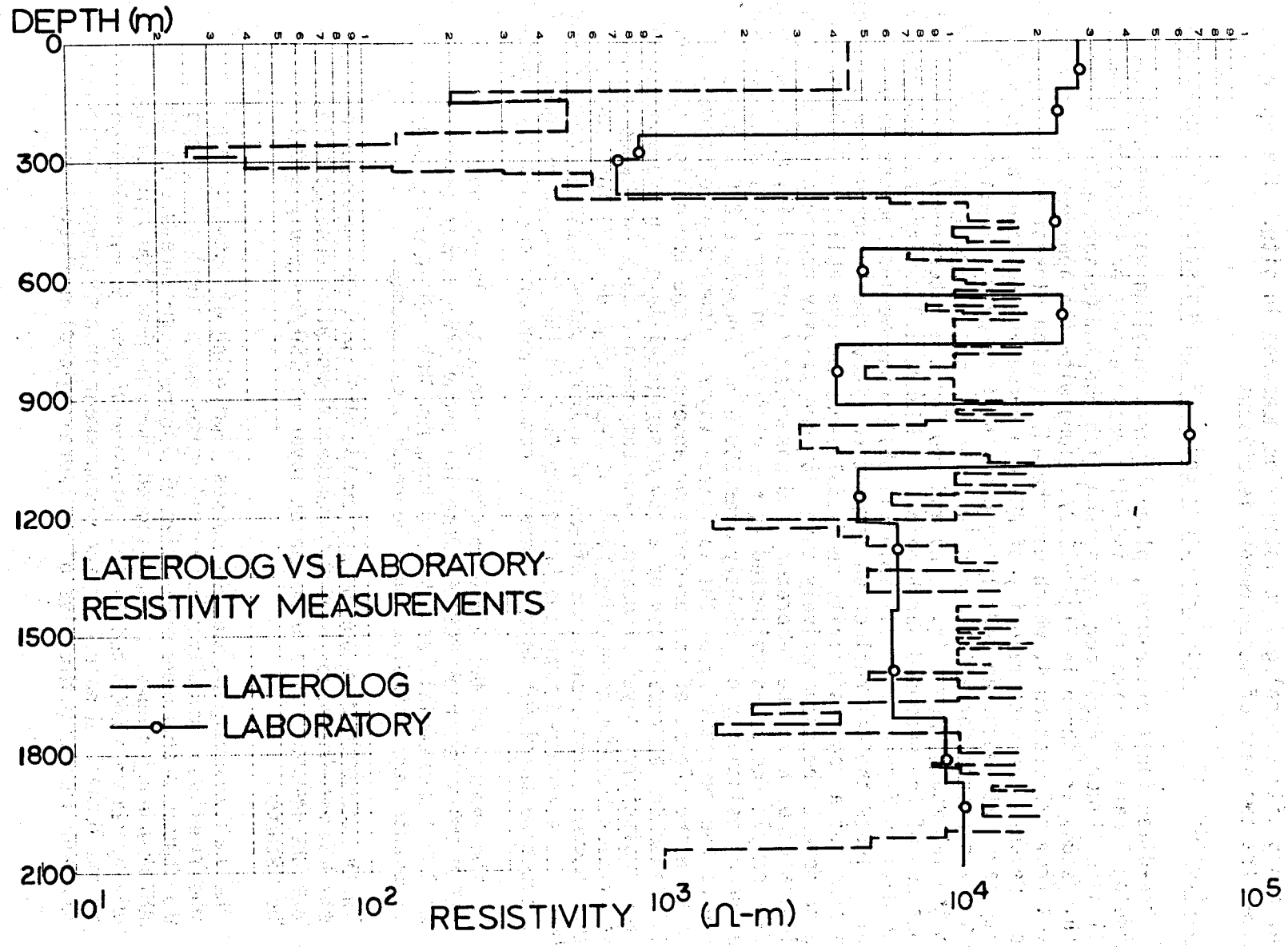

FIGURE E.36. D.C. Measurements of Resistivity on Core Samples and Laterolog 7 Resistivities from Marysville Drill Site

Figure E.36 shows the results of D.C. measurements on cores from the drill site, along with Laterolog 7 resistivities measured in situ. The agreement between the two sets of measurements is obvious.

Comparison of AMT Data with Laboratory and In-Situ Resistivity Measurements

One-dimensional plane-wave, plane-layered modeling was done with the Laterolog 7 data and with the resistivity measurements on the cores from the drill site (Figure E.36) for comparison with the AMT measurements. Results of this study are shown in Figure E.37, along with the apparent resistivity curves from AMT station 4, which was the AMT station closest to the drill site. Because the vast majority of AMT measurements indicated a low resistivity layer at depth, an underlying basal half space with resistivity of 100 Ω-m was chosen for all the models. Three separate models were inferred from the lab measurements (x, o, Δ) and two for the Laterolog 7 data (□, ○). Comparison of the proposed earth models in Figure E.37, with the resistivity-depth data in Figure E.36 will show the philosophy behind the choice of models. These choices reflect an attempt to study the effect of the presence or absence of a low resistivity surficial layer on the ability of the AMT data to detect the comparatively thin, low resistivity region at depth which is indicated both in the laboratory and Laterolog 7 resistivity measurements. Surface sample Pɛe 9 was collected in the vicinity of the drill site and had a measured resistivity of slightly over 200 Ω-m. Therefore 200 Ω-m was chosen as the resistivity of the surficial layer. Comparison of curves x and Δ show the effect of the presence or absence of the low resistivity surficial layer on the resolution of a 150 m surficial layer in the absence of the low resistivity layer at depth. The Laterolog 7 data indicated lower resistivities for the conductive layer at depth than did the lab measurements. Curves □ and ○ show the effect of a 175 m thick layer of resistivity of 100 Ω-m as inferred from the Laterolog data in the presence or absence of the conductive surficial layer. Several conclusions are immediately apparent.

1) In the absence of the low conductivity surficial layer, both a 150 m thick layer of 800 Ω-m material and a 175 m thick layer of 100 Ω-m material, as inferred from the lab and laterlog measurements respectively, would be readily detectable.

2) In the presence of a conductive surficial layer, the presence of the 150 m thick layer of 800 Ω-m material would be undetectable, but the presence of a 175 m thick layer of 100 Ω-m would still be detected.

3) The vast majority of the AMT curves (including all stations in the immediate vicinity of the drill site) were similar in shape to station 4 and were indicative of 3 layer structure within the AMT frequency range. It is assumed that the low (100 Ω-m) resistivity region indicated by the Laterolog 7 data is a reflection of the localized nature of the measurement in a fractured environment and is not indicative of the more regional resistivity

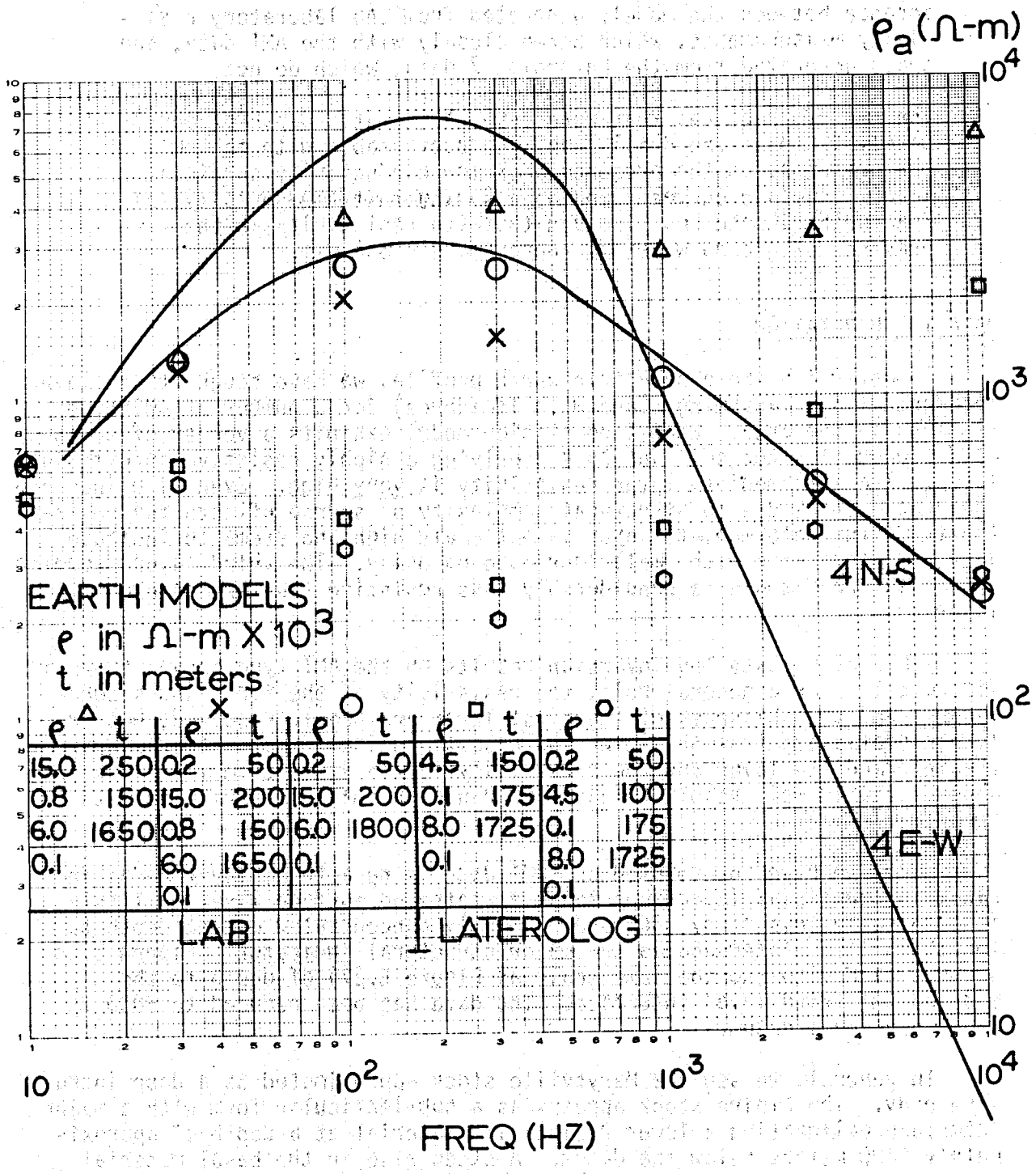

Δ ρ	Δ t	× ρ	× t	○ ρ	○ t	□ ρ	□ t	○ ρ	○ t
15.0	250	0.2	50	0.2	50	4.5	150	0.2	50
0.8	150	15.0	200	15.0	200	0.1	175	4.5	100
6.0	1650	0.8	150	6.0	1800	8.0	1725	0.1	175
0.1		6.0	1650	0.1		0.1		8.0	1725
		0.1						0.1	

FIGURE E.37. Laterlog 7 Model and AMT Station 4 Apparent Resistivity Versus Frequency

structure. This conclusion is reached in view of the vast difference between the models generated from the laboratory resistivity measurements, which agree closely with the AMT data, and those generated from the Laterolog 7 data, which do not.

4) The set of fractures that were encountered at a depth of approximately 500 m at the drill site are undetectable with the AMT measurements, in the presence of a low conductivity surficial layer, (compare curves x and o) assuming that the porosity and fracturing in the rock is such that its resistivity in the presence of ground water is approximately 800 Ω-m.

DATA INTERPRETATION

To determine the geoelectric earth profile, we have sought three layer interpretations (assuming plane wave incidence) for a number of AMT type stations in the area. Each type station model exhibits a veneer of weathered, conductive top soil and rock overlying a highly resistive intermediate layer. The intermediate layer resistivity is very high. Even with increase (decrease) of ρ_a due to structural complexity or source effects the resistivity of the intermediate layer is extremely high and seems to indicate very competent rock with small intrinsic porosity. The third layer, modeled as a basal half space is considerably less resistive than the intermediate layer.

Table E.10 lists the inversion results on the AMT type curves shown in Figure E.31. As a general rule, the resistivity of the first and second layers, and the thickness of the first layer are poorly resolved, but the linear statistics from the inversion process indicate that the thickness of the intermediate layer and the resistivity of the AMT bottom layer are in general fairly well resolved, assuming random normally distributed data error.

Since we have interpreted our AMT data using a three layer model and since the surficial layer represents a weathered surface layer of little importance in this study, we have primarily concentrated on the depth to the third layer interface as the major structural indicator. Figure E.38 shows a plan view (to the same scale as Figure E.27) of depth to the modeled AMT third layer interface. The data has been reduced to 5000 ft above sea level datum.

In general, we see the Marysville stock approximated as a deep intrusive body. The Empire stock appears as a sub-lenticular form with a major interface delineating a lower resistivity material at a depth of approximately 2400 meters below the datum. A steep rise in the basal material between the two stocks may be indicative of a fault as a set of faults are exposed at the surface in this area. In general, the resistivities in the southwest corner of the Marysville area are extremely low ($\sim$10 Ω-m) even at the very long MT periods. The shales, etc., in this region can be expected

TABLE E.10. AMT Type Curve Inversion Results

	ρ ± s (Ω - m)	t ± s (m)		ρ ± s (Ω - m)	t ± s (m)		ρ ± s (Ω - m)	t ± s (m)
AMT 5N-S	8.4 ± 130	5.4 ± 85	AMT 20N-S	17 ± 450	5.8 ± 150	AMT 50	67 ± 150	16.5 ± 45
	4720 ± 26K	710 ± 170		24.4K ± 702K	2160 ± 290		900 ± 210	740 ± 90
	47 ± 18			46 ± 50			24 ± 12	
AMT 9E-W	130 ± 190	27 ± 43	AMT 37N-S	250 ± 370	41 ± 70	AMT 54	5 ± 110	4 ± 80
	3700 ± 770	2110 ± 210		9620 ± 4390	1890 ± 190		4370 ± 68K	410 ± 180
	24 ± 38			110 ± 60			63 ± 15	
AMT 10N-S	69 ± 730	95 ± 110	AMT 39N-S	90 ± 4760	11 ± 580	AMT 71R	76 ± 360	6.5 ± 30
	990 ± 255	680 ± 150		120K ± 780K	2690 ± 1390		476K ± 1020K	7010 ± 510
	54 ± 17			5810 ± 1180			140 ± 250	
AMT 14	290 ± 1650	42 ± 250	AMT 43N-S	110 ± 500	16 ± 110			
	44.8K ± 185K	2135 ± 500		410 ± 90	440 ± 150			
	590 ± 190			59 ± 14				

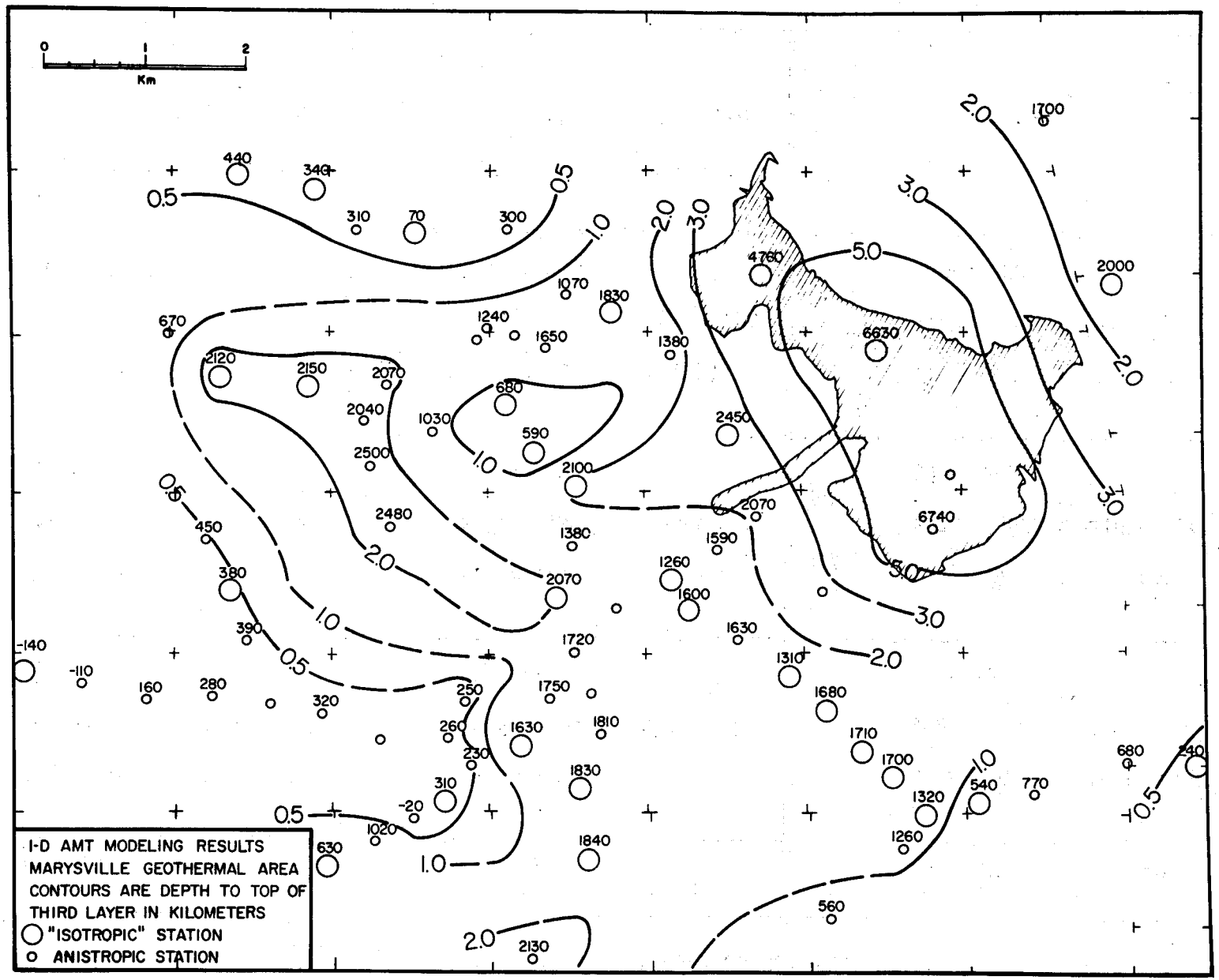

FIGURE E.38. Plan View of Depth to Third Layer Interface from AMT Measurements. A datum of 5000 feet above sea level has been chosen.

to have a low resistivity but the low resistivity seen at extremely long periods is not understood at present. Paucity of data in this region further complicates any attempt at interpretation at this time.

Figure E.39 shows three cross sections marked AA', BB' and CC' on Figure E.27. These cross sections have been interpreted using one-dimensional interpretations of AMT data and include information from other geophysical and geological surveys by Blackwell et al. (1973). In particular, the apparent form of the Empire stock with a low (100 Ω-m) interface at depth and possible fault between the Empire and Marysville stock are shown rather dramatically, particularly in profile BB'.

Data Interpretation - Two-Dimensional Results

To determine the effects of lateral inhomogenieties on the MT/AMT data, we have attempted to model profile AA' (Figure E.27) with a 2-D transmission surface analogy modeling program. Figures E.40 and E.41 show the models and station locations for which apparent resistivity data are presented. Theoretical and observed apparent resistivity data are shown in Figures E.42, E.43 and E.44 as follows:

Model Station No.	MT Station No.	AMT Station No.
S_1	MT-5	AMT 31a
S_2	MT-2	AMT 16
S_3	MT-12	AMT 71

The two-dimensional model shown in Figure E.40 was constructed using MT/AMT one-dimensional modeling results along with results of magnetic data modeling by Blackwell et al. (1974). A 1000 Ω-m half-space at a depth of approximately 13 km was initially included in the model to represent a fairly resistive basement material. Examination of the TE and TM modes from this model shows general agreement with the observed data at AMT frequencies. In the MT frequency range, however, the fit becomes poorer, although the general shapes of curves are fairly well preserved.

Model 2, shown in Figure E.41, was used for modeling at frequencies lower than 1 Hz. At these frequencies the model can be simplified because of associated large skin depths. Note that the 1000 Ω-m basal half space has been omitted in this model. Model 2 results for both modes are also shown in Figures E.42, E.43, and E.44 for the three selected stations.

The excellent fit of the observed data to Model 1 results at long periods for station S_3 in both modes and for stations S_1 and S_2 for the E-parallel mode, indicate a need to at least deepen the 1000 Ω-m basal half space. Station S_3 exhibits a fairly good fit in both modes with no half space at all; however, the E-perpendicular mode for stations S_1 and S_2

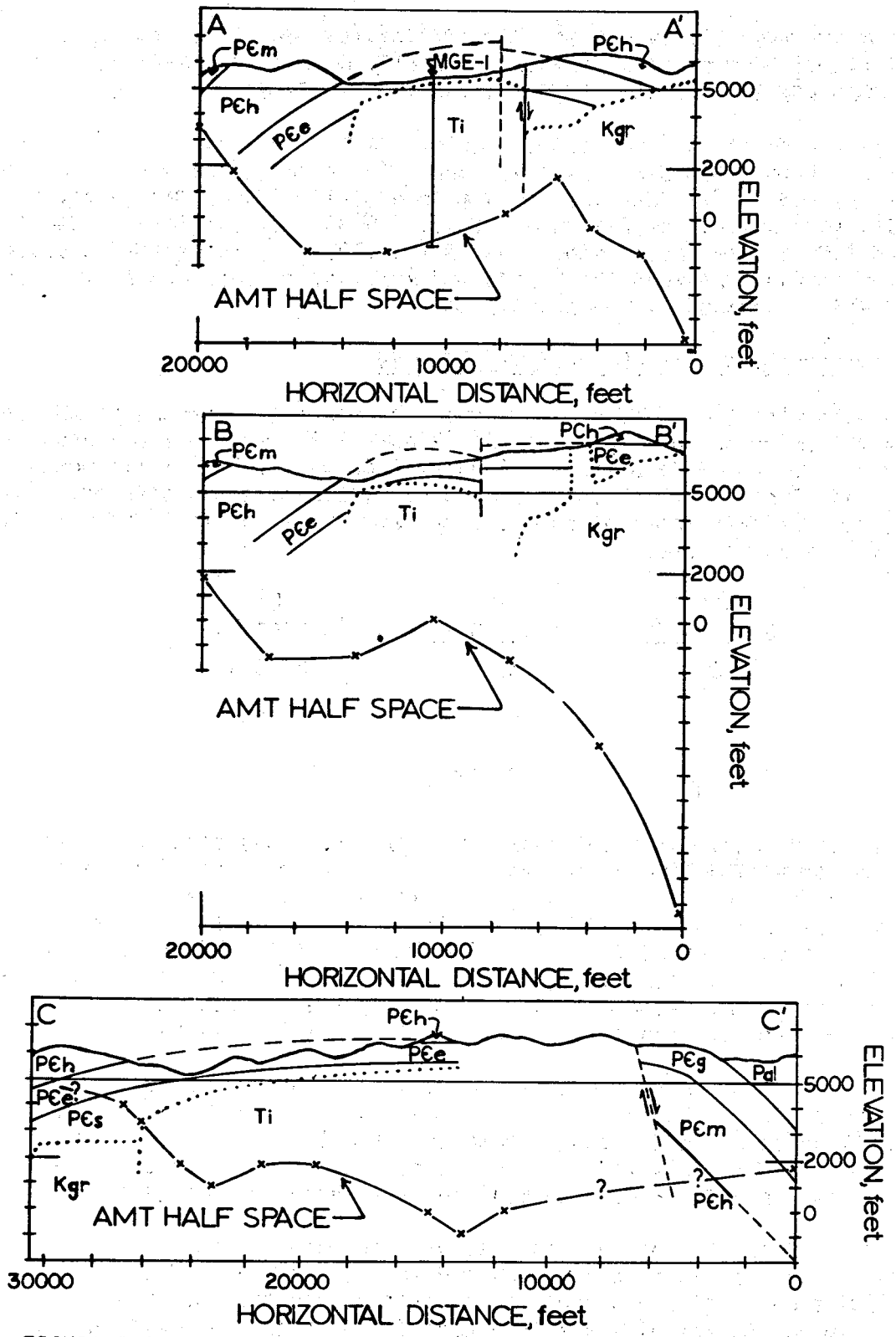

FIGURE E.39. Three Cross Sections of the Marysville Area Based Primarily on the MT/AMT Information

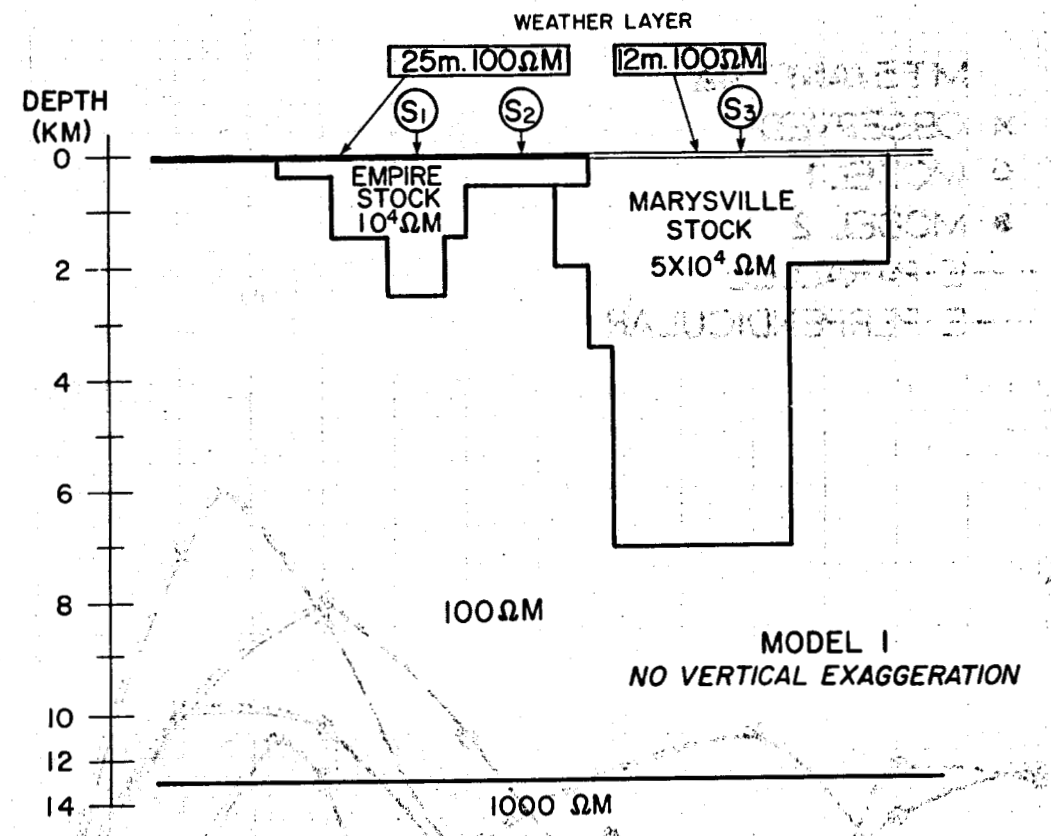

FIGURE E.40. Two-Dimensional Model 1

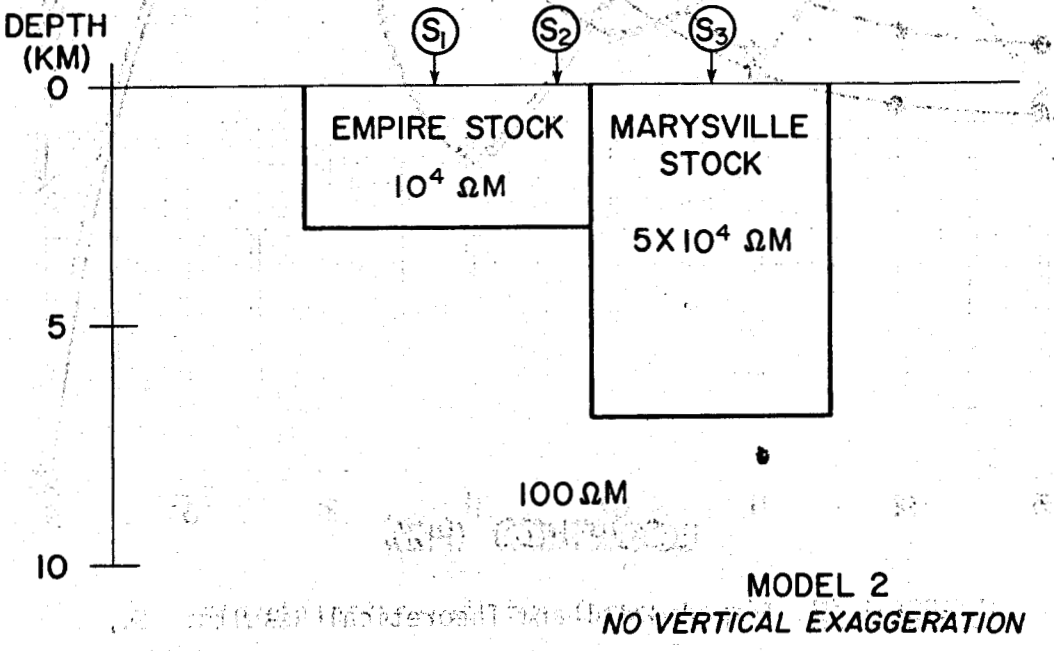

FIGURE E.41. Two-Dimensional Model 2

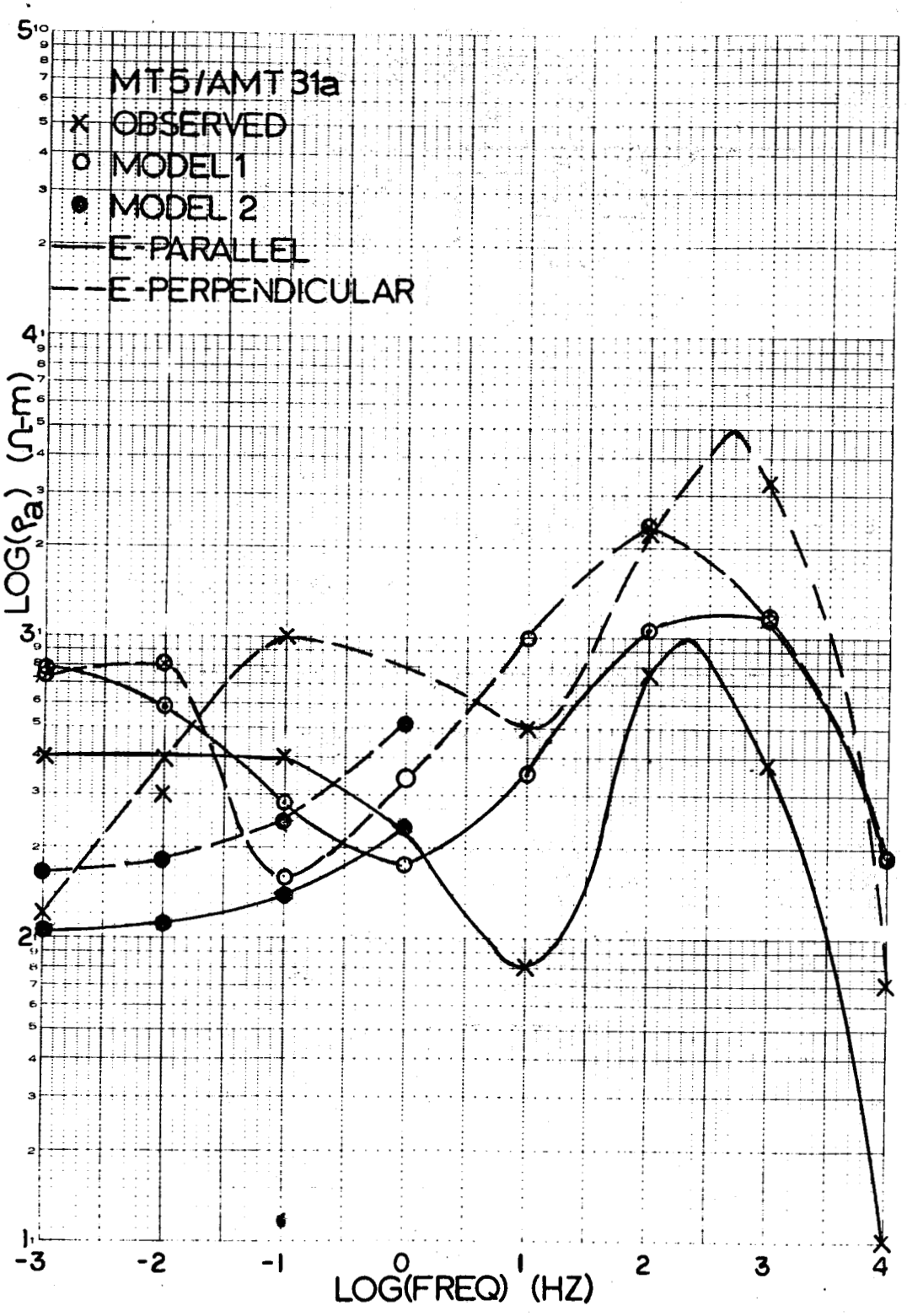

FIGURE E.42. Experimental and Theoretical Results: S_1

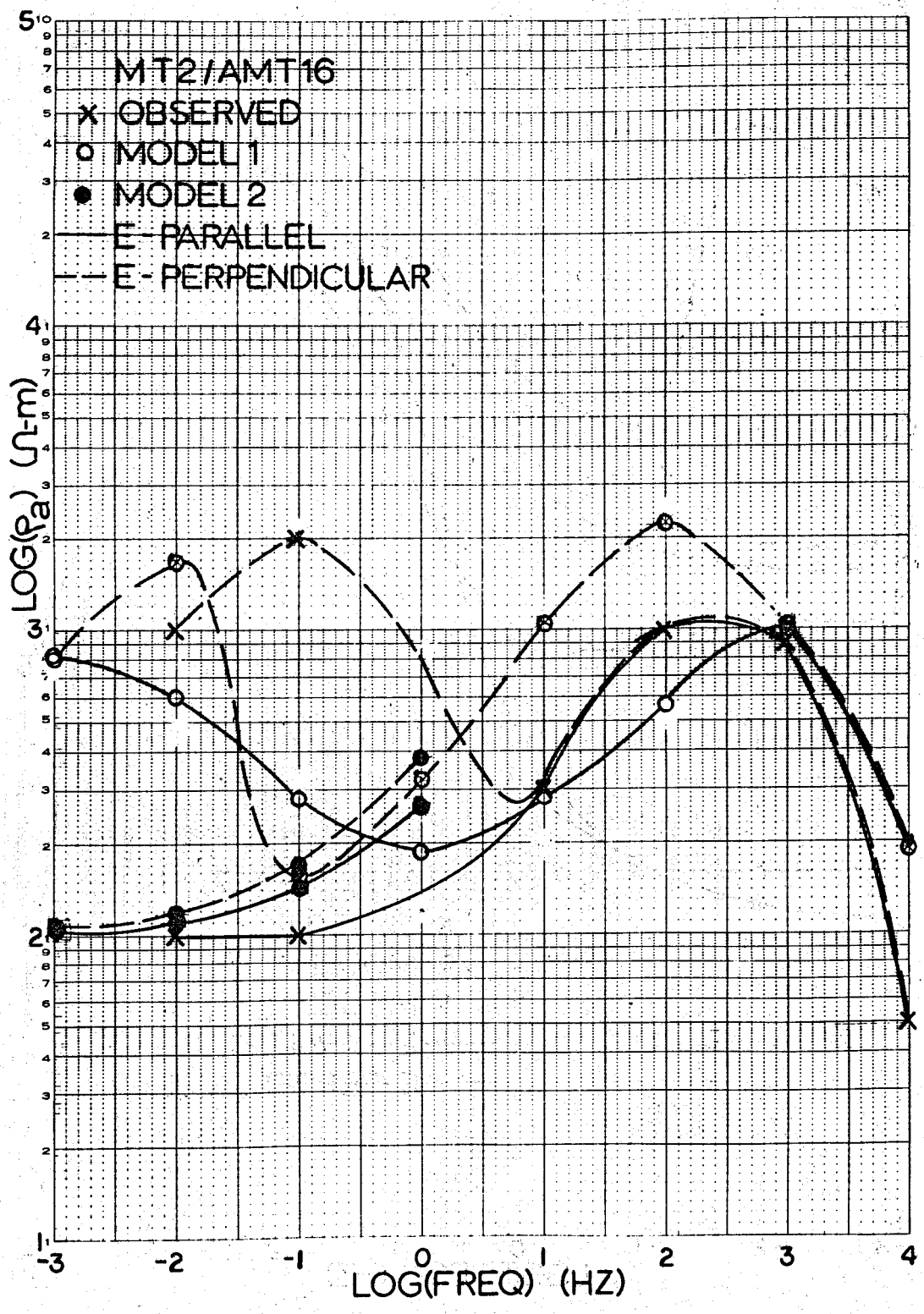

FIGURE E.43. Experimental and Theoretical Results: S_2

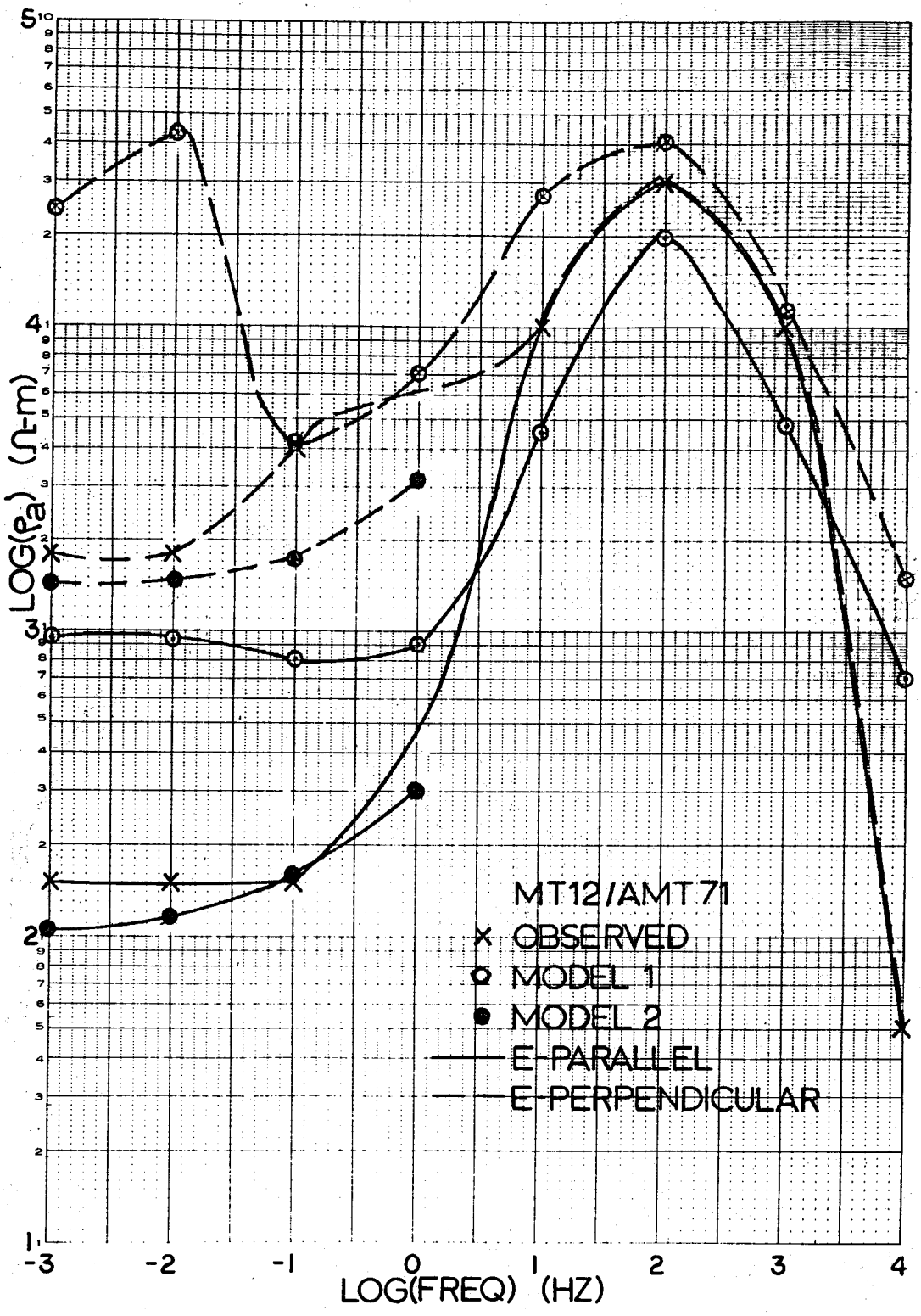

FIGURE E.44. Experimental and Theoretical Results: S_3

appear to require a more complex model to satisfy the observed data. Comparison of the long period results from both models suggests that at least the character of the observed curves can be approximated by the introduction of a higher resistivity material at depth. However, the shape of the observed curves is undoubtedly a reflection of three-dimensional conductivity structure both at depth and laterally, which can be modeled only approximately with a two-dimensional program.

In complicated two-dimensional geometries the TE mode will give a good indication of the vertical resistivity profile. Qualitative arguments would suggest that for three-dimensional geometries with a reasonable strike length, the apparent resistivities obtained from electric fields parallel to strike should still be indicative of the vertical resistivity profile.

Our data indicates that the apparent resistivities from the electric field parallel to strike agree generally with two-dimensional modeling results, suggesting that the vertical resistivity profile primarily controls apparent resistivities with lateral changes having a much reduced effect.

CONCLUSIONS

The MT/AMT resistivity data, combined with laboratory rock resistivity measurements, indicate the following:

1) A very thin veneer of weathered surficial material overlies the entire area covered in this survey. This veneer thins over the Marysville stock.

2) The Empire stock is clearly indicated in the data as a high resistivity material. Within the accuracy of the AMT data, no fracture zones are delineated. The Empire stock high resistivity material appears to extend to approximately 2.4 km in the vicinity of Lost Horse Creek. At this point, the AMT data indicates the transition to material of a low resistivity in the order to 100 Ω-m. This low resistivity material may be an actual material change or may represent a more extensively fractured medium than previously encountered at shallower depths in which hydrothermal water is flowing. The MT/AMT data of course cannot distinguish between the two (or more?) possibilities mentioned above.

   The Empire stock thins away from the Lost Horse Creek area. The thinning is less pronounced southward than eastward. The resistivity data is consistent with a model in which the Empire stock extends to and abutts against the Marysville stock.

   Other geophysical information must be relied on to determine the western boundary of the Empire stock, because of the paucity of MT-AMT data in this region, and the presence of low resistivity overlying formations lessens the exploration depth of the data. There

are indicators that the Empire stock extends to the south or southwest off the mapped area (Figure E.27) and thickens but again paucity of data in this region makes this conclusion speculative.

3) The Marysville stock appears as a thick intrusive plug. This stock seems to be underlain by low resistivity material (∿100 Ω-m); however, this could be a manifestation of three-dimensional effects and the stock may extend deeper than the modeled depth of 7 to 8.5 km.

4) At a depth of approximately 9 km, the MT data may indicate a transition to higher resistivity material (200-1000 Ω-m) in the study region. This material could extend to the west of the Empire stock.

5) The resistivity structure at depth in the southwest and southeast corners of the map is indeterminate because of the presence of near surface low resistivity material. The Marsh shale outcrops in both these areas, overlain in places by the Black Mountain and Greenhorn Mountain quartzites respectively. It is suspected that the AMT Soundings in these areas delineate the contact between the quartzite and the Marsh shale. A thin veneer of low resistivity weathered material controls the curve at the high frequencies, with the quartzite representing a fairly resistive intermediate layer of moderate thickness. The conductivity and thickness of the Marsh shale are apparently great enough so that penetration through this material is not achieved at the AMT frequencies. Complex geology in this area further complicates any interpretation.

6) Measurements along the ridge to the north of the drill site above Empire Creek provide models with depth to a low resistivity layer which approximately coincide with the contact of the Empire shale and the Spokane argillite, according to geologic cross-section CC' by Blackwell, et al. (1975). Both the Helena limestone and the Empire shale (sample Pεe8), which are the overlying formations in this area, have exhibited high measured resistivities in both laboratory and drill hole via Laterolog 7 measurements and presumably make up the resistive intermediate layering in this area. Again, a low conductivity surficial layer is present which controls the curves at high frequencies.

7) A low resistivity anomaly (∿20 Ω-m) in the vicinity of station MT 10 at the western edge of the study area appears to extend to at least 10^{-2} Hz. The skin depth for 20 Ω-m material at 10^{-2} Hz is 22.5 km indicating a deep seated low resistivity region and/or much lateral inhomogeneity.

8) We believe at this point that the data is inconsistent with previously suggested models of a "magma chamber" at shallow depths (2 to 3 km) under the exposed Empire shale. The experimental

resistivity values appear too large to be consistent with material at elevated temperatures. We do not understand the low ($\sim$10 Ω-m) values of resistivity in the southwest corner of Figure E.27. The paucity of data from various geophysical experiments (including MT/AMT) makes any conclusion highly tentative in this region. We feel that the area to the south and west of the area studied during 1974 should be investigated further to determine the entire structural picture at depth for this region.

9) We would speculate that the region below 2.4 km under the exposed Empire shale is the reservoir for a hydrothermal system and fracturing through the Empire stock ($\leq$2.4 km?) serves as a conduit for the hydrothermal system.

REFERENCES

Baagsaard, H., R.E. Folinsbee and J. Lipson, Potassium-argon dates of biotites from Cordilleran granites, Bull. Geol. Soc. Amer., 72, 689-702, 1961.

Bailey, R.C., Proc. Roy. Soc. Ser. A, 315, 185, 1970.

Bevington, P.R., Data Reduction and Error Analysis for the Physical Sciences. McGraw-Hill Book Co. Inc., New York, 1969.

Blackwell, D.D., Heat flow determinations in the northwestern United States, J. Geophys. Res., 4, 74, 992-1007, 1969.

Blackwell, D.D., et. al., Geophysical Geothermal exploration at Marysville Geothermal area; 1973 results, Technical Report - April, 1974 under NSF-RANN Grant No. GI 38972.

Brace, W.F., Orange, A.S., and T. R. Madden. The effect of pressure on the electrical resistivity of water saturated crystalline rocks, J. Geophys. Res., 70, 22, 5669-5678, 1965.

Cagnaird, L., Basic theory of the magnetotelluric method of geophysical prospecting, Geophys., 18, 605-635.

Draper, N.R., and H. Smith, Applied Regression Analysis, John Wiley and Sons, Inc., New York, 1966.

Eardley, A.J., Structural Geology of North America, Harper and Row, New York, 1962.

Glenn, W. E., Ryu, J., Ward, S.H., Peeples, W.J., and Phillips, R.J., The inversion of vertical magnetic dipole data. Geophys., 38 1109-1129, 1973.

Hamilton, W.C., Statistics in Physical Sciences, Estimation, Hypothesis Testing, and Least Squares, Ronald Press Co., New York, 1964.

Inman, J.K., Ryu, J., and S.H. Ward, Resistivity Inversion, Geophys., 38, 6, p. 1088-1108, 1973.

Jackson, D.D., Interpretation of inaccurate, insufficient and inconsistent data, Geophys. J. Roy. Astron. Soc., 28, 97-109, 1973.

Jenkins, G.M., and D.G. Watts, Spectral Analysis and its Applications, Holden Day, San Francisco, 1968.

Johnson, I.M., and D.E. Smylie, Geophys. J. Roy. Astron. Soc., 22, 41, 1970.

Knopoff, L., An aversion to inversion, in Mantle and Core in Planetary Physics, Academic Press, New York, 1971.

Kunetz, G., Correlation et recurrence des variations des courants tellureques et du champ magnetique, Actes du Congres de Lux, 72 eme Seo. de l'Association pour l'Advancement des Sciences, 1953.

Lanczos, C., Linear Differential Operators, D. Van Nostrand Co., Princeton, New Jersey, 1961.

Marquardt, Donald W., An algorithm for least squares estimation on non-linear parameters. J. Soc. Indust. Appl. Math., 11, 2, 431-441, 1963.

Mazzella, F.E., A thermal and gravity model of a geothermal anomaly near Marysville, Montana, M.S. Thesis, Southern Methodist University, 1974.

Parker, R.L., Geophys. J. Roy. Astron. Soc., 22, 121, 1970.

Patrick, F.W., and F. S. Bostick, Jr., Magnetotelluric Modeling Techniques: Elec. Geophys. Res. Lab., Tech. Rept. No. 59, Elec. Res. Cntr., Univ. Texas, Austin, Texas, 100p. 1969.

Rankin, D., and I.K. Reddy, Crustal conductivity anomaly under the Black Hills: A Magnetotelluric study, Earth Plan. Sci. Letters, 20, 275-279, 1973.

Schlumberger, M., and G. Kunetz, Variations rapides simultanus de champ tellurique en France et a Madagascar, C. R. Acad. Sci. Paris, 223, 551-553, 1946.

Smith, B., Ph.D. Thesis, University of Utah, 1974.

Wiggins, R.H., The generalized inverse problem, Rev. Geophys. and Space Sci., 10, 1, 251-286, 1972.

UNIVERSITY OF ALBERTA SUBCONTRACTOR'S REPORT TO THE UNIVERSITY OF UTAH: RESULTS OF MT DATA COLLECTION

by
D. Rankin
University of Alberta

September 1975

APPENDIX E.1

RESULTS OF MT DATA COLLECTION

D. Rankin
University of Alberta

MAGNETOTELLURIC SURVEY

A magnetotelluric survey was conducted in the Marysville area in the summer of 1974. This is a region of abnormally high heat flow and was considered a suitable target for geothermal exploration. The magnetotelluric method was used because of its potential for determining resistivity anomalies which are thought to be associated with thermal anomalies. The area itself is rugged. Considerable difficulty was encountered in locating suitable recording sites and in transporting the instruments. Usable data was obtained at 12 sites and these stations are shown on the map in Figure E.45, except for station MT 11 which is near Helena, Montana and is used as a control.

Harmonic analysis of the data was carried out using the Fast Fourier technique. Tensor impedances were computed and the principle directions, the skew and β factor were obtained. The apparent resistivities in the principle directions are shown for stations 1, 7 and 10 in Figures E.46, E.47 and E.48 and the associated parameters in Figures E.49 and E.50. The apparent resistivity values in the major direction are contoured in Figures E.51, E.52 and E.53 for periods of 0.1, 10 and 100 sec.

Rankin and Reddy have shown (work to be submitted for publication) that for continuously variable conductivity in the lateral direction, a two or three dimensional structure can be interpreted to a good first order approximation by one-dimensional considerations.

From this result and those shown in Figures E.51, E.52 and E.53 it appears that if a subsurface thermal anomaly exists, it lies

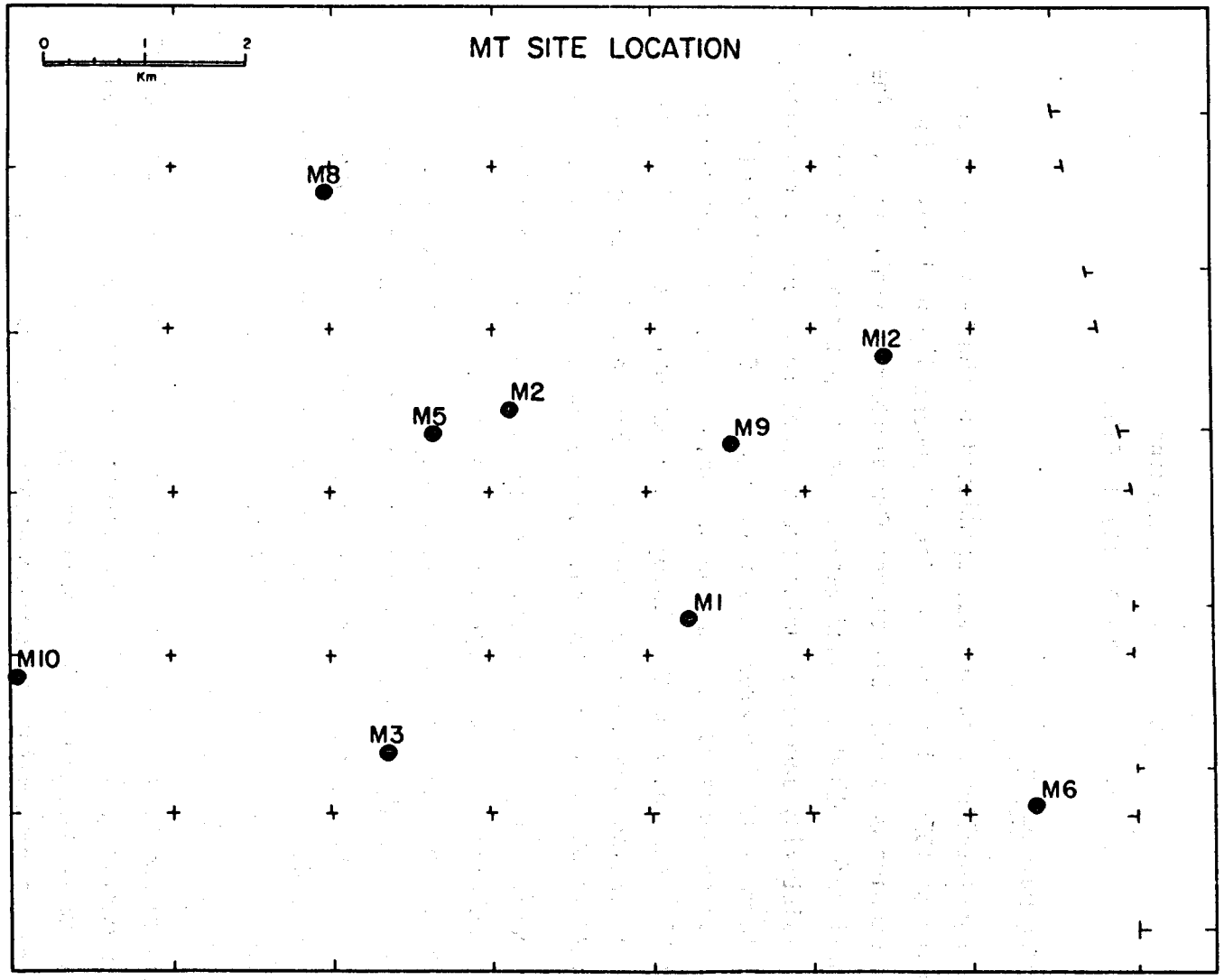

FIGURE E.45. Map of MT Site Locations

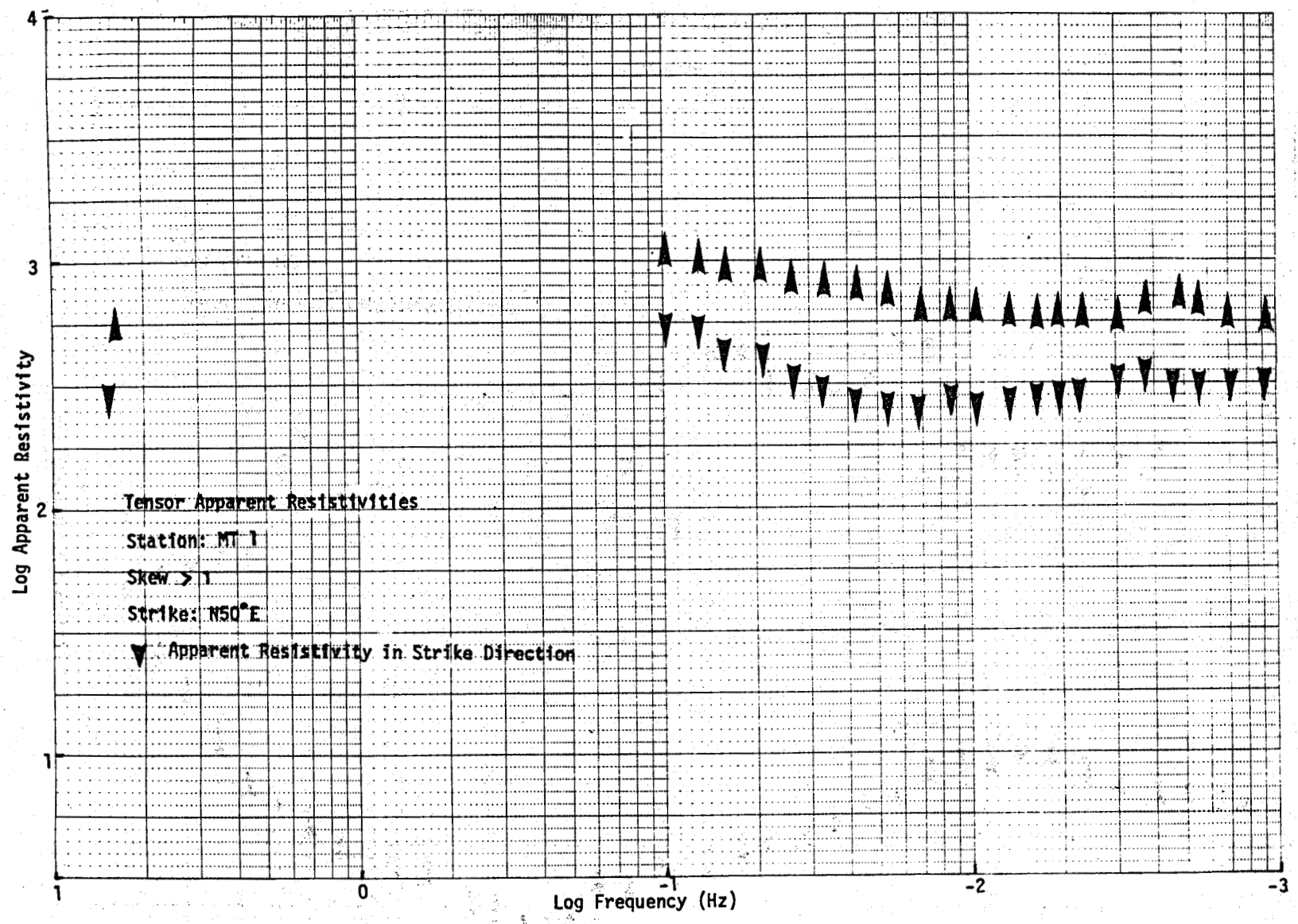

FIGURE E.46. Apparent Resistivities for MT Station 1

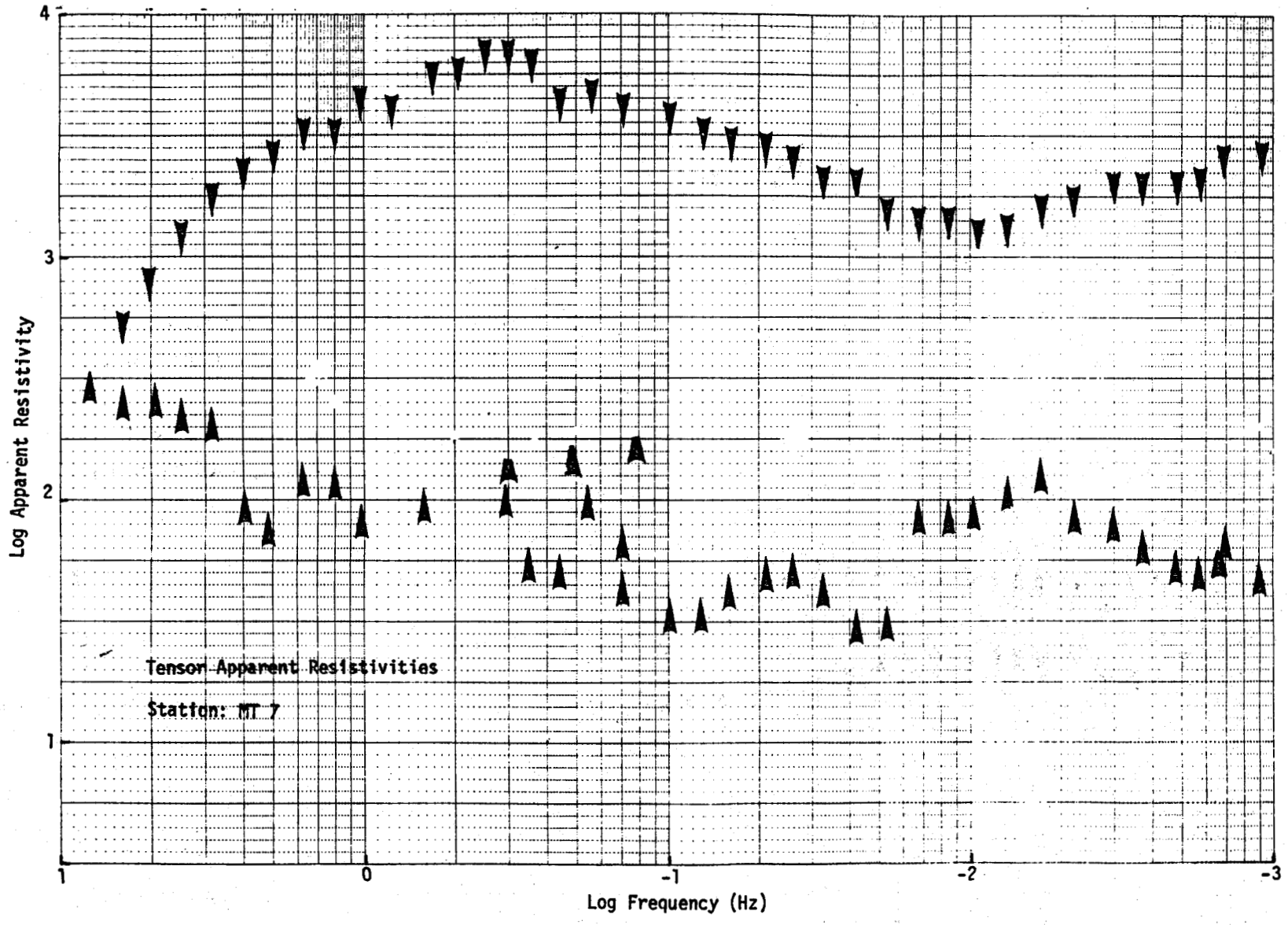

FIGURE E.47. Apparent Resistivities for MT Station 7

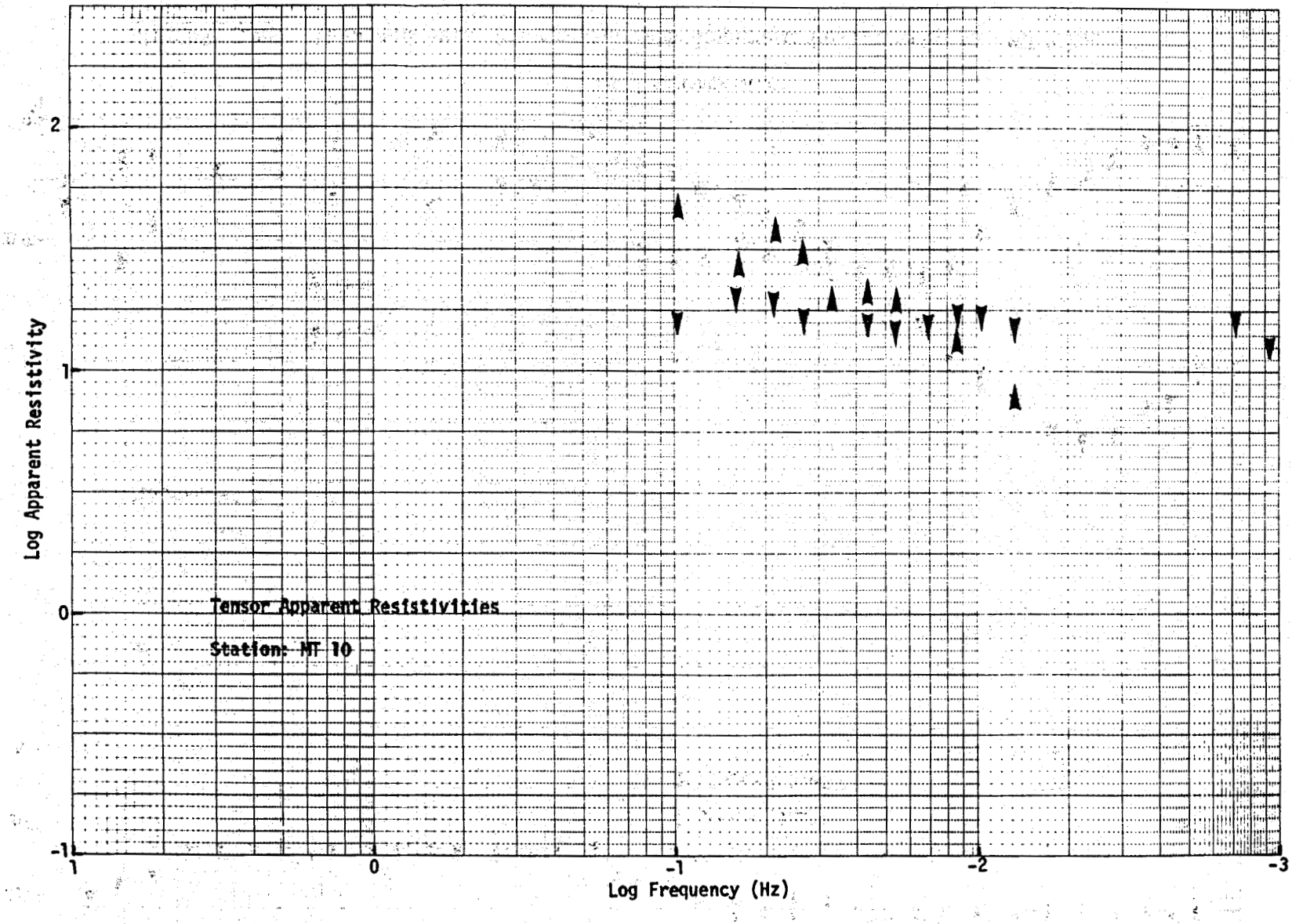

FIGURE E.48. Apparent Resistivities for MT Station 10

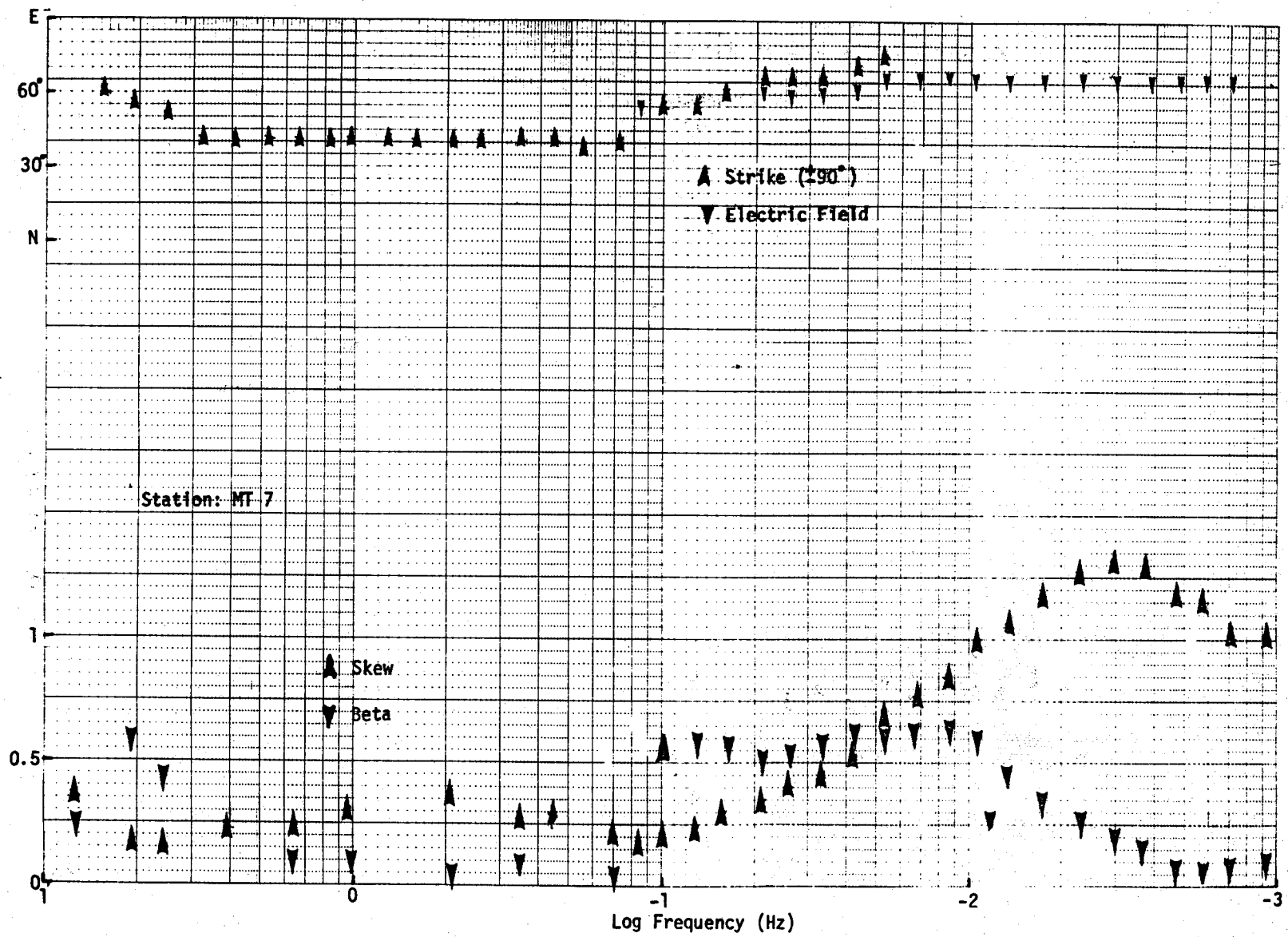

FIGURE E.49. Skew and Beta Associated with Apparent Resistivity for MT Site 7

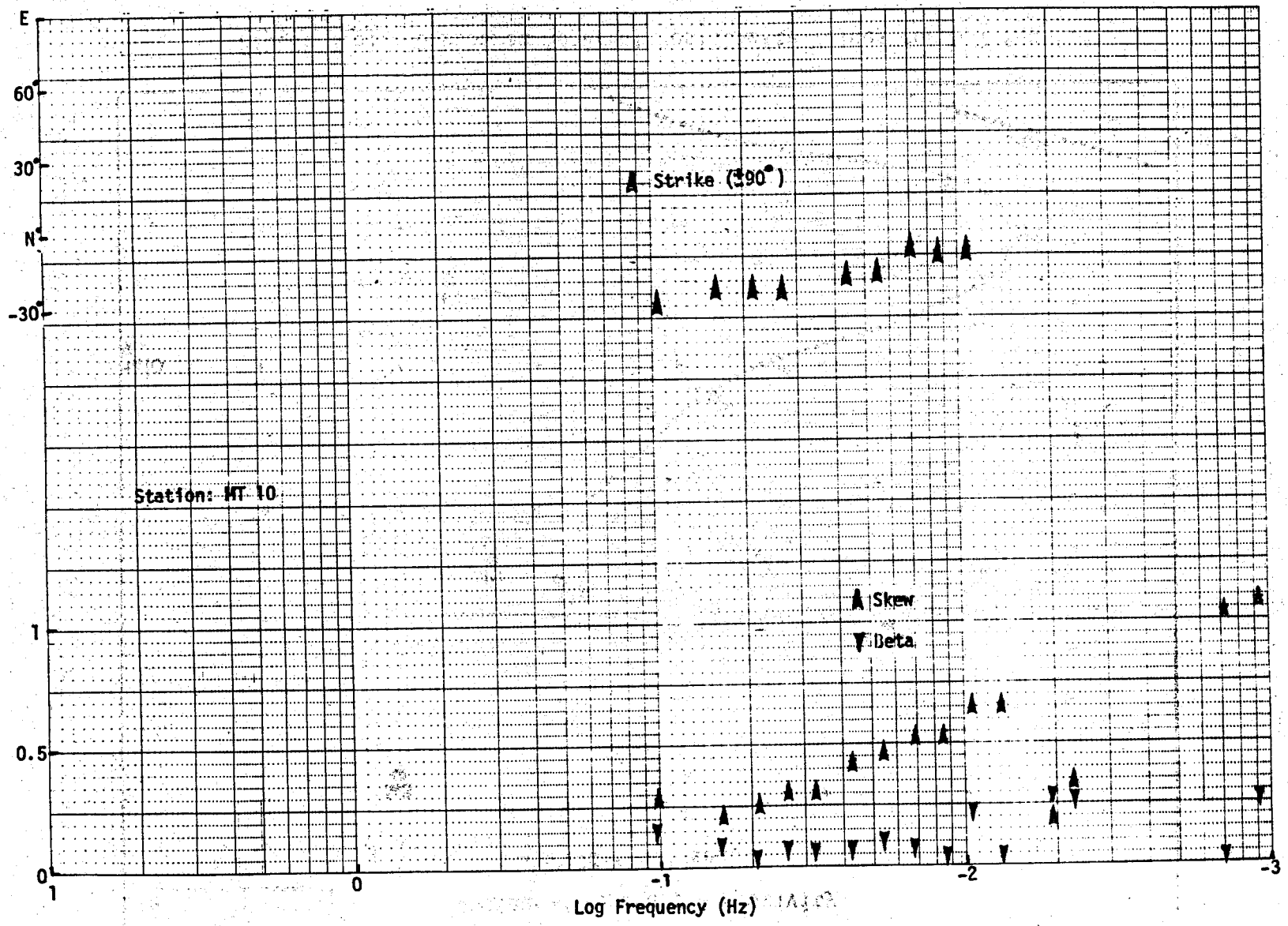

FIGURE E.50. Skew and Beta Associated with Apparent Resistivity for MT Site 10

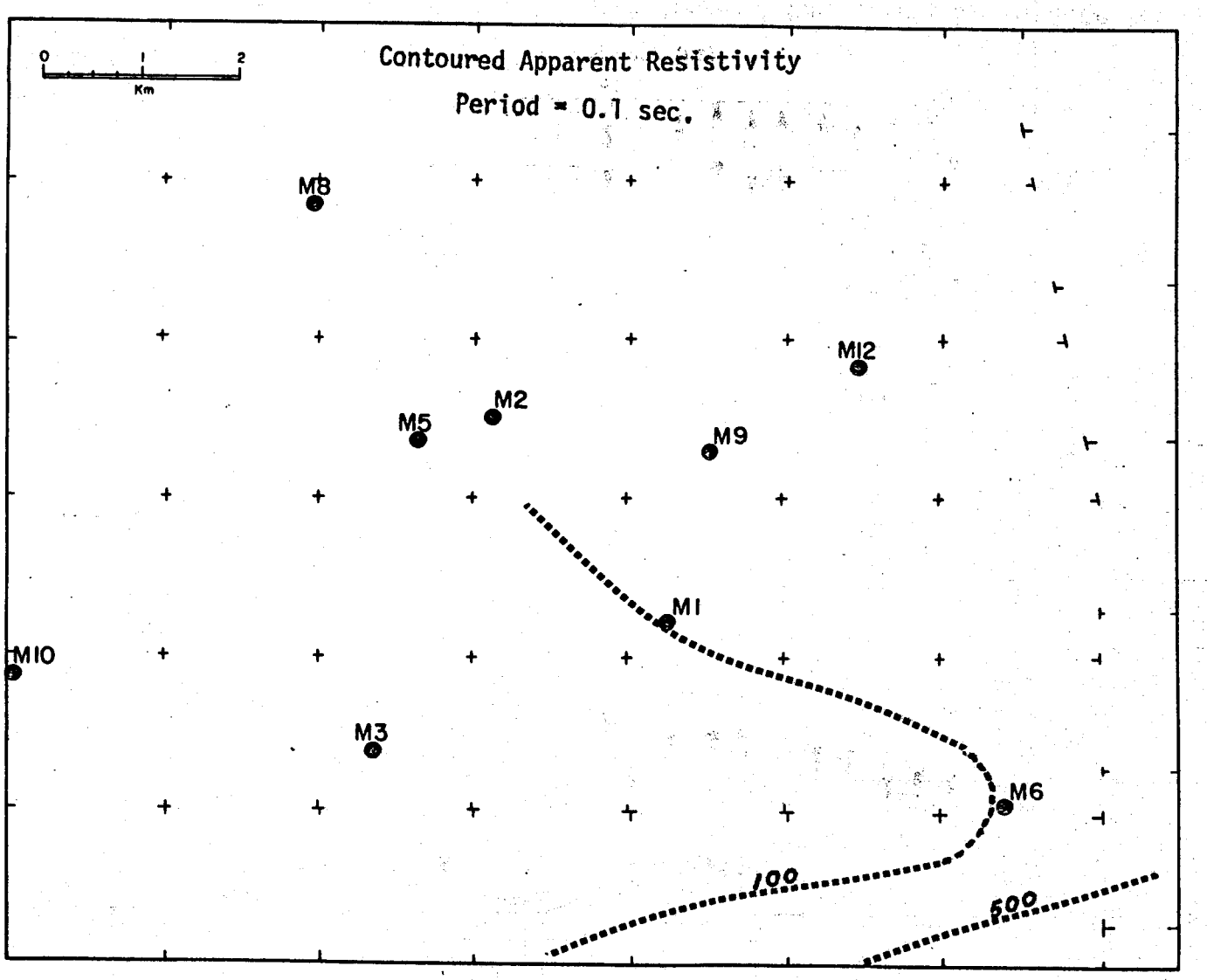

FIGURE E.51. Contoured Apparent Resistivity Values for 0.1 Sec

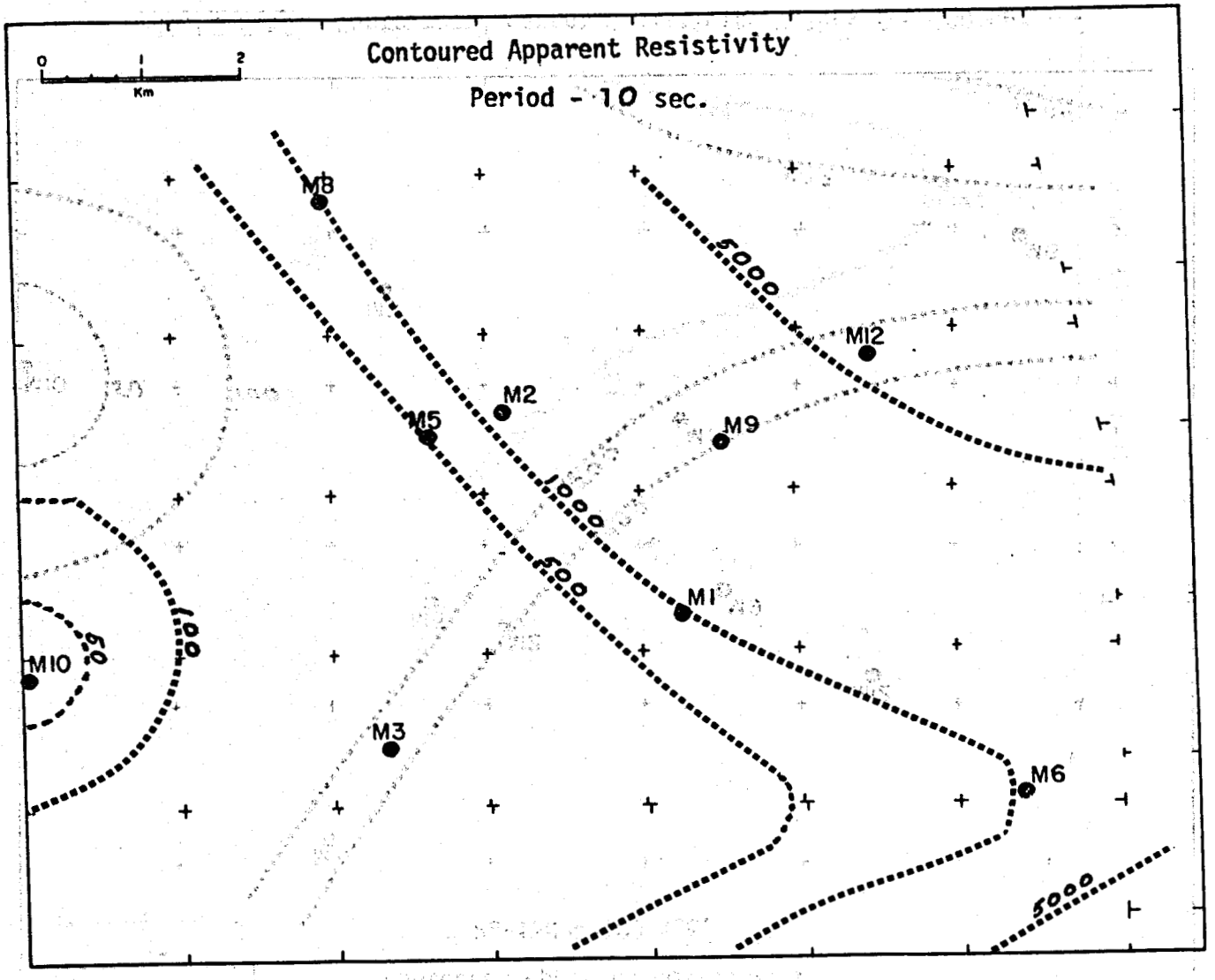

FIGURE E.52. Contoured Apparent Resistivity Values for 10 Sec

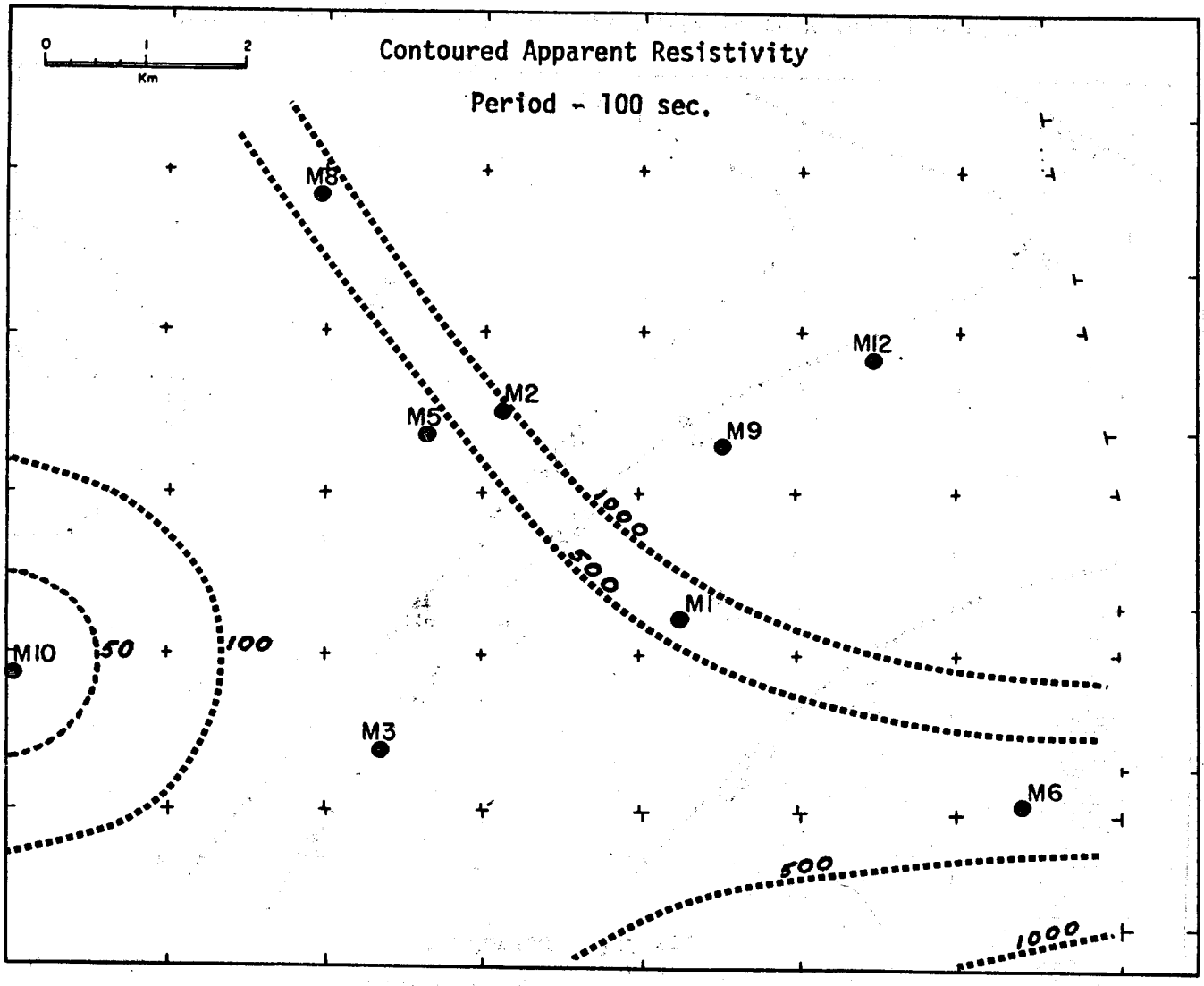

FIGURE E.53. Contoured Apparent Resistivity Values for 100 Sec

considerably to the west of the surface manifestation, which was located by heat flow measurements, to be near the Drill Site. These plots show, however, that the Drill Site is located near a region of rapidly changing resistivity which is interpreted to be a fault structure along which heat might conduct more readily to produce the superficial effect which is measured near surface. A similar result was obtained by Rankin and Reddy (1973) in the Black Hills region in which the hot springs shown at "H" in Figure E.54 is approximately 30 km from the thermal anomaly shown at "C." The negative results of this work with respect to the anomaly at the Drill Site is consistent with the results of the microseismic study.

It would be useful to extend this survey to the region about Station MT 10.

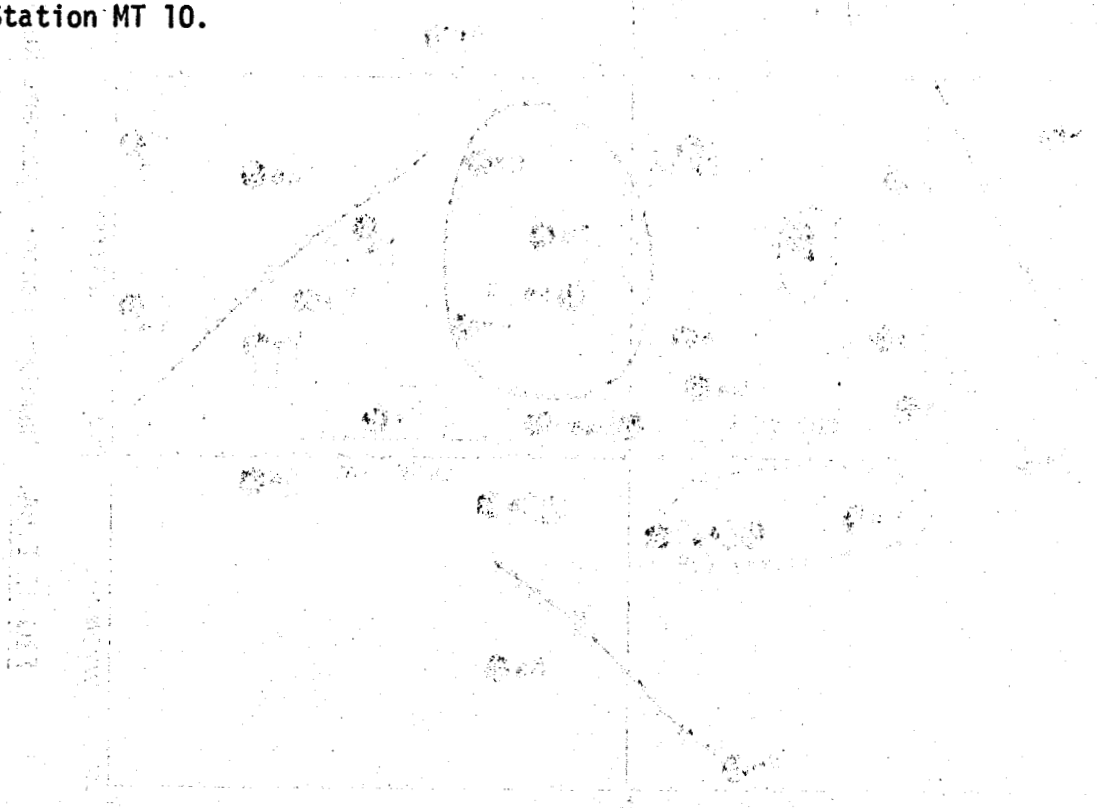

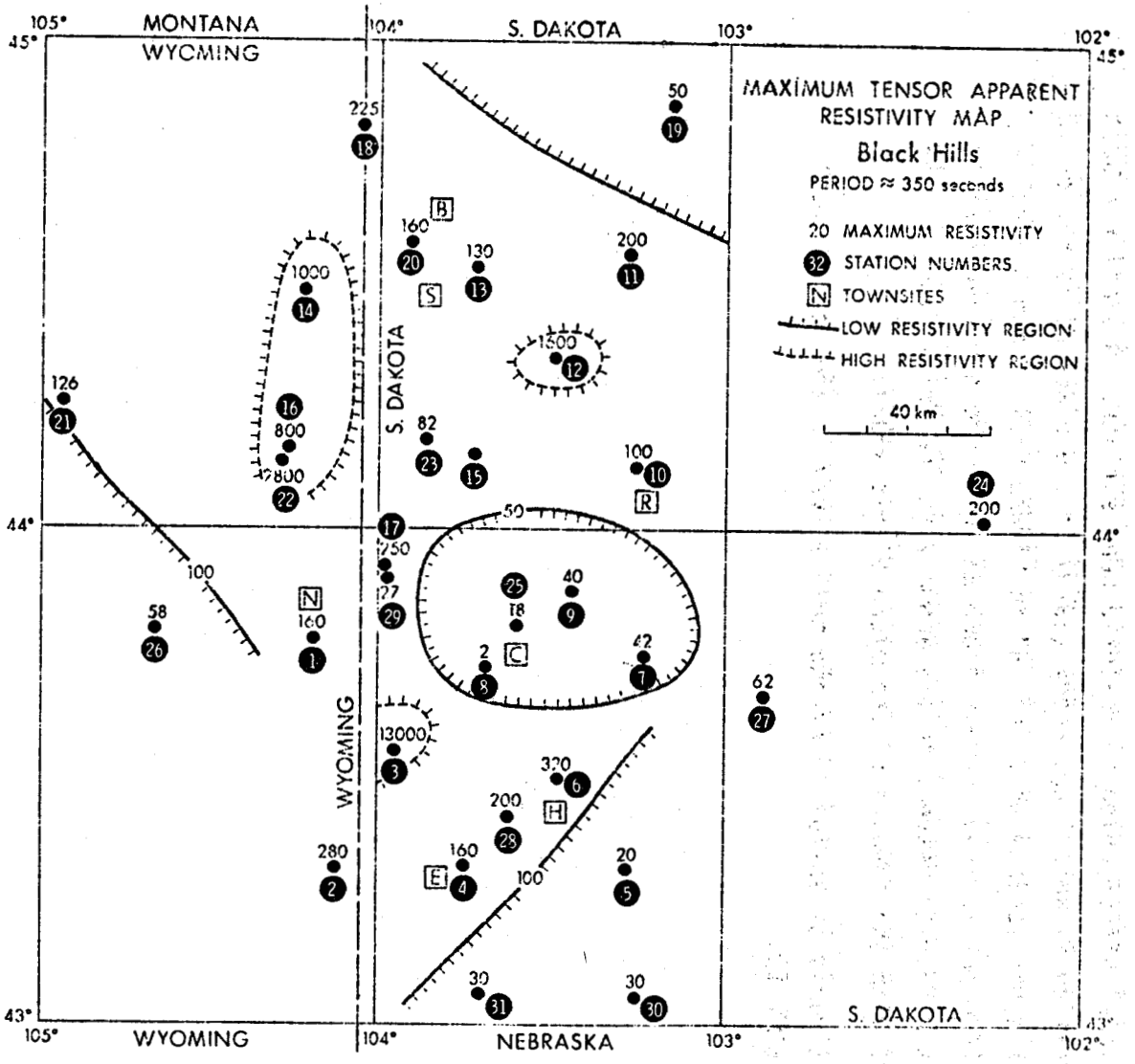

FIGURE E.54. Maximum Tensor Apparent Resistivity Map

APPENDIX E.2

BASIC MAGNETOTELLURIC THEORY

The basic theory of magnetotelluric fields is contained in a boundary value problem involving Maxwell's equations and the resultant electromagnetic wave equation. The relationship between orthogonal components of the electric and magnetic fields measured at the surface of the earth are a measure of the electrical properties of the earth.

The reference coordinate frame for the theoretical development which follows is a right-handed cartesian system with the positive x axis northward and z vertically downward. The earth is initially considered to consist of N horizontally stratified, isotropic, homogeneous conducting layers above a basal half space. The origin of the coordinate system lies on the upper surface of the first layer. The rationalized MKS system will be used in the theoretical discussion.

The natural electromagnetic disturbace fields are thought to originate in the ionosphere or magnetosphere at altitudes of 100 kilometers and greater and these fields then propagate downward to the surface of the earth. The similarity of the magnetotelluric field over large regions at the earth's surface was noticed by Schlumberger and Kunetz (1946) and Kunetz (1953); thus Cagnaird (1953) made the *a priori* assumption that the natural electromagnetic disturbances could be treated as plane waves.

Since the layers of the model are assumed to contain no primary sources, Maxwell's equations in the i^{th} layer are given by:

$$\nabla \times \vec{E} = -\frac{\partial \vec{B}}{\partial t} \qquad \text{A2.1}$$

$$\nabla \times \vec{H} = \vec{J} + \frac{\partial \vec{D}}{\partial t} \qquad \text{A2.2}$$

$$\nabla \cdot \vec{D} = \rho = 0 \qquad \text{A2.3}$$

$$\nabla \cdot \vec{B} = 0 \qquad \text{A2.4}$$

where $\vec{J} = \sigma\vec{E}$, $\vec{D} = \epsilon\vec{E}$, and $\vec{B} = \mu\vec{H}$.

For a steady state sinusoidal time dependence of the form $e^{-j\omega t}$ for the electric and magnetic fields, equations A2.1 and A2.2 can be written:

$$\nabla \times \vec{E} = j\omega\mu\vec{H} \qquad \text{A2.5}$$

$$\nabla \times \vec{H} = \sigma\vec{E} - j\omega\epsilon\vec{E}. \qquad \text{A2.6}$$

Taking the curl of equations A2.5 and A2.6 and assuming ϵ and σ are constant within each layer, we obtain two vector Helmholtz equations

$$\nabla^2 \begin{bmatrix} \vec{E} \\ \vec{H} \end{bmatrix} + k^2 \begin{bmatrix} \vec{E} \\ \vec{H} \end{bmatrix} = 0 \qquad \text{A2.7}$$

where $k^2 = j\omega\sigma\mu + \epsilon\mu\omega^2$. Solutions of the Helmholtz equations are given by:

$$\begin{bmatrix} \vec{E} \\ \vec{H} \end{bmatrix} = \begin{bmatrix} \vec{E}_o \\ \vec{H}_o \end{bmatrix} e^{j\vec{K}\cdot\vec{r} - j\omega t} \qquad \text{A2.8}$$

where

$$\vec{K} = (k_x, k_y, k_z,)$$

$$\vec{r} = (x, y, z).$$

The frequencies considered in magnetotelluric (but not audio-magnetotelluric) methods are nearly always less than 10 Hz. Using normal parameters of conductivity, permittivity, and permeability appropriate to materials composing the earth, the displacement currents are negligible in comparison the conduction currents for the low frequencies considered herein

$$|j\omega\sigma\mu| >> |\epsilon\mu\omega^2|.$$

The Helmholtz equations then reduce to diffusion equations with a diffusion

constant (skin depth) given by

$$\delta = \sqrt{\frac{2}{\mu\omega\sigma}} \, . \qquad \text{A2.9}$$

Since the wave number of the electromagnetic field in air is much less than in the earth,

$$k^2_{Air} = \varepsilon_o\mu_o\omega^2 << | \, j\omega\mu\sigma \, | = k^2_{Earth}$$

at the air-earth interface the incident plane waves are refracted and propagate through the earth nearly parallel to the vertical axis for nearly all incident angles.

For the geometry and conditions stated above, $\vec{E}$ and $\vec{H}$ are independent of x and y and thus all derivatives of the field with respect to x and y vanish. Thus, in the i^{th} layer a solution of equation A2.7 is given by

$$E_{1y} = E_o[\exp(-ik_{1z}z) + R_{TE}\exp(+ik_{1z}z)]\exp(-ik_{1x}x + i\omega t), \qquad \text{A2.10}$$

in which E_o is the amplitude of the incident electric field and R_{TE} is the reflection coefficient for perpendicular polarization defined as $R_{TE} = E_{reflected}/E_{incident}$. Using this solution and Eqs. A2.5 we obtain the solution for the magnetic field as

$$H_{1x} = \frac{k_{1z}E_o}{\mu\omega}[\exp(-ik_{1z}z) - R_{TE}\exp(+ik_{1z}z)]\exp(-ik_{1x}x + i\omega t). \qquad \text{A2.11}$$

If we take the ratio of tangential electric and magnetic fields on the upper side of the surface at z = 0, we obtain

$$\left.\frac{E_{1y}}{H_{1x}}\right|_{z=0} = \frac{\mu\omega}{k_{1z}}\left(\frac{1+R_{TE}}{1-R_{TE}}\right) = \frac{Z_1}{\cos\theta_1}\left(\frac{1+R_{TE}}{1-R_{TE}}\right), \qquad \text{A2.12}$$

where Z_1 is the impedance of the upper region. In the lower region, we have

$$E_{2y} = E_oT_{TE}\exp(-ik_{2z}z - ik_{2x}x + i\omega t),$$

and

$$H_{2x} = \frac{k_{2z}E_oT_{TE}}{\mu\omega}\exp(-il_{2z}z - ik_{2x}x + i\omega t), \qquad \text{A2.13}$$

where T_{TE} is the amplitude transmission coefficient for perpendicular polarization. Since we must have $k_{1x} = k_{2x}$ in the limit at $z = 0$, then we find

$$\left.\frac{E_{2y}}{H_{2x}}\right|_{z=0} = \frac{\mu\omega}{k_{2x}} = \frac{Z_2}{\cos\theta_2} = Z_2', \qquad \text{A2.14}$$

and Z_2 is the impedance of the lower region. At $z = 0$, tangential E and H must be continuous, therefore we find

$$R_{TE} = (Z_2 - Z_1)/(Z_2 + Z_1). \qquad \text{A2.15}$$

We now extend our lower half space to a model of the Earth which is composed of a number of parallel homogeneous plane layers. For any layer p we have a solution

$$E_{py} = E_o[A_p\exp(-ik_{pz}z) + B_p\exp(+ik_{pz}z)]\exp(-ik_{px}x + i\omega t),$$

$$H_{px} = \frac{E_o}{I_p}[A_p\exp(-ik_{pz}z) - B_p\exp(+ik_{pz}z)]\exp(-ik_{px}x + i\omega t), \qquad \text{A2.16}$$

where I_p is the intrinsic impedance of the p^{th} layer. If Z_p is the input impedance at the p^{th} interface, then at $z = 0$

$$Z_1 = \left.\frac{E_{oy}}{H_{ox}}\right|_{z=0} = I_o\left(\frac{1+R_{TE}}{1-R_{TE}}\right)$$

$$Z_1 = \left.\frac{E_{1y}}{H_{1x}}\right|_{z=0} = I_1\left(\frac{A_1+B_1}{A_1-B_1}\right) = I_1\left(\frac{1+B_1/A_1}{1-B_1/A_1}\right). \qquad \text{A2.17}$$

To solve for Z_1, we must determine the unknown ratio B_1/A_1. At the interface $z = d_1$

$$Z_2 = \left.\frac{E_{1y}}{H_{1x}}\right|_{z=d_1} = I_1\left(\frac{e^{i2\phi_1}+B_1/A_1}{e^{i2\phi_1}-B_1/A_1}\right), \qquad \text{A2.18}$$

where $\phi_1 = k_{1z}d_1$. Solving Eq A2.18 for B_1/A_1 and substituting into Eq. A2.17 we obtain

$$Z_1 = I_1 \quad \frac{Z_2 + iI_1 \tan \phi_1}{I_1 + iZ_2 \tan \phi_1} \qquad \text{A2.19}$$

This is a special case of the more general relation

$$Z_p = I_p \quad \frac{Z_p + iI_p \tan \phi_p}{I_p + iZ_{p+1} \tan \phi_p} \qquad \text{A2.20}$$

in which $\phi_p = k_{pz} d_p$; $2 \leq p \leq N$, in which p corresponds to the layer number and Z_{N+1} equal I_{N+1}.

The apparent resistivity of the medium can now be defined as:

$$\rho_\alpha(\omega) = \frac{1}{\omega\mu} \mid Z_1(\omega) \mid^2 . \qquad \text{A2.21}$$

The apparent resistivity thus represents a weighted resistivity value for all layers and is the resistivity of an equivalent homogeneous half space at a particular frequency.

APPENDIX E.3

THE INVERSE PROBLEM

INTRODUCTION

Much effort has been expended in solving classical boundary value problems to find analytic solutions for particular problem geometries.

We shall now attempt to delineate the inverse problem. Assuming that the forward problem for a particular geometry can be solved analytically or numerically, we now attempt to use this solution together with a given set of observations to determine the physical parameters of our model which yield a good approximation to our experimental results. Our understanding of the inverse problem has been greatly aided by the studies of Backus and Gilbert (1967,1968, 1970), Bailey (1970), Johnson and Smylie (1970), Parker (1970), Knopoff (1971), Wiggins (1972), and many others.

In this section we will cast the inverse problem into a general linear inverse problem with a simple matrix algebra which can, hopefully, estimate a number of the linear or quasilinear unknown parameters of the mathematical model of a physical system. For a detailed review of general linear inversion, the reader is referred to Wiggins (1972).

GENERALIZED LINEAR INVERSION

We shall assume a model, a mathematical abstraction of the real world which suffices for some geophysical observation, for the physical system under consideration. This model will, of necessity, be represented by a finite number of parameters x_i, $i = 1,M$ and we shall

denote a particular madel as

$$M_j\ (x_1, x_2, \ldots, x_m) = M_j(X), \qquad \text{A3.1}$$

where the subscript j represents the model for a particular combination of x_i. A rule which maps the model into gross predicted data, y^{pred}, shall be called a gross functional f and we have the relationship

$$y_j^{pred} = f\,[M_j(X)]. \qquad \text{A3.2}$$

The corresponding number representing actual physical observations is denoted by y_j^{obs}

One objective of our investigation is to find a set of parameters X for our particular model which minimize in some fashion the differences $|y_j^{obs} - y_j^{pred}|$ for all measurements. To achieve this minimization, we shall linearize our problem by expanding the gross functional in a Taylor's series and rejecting the second and higher order terms:

$$y_j^{obs} - y_j^{pred} = \sum_{i=1}^{M} \frac{\partial f[M(X)]}{\partial x_i}\,\Delta x_i; \qquad j = 1,\ldots,N. \qquad \text{A3.3}$$

The precesses of parameterization and linearization have now left us with a set of N simultaneous equations in M unknown which must be solved. We shall now adopt the following notation:

$$\Delta Y = \begin{bmatrix} y_1^{obs} - y_1^{pred} \\ y_2^{obs} - y_2^{pred} \\ \vdots \\ y_n^{obs} - y_n^{pred} \end{bmatrix} \qquad \Delta X = \begin{bmatrix} \Delta x_1 \\ \Delta x_2 \\ \vdots \\ \Delta x_m \end{bmatrix} \qquad \text{A3.4}$$

and

$$A = \begin{bmatrix} \frac{\partial M_1}{\partial x_1} & \frac{\partial M_1}{\partial x_2} & & \frac{\partial M_1}{\partial x_M} \\ \frac{\partial M_2}{\partial x_1} & \frac{\partial M_2}{\partial x_2} & & \frac{\partial M_2}{\partial x_M} \\ \vdots & & & \\ \frac{\partial M_N}{\partial x_1} & \frac{\partial M_N}{\partial x_2} & & \frac{\partial M_N}{\partial x_M} \end{bmatrix} \qquad \text{A3.5}$$

which allow us to write the simultaneous equations in matrix form

$$A\Delta X = \Delta Y \qquad \text{A3.6}$$

THE LEAST SQUARES INVERSE

The method of finding a least square inverse to linear and non-linear problems has been discussed in excellent developments by Hamilton (1964), Draper and Smith (1966), and Bevington (1969). Glenn et. al. (1973) and Inman, Ryu and Ward (1973) have given detailed accounts of the application to electromagnetic resistivity sounding problems. The linearized form of geophysical problem can be written as

$$[A] \langle \Delta x \rangle = \langle \Delta y \rangle + \langle e \rangle \qquad \text{A3.7}$$

Equation A3.7 represents a truncated Taylor Series expansion with the truncation error given by $\langle e \rangle$. When $\langle e \rangle$ contains small values, the least square solution of A3.7 for $\langle \Delta x \rangle$ is given by

$$\Delta X = \{[A]^T[A]\}^{-1}[A]^T \langle \Delta y \rangle \qquad \text{A3.8}$$

where superscript T denotes matrix transpose and superscript -1 denotes matrix inverse. The inverse operator is given by

$$[H] = \{[A]^T[A]\}^{-1}[A]^T \qquad \text{A3.9}$$

The derivatives required to formulate [A] can be evaluated nicely by the scheme shown by Patrick and Bostick (1969).

The least square error of the solution, ξ_y^2, is computed from

$$\xi_y^2 = \langle \Delta y \rangle^T \langle \Delta y \rangle \qquad \text{A3.10}$$

DESCRIPTION OF STATISTICAL ESTIMATES

The following demonstrates statistical techniques used in evaluation of geophysical measurements. We will not derive basic statistical principles but refer the reader to Hamilton (1964) and Bevington (1969).

Analysis of the model depends upon statistical estimates of the model *parameters* or the parameter covariance matrix, which has diagonal elements of variances and off-diagonal elements of mutual variances or covariances. Computation of the *parameter change* covariance matrix. has been outlined by Jackson (1973) and Wiggins (1972).

The parameter change covariance matrix is formally defined in terms of the expected value of the parameter change as

$$[\text{cov}\Delta x] = E\ \{(\langle \Delta x \rangle - E\langle \Delta x \rangle)\ \ (\langle \Delta x \rangle - E\langle \Delta x \rangle)^T\} \qquad \text{A3.11}$$

where E denotes expectation. The data difference covariance matrix is defined in the same manner as

$$[\text{cov}\Delta y] = E\ \{[\ \langle \Delta y \rangle - E\langle \Delta y \rangle)\ (\langle \Delta y \rangle - E\langle \Delta y \rangle)^T\} \qquad \text{A3.12}$$

It can easily be shown that

$$[\text{cov}\Delta x] = [H]\ [\text{cov}\Delta y]\ [H]^T \qquad \text{A3.13}$$

If the data differences are statistically independent and have a uniform variance, ξ_y^2, then A3.13 becomes

$$[\text{cov}\Delta x] = [H]\ [H]^T\ \xi_y^2$$

$$[\text{cov}\Delta x] = \{[A]^T[A]\}^{-1}\xi_y^2 \qquad \text{A3.14}$$

Smith (1974) has shown that assuming:

1) The numerical error in computation of the forward problem and derivatives are much smaller than the observation errors,

2) truncation of the Taylor Series expansion produces smaller error than the observation error,

3) the observation errors are statistically independent with a uniform standard deviation and

4) the model describing the earth correctly describes the terrain in which the geophysical measurements are made

the covariance of Δx is the same as covariance of x, the vector of parameters (solution to the problem), i.e.

$$[\mathrm{cov}\Delta x] = [\mathrm{cov}x]$$

that is $$[\mathrm{cov}x] = \{[A]^T[A]\}^{-1} \quad \xi_y^2 \qquad \text{A3.15}$$

The data variance, ξ_y^2, scales [covx] as given by equation A3.15. An estimated value of the data variance is given by

$$\xi_o^2 = \frac{\langle \Delta c \rangle^T \langle \Delta c \rangle}{N-M} \qquad \text{A3.15}$$

where N is the number of observations and M the number of parameters. The parameter covariance, then, is estimated by substitution of ξ_o^2 for ξ_y^2 given in equation A3.15.

The magnitude of parameter standard deviation, $(\mathrm{covx}_{i,i})^{1/2}$, reflects the magnitude of the mean value of the parameter $(E\{x_i\})$.

The standard deviation is given as a percentage of the parameter or

$$(\xi_p^{\%})j = \left(\frac{(\xi_p)_j}{P_j} \right) x\ 100 \qquad \text{A3.16}$$

Percentage parameter standard deviations have the desirable advantage of being dimensionless and independent of the parameter mean value (Jenkins and Watts, 1968).

The remaining important statistical estimates are given by the parameter correlation matrix which has i^{th}, j^{th} elements defined as

$$corrx_{ij} = \frac{covx_{ij}}{(covx_{ii} \cdot covx_{jj})^{1/2}} \quad . \qquad \text{A3.17}$$

Near unity values for the off-diagonal elements of the correlation matrix *implies* a linear relationship between parameters of the earth model. For example the first parameter, p_1, can be written in terms of the other parameters as

$$P_1 = \Sigma_{i=2}^{M} \frac{(\xi_p)_1}{(\xi_p)_j} \; (covp_{ij}) \cdot P_j \qquad \text{A3.18}$$

Equation (19) also suggests that for near unity values of correlation coefficients, two or more parameters can be combined as a single parameter. For example suppose that the correlation coefficient for σ_1 and D_1 is near unity and greater than zero. Then a change in one will be proportional to a change in the other. Hence the ratio D/σ_1 or the product $\rho_1 D_1$ (resistivity-thickness) will remain approximately a constant.

MARQUARDT CONSTRAINTS

Problems with convergence to a minimum of the objective function (least square error) arise in the linearized inversion process when the difference between the largest and smallest eigenvalue of the matrix A^TA (condition number) is large. A small eigenvalue associated with a particular parameter implies that the data contains little information about that parameter. This in turn implies that large changes in the value of that parameter will have little effect on the theoretically generated data (forward solution). Because of this, large steps in parameter space may result during unconstrained iteration. The least squares linearized inversion technique always produces a step in a direction which will decrease the value of the objective function.

But the objective function in parameter space may have many local minima, maxima, or saddle points, depending on how non-linear the actual problem is. The magitud of the step in parameter space becomes important in this case, since it is possible to overshoot a minimum in the objective function by taking too large a step.

The Marquardt technique provides a means of controlling the step taken in parameter space by weighting the diagonal elements of the matrix $[A^TA]^{-1}$. The weighting is performed in the following manner (see Chapter 3, Lanczos, 1961 for notation)

$$A = U\Lambda V^T \qquad A^T = V\Lambda U^T$$

$$A^TA = V\Lambda^2V^T = \sum_{i=1}^{m} \lambda_i^2 v_i v_i^T$$

Unweighted

$$[A^TA]^{-1} = \sum_{i=1}^{m} \frac{1}{\lambda^2} v_i v_i^T$$

Weighted

$$\sum_{i=1}^{m} \frac{1}{(\lambda_i^2+\omega)} v_i v_i^T = [A^TA+\omega]^{-1}$$

where U = matrix of data eigenvectors

V = matrix of parameter eigenvectors v_i, i = 1 to m

Λ = diagonal matrix of eigenvalues of A

I = identity matrix

ω = Marquardt weight

The Marquardt weight ω is determined by experiment to allow convergence to a minimum of the objective function upon iteration. Values of ω used in this study ranged from 0.05 to 0.2. The effect of this weighting on iteration is to decrease the step size in parameter space and to rotate the direction of the step towards the steepest descent direction of the objective function, with the larger values of ω having the greater effect.

DISTRIBUTION

No. of Copies	
30	David D. Blackwell Department of Geological Sciences Southern Methodist University Dallas, TX 75222
15	W. F. Bott Rogers Engineering Company, Inc. San Francisco, CA 94100
1	Lynn A. Brant Montana Department of Natural Resources and Conservation Energy Planning Division Sam W. Mitchell Bldg. Helena, MT 59601
1	T. L. Britt Salt Lake City, UT 84100
1	John Burnham Battelle-Northwest Richland, WA 99352
25	Ritchie B. Coryell Office of Systems Integration and Analysis National Science Foundation Washington, DC 20550
1	W. T. Cruse Montana Club Helena, MT 59601
1	Dr. Jesse Denton, Director National Center for Energy and Power Management 260 Towne Bldg. University of Pennsylvania Philadelphia, PA 19174
1	F. E. Diebold Montana Tech. Butte, MT 59701
2	Raymond Dominick Communications Editor Montana Department of Intergovernmental Relations Capitol Station Helena, MT 59601
1	D. R. Draper Montana Department of Intergovernmental Relations Capitol Station Helena, MT 59601
15	Dr. Russell Duff Radiation and Fluid Physics Division Systems, Science & Software P.O. Box 1620 LaJolla, CA 92037
1	Robert Duncan Montana Department of State Lands State Capitol Helena, MT 59601
1	J. R. Eliason Battelle-Northwest Richland, WA 99352
1	L. O. Foley Battelle-Northwest Richland, WA 99352
1	P. Groth Pam Am Oil Co. Denver, CO 80200
1	Ron Guse Montana Department of Natural Resources and Conservation Energy Planning Division Sam W. Mitchell Bldg. Helena, MT 59601

DISTRIBUTION (Continued)

No. of Copies

1 D. Harriott
Livingston, MT 59047

1 A. J. Haverfield
Battelle-Northwest
Richland, WA 99352

1 A. Hellesmark
Livingston, MT 59047

1 W. R. Hotchkiss
U.S. Geological Survey
Helena, MT

Gerald W. Johnson
TRW
Redondo Beach, CA 90277

2 James T. Kuwada
Rogers Engineering Company, Inc.
16 Beale St.
San Francisco, CA 94105

5 D. B. Lombard
U.S. Energy Research and Development Administration
Division of Geothermal Energy

1 Frank McChesney, Director
Montana Department of Intergovernmental Relations
Capitol Station
Helena, MT 59601

2 William R. McSpadden
Battelle-Northwest
Richland, WA 99352

1 B. J. Melton
ERDA Richland Operations Office
Program Division
Richland, WA 99352

No. of Copies

1 L. J. Patrick Muffler
U.S. Geological Survey
Geochemistry and Petrology
345 Middlefield Road
Menlo Park, CA 94025

2 Robert Newman
Bureau of Land Management
P.O. Box 1227
Missoula, MT 59801

1 James Posewitz
Montana State Fish and Game Department
Sam Mitchell Bldg.
Helena, MT 59601

1 Dan H. Pyfer
Manager Area Development
Montana Power Company
40 E. Broadway
Butte, MT 59701

1 Dr. Henry J. Ramey, Jr.
Department of Petroleum Engineering
Stanford University
Stanford, CA 94305

1 L. C. Schmid
Battelle-Northwest
Richland, WA 99352

25 Col. S. Schwiller
U.S. Energy Research and Development Administration
Division of Geothermal Energy

1 R. C. Scott
U.S. Environmental Protection Agency
San Francisco, CA 94100

1 M. C. Smith
Los Alamos Scientific Laboratory
Los Alamos, NM 87544

DISTRIBUTION (Continued)

No. of Copies		No. of Copies	
1	R. B. Smith University of Utah Salt Lake City, UT 84100	1	Montana Associated Utilities, Inc. Great Falls, MT 59401
1	Shannon Soloman Montana Department of State Lands State Capitol Helena, MT 59601	1	Montana Tech. Physics Department Butte, MT 59701
5	D. H. Stewart Battelle-Northwest Richland, WA 99352	27	Technical Information Center
1	N. A. Stoll Oregon National Building Portland, OR 97200	3	Technical Information Files
1	L. K. Stone Department of Interior Washington, DC 20000		
1	W. M. Taliaferro U.S. Forest Service Helena National Forest		
1	W. Templeton Battelle-Northwest Richland, WA 99352		
1	G. Wicks Montana Department of Natural Resources and Conservation Energy Planning Division		
1	R. Zahradnik National Science Foundation Washington, DC 20000		